Polythiophene-Containing Block Copolymers for Organic Photovoltaic Applications

A DISSERTATION
SUBMITTED TO THE FACULTY OF THE GRADUATE SCHOOL
OF THE UNIVERSITY OF MINNESOTA
BY

Bryan W. Boudouris

IN PARTIAL FULFILLMENT OF THE REQUIREMENTS
FOR THE DEGREE OF
DOCTOR OF PHILOSOPHY

C. Daniel Frisbie and Marc A. Hillmyer, Advisors

August 2009

Acknowledgements

It has been a true privilege to attend graduate school at the University of Minnesota in the Chemical Engineering and Materials Science (CEMS) Department. Numerous individuals at Minnesota have helped challenge, inspire, and nurture my intellectual and personal growth. First and foremost, I thank my advisors, Professors Dan Frisbie and Marc Hillmyer. They were mentors in every sense of the word. They provided amazing guidance while still allowing me to engineer my own research project, and always found new ways to test my creativity. Observing your two different management styles and personalities showed me how to generate productive collaborations, and has made me a better scientist. Professor Russ Holmes also has played a crucial role in my classroom and laboratory development. His readiness to engage in informal discussions on any number of topics for hours at a time was very much appreciated. Additionally, his willingness to allow me to assist in teaching his introductory materials science class leaves me forever indebted to him.

I would also like to thank our collaborators in Professor David Blank's group in the Chemistry Department, specifically Dr. Nathan Wells, Dr. Andrew Healy, and Francesc Molins. The experiments they performed and the conversations I have had with them and Professor Blank greatly improved my understanding of how charge is generated and transferred in organic semiconductors. Perhaps even more impressive was their ability to gather so much important data from only milligram quantities of material! I must also thank our colleagues at the National Renewable Energy Laboratory (NREL), Dr. Sean Shaheen and Dr. Nikos Kopidakis. Their help in teaching me the proper fabrication and testing techniques for polymer solar cells was central in the development of my practical organic photovoltaic knowledge.

Thank you to all of the past and current members of the Frisbie and Hillmyer research groups. An innumerable amount of useful conversations have occurred thanks to the wonderful colleagues that compose these two groups. I would like to especially thank the following Frisbie group members and alumni: Salil, Seongho, Dave, Vivek, Moon, Yan, Xia, Xiuyu, Lei, Sandy, Chris, and Vince. I would also like to specifically

thank the following Hillmyer group members and alumni: Mark Amendt, Will Gramlich, Chun, Jennifer, Louis, Marc Rodwogin, Zach, John, Will Edmonds, Kathleen, Adam, Javid, Mahesh, and Raji. Your camaraderie in the office and laboratory has made graduate school a very enjoyable experience. I would like to send a special thank you to Frisbie group alumnus Professor Matthew Panzer whose friendship, both inside and outside of the laboratory, has been very much appreciated and will never be forgotten. Finally, I must thank the small photovoltaics group that includes: Derek Stevens, Dr. Jung Yong Kim, Dr. Yang Qin, and Josh Speros. Derek deserves extra thanks for carefully and quickly proofing the entirety of this thesis. Your diligent work is very much appreciated.

Thank you to my office compatriots of the Holmes group: Nick, Richa, Kai, Grant, and Wade. Since the formation of the group, your friendships have made coming to the office a great experience. Particularly, I would like to thank Wade Luhman for proofing parts of this work. A large thank you goes out to Julie Prince, Teresa Bredahl, Mary Haverkost, Mary Nissen, and the entire CEMS Department staff for everything that you continue to do. It would be fair to say that the research presented within would not be possible without your help. Outside of the University, I have met many strangers that became friends while in Minnesota including: Heather, Rob, Tina, Bob, Eric, Crystal, and, of course, Nicole. I would like to thank them for their camaraderie and support during my time here.

Last, but certainly not least, I must thank all of my friends and family from Illinois. I thank the friends from Highland, Champaign, and the Chicago areas that have sent their well-wishes, participated in fantasy sports, and visited the Twin Cities while I have attended the University. Specifically, I would like to thank Emily for serving as an amazing friend, and always finding new ways to keep me grounded during the past five years. Finally, I must thank my parents, brother, and grandparents for their never-ending support. Your love and understanding have buoyed my spirits during my time here. You are always with me.

Dedication

This dissertation is dedicated to my parents and grandparents.

William and Teresa Boudouris

Nick and Kathryn Boudouris; Donald and Leola Wall

Abstract

Poly(3-alkylthiophene)s (P3ATs) have become the most common electron-donating material in organic photovoltaics (OPVs), and recent advances in the fabrication of polythiophene–fullerene bulk heterojunction solar cells have allowed for devices with power conversion efficiencies of up to ~6% to be realized. This efficiency has only been possible through enhancements in the active layer microstructure. This key factor allowed for better separation of the bound electron-hole pair (exciton), generated by absorption of light. Understanding how exciton dissociation and the active layer morphology affect device performance will facilitate cell optimization, ultimately leading to higher device efficiencies. Consequently, we developed two new classes of polythiophene-based block copolymers to better understand these phenomena.

First, we synthesized well-defined diblock and triblock copolymers with the structures: poly(3-alkylthiophene)-*b*-polylactide (P3AT-PLA) and polylactide-*b*-poly(3-alkylthiophene)-*b*-polylactide (PLA-P3AT-PLA). We have observed that kinetic factors dominate phase separation for a semicrystalline polythiophene block. However, if the polythiophene moiety was amorphous the polymers self-assembled into thermodynamically stable, ordered microstructures with domain spacings on the scale of interest for charge separation in OPV cells (ca 30 nm). Polylactide was chosen as the second moiety in the block copolymers because it could be selectively etched from the polythiophene matrix with a gentle alkaline bath. This procedure led to the formation of nanoporous templates that could generate ordered bulk heterojunctions.

In the second approach, P3AT chain ends were terminated with fullerene to create an internal electron acceptor-donor-acceptor, methylfulleropyrrolidine-poly(3-alkylthiophene)-methylfulleropyrrolidine (C_{60}-P3AT-C_{60}). Microphase separation occurred between the polymer chain and fullerene end groups, which suggested the creation of two distinct semicrystalline regimes. A compositionally similar blend of P3HT and C_{60} showed a similar microstructure. This comparable domain formation, coupled with the possibility of enhanced charge transfer, makes C_{60}-P3AT-C_{60} a promising candidate as a material in bulk heterojunction organic photovoltaic devices.

Table of Contents

List of Tables

List of Figures

1 Introduction

In 1986 the Eastman Kodak Corporation introduced the first notably efficient bilayer organic photovoltaic (OPV).[1] While only ~1% efficient, this first plastic solar cell offered the promise of a power source that was lightweight, thin, mechanically robust, and flexible.[2,3] This was a monumental shift from traditional inorganic (*i.e.* silicon) photovoltaics, which are thick, rigid, and fragile. Additionally, the largest advantage of this new class of photovoltaics was the possibility for device fabrication using low-cost, large-area techniques (*e.g.*, roll-to-roll printing).[4] The opportunity to maneuver away from the expensive and energy-intensive clean room fabrication of inorganic devices has generated a new paradigm in the field of PVs. While these devices show much promise there are still hurdles for the OPV community to overcome. For instance, some device design rules exist,[5] but it is still difficult to predict the success of a particular semiconductor or device a priori. Consequently, the field of organic photovoltaics must continue to learn from the more developed organic light-emitting diode (OLED) and inorganic photovoltaic literature while attempting to create and nurture new classes of materials and devices. This affords researchers in the relatively new field of organic photovoltaics opportunities to address both fundamental and practical engineering questions in order to develop systems that allow for the commercialization of OPVs.

In the past twenty years many modifications to OPVs have been made and include new photoactive materials, deposition techniques, device architectures, and electrode materials.[6,7] These changes and fine-tuning have led to certified power conversion efficiencies of 6%.[8] While this is an impressive milestone, organic photovoltaics remain below the 10% efficiency of amorphous silicon devices, a benchmark that needs to be reached to create a large investment from the private sector. At present, obstacles such as the inherent low carrier mobilities in organic semiconductors, the absence of low band gap materials, the lack of a wide variety of electron-conducting semiconductors, and the environmental instability of the photoactive layer have prevented the fabrication

of higher efficiency devices. Another large challenge currently preventing researchers from overcoming the 10% efficiency mark, which is addressed in this work, is the lack of control over the morphology of the device active layer and understanding how this morphology affects device performance.[7,9,10]

1.1 Thesis Overview

The motivation of the research presented here was to synthesize and understand the microstructure of functional block copolymers. Eventually these molecules could be used as active layer materials for organic photovoltaics. While many different polymer systems could have been chosen, this work focused on polythiophene-based block copolymers because the large variety of materials within the polythiophene family have attracted much attention in the field of organic electronics due to their high hole transport (p-type) performance, their chemically tunable electronic properties, and their processibility from numerous solvents.[11-13] End-functionalized polythiophenes were used as the building blocks for the addition of a second or third segment to the ends of the semiconducting chains where the additional moieties were of two types. The first was a selectively etchable polyester block and the second type was an electron-transporting (n-type) material. In the first instance, nanoporous poly(3-alkylthiophene) films were generated, and the microstructures of the block copolymers varied greatly depending on the regioregularity of the polythiophene block. The second case illustrated how the covalent linkage of electron-accepting and donating materials could lead to interesting optical properties, charge transfer phenomena, and microstructures. Both of these systems offered advantages for controlled active layer morphologies in organic photovoltaic cells. The use of the materials developed in this work could generate a better understanding of the crucial structure-transport relationship in organic photovoltaics; this, in turn, should allow researchers develop more efficient organic photovoltaics.

Chapter 2 introduces general techniques for the synthesis of block copolymers; also described are the theoretical and commonly observed microstructures. The synthetic protocols and morphologies are described for two system types: 1) block

copolymers composed entirely of flexible bonds along the backbone of the polymer (*i.e.* coil-coil diblock copolymers) and 2) block copolymers where at least one of the segments contains a more rigid polymer (*i.e.* rod-coil block copolymers). The differences in synthetic protocols are noted and the mechanisms that drive phase separation and the observed microstructures are compared and contrasted. The chapter concludes by reviewing the use of block copolymers as nanotemplates in applications ranging from lithography to separations.

Chapter 3 begins with an introduction to the molecular structures for a number of small molecules and polymers commonly used in organic photovoltaic devices. A comparison of the operating principles in inorganic and organic photovoltaics follows. A focused review of the various device architectures currently used in organic photovoltaics introduces the concept of the ordered bulk heterojunction. Finally, a proposed route to a well-ordered, all-organic bulk heterojunction through the use of block copolymer templates is outlined.

Chapter 4 has been published as "Nanoporous Poly(3-alkylthiophene) Thin Films Generated from Block Copolymer Templates," by B. W. Boudouris, C. D. Frisbie, and M. A. Hillmyer, *Macromolecules* **2008**, *41*, 67–75. Block copolymers of poly(3-alkylthiophene)-*b*-polylactide (P3AT-PLA) are synthesized and the alkyl chain length of the polythiophene block is either six or twelve carbons long. After molecular and thermal characterization it was found that poly(3-dodecylthiophene) (P3DDT) is a better choice for study because the melting temperature of poly(3-hexlythiophene) (P3HT) is above the degradation temperature of PLA; therefore, P3DDT-PLA has a more robust processing window than P3HT-PLA. Thin films of P3DDT-PLA were selectively etched to remove the PLA moiety and leave a nanopitted P3DDT film. Long-range order is not observed because phase separation of the blocks is dominated by the crystallization of the polythiophene moiety.

Chapter 5 explores the effect of the regioregularity of the polythiophene moiety in the block copolymers on the observed microstructures. These materials are ABA-type triblock copolymers, polylactide-*b*-poly(3-alkylthiophene)-*b*-polylactide (PLA-P3AT-

PLA), where the polythiophene moiety is the middle (B) block. When the polythiophene segment is semicrystalline phase separation is dominated by the kinetics of crystallization; this is similar to the diblock copolymer case described in Chapter 4. However, when the polythiophene block is amorphous the phase separation observed is independent of crystallization effects. It is proposed that this type of phase separation is more useful than the crystallization-induced phase separation for functional block copolymer solar cells. However, long-range order was not observed for the completely amorphous PLA-P3AT-PLA block copolymers presumably because the polythiophene block is composed of polymer chains with an extremely large distribution in molecular weights.

Chapter 6 shows the synthesis, molecular, thermal, and structural characterization of a novel series of polythiophene-containing block copolymers, polylactide-*b*-poly(3-dodecylthiophene-*co*-thiophene)-*b*-polylactide (PLA-coPT-PLA). Because the dihydroxyl-terminated poly(3-dodecylthiophene-*co*-thiophene) (HO-coPT-OH) macroinitiator is synthesized using a controlled polymerization technique, the block copolymers have relatively narrow molecular weight distributions. The incorporation of 3-dodecylthiophene and thiophene repeat units into the semiconducting polymer backbone causes the homopolymer, and the subsequent triblock copolymers, to be completely amorphous as evidenced by DSC and WAXS. Because these triblock copolymers are completely amorphous and have narrow molecular weight distributions, they offer the promise of self-assembling into thermodynamically-controlled thin film microstructures with long-range order.

Chapter 7 has been published as "Synthesis, Optical Properties, and Microstructure of a Fullerene-Terminated Poly(3-hexylthiophene)," by B. W. Boudouris, F. Molins, D. A. Blank, C. D. Frisbie, and M. A. Hillmyer, *Macromolecules* **2009**, *42*, 4118–4126. Fullerene end-functionalized poly(3-hexlythiophene) (C_{60}-P3HT-C_{60}) is synthesized using a controlled polymerization scheme to create an internal electron acceptor-donor-acceptor macromolecule. Covalent linkage of the fullerene to the ends of the polythiophenes is determined using ^{1}H NMR spectroscopy, ultraviolet-

visible (UV-Vis) light absorbance spectroscopy, and fluorescence spectroscopy. Wide-angle and small angle x-ray scattering (WAXS and SAXS) of C_{60}-P3HT-C_{60} powders suggest the formation of two distinct semicrystalline regimes; one of the regimes is associated with the crystalline regions of poly(3-hexlythiophene) while the other is associated with fullerene. Fast Fourier Transform (FFT) data indicate that this microstructure is also present in C_{60}-P3HT-C_{60} thin films.

Chapter 8 suggests future experiments related to the work presented within this thesis. Preliminary results detailing the thin film microstructures of the PLA-coPT-PLA triblock copolymers synthesized in Chapter 6 are shown, and future experiments to generate a nanoporous thin film with long-range order are suggested. Next, strategies for infiltrating nanoporous polymer films with a second organic semiconductor to create an all-organic ordered bulk heterojunction are discussed. The synthetic techniques utilized in Chapter 7 are used to generate a series of C_{60}-P3HT-C_{60} polymers where the average number of repeat units varies from 10–150. Thin film microstructures for the lowest molecular weight C_{60}-P3HT-C_{60} polymer are also explored. Finally, preliminary results detailing the use of the C_{60}-P3HT-C_{60} in organic electronic devices are shown.

Chapter 9 contains appendices relevant to this thesis, including: copyright permissions for the material in Chapters 4 and 7 as well as additional experimental details and characterization associated with the polymers presented in Chapters 5, 6, and 7. The standard operating procedures for the vacuum-inert atmosphere manifold in 482 Amundson Hall are also provided for reference.

1.2 References

[1] Tang, C. W. *Appl. Phys. Lett.* **1986**, *48*, 183–185.

[2] Shaheen, S. E.; Ginley, D. S.; Jabbour, G. E. *MRS Bull.* **2005**, *30*, 10–15.

[3] Loo, Y. L.; McCulloch, I. *MRS Bull.* **2008**, *33*, 653–658.

[4] Brabec, C. J.; Durrant, J. R. *MRS Bull.* **2008**, *33*, 670–675.

[5] Scharber, M. C.; Mühlbacher, D.; Koppe, M.; Denk, P.; Wadauf, C.; Heeger, A. J.; Brabec, C. J. *Adv. Mater.* **2006**, *18*, 789–794.

[6] Sun, S.; Sariciftci, N. S.; Eds. *Organic Photovoltaics: Mechanisms, Materials, and Devices*; Taylor & Francis: Boca Raton, FL, 2005.

[7] Thompson, B. C.; Fréchet, J. M. J. *Angew. Chem., Int. Ed.* **2008**, *47*, 58–77.

[8] Park, S. H.; Roy, A.; Beaupré, S.; Cho, S.; Coates, N.; Moon, J. S.; Moses, D.; Leclerc, M.; Lee, K.; Heeger, A. J. *Nat. Photonics* **2009**, *3*, 297–303.

[9] Müller, C.; Ferenczi, T. A. M.; Campoy-Quiles, M.; Frost, J. M.; Bradley, D. D. C.; Smith, P.; Stingelin-Stutzmann, N.; Nelson, J. *Adv. Mater.* **2008**, *20*, 3510–3515.

[10] Peet, J.; Senatore, M. L.; Heeger, A. J.; Bazan, G. C. *Adv. Mater.* **2009**, *21*, 1521–1527.

[11] Nalwa, H. S.; Ed. *Handbook of Organic Conductive Molecules and Polymers*; J. Wiley & Sons: New York, 1996.

[12] McCullough, R. D. *Adv. Mater.* **1998**, *10*, 93–116.

[13] Osaka, I.; McCullough, R. D. *Acc. Chem. Res.* **2008**, *41*, 1202–1214.

2 Synthesis and Physics of Block Copolymers

Polymers are macromolecules composed of distinct sections that may number from tens to millions of repeating units. These distinct units originate from reactions (*e.g.*, chemical, electrochemical, photochemical) of monomers that covalently attach to one another to form repeating elements and create a unique polymer chain. If the chemical structure of the repeat unit is the same throughout the chain the polymer is termed a homopolymer. However, a polymer may be composed of two chemically distinct and covalently bound repeat units; these molecules are known as copolymers. The exact sequencing of the chemically distinct repeat units can be controlled by a variety of synthesis conditions such as the polymerization initiator functionality, the monomer addition sequence and rate, and the feed ratio of the different monomers.

Examining systems where the copolymers are constrained to compositions generated from only two distinct monomer feeds leads to nomenclatures of a variety of common copolymers.[1-3] Schematic representations of these polymers are shown as black and white circles in Figure 2.1. Perhaps the simplest copolymer is the statistical copolymer where repeat units are distributed in a random manner along the length of the polymer chain. A more ordered structure is shown by the alternating copolymer where the black and white repeat units appear exactly at every other position. Gradient copolymers are molecules that have a higher concentration of chemically similar repeat units towards the beginning and terminus of the polymer chains. For instance, white repeat units dominate the left-hand side of the chain in Figure 2.1d with black repeat units slowly added to the chain; a gradient of white to black repeat units begins to form until, eventually, the right-hand side of the chain is dominated by black repeat units. To this point, only linear polymers have been discussed. These polymers are ones in which the addition of repeat units continually occurs at the end of the polymer chain. However, branched copolymers can also be synthesized; these macromolecules include geometries such as star and comb copolymers (Figure 2.1e,f).

While all of the polymers discussed to this point are important in a variety of commercial applications, the focus of this work is block copolymers. Block copolymers are macromolecules where the repeat units are broken into distinct segments (*i.e.* blocks) where each segment is composed of the same types of repeat units and these segments are covalently linked to one another. In the simplest case, a segment of white repeat units (A block) are covalently attached to a segment of black repeat units (B block) to form an A-B diblock copolymer (Figure 2.1g). Other commonly synthesized constructs include A-B-A triblock and A-B-A-B-A pentablock terpolymers.

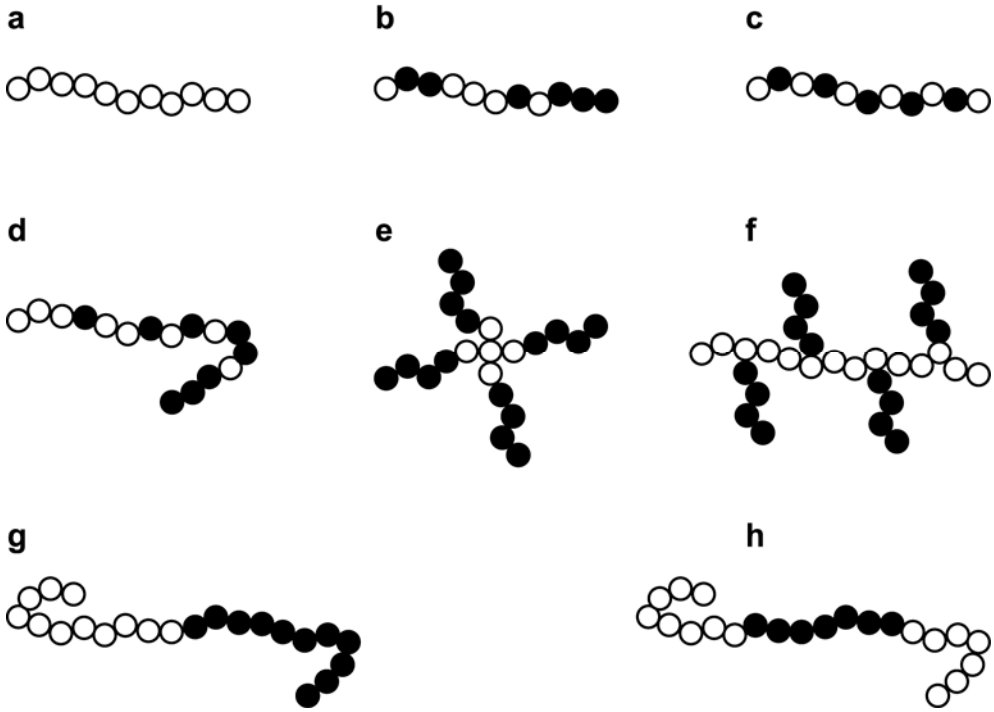

Figure 2.1 Schematic examples of (a) a homopolymer composed of white circle repeat units, and copolymers composed of chemically distinct black and white repeat units in a variety of constructs such as a: (b) statistical copolymer, (c) alternating copolymer, (d) gradient copolymer, (e) four-arm star copolymer, (f) comb copolymer, (g) A-B diblock copolymer, and (h) A-B-A triblock copolymer.

Covalently binding distinct moieties in block copolymers can lead to materials properties that are similar to that of the individual homopolymers but can also lead to strikingly different behavior. One remarkable example occurs due to the chemical

dissimilarity between the covalently bound blocks. Specifically, microphase separation readily occurs in these materials forming nanoscopic geometries. This phenomenon results from the interplay of entropic and enthalpic contributions as the system seeks to lower its total free energy while still maintaining its chemical linkage.[2,4,5] Understanding the complex morphologies that can form requires knowledge of the molecular structure of the polymer in question and, importantly, a firm grasp of the flexibility of the individual blocks. The first point is usually well-established based on the mechanism of the synthetic route taken and can be verified by using appropriate characterization techniques. On the other hand, the second point is more subtle and usually overlooked, as the majority of block copolymers synthesized contain segments where each moiety is composed of a polymer that adopts a Gaussian coil in the melt due to the flexibility of the molecular backbone of the homopolymer (a coil-like polymer).[6-8] Block copolymers where at least one of the segments is considered inflexible (a rod-like polymer) are becoming increasingly important for applications ranging from organic electronics to biotechnology.[9,10] Comparing the synthetic techniques available, how these mechanisms can be used to generate linear A-B and A-B-A block copolymers, and the observed microstructures of coil-coil and rod-coil block copolymers will facilitate the discussion of the results presented later.

2.1 Completely Coil-like Block Copolymers

The most widely studied class of block copolymers are those with moieties whose backbones are coil-like in nature.[4,11-13] Therefore, there are a number of common synthetic routes that can lead to block copolymers where the molecular weight and sequencing of the copolymer segments can be precisely tuned while still maintaining a low molecular weight distribution. Additionally, the equilibrium morphologies for these types of systems in the melt have been widely studied both theoretically[14-16] and experimentally.[17-19] By refining the synthetic protocols and utilizing x-ray scattering and microscopy tools researchers have been able to establish important structure-property relationships for coil-coil diblock copolymer systems, and applications based around these unique materials have emerged commercially.[13]

2.1.1 Synthetic Techniques

Unlike the majority of rod polymers, the synthetic schemes for coil polymers generally fall into the class of polymerizations known as chain-growth. In the chain-growth mechanism, an active center is introduced into the reaction flask containing monomers. The active center adds repeat units to the polymer chain by consuming monomers until a termination event occurs. These events are summarized in Equations 2.1 – 2.3.

$$I \rightarrow I^* \tag{2.1}$$

$$I^* + M \rightarrow I - M^* + M \rightarrow\rightarrow\rightarrow P_i^* \tag{2.2}$$

$$P_i^* + P_j^* \rightarrow P_{i+j} \tag{2.3}$$

In these reactions, the active initiator species (*I**) is formed from the dissociation or decomposition of the initiator (*I*). *I** reacts with a monomer and transfers the active species to the beginning of the polymer chain. After this point, the growing polymer chain continues to consume free monomer and reaches some degree of polymerization with *i* repeat units. Finally, the polymer chain can terminate through a variety of mechanisms that are more or less likely depending on the exact polymerization conditions. In the particular instance shown (Equation 2.3), two polymer chains with *i* and *j* repeat units couple to create a chain with *i*+*j* repeat units and no active centers.

Within chain-growth, the polymerizations can fall into two broad classes: controlled or uncontrolled polymerizations. Controlled polymerizations are termed as those in which the molecular weight of the polymer can be precisely tuned by reaction conditions and the molecular weight distribution, or polydispersity index (PDI), is kept narrow. The polydispersity index can be thought of in terms of the standard deviation (σ) away from the number-average molecule weight (M_n). Equation 2.4 shows that as the PDI goes to 1 the standard deviation becomes smaller.[2]

$$\sigma = M_n \left[PDI - 1\right]^{1/2}; \; PDI \equiv \frac{M_w}{M_n} \tag{2.4}$$

Keeping the polydispersity index low through controlled polymerization techniques is practical on the bench top or pilot plant level, but uncontrolled polymerizations are the

workhorses of industrial applications.[1-3] These schemes are used because they rapidly produce large amounts of valuable commodities and do not require maintaining a high level of purity in the reagents and reaction vessels. Controlled polymerizations give narrow molecular weight distributions (PDI < 1.2). They are the preferred synthetic routes in the field of block copolymers because a narrow distribution helps prevent confusion when tracking the phase behavior of block copolymers as a function of molecular weight; however, high molecular weight distribution coil-like block copolymers (PDI > 1.5) are attracting more interest, as PDI can be used as another knob in controlling the microphase separation.[20-22]

A special class of controlled polymerizations is the living polymerization. While exact criteria have been suggested for defining how "living" a polymerization is,[23,24] polymers generated in this manner have finely tuned molecular weights, very narrow molecular weight distributions, and can be used to produce block copolymers and end-functionalized polymers. These reactions are defined such that irreversible termination and chain transfer are not present. If the rate of initiation is much faster than the rate of propagation, all chains have equal reactivity, and the rate of polymerization is much faster than the rate of depolymerization, the polymer molecular weights are characterized by a Poisson distribution; it then can be shown that Equation 2.5 holds.[2]

$$\frac{M_w}{M_n} = PDI \approx 1 + \frac{1}{N} \tag{2.5}$$

In this equation M_w is the weight-average molecular weight, M_n is the number-average molecular weight, and N is the number of repeat units in the polymer. Therefore, the molecular weight distribution approaches unity as the molecular weight of the polymer increases. For example, a modest molecular weight polymer with $N = 1000$ has a PDI = 1.001. While this may be difficult to achieve (or measure) in practice, similar narrow molecular weight distributions can be easily reached and this greatly simplifies block copolymer microstructural analysis. Importantly, even in the case when a controlled polymerization is not necessarily living, the molecular weight distributions experimentally realized for controlled polymerizations (the most common reaction for

the synthesis of coil polymers) are much lower than the PDI values for step-growth polymerization (the most common reaction for the synthesis of rod polymers). This point will be readdressed in Chapters 4 and 5.

Anionic polymerization, one of the most common controlled polymerization techniques for coil-like polymers, generally is living and has been employed since 1956.[25] In order to utilize living anionic polymerizations, an unsaturated bond (such as a vinyl group or cyclic structure) must be present in the monomer. These polymerizations proceed via organometallics sites, carbanions with metallic counterions.[26] This means that the active species is nucleophilic; therefore, the substituent group must be electroattractive in the vinyl monomer example. Finer points, including monomer and solvent purity, counterion size and the polarity of the solvent, must also be considered in order to achieve narrow molecular weight distributions, but routes to optimize these reaction conditions are usually well-known.[13,26] One built-in feature that allows this mechanism to be living is that termination by chain coupling is not favored because the reaction of two anions is highly unlikely. To terminate a living anionic polymerization to create a homopolymer simply requires the introduction of a proton source to quench the growing chains, and anionic polymerization is also readily amenable to block copolymer synthesis.

The most general method to create an A-B diblock copolymer is the sequential addition of a B monomer after the polymerization of A is completely exhausted. Care must be taken that the carbanions of A are able to initiate the polymerization of B and that the addition of B monomer is done in a way that does not terminate A to leave homopolymer A chains. A second method relies on protecting the end of the growing A block by the addition of a bulky functional group or counterion that is less reactive to A and more reactive to B. Sequential monomer addition can also be used to synthesize A-B-A triblock copolymers. This technique can be difficult to achieve in practice because monomers A and B must be chosen so that the carbanions of A can initiate the polymerization of B and the carbanions of B can initiate the polymerization of A. Additionally, if the polymer is to be truly symmetric, exact equimolar amounts of A

monomer must be added at the beginning of the first and third polymerization steps. A more realistic strategy is to couple two A-B diblock copolymers that are half the molecular weight of the intended triblock copolymer molecular weight. The diblock copolymers could be synthesized using the sequential monomer addition route and coupled using a difunctional agent. Usually, coupling is not complete and A-B diblock copolymers must be separated from the coupled A-B-A triblock copolymers, a purification that can be difficult. Perhaps the most experimentally practical route to A-B-A triblock copolymers is to utilize a difunctional initiator to synthesize the B block first. Sequential monomer addition of A could then be employed to generate the two exterior A blocks, assuming that the B carbanions can initiate the A monomer.

While not as often employed as anionic polymerization, cationic polymerization was shown to be a tangible method for the synthesis of living polymers in 1984.[27,28] Cationic polymerizations are technically relevant as some monomers (such as isobutylene and vinyl esters) can only be polymerized using this technique due to the chemistry of their substituents. The lag between the discovery of living anionic and living cationic polymerizations is of note. Just as in anionic polymerization, the probability of termination due to chain combination is very low due to carbocations trying to avoid interactions with other positive charges. The carbocations tend to prevent a true living polymerization as they have a propensity to be unstable, and it becomes more difficult to control side and termination reactions in cationic polymerizations versus anionic polymerizations.[1,2] However, these side reactions can be overcome by stabilizing carbocationic intermediates.[29] Additionally, cationic polymerizations tend to need co-initiators and total dissociation of the initiator can be problematic; therefore, instantaneous initiation of all the polymer chains can be difficult in practice. Many of the same techniques used to generate block copolymers using anionic techniques are directly applicable to cationic polymerizations as well. Reaction conditions are much more sensitive for cationic polymerizations relative to anionic and care must be taken when choosing reagents and temperatures for use. Of special interest for techniques such as sequential monomer addition is that the order of monomer

addition becomes even more crucial in the cationic case. Due to this complication, the only practical method to generate A-B-A polymers is through the use of difunctional cationic initiators.

The ionic classes of controlled (and living) polymerizations have dominated the block copolymer landscape, but controlled radical polymerizations are making significant headway in the coil-like polymer community as they offer comparable molecular weight size and distribution control while also being more robust to monomer chemistry and environmental conditions. The three most commonly used subgroups are atom transfer radical polymerization (ATRP),[30] nitroxide-mediated polymerization (NMP),[31] and reversible addition-fragmentation transfer (RAFT) polymerization.[32] Unlike their free radical polymerization counterparts, these polymerization schemes yield narrow polydispersity polymers by limiting the number of growing polymer chains (those with an active radical center) at one instant during the reaction; this significantly lowers the possibility of chain termination by bimolecular recombination.

In order to keep the number of active chain ends low, ATRP and NMP cap the ends of the polymer chains with groups that can reversibly terminate the chain-growth. In this way a particular polymer chain remains dormant for long periods of time while the leaving group is on the end of the polymer chain. Upon spontaneous dissociation of the leaving group, the polymer becomes active and is free to consume monomer units in a chain-growth reaction mechanism, which is analogous to free radical polymerizations. After a certain number of repeat unit additions (which can be controlled by the reaction conditions), the leaving group once again adds to the end of the polymer chain and makes the chain dormant. By slowly growing individual polymer chains and keeping the concentration of active radicals at a minimum, a narrow molecular weight distribution is achieved. In a RAFT polymerization the number of active polymer chains is also kept small, but instead of a reversible termination step, as the name implies, a reversible chain transfer step is used. In RAFT a dormant polymer chain is capped with a chain transfer agent and becomes active by reacting with an active chain to donate the chain transfer agent to the previously active chain. This “passing” of the chain transfer

agent from chain to chain, once again, creates a small number of active radical species in the reaction. Most A-B diblock copolymers synthesized by controlled radical techniques use the sequential monomer addition technique. An advantage of using controlled radical over ionic schemes is that the product formed after the polymerization of the A block is generally air stable and can be purified prior to the addition of the B monomer. A-B-A triblock copolymers are generally synthesized using a difunctional initiator to first polymerize the B block and then the A blocks in controlled radical schemes.

Ring-opening polymerization (ROP) is an important class of controlled polymerizations in this work as the coil blocks are synthesized from rod macroinitiators in this fashion (Chapter 4 and 5). In contrast to the aforementioned polymerizations, the chemical linkage of the monomer is the same as in the polymer for these reactions; in the case of the anionic polymerization of styrene, for instance, the carbon-carbon double bond is converted to a single bond during the polymerization. In ring-opening polymerizations, a particular bond in the cyclic structure is broken, which leads to an active growth center but does not change the type or order of bonds in the structure except at the beginning and end of the polymer chain. Thus, it is the release of ring strain the drives these polymerizations. Rising to the forefront of the ring-opening polymerization class is a special case termed ring-opening metathesis polymerization (ROMP). In the polymerization a strained cycloalkene is converted to a linear polymer containing unsaturated bonds along its backbone through an olefin metathesis route. ROMP polymerizations are mediated by transition metals that have historically been tungsten,[33] molybdenum,[34] or ruthenium-based.[35] The exact mechanism of this reaction is described elsewhere,[36] but if experimental conditions such as the coinitiators and transition metals are properly chosen, the polymerization can proceed in a controlled manner. In fact, large steps have been taken in adjusting the catalyst chemistry such that ROMP polymerizations can accommodate a wide variety of monomers, initiators, and reaction solvents. Like many of the other controlled polymerization schemes, sequential monomer addition is the most common method for generating A-B diblock copolymers.

The most common route to A-B-A triblock copolymers synthesized completely by ROMP is also sequential monomer addition as the concept of a difunctional initiator tends to break down in terms of the ROMP mechanism.

2.1.2 Synthesis of Polylactide

Attention is now devoted to a particular monomer for ring-opening polymerization, lactide. Polylactide (PLA) has been used in a number of well-ordered block copolymer systems. One advantage to polylactide is that it is a biodegradable polymer that can be synthesized from biorenewable resources.[37] Another benefit of incorporating polylactide into self-assembled block copolymers is that PLA can be selectively etched from a polymer matrix using a gentle alkaline bath to render a nanoporous template (Section 2.4). If reaction conditions are controlled, multiple synthetic routes exist for the controlled polymerization of PLA. One hurdle that must be overcome to generate well-defined PLA is the transesterfication side reactions that generally occur with polyesters.[38] The second challenge to minimizing the polydispersity is realizing that the polymerization is an equilibrium reaction; therefore, chemists usually quench the reaction prior to full conversion to prevent a broadening of the molecular weight distribution. Researchers have found methods to curtail these adverse effects and ring-opening polymerizations of lactide are generally considered to be well-controlled.[39]

The lactide monomer and PLA structures are shown in Figure 2.2. Note that two carbons in lactide are stereocenters and three possible stereoisomers are possible: D-lactide, L-lactide, and D,L-lactide. Polymers synthesized from D-lactide or L-lactide can be semicrystalline while polymers having D,L-lactide as the monomer are amorphous. The glass transition temperature of all forms of PLA is T_g ~55 °C and the melting temperatures of the semicrystalline forms is T_m ~170 °C.[40] Also of note is that the semicrystalline polylactides are much more resistant to degradation than their amorphous counterparts;[41] therefore, D,L-lactide is the monomer of choice when an application requires a selective etch of the polylactide domain. Note that confusion can sometimes exists because polylactide is also known as poly(lactic acid) as the step-

growth condensation (Section 2.2) of two lactic acid monomers yields the same polymer structure as the chain-growth polymerization of lactide. The chain-growth mechanism is preferred for applications where low polydispersity polymers are needed.

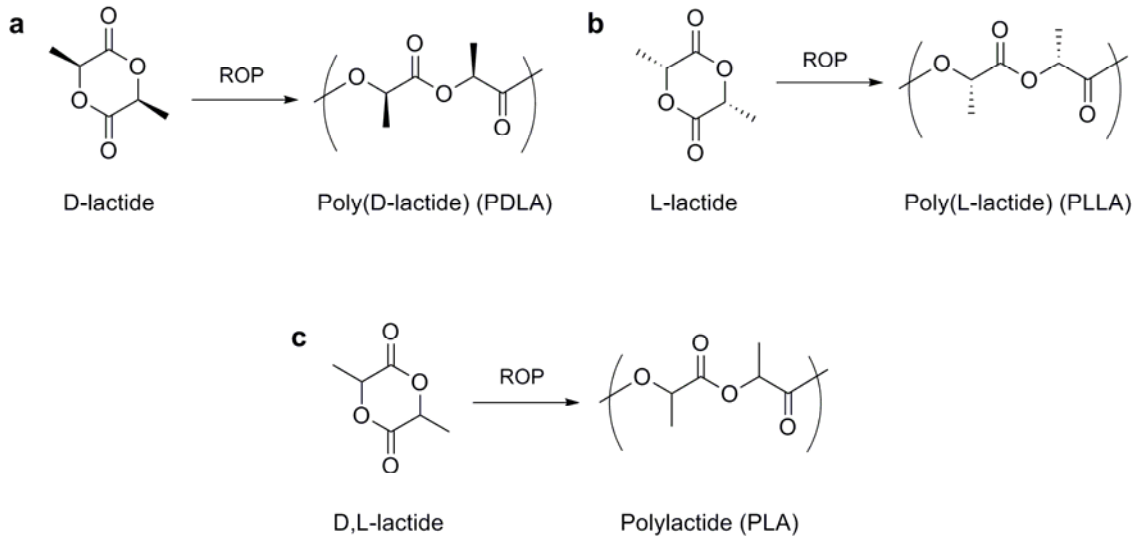

Figure 2.2. Synthesis of polylactide from (a) D-lactide, (b) L-lactide, and (c) D,L-lactide.

PLA can be synthesized using anionic routes.[42-44] In these situations an initiator consisting of a nucleophilic species and a balancing cation (usually a monovalent metal such as lithium or potassium) is introduced to the monomer solution. The lactide monomer is then ring-opened at an acyl-oxygen bond, and this oxygen, which now appears at the terminus of the chain, becomes the propagating center for the polymerization. As with other anionic techniques, this route is sensitive to reaction conditions, especially protic impurities. The more common strategy for polylactide synthesis, and the one used in this work, is through a metal-catalyzed coordination insertion polymerization (Figure 2.3). As shown, the oxygen of the carbonyl coordinates with the ligand (L_n) encased metal (M) and this leads to initiation and propagation of the polymer chain. In the homopolymer polymerization of PLA, OR generally represents an alcohol species. It should be noted that a growing field is emerging that will not be described, namely research related to metal-free PLA initiator systems.[45-4647]

These molecules are interesting as they tend to be air stable and they also avoid the need for the removal of heavy metals from the polymer, particularly important for biomedical applications.

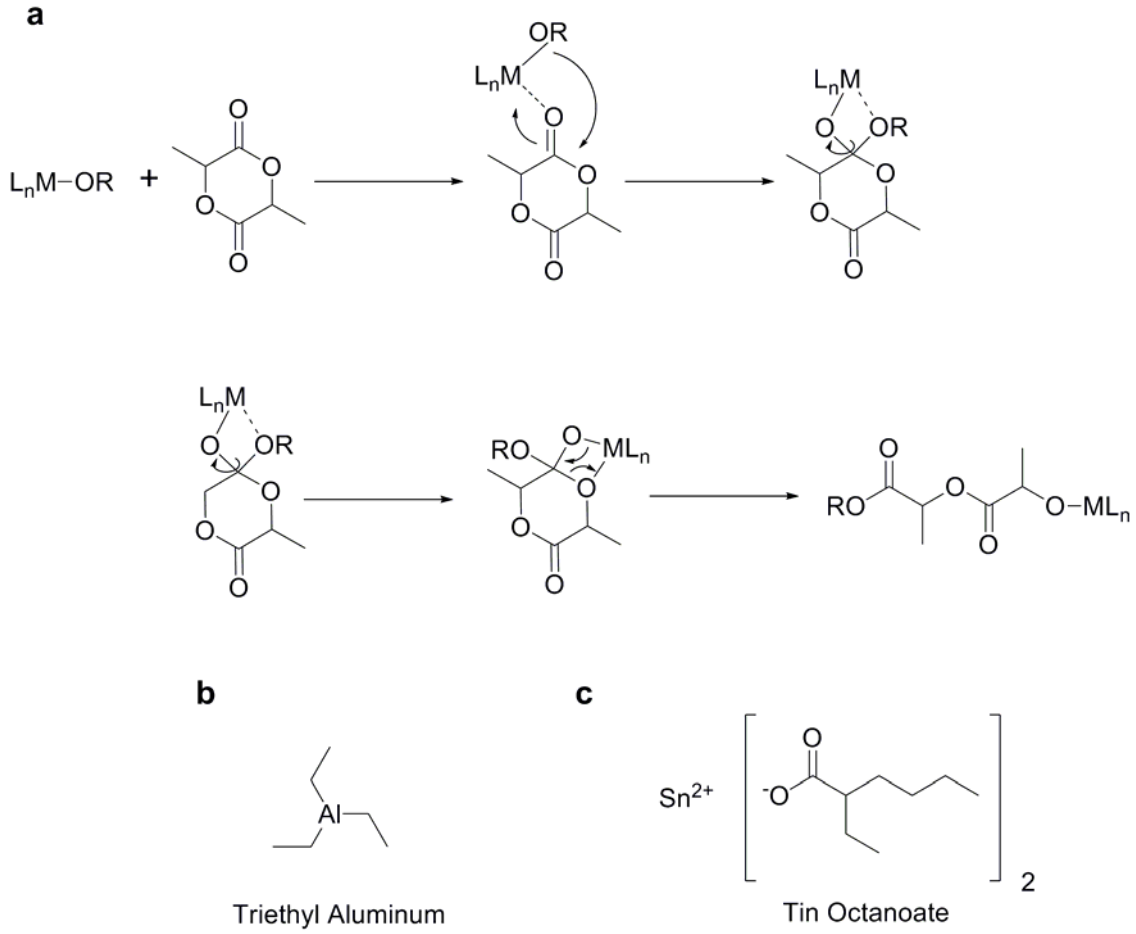

Figure 2.3. (a) Coordination insertion mechanism of the metal-catalyzed ring-opening polymerization of PLA. Here L_n is the ligand encasing the metal (M) and OR generally represents an alcohol species. The molecular structures of the metal complexes used for the polymerization of lactide in this work: (b) triethyl aluminum and (c) tin octanoate.

While a vast number of metal-ligand combinations have been studied (ranging from zinc to titanium complexes),[48-51] one of the most common metals used in complexes for the ROP of PLA is aluminum. One particular example is triethyl aluminum ($AlEt_3$); this species allows for the synthesis of polylactides with predictable molecular weights and narrow polydispersities.[52,53] When mixed with an alcohol the alkyl aluminum

compound will react to yield the corresponding aluminum alkoxide and alkane byproduct. The alkoxide then acts as the initiator for the polymerization. Another commonly used catalyst for the polymerization of PLA is tin octanoate ($SnOct_2$, 2.3c).[54-56] This material is less sensitive to water and oxygen than triethyl aluminum. Despite some disagreement as to the exact reaction mechanism of the $SnOct_2$-PLA polymerization, it is still able to generate high molecular weight, low PDI polymers. However care must be taken when using tin octanoate as it is active only at higher temperatures, which can promote side reactions such as transesterfication and, thus, broadens the polydispersity.[54-56]

Block copolymers that include a PLA moiety can be synthesized in a variety of manners. In many cases, a first block is polymerized and capped with an alcohol group which can act as an initiator upon the addition of a metal complex.[57,58] In other cases, PLA is initiated with a small molecule alcohol(R-OH)/metal complex. The resultant polymer has the structure R-PLA-OH. The hydroxyl end-cap can be converted to a functional group so that the PLA can be used for a macroinitiator of another polymerization.[59,60] Block copolymers containing PLA can also be synthesized in a grafting to approach; for instance, in the tailoring of miktoarm star copolymers containing a PMMA core and PLA arms.[61,62]

Clearly, there are a variety of techniques available to the polymer community that allow for large-scale, quick syntheses of low polydispersity and tunable molecular weight coil-like polymers; these materials can then be converted through the same techniques to diblock or triblock copolymers. Because the monomers of *most* rod-like polymers are not cyclic or vinyl in nature, the techniques discussed so far will be inapplicable to the synthesis of semiconductor polymers. Note that other controlled polymerization schemes exist and only the most commonly used synthetic strategies for completely coil-like, linear block copolymers have been discussed. Additionally, appropriate sequencing, end-capping, coupling, or macroinitiating of polymers can yield block copolymers through combinations of any of the above mentioned polymerization mechanisms. This wide variety of polymerization mechanisms that produce easily tuned

and well-defined coil block copolymers has allowed for many systematic studies of the experimentally observed morphologies in which these macromolecules microphase separate.

2.1.3 Phase Behavior

The phase behavior of coil-like block copolymers is an active area of research because controlling the molecular design of the block copolymers leads to many interesting and commercially relevant microstructures. The exact size of the domains can be tailored simply by controlling the molecular weight of the constituent blocks. This becomes quite easy to do in practice because of the various controlled polymerization techniques outlined above. To date, theory has helped to explain observed polymer phase behavior. Many caveats and special cases arise in the treatment of completely coil block copolymers, even though these systems are relatively easier to explain than rod-containing systems. While more in-depth reviews of coil block copolymer phase separation are plentiful,[4,13,63-66] the discussion will focus exclusively on the equilibrium microstructures of monodisperse, symmetric A-B and A-B-A linear block copolymers in the melt.

Miscibility of coil-like polymer blends was first described by Flory and Huggins and is directly related to regular solution theory.[67,68] It has be shown for a blend of polymers 1 and 2 that the Gibbs' free energy of mixing (ΔG^m) follows Equation 2.6.

$$\frac{\Delta G^m}{k_B T} = \frac{\phi_1}{N_1}\ln\phi_1 + \frac{\phi_2}{N_2}\ln\phi_2 + \phi_1\phi_2\chi_{12} \tag{2.6}$$

Here, k_B is the Boltzmann constant, T is the temperature, N_i is the degree of polymerization of polymer i, and ϕ_i is the volume fraction of polymer i. It is important to note that N_i does not necessarily represent the number of repeat units but instead accounts for the number of segments in a defined reference volume. Finally, χ_{12} represents the polymer-polymer (Flory-Huggins) interaction parameter and is a function of the chemical nature of the polymers in the system, inversely proportional to temperature. The first two terms on the right hand side of Equation 2.6 occur due to the entropy of mixing and are always negative, representing a favorable free energy change

upon mixing. The entropic terms are usually very small, however, because they are scaled by the inverse of degree of polymerization, which for polymers is usually very large. The final term on the right hand side of the equation accounts for the enthalpy of mixing, which for two chemically distinct polymers is usually (but not always[69]) greater than zero. Therefore, enthalpy overcomes entropy and phase separation is promoted in the majority of cases. Macrophase separation of polymer blends limits the usefulness of the polymers in applications. However, if the polymers are covalently tethered to one another (*i.e.*, block copolymers) interesting materials properties and microstructures can arise.

In an effort to minimize their free energy coil-coil A-B diblock copolymers in the melt organize into equilibrium structures and arrange the A and B segments on opposite sides of interfaces to create domains that are rich in A and B. Periodically ordered morphologies occur when the enthalpic terms that drive phase separation are balanced by the interfacial tension and entropic stretching terms. In a similar manner to Flory-Huggins theory, block copolymer phase diagrams are characterized by three parameters: the total number of repeat units ($N = N_A + N_B$), the segment-segment (Flory-Huggins) interaction parameter (χ_{AB}), and the volume fraction of the A block (f_A). Once again, the overall degree of polymerization is not exactly the number of repeat units of A and B, but rather the total number of segments of A and B in a certain reference volume. The theoretically predicated phase diagram for symmetric A-B block copolymers are shown in Figure 2.4a. Note that the vertical axis of the phase diagram is plotted as the product of χN. Above a critical χN value phase separated morphologies exist and below this value the system is disordered (Dis). Note that because χ is inversely proportional to temperature, a higher χ value promotes phase separation. As the volume fraction of the A block is changed the predicted morphology can also chain for a given value of χN. The real space equilibrium microstructures for the regions of the phase diagram are shown in Figure 2.4b for the case of a "red" A block and a "blue" B block.

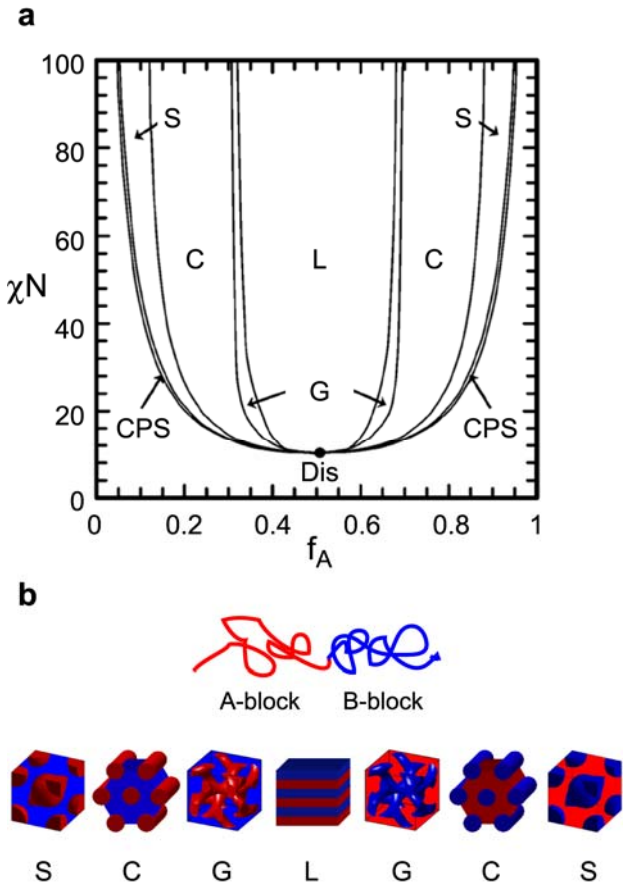

Figure 2.4. (a) Theoretical phase diagram for coil-coil A-B (red-blue) diblock copolymers. "Dis" indicates the disordered region. The ordered morphologies include: close-packed (face-centered cubic) spheres (CPS), body-centered cubic spheres (S), hexagonal packed cylinders (C), a bicontinuous gyriod network (G), and a lamellar phase (L). (b) Real space representations of the S, C, G, and L morphologies with the A block as both the minority (left) and majority (right) phase. Figure 2.4a is reproduced from Ref. 16.

The ordered microstructures (for low volume fractions of A) begin with ordered red spheres (S) of the minority polymer, A, on a body-centered cubic (BCC) lattice surrounded by a matrix of B. As f_A is increased towards the center of the diagram, the system undergoes order-to-order transitions (OOTs) and the minority phase forms hexagonally packed cylinders (C), then a bicontinuous gyriod network (G), and as f_A = 0.5 is approached, lamellae of A and B form. Because the phase diagram is symmetric, the observed microstructures are the same as the volume fraction of the A block is

increased, but now A is the majority phase and this polymer is the matrix for the hexagonally packed and body-center cubic geometries.

The theoretically predicted structures for A-B block copolymers have also been observed experimentally. In fact, phase diagrams for select systems have been generated experimentally.[17-19,70,71] While qualitatively similar to the theoretical phase diagrams a few strikingly different features should be noted. First, none of the known A-B block copolymer phase diagrams are symmetric about $f_A = 0.5$ as predicted by theory. This is due to the conformational asymmetry that exists in real block copolymer systems.[72] Secondly, the ordered bicontinuous double diamond and perforated lamellae morphologies not theoretically predicted were observed experimentally.[73-76] After much debate, it is now agreed upon that these structures are non-equilibrium morphologies but can have energies that compete with hexagonally packed cylinders and the gyroid and lamellar phases.[77] Thanks in large part to the early experimental and theoretical work outlined above, researchers are now able to easily tune the morphology of A-B block copolymers by manipulating the molecular weight, volume fraction, and chemical compatibility of the respective blocks.

The predicted morphologies of A-B-A triblock copolymers are the same as those discussed for A-B diblock copolymers; however, interesting shifts in the phase diagram occur.[78] The theoretically predicted phase diagram for a completely coil-like, symmetric A-B-A triblock copolymer is shown in Figure 2.5.

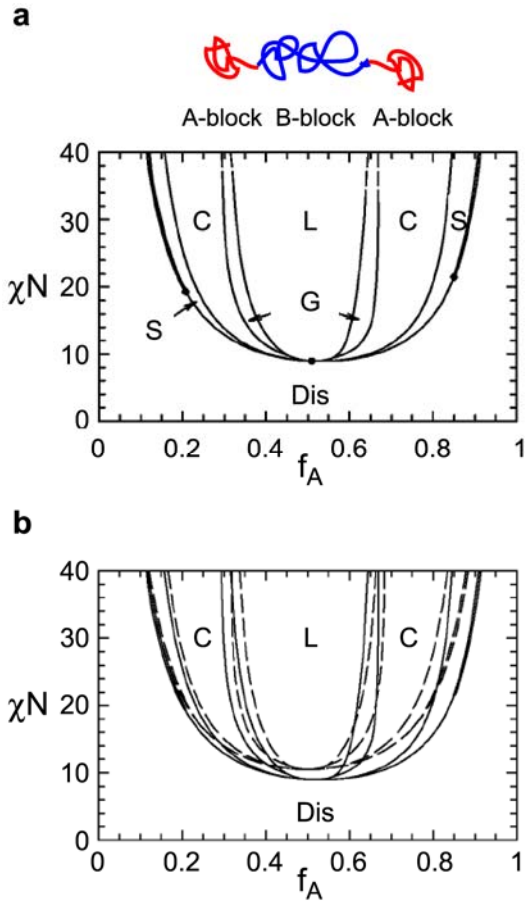

Figure 2.5. (a) Theoretical phase diagram for coil-coil A-B-A (red-blue-red) triblock copolymers. "Dis" indicates the disordered region. The ordered morphologies include: body-centered cubic spheres (S), hexagonal packed cylinders (C), a bicontinuous gyriod network (G), and a lamellar phase (L). (b) Overlay of A-B diblock copolymer (dashed) and symmetric A-B-A triblock copolymer (solid) theoretical phase diagrams showing a lowered order-disorder transition (ODT) χN value and wider order-order transition (OOT) windows in the interior microphase separated regions. Reproduced from Ref. 77.

Thinking of an A-B diblock as an A-B-A triblock copolymer that has been halved in the middle of the B block makes for more end segments in a melt of the A-B diblock. Because the triblock copolymer has fewer end segments, it has a higher degree of segregation, and, thus, will remain ordered for lower values of χN (higher ODT temperature). Theory also predicts that because the B block no longer has a free end, it is easier to stretch than in the A-B diblock case. This causes domain spacings in A-B-A

triblock copolymers to be larger than those for A-B diblock copolymers with the same overall degrees of polymerization of the A and B blocks. Stretching of the middle block also causes phase regions to be altered towards smaller A-block compositions.

The synthesis and phase behavior of a wide variety of coil-coil A-B diblock and A-B-A triblock copolymers have been studied in the literature. These polymers have helped researchers gain better understanding of how chemistry can affect the microstructure of these materials, and, in turn, their potential applications. New classes of functional polymers whose self-assembling characteristics are much less well-understood are starting to emerge. These macromolecules, in which one of the moieties is much more rigid than the other, are termed rod-coil block copolymers.

2.2 Rod-containing Block Copolymers

Rod-containing block copolymers are becoming of greater interest as cutting-edge research starts investigating nanoscopic properties. Many applications require a material that not only self-assembles on the nanoscale but also contains inherent electronic or biological functionality. Unlike the coil-coil systems outlined above, synthetic techniques for rod polymers are not always as well-developed and the phase behavior is not as easily discerned. Because established synthetic routes are not always available the molecular weights of the polymers can be very low and the polydispersity can be very high (PDI > 2). This only complicates systems where the phase behavior of block copolymers is difficult to understand. One of the largest obstacles to overcome when determining the phase behavior of rod-coil block copolymers is that Flory-Huggins theory, which described coil-coil systems so well, does not always hold. In most instances another parameter, which accounts for rod self-alignment, must be considered as it can dominate the observed microstructure. Both the synthesis and physics of rod-containing block copolymers are becoming better developed as chemists and engineers realize that theory from classical coil polymer systems does not always correspond well to rod-containing systems. A new class of materials is being developed that, while having many apparent limitations, also has many pathways for discovery and growth of applications.

2.2.1 Synthetic Techniques

In many instances the polymerizations used to synthesize rod-like polymers follow a step-growth mechanism. As the name suggests, the polymer chain grows one step at a time as a chemical reaction occurs between the polymer chain and a monomer in the reaction mixture. A generic mechanism for step-growth reaction steps is not as easily classified as with step-growth polymerizations (Equations 2.1 – 2.3). In many instances step-growth polymerizations occur through the condensation reaction of two functional groups (*e.g.* an alcohol and an acid). For instance, if a difunctional alcohol monomer (*AL*-*AL*) reacts with a difunctional organic acid (*AC*-*AC*) the beginning of a polymer chain will form by Equation 2.7.

$$AL - AL + AC - AC \rightarrow AL - al - ac - AC \tag{2.7}$$

In this sequence the *al* and *ac* monomers have reacted to become part of the polymer chain. The ends of the chain (*AL* and *AC*) are still able to react with other acid and alcohol monomers, respectively. Chain extension continues along this path until: 1) equilibrium is reached or 2) termination by either intentional or unintentional routes occurs. If reaction conditions are controlled, equilibrium reactions can be pushed to completion by the selective removal of the side-reaction products.

Unlike chain-growth polymerizations, step-growth polymerizations require high conversion to yield high molecular weight products. As the reactions are pushed to full conversion the polydispersity is increased, and it can be shown that the PDI increases for an increasing number of repeat units (N) according to Equation 2.8.[2]

$$\frac{M_w}{M_n} = PDI \approx 2 - \frac{1}{N} \tag{2.8}$$

Even in the idealized case (*i.e.* perfect stoichiometric balance, no solvent effects, no side reactions) as the polymer is pushed to higher molecular weights the polydispersity broadens and eventually reaches two. In the modest case of N = 10 the polydispersity index is already PDI = 1.9. This is much larger than the PDI values found by controlled chain-growth polymerizations.

As troublesome as the broad PDI initially appears, more recent work has shown that some rod polymers can be synthesized using reactions that are controlled; therefore, certain classes of rod polymers can be synthesized with tunable molecular weights, low polydispersities, and functionalized end groups.[79,80] The synthetic routes to rod-like polymers are not as commonly used nor are they as easily classified as those for coil-like polymers. Consequently, only poly(phenylene vinylene) (PPV) and polythiophene (PT) derivatives will be discussed as these materials have become the most commonly studied materials for organic electronics. The molecular structures of PPV and PT are shown in Figure 2.6. Substituted PPVs and PTs are required because unsubstituted PPV and PT are not soluble in common organic solvents. Generally alkyl chains are added to the conjugated ring in the repeat unit to aid in solubility. Additionally, the synthetic schemes that yield well-defined block copolymers have been developed for macromolecules that contain these materials. Because controlled reactions are used to synthesize PPVs and PTs the phase behavior of block copolymers containing these rod-like polymers has been better developed.

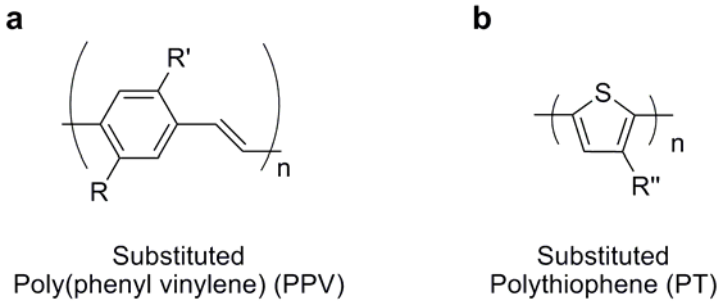

Figure 2.6. Molecular structures of (a) poly(phenylene vinylene) (PPV) and (b) polythiophene (PT). The R, R', and R'' groups represent substitutions to the repeat unit structures. These could be added for a variety of reasons and depend on the exact application.

Original efforts to synthesize poly(phenylene vinylene)s included the McMurray reaction,[81] Hofman elimination,[82] Wittig reaction,[83] and a paracylcophene route.[84] However, whenever high molecular weight species were made using these routes significant configurational problems (*i.e.* saturated carbon centers) occurred. In 1991

Kretzschmann and Meier used the Siegrist reaction to condense monomers containing both an azomethine and aromatic methyl functional groups.[85] This polymerization mechanism has proven to yield PPV derivatives with controllable molecular weights and low polydispersities. Additionally, the mechanism of the reaction dictates that one end group of the polymer chain is an aldehyde; this gives chemists a handle to grow a second block from a rod-like macroinitiator. Because of all the advantages that the Siegrist polymerization affords, it has become the predominate method for generating rod-coil block copolymers containing PPV derivatives.

Much of the early work in the synthesis of PPV-containing block copolymers focused on coupling an end-functionalized PPV block with a growing coil block.[86,87] This technique is effective in many respects as it creates a well-defined coil block. In fact, this method is still used today and has led to the synthesis of PPV-containing rod-coil block copolymers where the coil block has polyisoprene (PI)[88] or poly(methylmethacrylate) (PMMA).[89] A disadvantage to this route, however, is that the block copolymer must be separated from uncoupled homopolymer. A way to circumvent this potentially problematic purification step is to use the functionalized PPV block as a macroinitiator for the polymerization of the coil block. Because ionic polymerization techniques are sensitive to reaction conditions it can be easier to use controlled radical polymerizations in these macroinitiator situations. One of the earliest PPV-containing rod-coil block copolymers was synthesized by converting the end group of an aldehyde-terminated poly(phenylene vinylene) derivative (PPV-CHO) to an initiator suitable for a controlled nitroxide-mediated polymerization.[90,91] A statistical copolymer of polystyrene and poly(chloromethyl styrene) (PCMS) was then polymerized as the coil block. Subsequent reactions via either atom transfer[92] or an azide intermediate[93] were used to convert the chloromethyl substituent to a buckminsterfullerene (C_{60}) group to create an internal donor-acceptor (Chapter 3) block copolymer. More recently, PPV-PMMA was synthesized using ATRP for the growth of the coil block. In this case, the PPV-CHO was reduced to the corresponding alcohol which was then converted to a bromine-containing ATRP end group.[94]

Early reports of the polymerization routes for unsubstituted thiophene were metal-catalyzed condensation reactions.[95-96] Another commonly employed technique uses iron (III) chloride to oxidatively polymerize thiophene monomers. While these techniques are successful in polymerizing thiophene, polythiophene is not soluble in common organic solvents; as such, the majority of the synthetic techniques developed for PTs have focused on substituted polythiophenes. The most studied of the substituted polythiophenes are poly(3-alkythiophene)s (P3AT)s. Importantly, the optoelectronic properties of P3ATs are heavily dependent on the regiochemical couplings along the polymer chain. The three possible linkages between thiophene repeat units is shown in Figure 2.7. In order to achieve good crystal packing and electrical transport properties, the P3AT must be regioregular; this means that almost all of the linkages along the polymer chain are of the same type (usually head-to-tail).

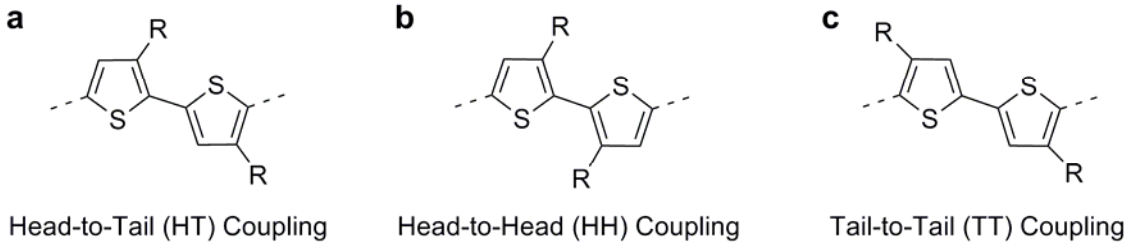

Figure 2.7. Regiochemical couplings of poly(3-alkylthiophene)s (P3ATs); specifically (a) head-to-tail (HT), (b) head-to-head (HH), and (c) tail-to-tail (TT).

The routes referenced for the synthesis of polythiophene are also applicable for P3ATs. However, these schemes lead to regioirregular (regiorandom) P3ATs. Additionally, these methods generally produced low molecular weight polymers with broad PDIs and offer no control over molecular weight. In order to overcome these limitations, much research went into developing pathways that would give completely regioregular P3ATs with narrow molecular weight distributions. In 1992, two new methods emerged: the McCullough method[97] and the Rieke method.[98] In the McCullough method 2-bromo-5-bromomagnesio-3-alkylthiophene monomers are cross-coupled together with 1,3-bis(diphenylphosphino)propane nickel (II) chloride [Ni(dppp)Cl_2]. The Rieke method

uses activated (Rieke) zinc to generate the substituted thiophene monomer; the monomer was then coupled with a nickel catalyst. Both of these reaction methods generated regioregular P3ATs with tunable molecular weights and low PDIs, but they required cryogenic temperatures and highly reactive metals making large-scale production of P3ATs challenging. In 1999 McCullough and coworkers retooled his method and discovered the Grignard metathesis (GRIM) method (Figure 2.8).[99] This is the most commonly employed method for synthesizing well-controlled, highly regioregular, and economical poly(3-alkylthiophenes) but other polymerization techniques, such as Stille[100] and Suzuki[101] couplings, are also used. The GRIM polymerization mechanism begins with an oxidative insertion of the nickel catalyst to the end of the polymer chain.[102,103] This is followed by a transmetalation step between the Grignard metal present on a free thiophene monomer and the nickel catalyst at the end of the polymer chain. A reductive elimination is the final step where the thiophene monomer is added to the end of the polymer chain and the nickel catalyst is removed from the chain.

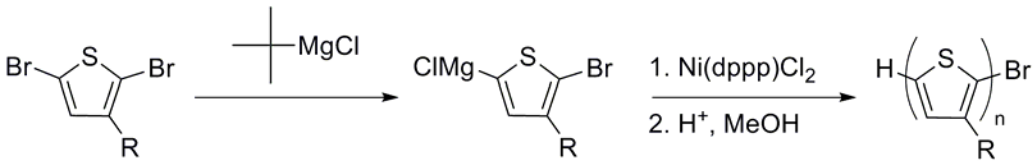

Figure 2.8. Common reaction conditions for the Grignard metathesis (GRIM) polymerization of poly(3-alkylthiohpene)s (P3AT)s. Note that Ni(dppp)Cl_2 is 1,3-bis(diphenylphosphino)propane nickel (II) chloride.

Another advantage of the GRIM method is that it allows for the *in situ* capping of P3AT chains with a functional end group that can easily be converted to a macroinitiating species.[104,105] It is this property of the polymerization scheme that has made P3ATs, specifically poly(3-hexylthiophene) (P3HT), some of the most widely studied rod blocks in rod-containing block copolymers.

The first P3AT-containing block copolymer was PS-P3HT.[106] The polystyrene block was polymerized anionically and capped with one 3-hexylthiophene repeat unit.

A solution of 3-hexylthiophene monomers and iron (III) chloride was then combined with the functionalized PS to oxidatively polymerize the P3HT block. A similar method was later used to synthesize poly(3-hexylthiophene)-poly(acrylate) diblock (P3HT-PA) and triblock copolymers (PA-P3HT-PA).[107] These synthetic routes are unique in that they are the only examples in the literature where a coil macroinitiator is used to polymerize the thiophene moiety. McCullough and coworkers used his original method to generate hydrogen/bromine-terminated P3HT (H-P3HT-Br) and subsequently coupled a functionalized thiophene repeat unit to the bromine end group. The end of the P3HT chain was then converted to an ATRP initiator for the polymerization of styrene and methylacrylate to generate poly(3-hexylthiophene)-*b*-polystyrene (P3HT-PS) and poly(3-hexylthiophene)-*b*-polymethylacrylate (P3HT-PMA) diblock copolymers.[108] The coupling of thiophene units through a nickel catalyst and a bromine end group has also been used to synthesize the internal donor-acceptor-donor triblock copolymer poly(3-hexylthiophene)-*b*-poly(cyano phenylene vinylene)-*b*-poly(3-hexylthiophene) (P3HT-CNPPV-P3HT).[109] Other works have shown that P3HT capped with groups containing carbon-carbon double bonds can be used to quench the anionic polymerization of styrene to generate P3HT-PS[110] diblock or PS-P3HT-PS triblock copolymers.[111]

Today, most research takes advantage of the GRIM method to end-functionalize the P3AT chain and uses this functionality to initiate the polymerization of the coil block. The first example of this was by the McCullough group in 2005 when they capped the end of P3HT product with a vinyl group at the end of the GRIM polymerization.[112] The vinyl group was then converted to an alcohol using a hydroboration/oxidation reaction. The alcohol was then converted to an ATRP group so that P3HT served as the macroinitiator for the controlled polymerization of polyacrylates; the exact synthetic conditions for this reaction were lately refined by Hawker's group.[113] McCullough et al. also showed that the P3HT end group could be converted to an NMP-type macroinitiator for the polymerization of polyisoprene (PI) to generate P3HT-PI,[114] and this technique was used later by anther group to make poly(3-hexylthiohpene)-*b*-poly(methylacrylate-*stat*-chloromethylstyrene) (P3HT-PMA-*stat*-

PCMS) where the PCMS block was later functionalized with fullerene to create an internal electron donor-acceptor polymer.[115] In the same paper,[114] McCullough showed that the end group could also be converted to a RAFT-type macroinitiator for polystyrene to polymerize P3HT-PS even though this had been previously shown.[116] An alcohol-terminated poly(3-alkylthiophene) was also used as the macroinitiator for the ring-opening polymerization of polylactide to generate P3AT-PLA diblock copolymers.[117] In 2007, researchers used a vinyl-terminated P3HT to initiate the anionic polymerization of poly(2-vinylpyridine) (P2VP) and through careful washing of the polymer were able to show low polydispersity, high molecular weight poly(3-hexylthiophene-*b*-poly(2-vinylpyridine) (P3HT-P2VP). Another group was able to use a difunctional P3HT with an unsaturated carbon-carbon bond on either end group to initiate the anionic polymerization of poly(methyl methacrylate) (PMMA) to synthesize PMMA-P3HT-PMMA triblock copolymers.[118] Click chemistry has even been used to synthesize P3HT-PS diblock and PS-P3HT-PS triblock copolymers.[119] The most recent use of a P3HT-macroinitiator was developed almost simultaneously by two competing groups wishing to create another internal electron donor-acceptor polymer. In both of these works, NMP was used to initiate the growth of perylene diimide derivatives from the ends of P3HT chains.[120,121]

Rod-containing block copolymers have attracted much attention over the past 10 years. Many different varieties of these macromolecules have been made using different synthetic techniques. The rod-like block synthetic techniques have become more developed and have led to polymers with controllable molecular weights and narrow polydispersities. Most of these techniques take advantage of the well-established controlled polymerization techniques to synthesize the coil block. Despite these advances by synthetic chemists, knowledge and models regarding the phase behavior of rod-coil block copolymers is still lagging behind completely coil-like systems.

2.2.2 Phase Behavior

The fundamental elements for the self-assembly of rod-containing block copolymers are different than for completely coil-containing block copolymers.[9,122] In a

rod-coil block copolymer the conformational entropies of the coil and rod blocks are not the same. Additionally, the space occupied by the two different types of moieties in the chain scales differently in the melt; coil blocks go as $N^{0.5}$ while the rod block goes as N. Also, the anisotropic rod blocks may desire to align in a liquid crystalline manner and this driving force may be much greater than the phase separation predicted by Flory-Huggins theory. Finally, and perhaps most problematic in seeing long-range order, many rod-like blocks can crystallize, resulting in phase behavior inherently limited by the kinetics of crystallization. This can be especially true in the organic electronics community as crystalline materials are desired in order to improve charge transport. Because of these complications, experiment has led theory in the field of rod-coil block copolymers.

The seminal work in the study of rod-coil block copolymer melt microstructures occurred in 1996 with the work of Chen et al.[123] In this work, poly(hexyl isocyanate)-*b*-polystyrene (PHIC-PS) block copolymers were anionically polymerized by subsequent monomer additions to yield high molecular weight, low polydispersity (PDI < 1.1) products. Transmission electron microscopy (TEM) images of the block copolymers revealed two new microstructures never before seen in coil-coil systems: the zigzag (Figure 2.9a) and arrowhead (Figure 2.9b) structures. Both of these structures have a lamellae-like morphology, the common motif in most phase separated rod-coil block copolymers.

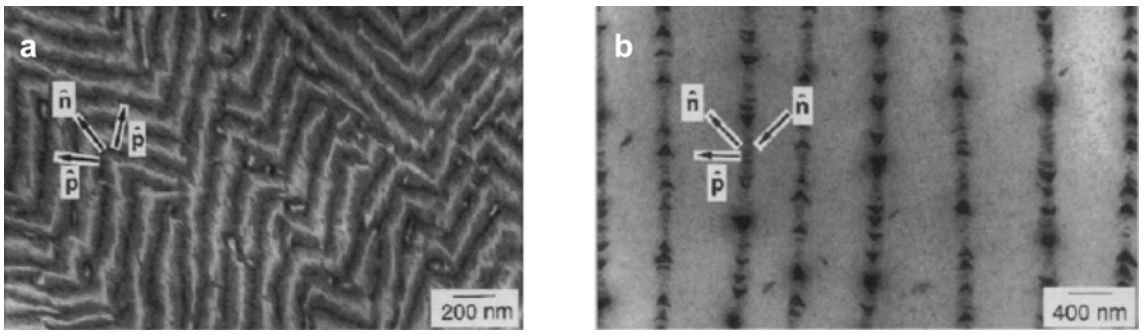

Figure 2.9. Transmission electron microscopy (TEM) images of poly(hexyl isocyanate)-*b*-polystyrene (PHIC-PS) showing (a) zigzag lamellar (f_{PS} = 0.27)and (b) arrowhead (f_{PS} = 0.04) microstructures. The polystyrene block is selectively stained black with ruthenium tetroxide. Reproduced from Ref. 120.

One of the earliest studied PPV-based rod-coil block copolymer systems was PPV-PS. In some instances the polystyrene block was unmodified and in others the PS was decorated with fullerene to generate an internal electron donor-acceptor macromolecule. In either case, lamellar structures were the most commonly observed morphology. However, if cast from carbon disulfide (CS_2), honeycomb structured films were observed, but the domain size for this system was on the order of micrometers.[92] This suggests some sort of solvent-driven phase separation instead of an equilibrium morphology. The most thorough systematic study of rod-coil block copolymers contained a PPV-based rod block (poly(2,5-diethylhexyloxy-1,4-phenylene vinylene)) and a polyisoprene (PI) coil block.[124-126] The large side group of the PPV block helped prevent self-alignment of the rods in the melt and, to a point, suppressed liquid crystalline behavior. In these systems, a lamellar ordered phase dominates before transitioning to a nematic liquid crystalline phase and then an isotropic phase at higher temperatures. At high coil volume fractions ($f_{coil} > 0.8$) and high molecular weights a small window exists on the phase diagram where hexagonal packed cylinders of the rod block are embedded in a coil matrix. While the observed morphologies for PPV-PI block copolymers have been limited to this point, manipulation of the rod-like polymer molecular structure could aid in accessing more microstructures for this synthetically robust and well-controlled system.

McCullough's group was the first to observe microphase separation in P3HT-based block copolymers using tapping mode atomic force microscopy (AFM).[108] They were able to see the formation of crystalline P3HT lamellae (sometimes termed nanofibrils) embedded in a matrix of amorphous PS. While many other P3HT-based A-B diblock and A-B-A triblock copolymer systems have been synthesized, the commonly detected morphology is what was originally found, a crystalline lamellae structure. An example AFM phase image of this nanofibril structure is shown in Figure 2.10b.

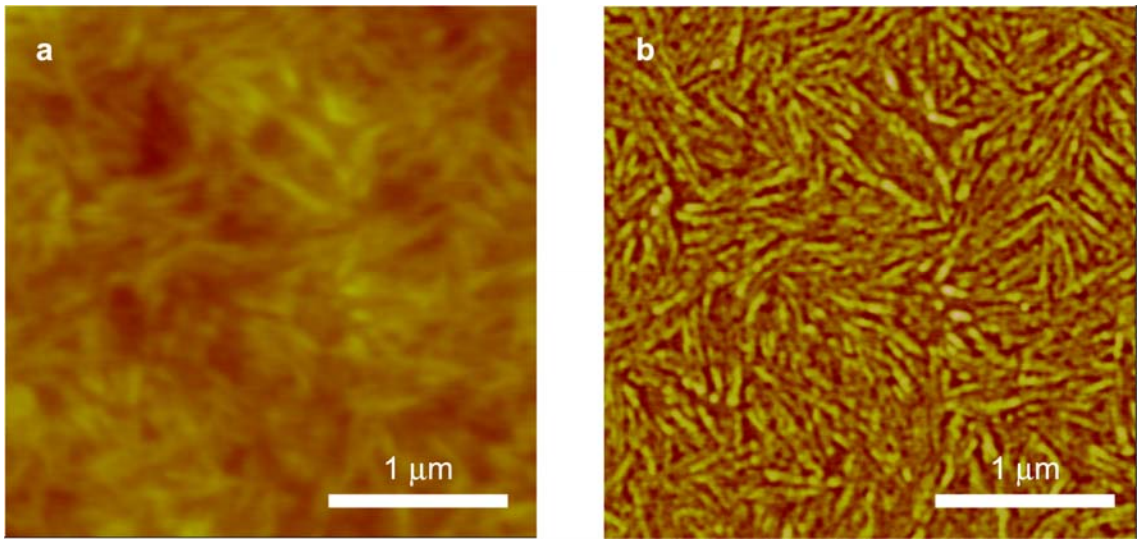

Figure 2.10. Atomic force microscopy (AFM) tapping mode (a) height and (b) phase images of a thin film of poly(3-hexylthiophene) (P3HT) spun-coat from a 2 mg of polymer in 1 mL of toluene solution at a rotation rate of 1000 rpm for 1 min. The height image shows a nearly flat film (RMS = 1.3 nm) while the phase image highlights the lamellae (nanofibrils) formed by the crystalline domains of P3HT. The height scale ranges from 0 – 30 nm. The phase scale ranges from 0 – 25°.

This phase separation is thought to occur because of the high melting temperature of P3HT (T_m ~220 °C). Any x-ray scattering or microscopy study performed at room temperature is far below the melting temperature of P3HT. This severe degree of undercooling almost necessitates the rapid crystallization of the thiophene moiety, which inhibits any possible microstructures from forming due to chemical dissimilarities. The one example contrary to this behavior was published in 2007.[127] Rod-coil block copolymers of poly(3-hexylthiophene)-*b*-poly(2-vinyl pyridine) (P3HT-

P2VP) showed microstructures similar to those of coil-coil systems for coil volume fraction up to $f_{coil} = 0.59$. Above this value, the commonly observed nanofibril structure was present (Figure 2.11). The authors cite the low molecular weight and the large chemical difference between the thiophene and vinyl pyridine blocks as the reasons for this remarkable phase separation in the P3HT-based block copolymers. However, the complicated solvent annealing protocol that the scientists used could have led to them observing non-equilibrium morphologies. The solvent used to anneal the block copolymers preferentially dissolves the P3HT block and could prevent the crystallization of P3HT while allowing the amorphous P2VP segments to vitrify into a glass where the microstructure is governed in a manner similar to a coil-coil system. When the remaining solvent vapor is removed, the P3HT is forced to crystallize in the confined domains. While this methodology leads to interesting microstructures, it is not as robust as systems where the observed morphologies are equilibrium-based.

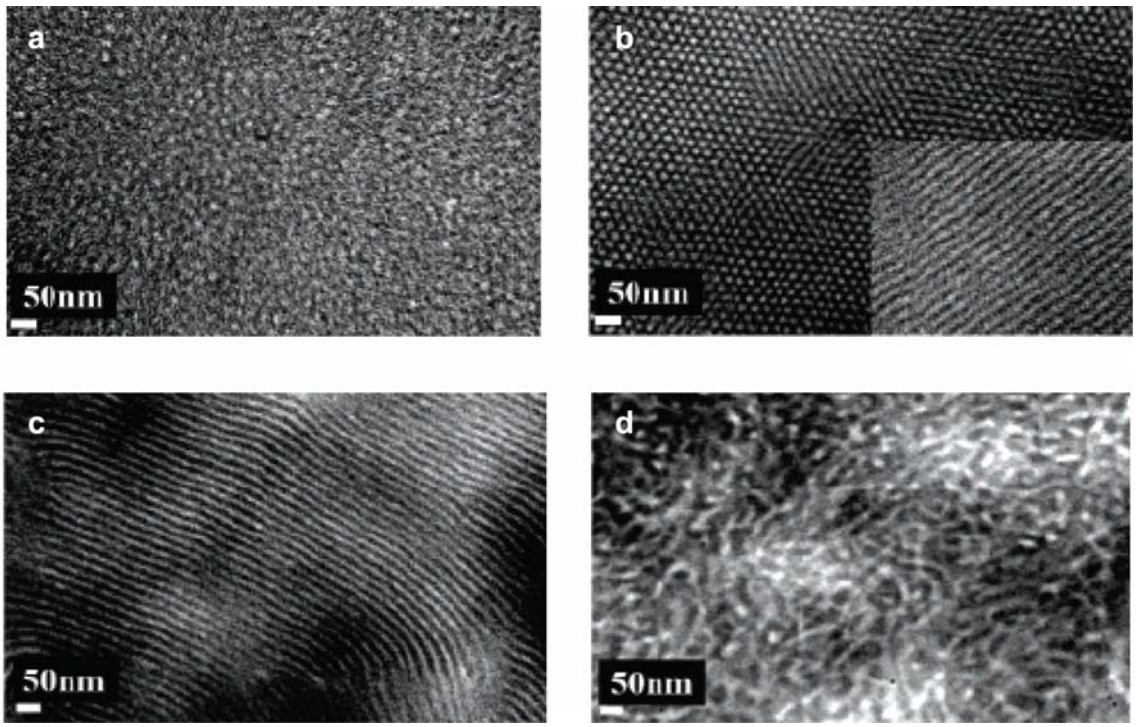

Figure 2.11. Transmission electron microscopy (TEM) images of poly(3-hexylthiophene)-*b*-poly(2-vinyl pyridine) (P3HT-P2VP) that contain (a) spherical (f_{P2VP} = 0.86), (b) cylindrical (f_{P2VP} = 0.75), (c) lamellar (f_{P2VP} = 0.59), and (d) nanofibril-like (f_{P2VP} = 0.30) morphologies. The inset of (b) shows the cross-sectional view of the P3HT cylinders. The P2VP block is selectively stained black with iodine. Reproduced from Ref. 125.

Many theoretical efforts have been employed to try to capture and understand the self-assembly behavior of rod-coil block copolymers. Early work focused on liquid crystalline transitions in rod-coil block copolymers: smectic (lamellar) to nematic,[128] smectic A to smectic A bilayers,[129] and smectic A to smectic C transitions.[130,131] In 1992 Holyst and Schick used both the Flory-Huggins (χ) and Maier-Saupe (μ) parameters to account for the segment-segment interactions and rod aligning interactions, respectively, in rod-coil block copolymers.[132] This work was expanded upon and it was shown that by varying the flexibility in the blocks of a diblock copolymer, the theoretical predications could be tuned from the coil-coil case shown by Liebler to the rod-coil case of Holyst and Schick.[133] The researchers also found that the ODT was

pushed to lower values of χN because the penalty for stretching the rod-like block was not as large as if it were a coil segment.

A powerful tool that led to the fundamental understanding of the predicted morphologies in coil-coil block copolymers is self-consistent field theory (SCFT). By combining this technique and the research of the works described above, rod-coil block copolymer phase behavior can be universally described by four parameters: the Flory-Huggins interaction (χN), the Maier-Saupe interaction (μN), the coil fraction (f_{coil}), and a parameter that accounts for the differences in lengths between the rod and coil blocks (v). Application of these four parameter using SCFT yielded theoretical results that showed the presence of smectic A, bilayers and arrowheads, smectic C, broken lamellas, and pucks.[130] If the Maier-Saupe parameter is neglected hexagonal microstructures can also be realized.[134] As a final note, coil-rod-coil A-B-A type triblock copolymers have also been studied using SCFT.[135] The computations predict that microstructures much more similar to those seen for completely coil systems will be present including: lamellar, gyriod, cylindrical, and spherical-like phases; however, full experiments studying the validity of these predictions have yet to be presented. This observation brings about a key point: despite the large amounts of effort in studying the theoretical and experimental aspects of rod-coil block copolymer self-assembly little work has been done to correlate the two fields. This is largely due to the lack of quantitative data on the experimental values for the computational parameters described above. Once again, the self-assembly of rod-coil block copolymers can be largely based on kinetic factors, making measurements of equilibrium values difficult. In spite of this, Olsen and Segalman have been able to show that their experimentally observed phase diagrams do match with theoretical predications.[126] These early results offer hope (and challenge) that, with the correct experimental systems, the theory of rod-coil block copolymers can become as well-understood as that of coil-coil systems.

2.3 Porous Templates from Block Copolymer Precursors

In order to generate a nanoporous structure using block copolymers, one of the moieties of the block copolymer must be able to be selectively etched and the other

block(s) must be able to support the remaining pattern.[136] Many different block copolymers have been used to generate nanoporous structures, and almost all of the studied nanoporous block copolymers are composed of completely coil block copolymers. In general, the most utilized morphologies are hexagonally packed cylinders and the gyroid phases where the etchable block is the minority phase. Using these microstructures generates materials that have continuous porous networks that are also able to remain intact upon complete removal of the etchable block. The utility of block copolymer precursors over other organic and inorganic materials for nanoporous templates has been well-documented[136,137] and applications range from catalysis[138] to gas and water separations.[139,140] This work will be limited to a discussion of three topics: 1) lithography, 2) nanoporous templates with polylactide as the etchable block, and 3) block copolymer templates for microelectronic applications.

The most widely studied application for block copolymer precursors is nanolithography and reviewing the most commonly used diblock copolymer used in this field will serve as a nice primer for other block copolymer templated systems. Polystyrene-*b*-poly(methyl methacrylate) (PS-PMMA) has been popularized for nanolithographic purposes by the Russell group.[141] PS-PMMA is synthetically convenient as it can be polymerized anionically by sequential monomer addition. When cast as a thin film, lamellar and cylindrical nanoscale domains can be aligned perpendicular to the substrate to generate long-range, ordered block copolymer films. Ordering can be tuned by an electric field,[142] controlling the casting conditions,[143] or by chemically modifying the substrates.[144] In order to create nanoporous films, PMMA acts as the sacrificial block and was originally removed by exposure to ultraviolet (UV) light followed by an acetic acid rinse.[145] Other scientists have shown that the PMMA block can also be etched by exposure to UV light while under vacuum, which reduces the need for a wet etch step.[146] Once PMMA has been degraded, many different systems have been patterned using the nanoporous PS template; the most common application being for the fabrication of nanodot arrays of metallic,[147-149] magnetic,[150] and semiconducting materials.[151-153]

Because parts of this work use polylactide (PLA) as the etchable moiety in block copolymers a brief review of other PLA-containing block copolymers used for porous templates follows. Polylactide-based block copolymers are particularly useful in generating nanoporous polymers because the PLA block can be etched by ester hydrolysis using a mild alkaline bath.[41] This is in contrast to the harsher chemical or UV-light conditions mentioned above that can lead to degradation or crosslinking, respectively, of the remaining matrix polymer. Because of this, many nanoporous materials have been generated by using a block copolymer where the etchable moiety was polylactide. The earliest systems to use PLA as the etchable block were monolithic polystyrenes from PS-PLA block copolymers with a cylindrical minority PLA phase in a PS matrix.[58] This block copolymer system was later spun-coat as thin films and used in the templating of magnetic nanoparticles.[154] PS-PLA was useful because cylinders with their long axis consistently perpendicular to the air-film interface form on a number of different substrates.[155] Eventually, additional blocks were added to PS-PLA to help in the ordering of thin film morphologies[156] or to give chemical functionality to the walls of the open cylinders running through the nanoporous polystyrene.[59,60] While polystyrene has been the workhorse matrix for nanoporous templates from PLA-containing block copolymers, poly(cyclohexylethylene)-*b*-polylactide (PCHE-PLA) block copolymers have also been used as nanoporous templates for some applications (see below) as PCHE has a higher thermal and chemical tolerance than PS,[157] and more mechanically robust blocks are currently being studied.[139]

Nanoporous block copolymers have also been used in the design of optoelectronic and semiconducting systems. An early work by the Russell group showed that nanoparticles of cadmium selenide (CdSe) could be sequestered in nanoporous PS where cylinders of PMMA had been removed.[158] Templates from PLA-etched block copolymers also have been used to synthesize nanoparticles of cadmium sulfide (CdS).[157,159] One of these reports also showed that conducting polypyrrole nanowires could be templated from a nanoporous poly(cyclohexylethylene) (PCHE) template (Figure 2.12a).[157] Lee et al. also generated polypyrrole nanowires from a PS-

PMMA block copolymer template.[160] In this instance the orientation of the polypyrrole wires was much more orientated (Figure 2.12b). A well-orientated device structure may be important for applications such as organic photovoltaics (OPVs).

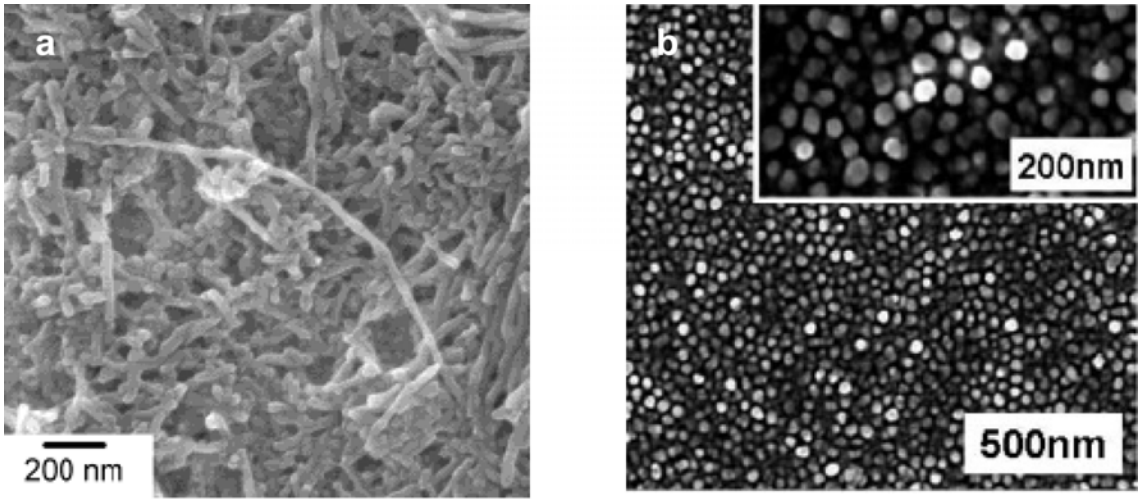

Figure 2.12. Scanning electron microscopy (SEM) images of (a) unordered (Reproduced from Ref. 128) and (b) ordered (Reproduced from Ref. 131) polypyrrole nanowires synthesized inside nanoporous block copolymer templates where the templates have been removed after nanowire growth. The polymer in (a) was synthesized by the oxidative polymerization of the monomer with iron (III) chloride while (b) was synthesized electrochemically with the substrate acting as the working electrode.

In addition to the synthesis of organic conducting nanowires, this technique has since been applied in the application of photovoltaic devices. Crossland et al. first demonstrated that high aspect ratio, ordered copper nanowires could be generated from a nanoporous template created by the removal of cylindrical PLA domains from a poly(fluorosytrene-*b*-polylactide) (PFS-PLA) film.[161] Using a similar strategy, they later used gyriod-shaped nanowires in the fabrication of reasonably efficient dye-sensitized solar cells (DSSCs)[162] and hybrid solar cells.[163]

Design of nanoporous templates from block copolymers is becoming a well-known option. The majority of the work in this field is focused on coil-coil block copolymers and their application in lithography. Templating by block copolymers is just

starting to emerge in the design of ordered photovoltaics, and most of this effort has been focused on templating a sacrificial coil-coil block copolymer matrix for the growth of an organic[160] or inorganic semiconductor.[162,] Only one example in the literature has shown a block copolymer composed of one semiconducting and one etchable block.[117] This molecular design gives inherent functionality to the matrix material that remains after selective etching and offers a future that includes an all-organic ordered bulk heterojunction solar cell. However, many synthetic and self-assembly hurdles must be overcome if long-range order is to be achieved in these complicated polymer systems.

2.4 References

[1] Odian, G. *Principles of Polymerization, 4th Ed.*; John Wiley & Sons, Inc: Hoboken, NJ, 2004.

[2] Hiemenz, P. C.; Lodge, T. P. *Polymer Chemistry*; CRC Press: Boca Raton, FL, 2007.

[3] Sperling, L. H. *Introduction to Polymer Science, 3rd Ed.*; John Wiley & Sons, Inc.: Hoboken, NJ, 2001.

[4] Bates, F. S.; Fredrickson, G. H. *Annu. Rev. Phys. Chem.* **1990**, *41*, 525–557.

[5] Leibler, L. *Macromolecules* **1980**, *13*, 1602–1617.

[6] de Genes, P. G. *Scaling Concepts in Polymer Physics*; Cornell University Press: Ithaca, NY, 1979.

[7] Doi, M.; Edwards, S. F. *The Theory of Polymer Dynamics*; Oxford University Press: New York, NY, 1986.

[8] Flory, P.J. *Principles of Polymer Chemistry*; Cornell University Press: Ithaca, NY, 1953.

[9] Olsen, B. D.; Segalman, R. A. *Mater. Sci. Eng., R* **2008**, *62*, 37–66.

[10] Scherf, U.; Gutacker, A.; Koenen, N. *Acc. Chem. Res.* **2008**, *41*, 1086–1097.

[11] Szwarc, M.; Levy, M.; Milkovich, R. *J. Am. Chem. Soc.* **1956**, *78*, 2656–2657.

[12] Schlick, S.; Levy, M. *J. Phys. Chem.* **1960**, *64*, 883–886.

[13] Hadjichristidis, N.; Pispas, S.; Floudas, G. A. *Block Copolymers: Synhtetic Strategies, Physical Properties, and Applications*; John Wiley & Sons, Inc.: Hoboken, NJ, 2003.

[14] Matsen, M. W. *J. Phys.–Condens. Mat.* **2002**, *14*, R21–R47.

[15] Matsen, M. W.; Bates, F. S. *Macromolecules* **1996**, *29*, 1091–1098.

[16] Cochran, E. W.; Garcia-Cervera, C. J.; Fredrickson, G. H. *Macromolecules* **2006**, *39*, 2449–2451.

[17] Bates, F. S.; Schulz, M. F.; Khandpur, A. K.; Förster, S.; Rosedale, J. H. *Faraday Discuss.* **1994**, *98*, 7–18.

[18] Zheng, W.; Wang, Z. G. *Macromolecules* **1995**, *28*, 7215–7223.

[19] Khandpur, A. K.; Förster, S.; Bates, F. S.; Hamley, I.; Ryan, A. J.; Almdal, K.; Mortensen, K. *Macromolecules* **1995**, *28*, 8796–8806.

[20] Lynd, N. A.; Hillmyer, M. A. *Macromolecules* **2005**, *38*, 8803–8810.

[21] Lynd, N. A.; Meuler, A. J.; Hillmyer, M. A. *Prog. Polym. Sci.* **2008**, *33*, 875–893.

[22] Hillmyer, M. A. *J. Polym. Sci. Pol. Phys.* **2007**, *45*, 3249–3251.

[23] Quirk, R. P.; Lee, B. *Polym. Int.* **1992**, *27*, 359–367.

[24] Darling, T. R.; Davis, T. P.; Fryd, M.; Gridnev, A. A.; Haddleton, D. M.; Ittel, S. D.; Matheson, Jr., R. R.; Moad, G.; Rizzardo, E. *J. Polym. Sci., Polym. Poly. Chem.* **2000**, *38*, 1706–1708.

[25] Szwarc, M. *Nature* **1956**, *178*, 1168–1169.

[26] Hsieh, H. L.; Quirk, R. P. *Anionic Polymerization, Principles and Practical Applications*; Marcel Dekker, Inc.: New York, NY, 1996.

[27] Miyamoto, M.; Sawamoto, M.; Higashimura, T. *Macromolecules* **1984**, *17*, 265–268.

[28] Miyamoto, M.; Sawamoto, M.; Higashimura, T. *Macromolecules* **1984**, *17*, 2228–2230.

[29] Higashimura, T.; Aoshima, S.; Sawamoto, M. *Makromol. Chem. Macromol. Symp.* **1998**, *14*, 457–471.

[30] Matyjaszewski, K. (Ed.) *Controlled/Living Polymerization: Progress in ATRP, NMP, and RAFT*; Oxford University Press: New York, NY, 2000.

[31] Matyjaszewski, K. *Chem. Rev.* **2001**, *101*, 2921–2990.

[32] Moad, G.; Rizzardo, E.; Thang, S. H. *Aust. J. Chem.* **2005**, *58*, 379–410.

[33] Kress, J.; Osborn, J. A. *J. Am. Chem. Soc.* **1983**, *105*, 6346–6347.

[34] Schrock, R. R.; DePue, R. T.; Feldman, J.; Schaverien, C. J.; Dewan, J. C.; Liu, A. H. *J. Am. Chem. Soc.* **1988**, *110*, 1423–1435.

[35] Nguyen, S. T.; Johnson, L. K.; Grubbs, R. H. *J. Am. Chem. Soc.* **1992**, *114*, 3974–3975.

[36] Piotti, M. E. *Curr. Opin. Solid State Mater. Sci.* **2000**, *4*, 539–547.

[37] Wanamaker, C. L.; O'Leary, L. E.; Lynd, N. A.; Hillmyer, M. A.; Tolman, W. B. *Biomacromolecules* **2007**, *8*, 3634–3640.

[38] Dubois, Ph.; Jacobs, C.; Jérôme, R.; Teyssié, Ph. *Macromolecules* **1991**, *24*, 2266–2270.

[39] Dove, A. P. *Chem. Commun.* **2008**, *48*, 6446–6470.

[40] Lou, X. D.; Detrembleur, C.; Jérôme, R. *Macromol. Rapid Commun.* **2003**, *24*, 161–172.

[41] Li, S. *J. Biomed. Mater. Res.* **1999**, *48*, 342–353.

[42] Kasperczyk, J. E. *Macromolecules* **1995**, *28*, 3937–3939.

[43] Hsueh, M. L.; Huang, B. H.; Wu, J. C.; Lin, C. C. *Macromolecules* **2005**, *38*, 9482–9487.

[44] Adamus, G.; Kowalczuk, M. *Biomacromolecules* **2008**, *9*, 696–703.

[45] Connor, E. F.; Nyce, G. W.; Myers, M.; Mock, A.; Hedrick, J. L. *J. Am. Chem. Soc.* **2002**, *124*, 914–915.

[46] du Boullay, O. T.; Marchal, E.; Martin-Vaca, B.; Cossio, F. P.; Bourissou, D. *J. Am. Chem. Soc.* **2006** *128*, 16442–16443.

[47] Bonduelle, C.; Martin-Vaca, B.; Cossio, F. P.; Bourissou, D. *Chem.–Eur. J.* **2008**, *14*, 5304–5312.

[48] Williams, C. K.; Breyfogle, L. E.; Choi, S. K.; Nam, W.; Young, V. G.; Hillmyer, M. A.; Tolman, W. B. *J. Am. Chem. Soc.* **2003**, *125*, 11350–11359.

[49] Chen, H. Y.; Tang, H. Y.; Lin, C. C. *Macromolecules* **2006**, *39*, 3745–3752.

[50] Lee, J.; Kim, Y.; Do, Y. *Inorg. Chem.* **2007**, *46*, 7701–7703.

[51] Chmura, A. J.; Cousins, D. M.; Davidson, M. G.; Jones, M. D.; Lunn, M. D.; Mahon, M. F. *Dalton Trans.* **2008**, 1437–1443.

[52] Kricheldorf, H. R.; Berl, M.; Scharnagle, N. *Macromolecules* **1988**, *21*, 286–293.

[53] Kowalski, A.; Duda, A.; Penczek, S. *Macromolecules* **1998**, *31*, 2114–2122.

[54] Kowalski, A.; Duda, A.; Penczek, S. *Macromol. Rapid Commun.* **1998**, *19*, 567–572.

[55] Kricheldorf, H. R.; Kreiser-Saunders, I.; Stricker, A. *Macromolecules* **2000**, *33*, 702–709.

[56] Ryner, M.; Stridsberg, K.; Albertsson, A. C.; von Schenck, H.; Svensson, M. *Macromolecules* **2001**, *34*, 3877–3881.

[57] Wang, Y.; Hillmyer, M. A. *Macromolecules* **2000**, *33*, 7395 – 7403.

[58] Zalusky, A. S.; Olayo-Valles, R.; Wolf, J. H.; Hillmyer, M. A. *J. Am. Chem. Soc.* **2002**, *124*, 12761–12773.

[59] Rzayev, J.; Hillmyer, M. A. *Macromolecules* **2005**, *38*, 3–5.

[60] Rzayev, J.; Hillmyer, M. A. *J. Am. Chem. Soc.* **2005**, *127*, 13373–13379.

[61] Smith, A. P.; Fraser, C. L. *Macromolecules* **2002**, *35*, 594–596.

[62] Bender, J. L.; Corbin, P. S.; Fraser, C. L.; Metcalf, D. H.; Richardson, F. S.; Thomas, E. L.; Urbas, A. M. *J. Am. Chem. Soc.* **2002**, *124*, 8526–8527.

[63] Lohse, D. J.; Hadijichristidis, N. *Curr. Opin. Colloid In.* **1997**, *2*, 171–176.

[64] Abetz, V.; Simon, P. F. W. *Adv. Polym. Sci.* **2005**, *189*, 125–212.

[65] Castelletto, V.; Hamley, I. W. *Curr. Opin. Solid State Mater Sci.* **2005**, *8*, 426–438.

[66] Kim, J. K.; Lee, J. I.; Lee, D. H. *Macromol. Res.* **2008**, *16*, 267–292.

[67] Flory, P. J. *J. Chem. Phys.* **1942**, *10*, 51–61.

[68] Huggins, M. L. *J. Am. Chem. Soc.***1942**, *64*, 1712–1719.

[69] Kuo, S.; Huang, W.; Huang, C.; Chan, S.; Chang, F. *Macromolecules* **2004**, *37*, 4164–4173.

[70] Schulz, M. F.; Khanpur, A. K; Bates, F. S.; Almdal, K.; Mortensen, K.; Hajduk, D. A.; Gruner, S. M. *Macromolecules* **1996**, *29*, 2857–2867.

[71] Floudas, G.; Vazaiou, B.; Schipper, F.; Ulrich, R.; Wiesner, U.; Iatrou, H.; Hadjichristidis, N. *Macromolecules* **2001**, *34*, 2947–2957.

[72] Matsen, M. W; Bates, F. S. *J. Polym. Sci. Pol. Phys.* **1997**, *35*, 945–952.

[73] Thomas, E. L.; Alward, D. B.; Kinning, D. J.; Martin, D. C.; Handlin, D. L., Jr.; Fetters, L. J. *Macromolecules* **1986**, *19*, 2197–2202.

[74] Herman, D. S.; Kinning, D. J.; Thomas, E. L.; Fetters, L. J. *Macromolecules* **1987**, *20*, 2940–2942.

[75] Hasegawa, H.; Tanaka, H.; Yamasaki, K.; Hashiomto, T. *Macromolecules* **1987**, *20*, 1651–1662.

[76] Hajduk, D. A.; Takenouchi, H.; Hillmyer, M. A.; Bates, F. S.; Vigild, M. E.; Almdal, K. *Macromolecules* **1997**, *30*, 3788–3795.

[77] Matsen, M. W.; Schick, M. *Phys. Rev. Lett.* **1994**, *72*, 2660–2663.

[78] Matsen, M. W.; Thompson, R. B. *J. Chem. Phys.* **1999**, *111*, 7139–7146.

[79] McCullough, R. D. *Adv. Mater.* **1998**, *10*, 93–116.

[80] Osaka, I.; McCullough, R. D. *Acc. Chem. Res.* **2008**, *41*, 1202–1214.

[81] Rehahn, M.; Schlüter, A. D. *Makromol. Chem., Rapid Commun.* **1985**, *11*, 375–379.

[82] Askari, S. H.; Rughooputh, S. D.; Wudl, F.; Heeger, A. J. *Polymer Preprints* **1989**, *30*, 157–160.

[83] Kossmehl, G.; Samandari, M. *Makromol. Chem.* **1985**, *186*, 1565–1574.

[84] Miao, Y.; Bazan, G. C. *J. Am. Chem. Soc.* **1994**, *116*, 9379–9380.

[85] Kretzschmann, H.; Meier, H. *Tetrahedron Lett.* **1991**, *32*, 5059–5062.

[86] Tew, G. N.; Pralle, M. U.; Stupp, S. I. *J. Am. Chem. Soc.* **1999**, *121*, 9852–9866.

[87] Li, W.; Wang, H.; Yu, L. *Macromolecules* **1999**, *32*, 3034–3044.

[88] Olsen, B. D.; Segalman, R. A. *Macromolecules* **2006**, *39*, 7078–7083.

[89] Ho, C. C.; Lee, Y. H.; Dai, C. A.; Segalman, R. A.; Su, W. F. *Macromolecules* **2009**, *42*, 4208–4219.

[90] Stalmach, U.; de Boer, B.; Videlot, C.; van Hutten, P. F.; Hadziioannou, G. *J. Am. Chem. Soc.* **2000**, *122*, 5464–5472.

[91] Stalmach, U.; de Boer, B.; Post, A. D.; van Hutten, P. F.; Hadziioannou, G. *Angew. Chem., Int. Ed.* **2001,** *40*, 428–430.

[92] de Boer, B.; Stalmach, U.; van Hutten, P. F.; Melzer, C.; Krasnikov, V. V.; Hadziioannou, G. *Polymer* **2001**, *42*, 9097–9109.

[93] van der Veen, M. H.; de Boer, B.; Stalmach, U.; van de Wetering, K. I.; Hadziioannou, G. *Macromolecules* **2004**, *37*, 3673–3684.

[94] Qu, G.; Jiang, F.; Zhang, S.; Usuda, S. *Mater. Lett.* **2007**, *61*, 3421–3424.

[95] Yamamoto, T.; Sanechika, K.; Yamamoto, A. *J. Polym. Sci., Polym. Lett. Ed.* **1980**, *18*, 9–12.

[96] Lin, J. W. P.; Dudek, L. P. *J. Polym. Sci., Poly. Chem.* **1980**, *18*, 2869–2873.

[97] McCullough, R. D.; Lowe, R. D. *J. Chem. Soc., Chem. Commun.* **1992**, *1*, 70–72.

[98] Chen, T. A.; Wu, X.; Rieke, R. D. *J. Am. Chem. Soc.* **1992**, *114*, 10087–10088.

[99] Loewe, R. S.; Khersonsky, S. M.; McCullough, R. D. *Adv. Mater.* **1999**, *11*, 250–253.

[100] Stille, J. K. *Angew. Chem., Int. Ed. Engl.* **1986**, *25*, 508 –524.

[101] Suzuki, A. *J. Organomet. Chem.* **1999**, *576*, 147–168.

[102] Yokoyama, A.; Miyakoshi, R.; Yokozawa, T. *Macromolecules* **2004**, *37*, 1169–1171.

[103] Sheina, E. E.; Liu, J.; Iovu, M. C.; Laird, D. W.; McCullough, R. D. *Macromolecules* **2004**, *37*, 3526–3528.

[104] Jeffries-EL, M.; Sauvé, G.; McCullough, R. D. *Adv. Mater.* **2004**, *16*, 1017–1019.

[105] Jeffries-EL, M.; Sauvé, G.; McCullough, R. D. *Macromolecules* **2005**, *38*, 10346–10352.

[106] François, B.; Widawski, G.; Rawiso, M.; Cesar, B. *Synth. Met.* **1995**, *69*, 463–466.

[107] de Cuendias, A.; Le Hellaye, M.; Lecommandoux, S.; Cloutet, E.; Cramail, H. *J. Mater. Chem.* **2005**, *15*, 3264–3267.

[108] Liu, J.; Sheina, E.; Kowalewski, T.; McCullough, R. D. *Angew. Chem., Int. Ed.* **2002**, *41*, 329–332.

[109] Tu, G.; Li, H.; Forster, M.; Heiderhoff, R.; Balk, L. J.; Scherf, U. *Macromolecules* **2006**, *39*, 4327–4331.

[110] Iovu, M. C.; Jeffries-EL, M.; Zhang, R.; Kowalewski, T.; McCullough, R. D. *J. Polym. Sci. Part A*, **2006**, *43*, 1991–2000.

[111] Higashihara, T.; Ohshimizu, K.; Hirao, A.; Ueda, M. *Macromolecules* **2008**, *41*, 9505–9507.

[112] Iovu, M. C.; Jeffries-EL, M.; Sheina, E. E.; Cooper, J. R.; McCullough, R. D. *Polymer*, **2005**, *46*, 8582–8586.

[113] Lee, Y.; Fukukawa, K.; Bang, J.; Hawker, C. J.; Kim, J. K. *J. Polym. Sci. Part A*, **2008**, *46*, 8200–8205.

[114] Iovu, M. C.; Craley, R.; Jeffries-EL, M.; Krankowski, A. B.; Zhang, R.; Kowalewski, T.; McCullough, R. D. *Macromolecules* **2007**, *40*, 4733–4735.

[115] Richard, F.; Brochon, C.; Leclerc, N.; Eckhardt, D.; Heiser, T.; Hadziioannou, G. *Macromol. Rapid Commun.* **2008**, *29*, 885–891.

[116] Boudouris, B. W.; Kasi, R. M.; Frisbie, C. D.; Hillmyer, M. A. *PMSE Preprints* **2006**, *95*, 103.

[117] Boudouris, B. W.; Frisbie, C. D.; Hillmyer, M. A. *Macromolecules* **2008**, *41*, 67–75.

[118] Higashihara, T.; Ueda, M. *React. Funct. Polym.* **2009**, *69*, 457–462.

[119] Urien, M.; Erothu, H.; Cloutet, E.; Hiorns, R. C.; Vignau, L.; Cramail, H. *Macromolecules* **2008**, *41*, 7033–7040.

[120] Sommer, M.; Lang, A. S.; Thelakkat, M. *Angew. Chem., Int. Ed.* **2008**, *47*, 7901–7904.

[121] Zhang, Q.; Cirpan, A.; Russell, T. P.; Emrick, T. *Macromolecules* **2009**, *42*, 1079–1082.

[122] Olsen, B. D.; University of California – Berkeley: Doctoral Thesis, 2007.

[123] Chen, J. T.; Thomas, E. L.; Ober, C. K.; Mao, G. P. *Science* **1996**, *273* 343–346.

[124] Olsen, B. D.; Segalman, R. A. *Macromolecules* **2005**, *38*, 10127–10137.

[125] Olsen, B. D.; Segalman, R. A. *Macromolecules* **2007**, *40*, 6922–6929.

[126] Olsen, B. D.; Shah, M.; Ganesan, V.; Segalman, R. A. *Macromolecules* **2008**, *41*, 6809–6817.

[127] Dai, C.; Yen, W.; Lee, Y.; Ho, C.; Su, W. *J. Am. Chem. Soc.* **2007**, *129*, 11036–11038.

[128] Semenov, A. N.; Vasilenko, S. V. *Zh. Eksp. Teor. Fiz.* **1986**, *90*, 124–140.

[129] Semenov, A. N. *Mol. Cryst. Liq. Cryst.* **1991**, *209*, 191–199.

[130] Pryamitsyn, V.; Ganesan, V. *J. Chem. Phys.* **2004**, *120*, 5824–5838.

[131] Matsen, M. W.; Barrett, C. *J. Chem. Phys.* **1998**, *109*, 4108–4118.

[132] Holyst, R.; Schick, M. *J. Chem. Phys.* **1992**, *96*, 730–739.

[133] Singh, C.; Goulian, M.; Liu, A. J.; Frederickson, G. H. *Macromolecules* **1994**, *27*, 2974–2986.

[134] Muller, M.; Schick, M. *Macromolecules* **1996**, *29*, 8900–8903.

[135] Chen, J. Z.; Zhang, C. X.; Sun, Z. Y.; Zheng, Y. S.; An, L. J. *J. Chem. Phys.* **2006**, *124*, 104907.

[136] Hillmyer, M. A. *Adv. Polym. Sci.* **2005**, *190*, 137–181.

[137] Olson, D. A.; Chen, L.; Hillmyer, M. A. *Chem. Mater.* **2008**, *20*, 869–890.

[138] Boger, T; Heibel, A. K.; Sorensen, C. M. *Ind. Eng. Chem. Res.* **2004**, *43*, 4602–4611.

[139] Phillip, W. A.; Rzayev, J.; Hillmyer, M. A.; Cussler, E. L. *J. Membrane Sci.* **2006**, *286*, 144–152.

[140] Phillip, W. A.; Martono, E.; Chen, L.; Hillmyer, M. A.; Cussler, E. L. *J. Membrane Sci.* **2009**, *337*, 39–46.

[141] Thurn-Albrecht, T.; Steiner, R.; DeRouchey, J.; Stafford, C. M.; Huang, E.; Bai, M.; Tuominen, M.; Hawker, C. J.; Russell, T. P. *Adv. Mater.* **2000**, *12*, 787–791.

[142] Morkved, T. L.; Lu, M.; Urbas, A. M.; Ehrichs, E. E.; Jaeger, H. M.; Mansky, P.; Russell, T. P. *Science* **1996**, *273*, 931–933.

[143] Peng, J.; Kim, D. H.; Knoll, W.; Xuan, Y.; Li, B.; Han, Y. *J. Chem. Phys.* **2006**, *125*, 64702.

[144] Stoykovich, M. P.; Müller, M.; Kim, S. O.; Solak, H. H.; Edwards, E. W.; de Pablo, J. J.; Nealey, P. F. *Science* **2005**, *308*, 236–239.

[145] Joo, W.; Yang, S. Y.; Kim, J. K.; Jinnai, H. *Langmuir* **2008**, *24*, 12612–12617.

[146] Asakura, S.; Hozumi, A.; Fuwa, A. *J. Vac. Sci. Technol., A* **2005**, *23*, 1137–1140.

[147] Thurn-Albrecht, T.; Schotter, J.; Kästle, G. A.; Emley, N.; Shibauchi, T.; Krusin-Elbaum, L.; Guarini, K.; Black, C. T.; Tuominen, M. T.; Russell, T. P. *Science* **2000**, *290*, 2126–2129.

[148] Park, M.; Chaikin, P. M.; Register, R. A.; Adamson, D. H. *Appl. Phys. Lett.* **2001**, *79*, 257–259.

[149] Guarini, K. W.; Black, C. T.; Milkove, K. R.; Sandstrom, R. L. *J. Vac. Sci. Technol. B* **2001**, *19*, 2784–2788.

[150] Asakawa, K.; Hiraoka, T.; Hieda, H.; Sakurai, M.; Kamata, Y.; Naito, K. *J. Photopolym. Sci. Tech.* **2002**, *15*, 465–470.

[151] Park, M.; Harrison, C.; Chaikin, P. M.; Register, R. A.; Adamson, D. H. *Science* **1997**, *276*, 1401–1404.

[152] Harrison, C.; Park, M.; Chaikin, P. M.; Register, R. A.; Adamson, D. H. *J. Vac. Sci. Technol. B* **1998**, *16*, 544–552.

[153] Black, C. T.; Guarini, K. W.; Milkove, K. R.; Baker, S. M.; Russell, T. P.; Tuominen, M. T. *Appl. Phys. Lett.* **2001**, *79*, 409–411.

[154] Olayo-Valles, R.; Lund, M. S.; Leighton, C.; Hillmyer, M. A. *J. Mater. Chem.* **2004**, *14*, 2729–2731.

[155] Olayo-Valles, R.; Guo, S.; Lund, M. S.; Leighton, C.; Hillmyer, M. A. *Macromolecules* **2005**, *38*, 10101–10108.

[156] Guo, S.; Rzayev, J.; Bailey, T. S.; Zalusky, A. S.; Olayo-Valles, R.; Hillmyer, M. A. *Chem. Mater.* **2006**, *18*, 1719–1721.

[157] Johnson, B. J. S.; Wolf, J. H.; Zalusky, A. S.; Hillmyer, M. A. *Chem. Mater.* **2004**, *16*, 2909–2917.

[158] Misner, M. J.; Skaff, H.; Emrick, T.; Russell, T. P. *Adv. Mater.* **2003**, *15*, 811–814.

[159] Lo, K. H.; Tseng, W. H.; Ho, R. M. *Macromolecules* **2007**, *40*, 2621–2624.

[160] Lee, J. I.; Cho, S. H.; Park, S. M.; Kim, J. K.; Kim, J. K.; Yu, J. W.; Kim, Y. C.; Russell, T. P. *Nano Lett.* **2008**, *8*, 2315–2320.

[161] Crossland, E. J. W.; Ludwigs, S.; Hillmyer, M. A.; Steiner, U. *Soft Matter* **2007**, *3*, 94–98.

[162] Crossland, E. J. W.; Nedelcu, M.; Ducati, C.; Ludwigs, S.; Hillmyer, M. A.; Steiner, U.; Snaith, H. J. *Nano Lett.* **2008**, *ACS ASAP*.

[163] Crossland, E. J. W.; Kamperman, M.; Nedelcu, M.; Ducati, C.; Wiesner, U.; Smilgies, D. M.; Toombes, G. E. S.; Hillmyer, M. A.; Ludwigs, S.; Steiner, U.; Snaith, H. J. *Nano Lett.* **2008**, *ACS ASAP*.

3 Organic Semiconductors and Photovoltaics

Current is the net flow of charge through a material in a defined direction over a given time. Here, charge carriers are thought to be either free electrons or holes. While electrons are more familiar, holes are also used to describe the motion of charge. A hole may be considered as a vacancy previously occupied by an electron. Therefore, a hole is oppositely charged relative to an electron and moves in the opposite direction of an electron under an applied electric field.[1] In order for charge to flow in matter, there must be some mechanism for charge carriers to freely move throughout the substance. The conduction mechanism varies depending on the material category where the three most common categories being metals, semiconductors, and insulators. Metals are a common class of materials that readily conduct current. The "electron sea" model is typically used to describe the flow of current in metals. In this representation the valence electrons associated with the nuclei of the metal atoms are highly delocalized due to the nature of the metallic bonds. Because of this delocalization the electrons can easily move in the sea upon application of an electric field.[2] Semiconductors, on the other hand, have electrons that are more tightly bound to the nucleus of their associated atom. Charge transport for inorganic semiconductors is generally described by band theory.[1,3,4] A basic concept of this theory is that the regular covalent bonding creates a crystal structure in inorganic materials and this allows for bands where charge can be transported. The valence electrons that are bound to the nuclei of the semiconducting atoms create the valence band. If an electron is provided enough energy to overcome its attraction to the nuclei, it is promoted to the conduction band (a hole is created in the valence band) where the electron can move freely in the semiconductor. The difference in energy between the valence and conduction bands is known as the band gap energy (E_g). Semiconductors have small band gap energies ($E_g < 4$ eV) so that a useful amount of electrons can be promoted from the valence band to the conduction band.[1-4] Inorganic insulators have the same type of band structure as semiconductors except that the band gap energy of an insulator is much larger than that of a semiconductor. As such, few to

no electrons are promoted to the conduction band and no current flows in these materials.

Most organic small molecules and polymers are insulating and have extremely large band gaps. Individual molecules are made by covalent bonds in an organic solid. Intermolecular interactions, however, are generally much weaker (usually van der Waals interactions) in organic solids than in inorganic solids and prevent the formation of band-like transport.[5] Organic semiconductors, on the other hand, share a trait in their bonding patterns: conjugation.[6] In these molecules carbon-carbon bonds alternate between single and double bonds such that there are only three atoms covalently bound to each carbon nucleus (*i.e.* sp^2-hybridization). It is this hybridization that allows valence p-orbital electrons to become delocalized and contribute to the current. The relatively small group of organic molecules that fall into the category of organic semiconductors are becoming of more interest today as applications arise where thin, flexible, and inexpensive devices trump high efficiency devices.[7,8] As may be expected, designing molecules that have this type of bonding pattern is not always trivial. Reviewing the structure of both small and macro molecular systems will aid in understanding subsequent device performance.

3.1 Molecular Structures of Organic Semiconductors

The use of small molecules and polymers in organic photovoltaic devices is prevalent in the literature as each class of organic semiconductor has its own advantages and limitations. Small molecules have discrete molecular weights and are generally deposited by thermal evaporation allowing for facile control of film thickness.[9] Combining well-characterized molecules and a well-controlled deposition technique leads to the growth of ordered films with a relatively high degree of crystallinity. In fact, some organic semiconductors can be grown as macroscopic single crystals.[10,11] On the industrial scale, thermal deposition is not always desired because it is thought to be more costly than solution processing as there are well-developed techniques already present for the roll-to-roll printing of inks and dyes for other applications. However, thermal evaporation can be used in an assembly line fashion. Even the most carefully

prepared polymer semiconductors have molecular weight distributions (Chapter 2) and the large number of covalent bonds prevents thermal deposition techniques as the molecule will decompose prior to evaporation. The large molecular weights and polydispersities of polymer semiconductors generally lead to films with less crystallinity than their small molecule counterparts. However, the fact that polymers can be deposited from solution is advantageous for reasons already mentioned. It should be noted that the previous discussion has oversimplified the two classes of materials as there are counterexamples of the implied limitations of each class. For example, much research has gone into producing solution processible small molecules[12-14] and semiconducting polymers with high thin film crystallinity.[15,16] However, the review of small molecule and polymeric semiconductors will be limited to the most prevalent materials used in the literature; these classic molecules follow the general trends that small molecule semiconductors are not soluble in common organic solvents and polymer semiconductors are not highly crystalline.

3.1.1 Small Molecule Semiconductors

As described above, organic semiconductors are generally referred to as electron donors (Figure 3.1) or electron acceptors (Figure 3.2). There are many more electron donors, or p-type materials, than electron acceptors (due to the instability of organic carbanions to water and oxygen[17,18]) so they will be addressed first. One of the most common classes of small molecule, hole-conducting semiconductors is metal phthalocyanines (MePc). The generic structure of these materials are shown in Figure 3.1a where the value of Me can be many different metals including, but not limited to, copper (Cu), zinc (Zn), platinum (Pt), and palladium (Pd). CuPc was used in the first efficient OPV[19] and is still commonly used today in small molecule cells due to its high absorption coefficient and hole mobility. In order to move the HOMO level of the electron donor farther away from vacuum, boron subphthalocyanine (SubPc) can be substituted for CuPc, and this improves the open-circuit voltage of devices (Chapter 3.2).[20] Oligoacenes are also used in organic photovoltaics (OPVs), with the prototypical material of this class being pentacene. This molecule is composed of five fused benzene

rings and serves as a benchmark for high charge transport in thin film organic field-effect transistors. The use of pentacene in OPVs has been somewhat limited due to its absorption spectrum, but relatively high efficiency pentacene-based devices have been fabricated.[21] Oligothiophenes with a host of different chemical functionalities[22] have also been used as the electron donors in OPVs as these materials generally have high charge carrier mobilities, high absorption coefficients, and form good thin films. Some of the most efficient oligothiophene-based devices contain *α,α-bis*(2,2-dicyanovinyl)-terminated oligothiophenes (DCVxT) with three (x = 3) to five (x = 5) thiophene rings present in the structure.[23,24] It should be noted that many other oligothiophene-based donors do exist but will not be discussed here.[25]

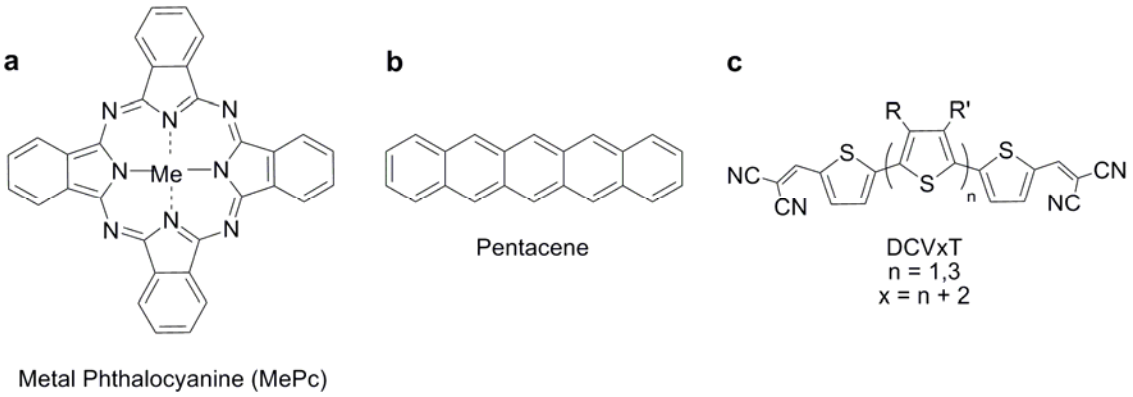

Figure 3.1. Small molecule, hole-conducting semiconductors commonly used in organic photovoltaics. (a) Metal phthalocyanines where typical elements for Me include Cu, Zn, Pt, and Pd. High-performing examples of (b) an oligoacene (pentacene) and (c) an oligothiophene (DCVxT). Here x represents the total number of thiophene units in the molecule.

As a final side note, the materials described in this section are some of the preeminent small molecule, hole-conducting materials used in OPVs; however, all of these molecules tend to have short exciton diffusion lengths and, as such, are inherently limited in bilayer OPVs (Chapter 3.2, 3.3). Current research is looking towards finding p-type semiconductors (or combinations of semiconductors) that have high exciton diffusion lengths to enhance device performance.[26]

The most widely used electron acceptors in organic photovoltaics are fullerene derivatives. Buckminsterfullerene (C_{60}) is commonly used if the electron acceptor is to be thermally evaporated;[27] however, recent results have shown that C_{70} may be a better electron acceptor due to its thin film absorption spectrum.[28] A more soluble derivative of C_{60} that gives the highest performance in OPVs is [6,6]-phenyl-C_{61}-butyric acid methyl ester[29] (PCBM), but other functionalized C_{60} have been studied.[30] The electron acceptor used in the original Tang cell[19] was 3,4,9,10-perylene tetracarboxylic *bis*-benzimidazole (PTCBI). Since that time, many other perylene derivatives have been used in organic electronic devices,[31,32] but despite better light absorption in the visible region, fullerene derivatives are usually favored over perylene derivatives due to the much longer exciton diffusion length in fullerene-containing moieties.

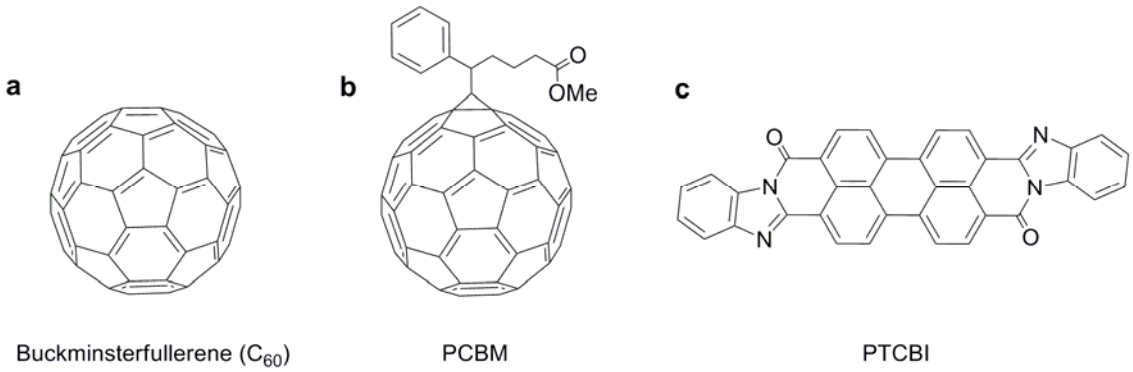

Figure 3.2. Small molecule, electron-conducting semiconductors commonly used in organic photovoltaics. (a) Buckminsterfullerene (C_{60}) and a soluble derivative (b) PCBM. (c) The perylene derivative used in the first efficient OPV, PTCBI.

Most of the small molecules described are not soluble in common organic solvents. With some exceptions, such as PCBM and a number of pentacene derivatives,[12,33] most solution processible organic semiconductors are macromolecules.

3.1.2 Polymeric Semiconductors

In general, polymeric semiconductors do not form films that are as crystalline as their small molecule counterparts. However, organic photovoltaics composed of either a blend of two polymers or a polymer and a small molecule (generally PCBM) have

comparable device efficiencies to small molecule solar cells. Polymer semiconductors are interesting because their properties can be affected not just by their chemical designs but also by their molecular weights.[34-36] Additionally, interesting film microstructures can be realized by blending two polymers or a polymer and a small molecule, and this is one of the main reasons why these lower crystallinity materials can compete with small molecule organic solar cells.

The most common electron donating polymers are based on polyfluorene (PF), poly(phenylene vinylene) (PPV) and polythiophene (PT) (Figure 3.3). The most commonly used polyfluorenes are poly(9,9-dicotylfluorene-2,7-diyl-*co*-*bis*-N,NN'-(4-butylpheneyl-*bis*-N,N'-phenyl-1,4-phenylenediamine)) (PFB) and poly(9,9-dioctylfluorene-2,7-diyl-*co*-benzothiadiazole) (F8BT).[37] It should be noted that F8BT is ambipolar (capable of transporting holes or electrons) and has been used as both an electron donor and an electron acceptor.[38] Poly(2-methoxy-5-(2'-ethyl-hexyloxy)-1,4-phenylene vinylene) (MEH-PPV)[39,40] and poly(2-methoxy-5-(3',7'-dimethyloctyloxy)-1,4-phenylene vinylene) (MDMO-PPV)[41,42] are the most common PPV derivatives used in devices. While many poly(3-alkylthiophene)s (P3ATs) have been used in organic photovoltaics, poly(3-hexylthiophene) (P3HT) has dominated the polymer solar cell literature since 2003.[43] These polymers have relatively low band gaps and form nice interpenetrating networks when cast from a solvent where electron accepting molecules have been codissolved.

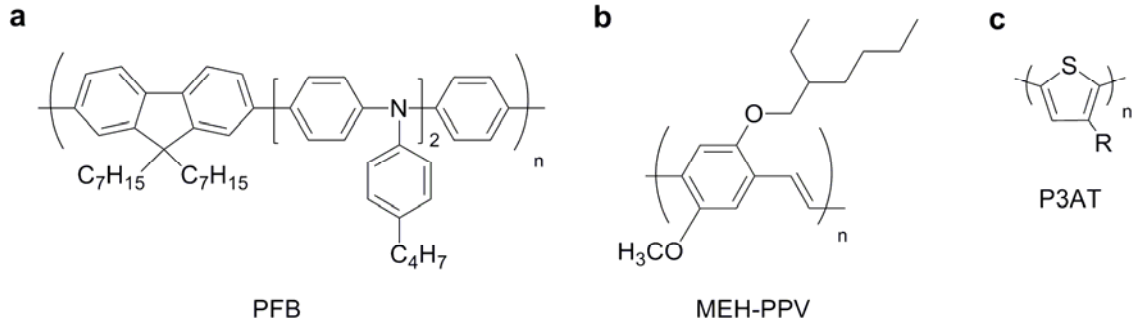

Figure 3.3. Macromolecular, hole-conducting semiconductors commonly used in organic photovoltaics. These include derivatives of (a) polyfluorene (PFB), (b) poly(phenylene vinylene) (MEH-PPV), and polythiophene (P3AT).

Other molecules have been synthesized to improve device efficiency. In some cases, the band gap of the polymers were lowered,[44-54] but these macromolecules generally have poor charge transport or have poor film morphologies, which leads to lower device efficiency than PF, PPV, or PT-based devices. Polymers with a higher degree of thin film crystallinity (to increase hole transport) have also been developed,[15,16] but implementation of these materials in OPVs has led to relatively low efficiency devices.[55,56]

Reports of electron-conducting polymers are rare,[18] and their uses in organic photovoltaics are even more uncommon; however, a few of the most readily used electron-conductors are shown in Figure 3.4. As previously mentioned F8BT is ambipolar and can be used as an electron acceptor.[38] Cyano group-modified PPV (CN-PPV) and MEH-PPV (CN-MEH-PPV) have also been used in organic electronic devices.[57,58] Recently, a copolymer of thiophene, cyano group-modified phenylene vinylene, and fluorene, poly{9,9-dioctylfluorene-2,7-diyl-*alt*-1,4-*bis*[2-(5-thienyl)-1-cyanovinyl]-2-methoxy-5-(3,7-dimethyl-octyloxy) benzene} (PF1CVTP), has also been used an electron-accepting material.[59]

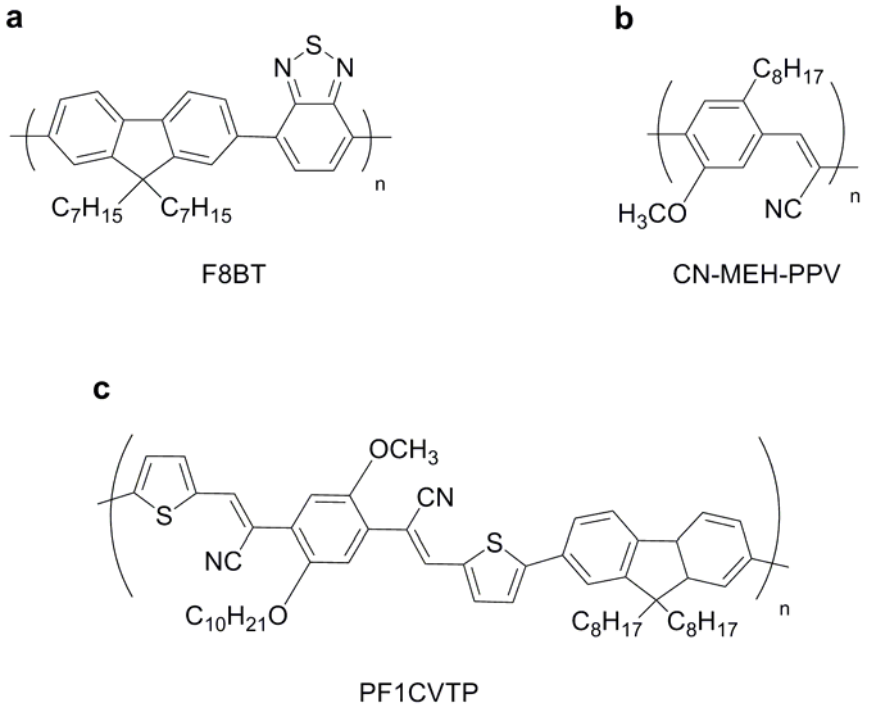

Figure 3.4. Macromolecular, electron-conducting semiconductors commonly used in organic photovoltaics. These include derivatives of (a) polyfluorene (F8BT); (b) poly(phenylene vinylene) (CN-MEH-PPV); and polyfluorene, poly(phenylene vinylene), and polythiophene (PF1CVTP). Note that F8BT is ambipolar and, thus, can act as an electron donor or as an electron acceptor.

One strategy to generate more macromolecular n-type materials is to functionalize an easily polymerized monomer with a functional group that is analogous to one of the small molecule electron-accepting materials described previously. It has been this technique that has led to polymers decorated with perylene[60-63] and fullerene[64,65] functionalities.

Before addressing how electron-donating and accepting materials are used in devices, a final class of materials that is quickly coming to the forefront of both small molecule and polymer organic photovoltaics needs to be addressed: internal electron donor-acceptors.[66,67] These materials are a combination of a p-type material that is covalently bound to an n-type material with a non-conjugated linker separating the two semiconducting segments. By having the two materials required for efficient OPVs present in one molecule, scientists are guaranteed that the electron donor and acceptor

phases are in intimate contact. High interfacial area between the electron donor and acceptor helps boost the efficiency of OPVs (Chapter 3.3). Most donor-acceptor materials synthesized to date have been small molecules based on oligo(phenylene vinylene)s and oligothiophenes (p-type) and fullerenes (n-type).[64,68-78] More recently, PPV and P3HT-containing block copolymers have been synthesized where the second block is an n-type semiconductor. In many cases, the n-type block is generated by functionalizing a common monomer unit (*e.g.,* styrene or methylmethacrylate) with a fullerene[64,65] or perylene derivative;[79,80] however, at least one case exists where only the end groups of the P3HT chain were converted to electron-accepting species.[81]

3.2 Photovoltaic Device Operating Principles

Photovoltaics offer the security of an environmentally friendly energy source that also decreases the United States' reliance on foreign fossil fuel sources that can prove to be unstable.[7] In fact, many applications currently exist for inorganic solar cells both in outer space and terrestrially.[82,83] Organic photovoltaics are a promising extension (or replacement) to inorganic systems for a number of economical and application-based reasons. As shown above, the optoelectronic properties of the semiconductors can be easily tuned in the chemistry laboratory by manipulating the chemical structure. This is not the case for the properties of traditional semiconductors, which are controlled by the inherent band structure of the materials. Additionally, organic semiconductors have a much higher absorption coefficient meaning that much more light is absorbed per unit of active layer; therefore, the same amount of light can be absorbed in a much thinner, lighter organic solar cell. This not only makes device fabrication cheaper because less material is used but also allows for the fabrication of flexible devices deposited on plastic substrates. Devices that are lightweight and flexible could prove to have a large share of niche markets (see Figure 3.5) where device portability and toughness outweigh the need for high efficiency (*i.e.*, tents, laptop bags, patio umbrellas). Because so many organic semiconductors can be deposited from solution, the possibility for well-developed printing techniques (*e.g.*, roll-to-roll coating) exists. This high-throughput strategy would significantly reduce the

cost of producing solar cells and allow for the quick fabrication of large-scale modules.[84,]

Figure 3.5. Example of a commericial organic photovoltaic module produced by Konarka Technologies that is printed on a flexible substrate. This module is being used to recharge a cellular telephone. Reproduced from Ref. 84.

Despite all of the possible advantages that organic photovoltaics offer, the power conversion efficiency of the best devices is still only ~5-6%.[85-87] In order to be commercially relevant, efficiencies of at least 10% are required.[88] Because the field of organic photovoltaics is relatively young compared to their inorganic counterparts, many fundamental questions still remain. These questions need to be answered in order to reach the device efficiencies desired by industry.

The critical player in the usage of photovoltaics is the sun and, more specifically, the radiative energy it produces from fusion reactions. The intensity of sunlight that reaches the outer surface of the Earth's atmosphere is referred to as air mass zero (AM0) and is equal to 1353 W/m^2.[89] After passing through the Earth's atmosphere the intensity of light is decreased due to absorption of light by components such as water vapor and ozone and scattering of light by dust particles. The amount of solar radiation that reaches a terrestrial observer depends on the person's exact location

on the Earth (as one moves closer to the equator there is a higher incidence of solar radiation). The commonly used standard for obtaining power conversion efficiencies of photovoltaics is air mass 1.5 (AM1.5) because it is fairly representative of the sunlight available in most of the contiguous United States and continental Europe. Specifically, it represents the average sunlight incident on a south-facing position at 37° N over the course of a year.[90] The solar spectrum at AM0 and AM1.5 are shown in Figure 3.6. It shows that most of the spectral irradiance is at wavelengths of less than 2000 nm. Also note that there is a large amount of sunlight present at wavelengths 750 nm < λ < 2000 nm that cannot be absorbed by many of the prototypical semiconductors described above due to their relatively wide band gaps. Therefore, an active area of current research is finding low band gap organic semiconductors (E_g < 1.5 eV) so that more of the incident radiation can be harvested.[44]

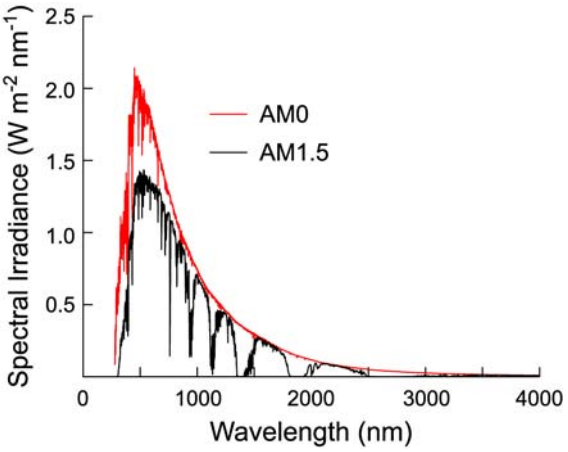

Figure 3.6. Solar spectra for AM0 and AM1.5 air mass conditions. Note that AM0 is the solar spectrum outside of the Earth's atmosphere and AM 1.5 is a similar to the solar irradiance on the planet's surface in the continental United States. Data acquired from Ref. 90.

It is interesting that the AM0 spectrum can be reasonably modeled by the blackbody radiation equation for an object at 5800 K.[4] Note that the dips in the terrestrial spectrum (AM1.5) that are not present in the AM0 spectrum are due to the aforementioned absorption and scattering of light by atmospheric components. The AM1.5 spectrum can be reproduced through the use of lamps and filters in the laboratory and many solar

simulators are commercially available. However, proper calibration of solar simulators can prove difficult, which can make comparisons of devices between different research groups complicated.[91] In the United States official certification of devices is performed at the National Renewable Energy Lab (NREL) in Golden, CO. Comparing device data between the certified solar simulator and a specific laboratory's simulator helps researchers to verify that their apparatus is properly calibrated.

3.2.1 Device Physics of an Inorganic Solar Cell: the p-n Junction

Band theory is generally used to describe the allowed electronic states in an inorganic semiconductor (see above). A p-n junction (the active layer of the photovoltaic device) made of a single semiconductor (with a single band gap), such as silicon, contains two distinct regimes: one that is doped with electron acceptors (p-type) and one doped with electron donors (n-type). When the p-type and n-type materials are brought into contact, there is diffusion and recombination of holes near the interface from the p-type region and electrons from the n-type region. The fixed dopant cores in both regions leaves the interfacial regions in the p-type material negatively charged and the n-type material positively charged (q) as shown in Figure 3.7a. Note that a one-dimensional geometry is used for simplification. This space-charge distribution creates an electric field (E) in the junction and, thus, a distribution of voltage (V) (Figure 3.7b,c) according to Equations 3.1 and 3.2.

$$\frac{dE}{dx} = \frac{q}{\varepsilon_r \varepsilon_0} \tag{3.1}$$

$$\frac{dV}{dx} = -E \tag{3.2}$$

Here, ε_r and ε_0 are the dielectric constant of the semiconductor and the permeability of free space, respectively. The total span of the charged p-type (x_p) and n-type (x_n) regimes is known as the depletion region (w) (Figure 3.7). The total width of the depletion region can be found if the doping concentrations, dielectric constant, and intrinsic carrier concentrations are known.

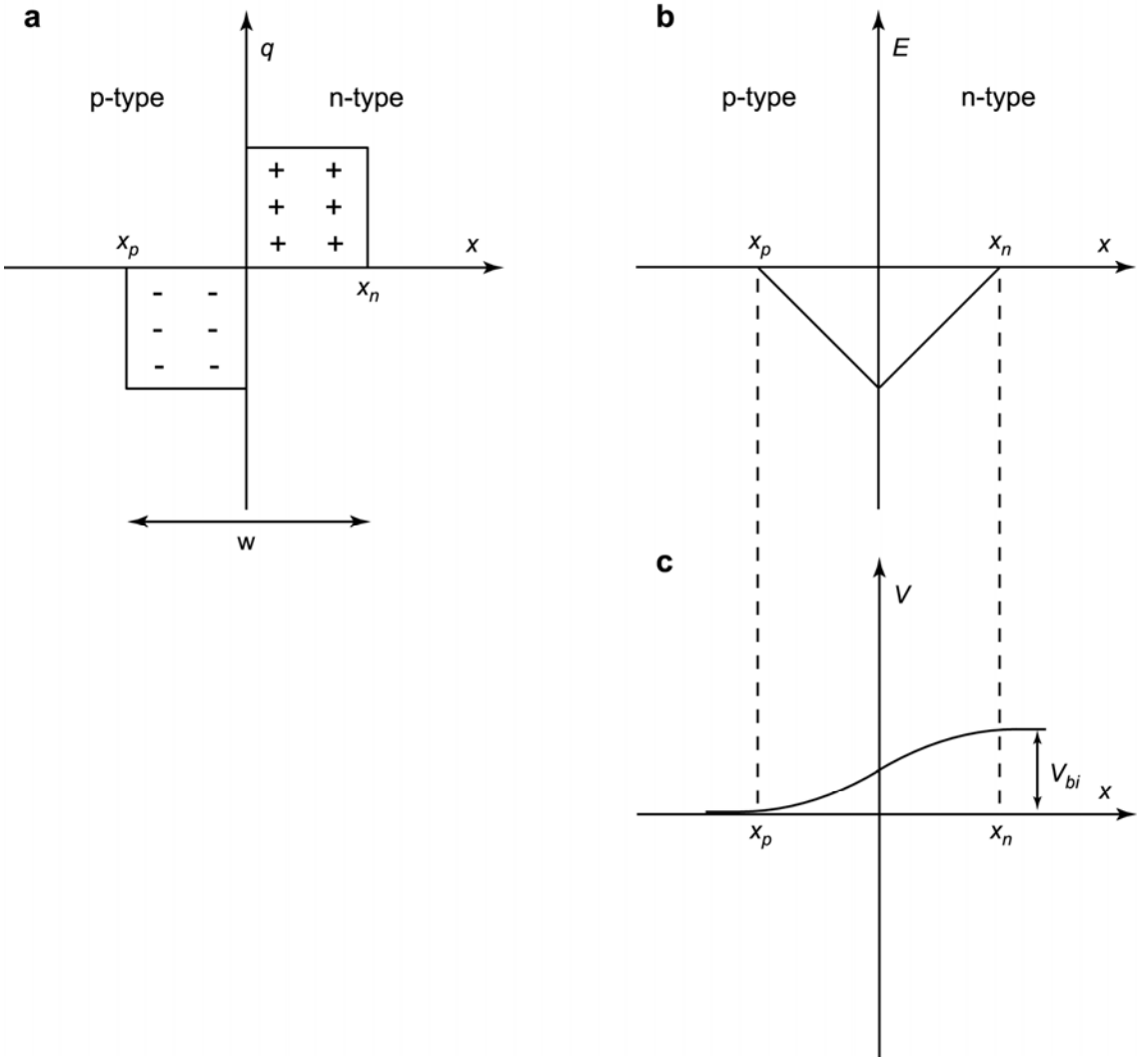

Figure 3.7. Illustration of (a) the space-charge (q) arrangement, (b) the electric field (E), and (c) voltage (V) of an inorganic p-n junction. When the two materials are put in contact electrons from the n-type semiconductor and holes from the p-type semiconductor recombine in the depletion region (w). This causes positively charged electron donor ions to remain fixed in the n-type semiconductor and negatively charged electron acceptor ions to remain fixed in the p-type semiconductor. This creates a built-in voltage (V_{bi}) across the depletion region of the p-n junction.

The formation of a p-n junction creates a diode, which is a device that allows current to flow in the forward bias regime but current does not flow in the reverse bias regime.[2,4] The physics behind this phenomenon may be explained through the use of a simple schematic. Figure 3.8 depicts the band diagrams, including the conduction band (E_c)

energy and valence band energy (E_v), for a p-n junction at equilibrium ($V = 0$), in the reverse bias ($V < 0$), and in the forward bias regimes ($V > 0$). Note that at zero bias the Fermi levels (E_F) of the two sides of the junction must align as a condition of equilibrium. This causes band bending in the p and n-type regions which brings about the built-in potential (V_{bi}). In reverse bias, the energy barrier that a charge carrier must overcome to go from one side of the junction to the other becomes even larger as the reverse bias voltage adds to the built-in voltage. In forward bias the energy required for a charge carrier to cross the junction becomes lower as one pushes to greater positive biases because the forward bias and built-in potential oppose one another. Note that the quasi-Fermi levels (E_{Fq}) on either side of the junction do not need to align in forward or reverse bias because these are no longer equilibrium conditions.

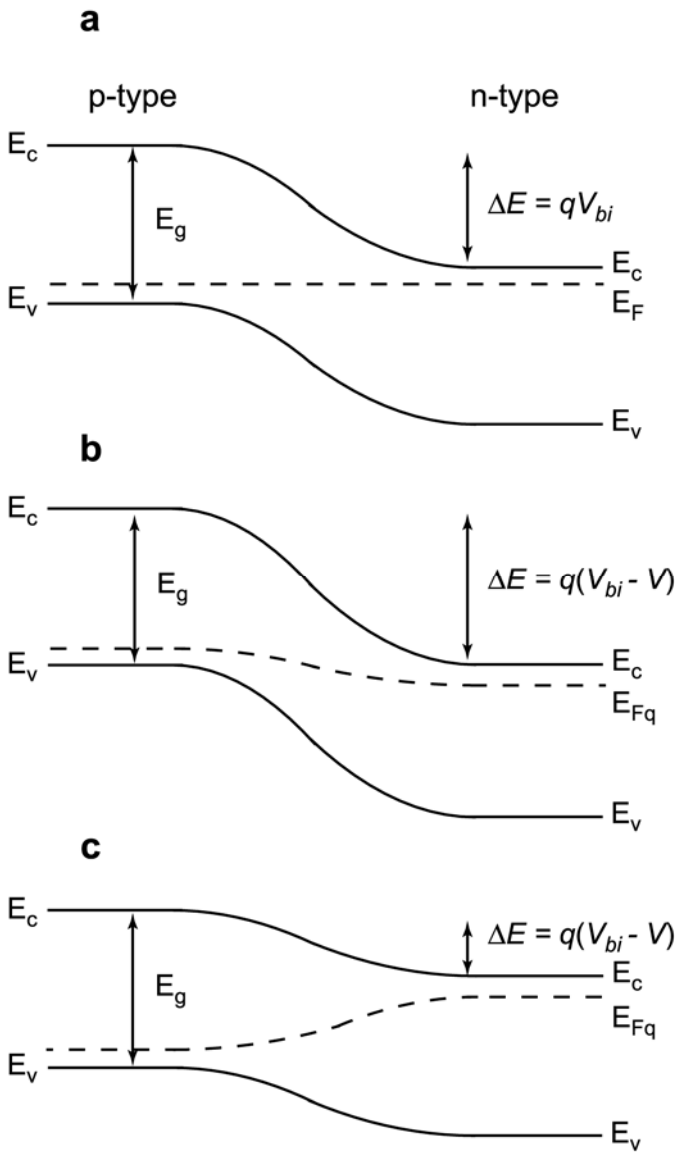

Figure 3.8. Energy band diagrams for an inorganic p-n junction (a) in equilibrium, (b) under reverse bias ($V < 0$), and (c) under forward bias ($V > 0$), assuming the p-type semiconductor is grounded. The conduction band (E_c), valence band (E_v), Fermi (E_F), quasi-Fermi (E_{Fq}), and band gap energies (E_g) are listed. The differences between the conduction (or valence) band energies (ΔE) of the p-type and n-type semiconductors is related to the built-in voltage (V_{bi}) and the applied voltage (V).

Using the conceptual arguments described above, the Shockley equation (Equation 3.3) relates the total current density (J) of an ideal diode in the dark to the saturation current

density (J_s) and the applied voltage (V).[92] Note that a current density is the current per unit cross-sectional area of the device.

$$J = J_s \left(e^{qV/kT} - 1 \right) \tag{3.3}$$

Here, q is the elementary charge, k is Boltzmann's constant, and T is the temperature. The saturation current density is the current density that is present in reverse bias and is usually orders of magnitude less than the current density observed in forward bias. Exact expressions for J_s will not be presented but can be found elsewhere.[4]

Before describing the equations that govern inorganic photodiode operation under illumination, a few key parameters used to describe photovoltaic power conversion efficiency will be described. It is important to note that these metrics are used to describe solar cell performance no matter the active layer composition (*i.e.*, inorganic vs. organic). Typical current density-voltage (J-V) photovoltaic curves, both in the dark and under illumination, are shown in Figure 3.9. Note that the dark current curve follows the form of the Shockley equation for a diode (Equation 3.3). Turning to the curve taken while the device is exposed to the solar spectrum (white light), the first point of interest is the current density at which the applied voltage is zero. This is termed the short-circuit current density (J_{sc}). Without the presence of a photocurrent, the value of the short-circuit current density would be zero as the system would be in equilibrium. Another important point is the voltage at which the overall current in the device is zero; this is the open-circuit voltage (V_{oc}). At this point, the photocurrent is balanced by an equal diode current with an opposite sign. Finally, the point along the J-V curve where the maximum power ($P = JV$) of the device is realized is called the maximum power density point (P_{MAX}). There are corresponding current-density (J_m) and voltage (V_m) values that, when multiplied together, yield the maximum density power at this point. If the power density of the sunlight (P_{in}) that the solar cell is exposed to is known, then the power conversion efficiency (η) of the device can be calculuated.[4]

$$\eta = \frac{J_m V_m}{P_{in}} \tag{3.4}$$

It is sometimes convenient to define a fill factor (*FF*), which is the ratio of the maximum power delivered and the potential power.[4]

$$FF \equiv \frac{J_m V_m}{J_{sc} V_{oc}} \tag{3.5}$$

In Figure 3.9, this parameter is the ratio of the shaded rectangle area to the area of the rectangle made from the intersection of J_{sc} and V_{oc}. The most commonly used expression for power conversion efficiency is found by substituting Equation 3.5 into Equation 3.4.

$$\eta = \frac{J_{sc} V_{oc} FF}{P_{in}} \tag{3.6}$$

Obviously, researchers attempt to increase the values of all three parameters in the numerator of this expression. The methods commonly employed for organic photovoltaics will be described below.

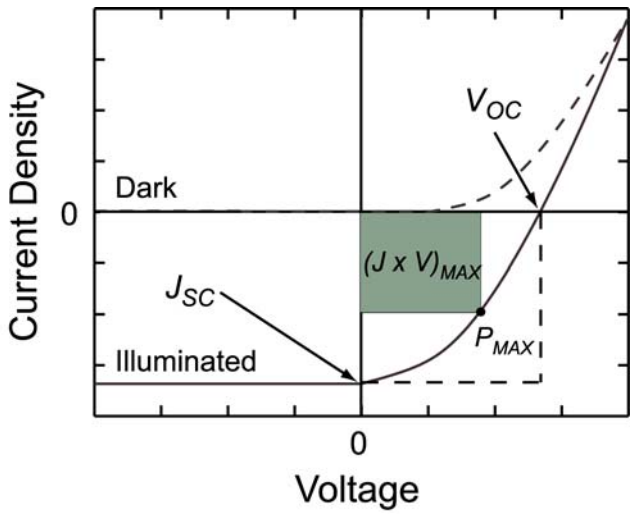

Figure 3.9. Representative current density–voltage (*J-V*) curve for a photovoltaic device in the dark (dashed line) and under illumination (solid line). The short-circuit current density (J_{sc}) and open-circuit voltage (V_{oc}) are labeled. The fill factor (*FF*) is the ratio of the area of the shaded rectangle $(J\text{-}V)_{MAX}$ to the area of the dashed rectangle.

Another important measure is the spectral response of the photovoltaic device. In this experiment, white light is replaced with monochromatic light and the photocurrent is

measured as a function of wavelength. This produces a quantity known as the external quantum efficiency (*EQE*), which is the ratio of the number of electrons (n_e) that are collected from a device to the number of photons (n_{ph}) incident on the device at a specific wavelength (λ). Equation 3.7 shows the full expression that includes Planck's constant (h), the speed of light (c), and the electrical charge (q), which are included for proper unit conversions.[5]

$$EQE = \frac{n_e}{n_{ph}} = \frac{J_{sc}}{P_{in}} \frac{hc}{q\lambda} \tag{3.7}$$

Returning to the case of a single inorganic material, ideal p-n junction, free charge carriers are generated upon illumination (this will not generally be the case for organic materials) and a new current source (the photocurrent density, J_L) is introduced into the system. The photocurrent guides electrons (and holes) in a direction opposite of the diode current. As such, Equation 3.3 becomes modified to yield the following.[4]

$$J = J_s \left(e^{qV/kT} - 1\right) - J_L \tag{3.8}$$

Absorption (with a Beers' law thickness dependence)[93] of photons and creation of free charge carriers occurs throughout the entirety of the p-n junction; therefore, a chemical potential gradient is not the driving force for the flux of electrons (holes). The photocurrent present in this device is caused by the gradient in electrical potential created by the built-in potential of the p-n junction. This is an important point and it is strikingly different than the mechanism for charge carrier flux in organic photovoltaics. The open-circuit voltage can also be found explicitly by setting the total current in Equation 3.9 equal to zero.[4]

$$V_{oc} = \frac{kT}{q} \ln\left(\frac{J_L}{J_s} + 1\right) \approx \frac{kT}{q} \ln\left(\frac{J_L}{J_s}\right) \tag{3.9}$$

Recall that the power density is the product of current density and voltage, and the maximum power point for the device can be found by taking the derivative of power with respect to voltage and setting this expression equal to zero.[4]

$$P = J \times V = J_s V \left(e^{qV/kT} - 1\right) - J_L V \tag{3.10}$$

$$J_m = J_s \frac{q}{kT} V_m e^{\frac{qV_m}{kT}}; V_m = \frac{kT}{q} \ln\left(\frac{\frac{J_L}{J_s} + 1}{1 + \frac{kT}{q} V_m} \right) \quad (3.11)$$

Now all parameters required to calculate the power conversion efficiency (Equation 3.6) have expressions except for the short-circuit current density. The theoretically predicted short-circuit current density can be estimated by integrating the photon energy of the solar spectrum over all energy wavelengths from the band gap of the material to infinity. Therefore, the theoretical power conversion efficiency for an ideal p-n junction device can be estimated. In fact, this analysis has been performed and it was found that the maximum efficiency of an ideal p-n junction silicon cell (E_g = 1.1 eV) would be η_{Si} = 36% and an ideal germanium cell (E_g = 0.67 eV) would be η_{Ge} = 28%. Based on the solar spectrum the ideal band gap energy for a single semiconductor p-n junction would be $E_g \approx 1.4$ eV.[94]

In real solar cells effects such as series and shunt resistances arise due to ohmic losses and leakage currents. These factors depend on the impurity concentrations in the p and n regions of the junction, the junction depth, materials properties, and the geometry of the device. In practice these effects are crucial to device performance and expressions that properly account for them have been found,[4] but they will not be covered here. To this point, it has been assumed that one free electron and one free hole are generated upon absorption of a photon in the active layer of a solar cell, which is the case for the inorganic solar cells. However, this is not the case in organic solar cells.

3.2.2 Device Physics of an Organic Solar Cell

The concept of conduction and valence bands is not typically used in the organic semiconductor literature. This is due to the fact that organic semiconductors are not as well-ordered as inorganic semiconductors as almost all are polycrystalline or completely amorphous. In lieu of the valence and conduction bands, the designated states for hole and electron transport are referred to as the Highest Occupied Molecular Orbital (HOMO) and Lowest Unoccupied Molecular Orbital (LUMO), respectively.[95,96]

Charge transport in organic semiconductors can be represented in many different manners including the hopping model,[95] the variable range hopping model,[97] and the multiple trapping and release model.[98] Given that transport in an individual organic semiconducting material is different than an inorganic material, it is not surprising that the mechanisms for device operations for inorganic and organic photovoltaics are different.

The most obvious distinction is that free charge carriers are created immediately upon photon absorption in inorganic solar cells. Because organic solar cells (OSCs) are composed of materials with lower dielectric constants ($\varepsilon_{Pentacene}$ ~3) than inorganic solar cells (ε_{Si} ~11), the excited electron remains bound to its corresponding hole by a Columbic interaction.[99,100] Remembering Coulomb's Law (Equation 3.12) will show that as the dielectric constant of a material (ε) decreases the force (F) between two opposite charges (with magnitude q) increases for a fixed distance of separation (r).[5]

$$F = \frac{q^2}{4\pi\varepsilon\varepsilon_0}\frac{1}{r} \tag{3.12}$$

Recall that ε_0 is the permittivity of free space. Absorption of a photon in OSCs leads to the creation of a bound electron-hole pair (exciton) that has a relatively short lifetime (~ 1 ns) before it recombines.[101,102] This Frenkel exciton is a mobile species that is neutral, and not affected by electric fields.[99,103] Therefore, separating excitons into free charge carriers becomes critical in extracting charges from organic photovoltaics. It should be noted that this exciton moves by a diffusion mechanism and, depending on the material, has a diffusion length (L_d) of ~10 – 40 nm. This means that the exciton can only explore a small amount of space prior to recombination. The predominant strategy to efficiently separate the exciton is to create a heterojunction of two materials which acts as the active layer of the photovoltaic device. One of these materials conducts holes (electron donor) and the other conducts electrons (electron acceptor). The electron donor is designed to have LUMO and HOMO levels closer to free vacuum than those same levels in the electron acceptor. Therefore, if an exciton reaches the donor-acceptor interface, it is energetically favorable to have the exciton dissociate so that the electron

and hole can lower their free energies. It should be noted that the exact mechanism of this dissociation process is still under debate.[104-106] Once the free electron and hole are generated, they can be transported through the organic semiconductors by a mechanism mentioned above[95,97,98] and collected at the appropriate electrode. A schematic representation of the five general steps required to generate current in an organic photovoltaic is shown in Figure 3.10.

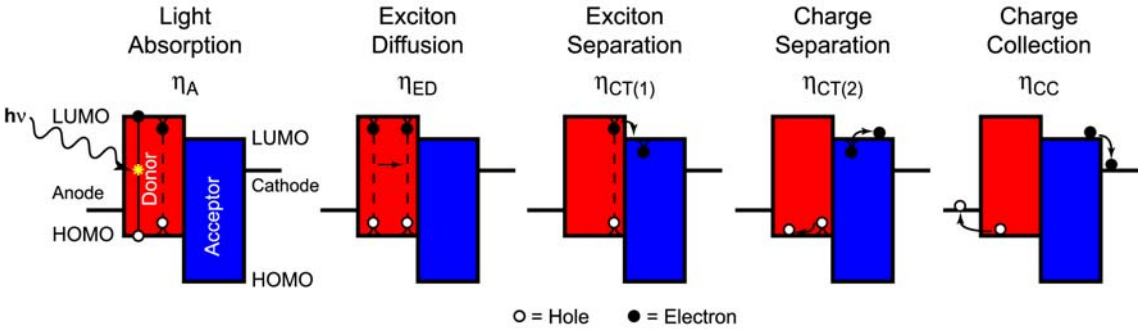

Figure 3.10. Illustration showing the charge generation and collection mechanism in organic photovoltaics at an electron donor (red)–acceptor (blue) interface. Light absorption creates a bound electron (black circle)-hole (white circle) pair called an exciton. The exciton diffuses through space and if it reaches an interface will separate into a free electron and hole. The charge carriers are then transported via chemical and electrical gradients through the electron donor (holes) and electron acceptor (electrons). Holes and electrons can then be collected at the anode and cathode, respectively. The efficiencies associated with step *i* are labeled as η_i (see text).

Another distinction between current generation in organic and inorganic solar cells can be explained mathematically by the electron and hole flux drift-diffusion equations. The gradients of electrical (U) and chemical (μ) potential energies are the driving forces for the one-dimensional current density of electrons [$J_n(x)$] and holes [$J_p(x)$].[3]

$$J_n(x) = n(x)\mu_n\left[\nabla U(x) + \nabla\mu(x)\right] \tag{3.13}$$

$$J_p(x) = p(x)\mu_p\left[\nabla U(x) + \nabla\mu(x)\right] \tag{3.14}$$

Here the gradients are weighted by the electron $n(x)$ and hole $p(x)$ densities. The electron and hole mobilities are given as μ_n and μ_p, respectively. Inorganic photovoltaics

generate free electrons and holes throughout the entire device. Additionally, any spatial distribution of free charge carriers is quickly erased because of the relatively high carrier mobilities in these materials.[99] Therefore, the gradient in electrical potential dominates the gradient in chemical potential for the inorganic photovoltaic generation of current density. On the other hand, exciton dissociation at the electron donor-acceptor interface creates a large charge gradient in organic photovoltaics, and the chemical potential gradient becomes a comparable (or even dominating) driving force for electron (hole) flux. In fact, efficient organic photovoltaics have been fabricated where the gradient in electrical potential was not present and all flux was due to the chemical potential gradient.[102] This is one advantage that organic photovoltaics has over inorganic photovoltaics, because the open-circuit voltage in OPVs is not necessarily limited by the built-in voltage, which is typically the case in inorganic photovoltaics.

3.2.3 Optimization of Organic Photovoltaics

In order to maximize OPV power conversion efficiency, the short-circuit current density, open-circuit voltage, and fill factor should all be optimized. Figure 3.11 shows a generic schematic of an active layer heterojunction organic photovoltaic. The bottom contact is composed of a transparent conducting oxide (TCO) and serves as the anode. The top contact is an opaque metal and serves as the cathode. This has been the traditional device geometry for OPVs and will be useful for this particular discussion; however, inverted solar cells, where the TCO serves as the cathode have recently become more popular.[107-109]

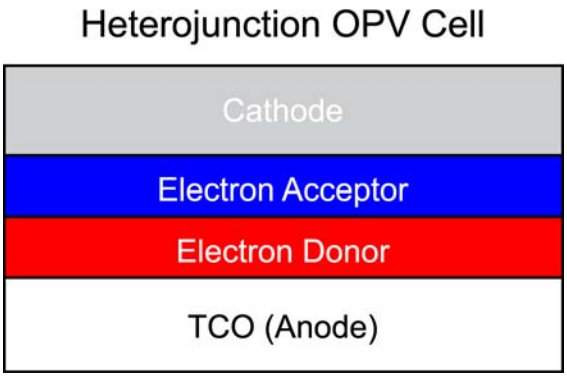

Figure 3.11. Schematic depiction of a generic heterojunction organic photovoltaic (OPV) cell. The electron donor is shown in red and the electron acceptor is in blue. The two layers are sandwiched between a transparent conducting oxide (TCO), which serves as the anode, and a cathode. Light enters the device through the TCO.

The short-circuit current can be increased by increasing the efficiency of each step shown in Figure 3.10 including: the absorption efficiency (η_A) of the active layer, the exciton diffusion efficiency (η_{ED}), the charge transfer efficiency (η_{CT}) between the electron donor and acceptor, and the charge collection efficiency (η_{CC}).[9] The amount of photons absorbed can be increased by increasing the thickness of the active layer. More photons also can be absorbed by selecting organic semiconductors with high absorption coefficients or with lower band gaps.[44] By finding materials with greater absorption coefficients, the thickness of OPVs can be decreased, and transport losses can be decreased. Most organic semiconductors used today have band gap energies $E_g \geq 1.9$ eV but Figure 3.6 clearly shows that a large number of photons with energies lower than 1.9 eV (corresponding $\lambda \geq 652$ nm) are present in the solar spectrum. Harvesting these lower energy photons will aid in increasing η_A.[110] While excitons can quench at organic-metal interfaces and at traps in an organic layer, generating free charge carriers from the bound electron-hole pair increases η_{ED} the most when dissociation occurs at an electron donor-acceptor interface.[99] It was noted above that one can increase the device thickness to increase the photon absorption efficiency; however, making a device too thick can decrease the short-circuit current density. A thick active layer can lead to a decrease in the excitons that can diffuse to the interface prior to recombination and

dissociate into electrons and holes, which decreases the number of free charge carriers. To balance these two effects (sometimes termed the exciton diffusion bottleneck),[9] experiments are conducted to determine the optimum device thickness. Increasing the exciton dissociation efficiency is a very active area of research, with different groups approaching this bottleneck in a variety of different manners that will not be discussed here.[26,111-114] The most common approach to increase η_{ED} is to increase the interfacial area between the electron-donating and accepting materials.[5,115] A detailed discussion of different active layer architectures that attempt to produce highly interdigitated structures will be shown in Chapter 3.3. The charge transfer efficiency (η_{CT}) in many heterojunction organic solar cells usually approaches unity.[9,116,117] The charge collection efficiency can also have values close to η_{CC} = 100%. Due to the relatively poor carrier mobility in organic semiconductors, however, there are some systems where free electrons and holes can recombine prior to being extracted at the electrodes. Electron and hole mobilities can be increased by selecting materials that have a large degree of crystallinity because transport is much easier through ordered domains relative to disordered, amorphous domains. Controlling film-formation[85,118] and annealing[119-121] conditions can help improve the crystalline nature of an organic semiconductor thin film. By tuning the synthesis of constituent molecules and the fabrication of the device structure, researchers have been able to create organic solar cells with short-circuit current densities in excess of 12 mA cm^{-2}.[85-87] This number is comparable to J_{sc} values found in amorphous silicon solar cells.[4]

Some have claimed that the open-circuit voltage is the largest hurdle to increasing OPV efficiencies.[110] This is because the band gap energy of many organic semiconductors is E_g ~2 eV but observed open circuit voltages are typically V_{oc} ~0.5 V – a loss of nearly 75% of the potential! Needless to say, the open-circuit voltage is one of the least well-understood and mostly heavily debated parameters in organic photovoltaics. The open-circuit voltage for inorganic solar cells is limited to the built-in voltage of the device. Because of the differences in the mechanisms of operation described above, this is not true for organic photovoltaics, and many results have shown

OPV devices with $V_{oc} > V_{bi}$.[99,122] The open-circuit voltage was originally thought of in terms of the metal-insulator-metal (MIM) model.[4,5] In this model, the open-circuit voltage is determined by the offset in work function of the anode and cathode metal contacts. Applications of the MIM model to organic solar cells have undergone many iterations. It has been shown the V_{oc} of OPVs can be affected by the LUMO level of the electron acceptor,[123] the HOMO level of the electron donor,[124] the active layer morphology,[125,126] the amount of dark current present in the device,[127] and the work function of the anode.[128] Recent results have suggested that the MIM model does not work at all for heterojunction active layers. The researchers found a useful rule of thumb for approximating the open-circuit voltage could be expressed in terms of the energy level of the electron donator HOMO (E_{HOMO}^{Donor}) and the electron acceptor LUMO ($E_{LUMO}^{Acceptor}$) for polymer-fullerene solar cells, if morphology effects are not included.[110]

$$V_{oc} = \frac{1}{q}\left(\left|E_{HOMO}^{Donor}\right| - \left|E_{LUMO}^{Acceptor}\right|\right) - 0.3\ V \tag{3.15}$$

While this result seems simple enough, other groups have shown that electrode modifications can greatly affect the open-circuit voltage and fill factor. The most common anodic material is the transparent conducting oxide, indium-doped tin oxide (ITO). Other anodes have been studied and have approximately the same performance.[129,130] The most common way to have ohmic contact between the anode and the electron-donating material is to coat the ITO with a thin layer of poly(ethylene dioxythiophene) doped with poly(styrene sulfonate) (PEDOT:PSS). Not only does this provide ohmic contact to a large number of commonly used electron-donating organic semiconductors, but it also provides a substrate that organic-based solutions wet better than ITO.[131] Traditionally, a low work function metal, such as aluminum, has been used as the cathode because of its common use in the organic light emitting diode (OLED) community. In 2002, Brabec et al. showed that an insertion of a thin layer of lithium fluoride (LiF) between the active layer and the aluminum contact greatly enhanced device efficiency.[132] Later, researchers at NREL showed that if the LiF layer was replaced by either barium or calcium layers device efficiency increased to an even

larger degree.[133] Because the phenomena that govern the open-circuit voltage in organic photovoltaics is not well understood, a large amount of parameters must be tuned to achieve an optimized V_{oc}.

A high efficiency device must also have a high fill factor. The fill factor is commonly described as a measure of the "squareness" of the *J-V* curve. In practice, the *FF* is affected by the choice of electrodes, all interfaces (metal/organic and organic/organic), and the morphology of the active layer. This complicated parameter can be related to physical conditions better by considering the resistances present in the device. Note that the inverse slope of the *J-V* curve in the linear regime under forward bias ($V > 0$) reflects the amount of series resistance in the device. Thus, one should minimize the series resistance of the device by optimizing the film's morphology and minimizing electrode contact resistances. The shunt resistance of the device is captured by the inverse of the slope of the *J-V* curve near the $J = 0$ axis. The fill factor is also increased by maximizing the shunt resistance (decreasing the leakage currents) in the device.

It should be clear that multiple materials are needed for the fabrication of efficient organic photovoltaics. How these materials are made into thin films and in what ratio greatly affects device performance. Optimization of the materials and thin film properties can go a long way in increasing the short-circuit current density, open-circuit voltage, and fill factor. Importantly, the geometry of the photoactive layers of these devices can also prove to be crucial. The delicate balance between light absorption, exciton diffusion, charge separation, charge transport, and charge collection has led researchers to explore a variety of architectures in order to maximize efficiency from a relatively small number of materials used in organic solar cells.

3.3 Organic Photovoltaic Active Layer Architectures

Three predominant architectures have been used to bring electron donors and acceptors into contact during the fabrication of heterojunction organic solar cells. These architectures are: the bilayer heterojunction, the bulk heterojunction, and the ordered bulk heterojunction (Figure 3.12).

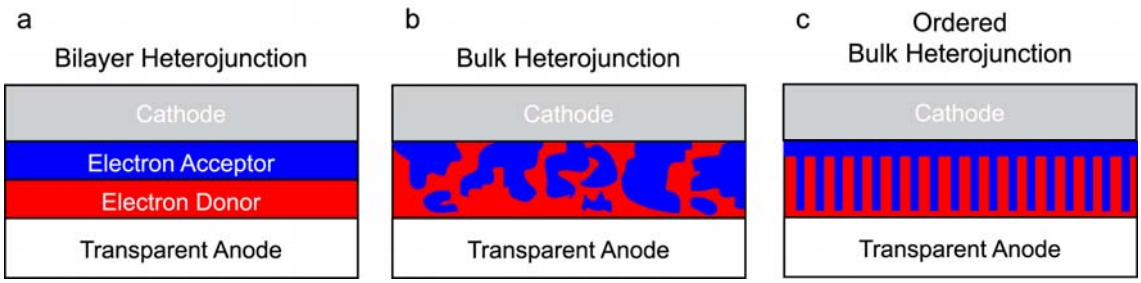

Figure 3.12. Schematic representation of (a) a bilayer, (b) a bulk heterojunction, and (c) an ordered bulk heterojunction. The electron donor is in red, and the electron acceptor is blue.

While modifications to these geometries, such as spacer layers[134] and stacking of heterojunctions[135,136] have been shown, the basic active layer structures that these heterojunctions provide dominate the literature. Each of these constructions has advantages and drawbacks that make it the preferred geometry for a specific situation.

The bilayer is the oldest of the heterojunctions and was first introduced by the Kodak Corporation in 1986.[19] The geometry is fabricated by sequentially depositing an electron donor and acceptor. In many cases this is accomplished by depositing small molecules from the vapor phase.[137] Bilayer heterojunctions can also be fabricated using solution coating techniques if orthogonal solvents[138] can be found or if the electron-donating layer can be crosslinked.[139] One of the largest advantages of the bilayer cell is that it allows for the formation of continuous pathways in which electrons and holes can travel to the appropriate electrodes. However, these charge carriers are most efficiently generated at the interface of the heterojunction. Because the exciton diffusion length of organic materials is usually small, only excitons generated near the interface are actually transformed into free electrons and holes. As the active layer thickness is decreased to increase the number of electron-hole pairs that are separated, the amount of light absorbed in the device is decreased. These competing effects dictate optimum electron donor and acceptor layer thicknesses, and these values are usually found through iterations of experiments. Because each lamella in the bilayer heterojunction is composed of a single material, it is a useful testbed for new organic photovoltaic

materials. Thus, this simple geometry will always be of great utility in the OPV community. Before discussing the bulk heterojunction, an important development in the small molecule OPV community that links the bilayer and bulk heterojunction will be mentioned. The Forrest group has shown that planar-mixed heterojunction devices are more efficient than bilayer devices composed of the same materials and can yield power conversion efficiencies of ~5%.[113,114]

In these devices, a layer of electron donor is evaporated onto an ITO-coated substrate. Instead of depositing a layer of pure electron-accepting material, the electron donor and electron acceptor are codeposited on top of the pure electron-donating layer. A layer of the electron acceptor is then deposited and the device is capped with the cathode. These devices are more efficient than bilayer solar cells because they increase the amount of interfacial area between the electron donor and acceptor, which leads to more exciton dissociation. The planar-mixed heterojunction geometry is an interesting design that is only just now being researched. This device geometry could prove to be very useful in generating highly efficient OPVs as it allows for both a high degree of electron donor-acceptor mixing and control of film morphology.

The geometry most commonly used to overcome the primary shortfall of the bilayer heterojunction is the bulk heterojunction solar cell,[140] and, to date, this active layer geometry has given the most efficient devices.[85-87] In the best performing of these systems the electron donor (a thiophene-based polymer) and acceptor (a fullerene derivative) are deposited as one layer. This may be done either by codeposition of materials from the vapor phase or, more commonly, by dissolving the semiconductors in a common solvent and coating the solution on a conducting substrate. By depositing the active layer in this manner there is a large increase in interfacial contact area between the electron-donating and accepting materials. By controlling the deposition[85] and post-fabrication annealing temperatures[120,141] researchers have been able to tune the morphology of specific systems to yield devices where the external quantum efficiency of devices reaches 80% for certain wavelengths. The annealing conditions allow the fullerene molecules to diffuse and aggregate to form crystals that nucleate and grow

with increasing time and temperature.[142] Using the appropriate combination of annealing times and temperatures allows for domain formation on the same length scale as that of the exciton diffusion length. Not only are appropriately sized domains formed, but interconnected paths of electron donating and accepting materials apparently exist so that charge collection can easily occur.[78,115] Even though these devices are state of the art, they are not completely optimized. As one would expect for a kinetically trapped morphology, the device performance is heavily dependent on exact annealing temperatures and times.[143,144] Consequently, prolonged exposure to heat or light can alter the morphology of the active layer and affect device performance. Interestingly, some researchers have used block copolymers (composed of blocks with properties similar to the electron donor and acceptor) as compatibilizers for active layer blends.[145] Even with only a small weight fraction of block copolymer, these ternary blends possess better thermal stability than the binary systems. Other ternary blends that include small molecule surfactants have also shown improved device performance, which reportedly occurs due to better control of the active layer morphology.[146,147] Perhaps the biggest drawback to bulk heterojunction active layers is the fact that one cannot predict (or subsequently easily measure[78]) the network morphology of the donor and acceptor phases. In fact, the best performing bulk heterojunction devices have required substantial materials optimization in order to achieve high power conversion efficiencies. Also troublesome is that there is no simple way to characterize the size and shape of the two distinct domains due to their stochastic nature. Therefore, modeling how these parameters affect device performance becomes difficult and it becomes non-trivial to grasp a true understanding of the geometric effects of the physics behind OPV performance.

In order to comprehend how spatial constructs influence device efficiency, researchers have begun to use ordered bulk heterojunction solar cells. Ideally, these active layers would combine the regular, continuous charge collection pathways of the bilayer heterojunction with the high exciton dissociation area of the bulk heterojunction. In fact, computational efforts have predicted that an ordered bulk heterojunction with

pillars running perpendicular to the electrodes is the optimal geometry for OPVs.[148,149] This assumes that the diameter and center-to-center distances of the pillars is on the order of the exciton diffusion length (L_d ~15 nm). Almost all ordered bulk heterojunctions fabricated to date have been hybrid solar cells where the electron acceptor is a metal oxide and the electron donor is a semiconducting polymer. In the seminal papers, the active layer consisted of the electron-accepting nanoporous titania (TiO_2) film that had been infiltrated by the electron-donating polymer, poly(3-hexylthiophene) (P3HT).[150,151] Researchers found that completely infiltrating these nanopores with a polymer can be difficult. Another approach to inorganic-organic ordered bulk heterojunctions is through the use of metal oxide nanowires. Both titania[152-154] and zinc oxide[155-157] (ZnO) nanowires have been grown from a TCO surface and subsequently backfilled with P3HT (Figure 3.13). Two issues have limited the performance of these devices. The first is that growing high aspect ratio metal oxide nanowires with diameters on the length scale of exciton dissociation is difficult. Adding to the difficulty is that deposition and infiltration of the polymer into the network can damage the nanowires.[157] The second problem is that charge transfer between the organic and inorganic species is much less efficient than charge transfer between two organic materials.[158,159] In fact, NREL researchers found that if a small molecule organic electron acceptor were added to the nanowire-polymer mixture, the efficiency of the devices increased fourfold.[155] The authors postulated that this was due to increased free charge carrier generation facilitated by the PCBM in the polymer matrix.

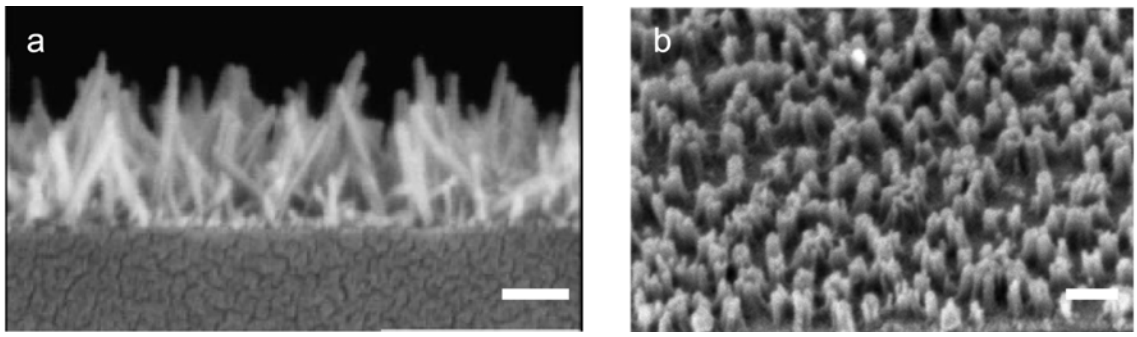

Figure 3.13. Scanning electron microscopy (SEM) images of nanowires composed of (a) zinc oxide (ZnO) (cross-sectional image) and (b) titania (taken at an angle 45 ° from the substrate). Both nanostructured films were subsequently backfilled with poly(3-hexylthiophene) (P3HT) to create hybrid ordered bulk heterojunctions. Both scale bars represent 100 nm. (a) is reproduced from Ref. 155 and (b) is reproduced from Ref. 154.

A few strategies have been used to fabricate all-organic ordered bulk heterojunctions, but all have had very limited success. The first approach by the Whitesides group used a novel "jelly roll" technique to fabricate their active layer.[138] In this technique a thin layer of an electron acceptor was spun-coat onto a thin layer of an electron donor using an orthogonal solvent. This bilayer-type device was thin lifted from the substrate and rolled into a tight package. The film was then orientated with the bilayers perpendicular to a substrate and the film was thinly sliced with a microtome. This layer was then sandwiched between an anode and a cathode to complete the device (Figure 3.14). While the device fabrication strategy was quite clever and the domain spacing of the electron donor and acceptor layers were on the order of the exciton diffusion length, these devices had poor performance. One of the main problems with these devices was that the active layer fabrication procedure led to poor films due to the multiple transfer steps. Additionally, because orthogonal solvents needed to be used for the spin-coating procedures, the electron donor and acceptor were not optimized with respect to their optoelectronic properties.

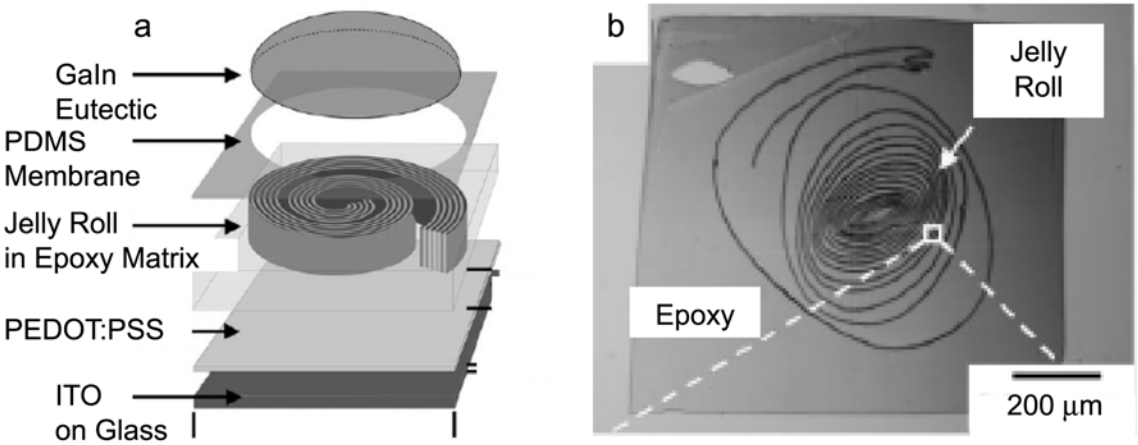

Figure 3.14. Jelly roll ordered bulk heterojunction (a) schematic fabrication procedure, and (b) an optical image of a jelly roll active layer embedded in an epoxy matrix. Note that the poly(dimethylsiloxane) (PDMS) membrane is used to localize the low viscosity gallium-indium (GaIn) eutectic. The width of each layer of the jelly roll was varied between 15–50 nm. The overall height of the roll (150 nm) was made by using a microtome. Reproduced from Ref. 138.

A more successful all-organic ordered bulk heterojunction was accomplished by structuring thin films of copper phthalocyanine (CuPc).[160] First CuPc was thermally evaporated onto ITO substrates. Upon solvent vapor annealing, nanostructured CuPc films were formed with the exact morphology depending on the solvent used (Figure 3.15). The CuPc film was then backfilled by solution coating PCBM from an orthogonal solvent and then evaporating a top cathode to complete the device. The CuPc films that had been exposed to acetone solvent vapor (Figure 3.15d) had photocurrents 2-3 times greater than that of the planar film, but full device characterization data were not shown. These devices could be optimized even further because the diameters of the nanorods were, at minimum, 50 nm.

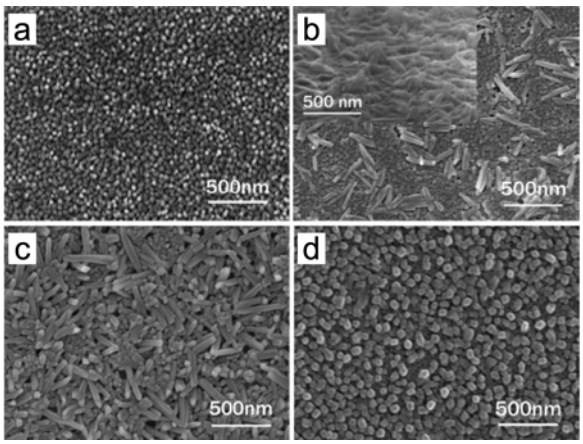

Figure 3.15. Top-down scanning electron microscopy (SEM) images of CuPc films (a) as-deposited on ITO-coated glass, (b) annealed with chloroform vapor, (c) annealed with toluene vapor, and (d) annealed with acetone vapor. Note that the well-ordered, nanostructured film shown in (d) gave the best device performance when used in a device. Reproduced from Ref. 160.

Some common limitations of the ordered bulk heterojunctions described above include: domain spacings much larger than the exciton diffusion length, difficulty infiltrating nanoporous networks with polymers, and poor charge transfer between the electron donor and acceptor (in hybrid cell cases). Using a block copolymer that both microphase separates on the scale of L_d and contains a semiconducting block could help alleviate these problems.

3.4 Strategy for an All-Organic Ordered Bulk Heterojunction

Here we present an approach towards an all-organic ordered bulk heterojunction that is derived from a nanoporous block copolymer template. It is this model that has motivated the block copolymer synthesis and microstructural analysis that dominates the contents of this thesis. Figure 3.16 schematically depicts the desired route to a well-ordered OPV active layer.

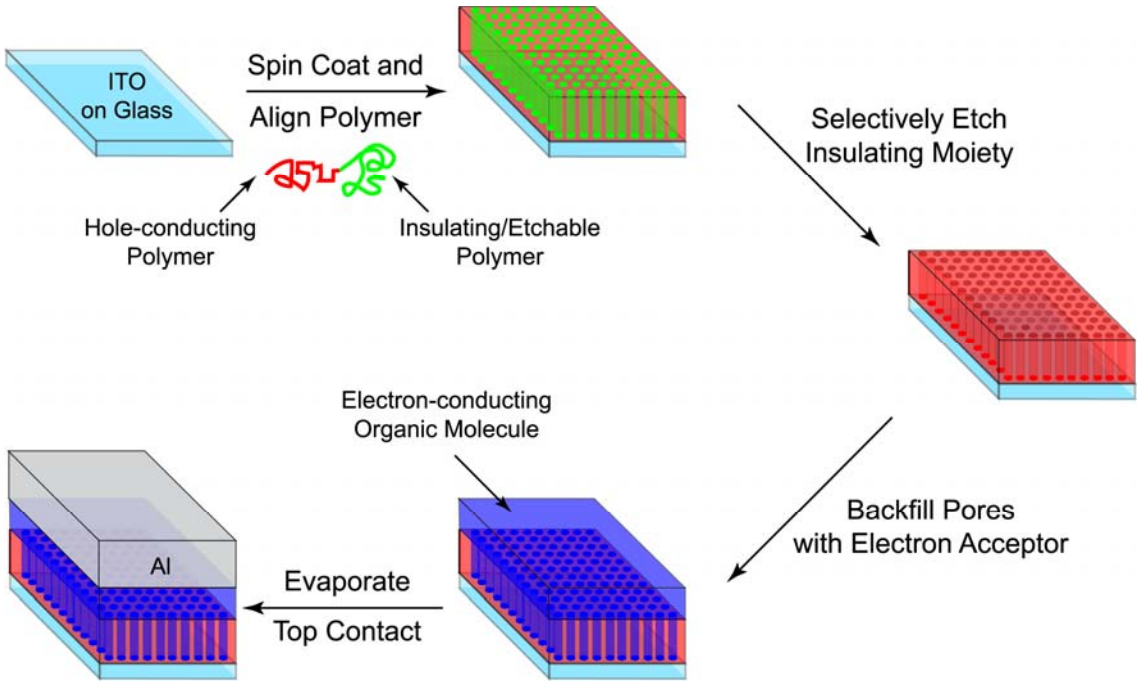

Figure 3.16. Schematic representation of the strategy to achieve an all-organic ordered bulk heterojunction solar cell. In this work, the hole-conducting polymer (red block) is a polythiophene and the etchable polymer is polylactide (green block). The electron acceptor (blue) could be either a small molecule or a polymer.

As with previous nanoporous thin films generated from block copolymer templates (Chapter 2), synthesis of a well-defined block copolymer is critical. In this work, polythiophene-containing block copolymers are used. Polythiophene derivatives (red block) were used because well-controlled polymerization schemes exist that also allow for end group control. Additionally, polythiophene derivatives have been used as the electron donors in some of the most efficient polymer-fullerene bulk heterojunction solar cells fabricated to date.[85,86] Polylactide (green blocks) was used as the etchable block (or blocks) as this polyester can be easily and selectively removed in a mild alkaline solution. As detailed in Chapter 2, the phase behavior of rod-coil block copolymers is very different than that of coil-coil block copolymers. Therefore, much of the work presented here focuses on understanding the microstructure of polythiophene-polylactide block copolymers, which behave as a rod-coil block copolymer system. It was found that generating well-ordered domains of the two moieties in thin films is

more difficult than shown in Figure 3.16. Despite this fact, the polylactide blocks were selectively removed from the polythiophene matrix (Chapter 4) to leave a nanoporous film.[161] In order to better tune the thin film microstructure of the block copolymer, the molecular structure of the polythiophene segment was changed. The results show that the stereolinkages of the thiophene repeat units greatly influence the phase behavior of polythiophene-polylactide block copolymers (Chapter 5). The last major hurdle of the schematic of Figure 3.16, backfilling with an electron acceptor, was never attempted with the nanoporous polythiophene films, but strategies for accomplishing this task are described in Chapter 8.

By using the approach outlined above, the problems associated with other ordered bulk heterojunction devices are avoided. First, the domain spacing and morphology of the block copolymer films can be controlled by tuning the molecular weight and volume fractions of the constituent blocks. Because the matrix polymer is also an electron-donating semiconductor, the film should be stable and structural failure should not be observed as in the some cases of metal oxide nanowires. Finally, this ordered bulk heterojunction is a better comparison relative to the high performing polymer-fullerene bulk heterojunction cells. The semiconducting materials that will be used in this device are completely organic and chemically very similar to those commonly used in the best performing plastic solar cells. While there is still much work to be done to understand the physics of phase separation in this system, the results outlined in the following chapters should provide a solid basis for achieving an all-organic ordered bulk heterojunction photovoltaic devices.

3.5 References

[1] Kittel, C. *Introduction to Solid State Physics, 8th Ed.*; John Wiley & Sons, Inc.: Hoboken, NJ, 2005.

[2] Callister, W. D. *Materials Science and Engineering: An Introduction, 7th Ed.*; John Wiley & Sons, Inc.: Hoboken, NJ, 2006.

[3] Pierret, R. F. *Advanced Semiconductor Fundamentals, 2nd Ed.*; Prentice Hall: Upper Saddle River, NJ, 2002.

[4] Sze, S. M. *Physics of Semiconductor Devices, 2nd Ed.*; John Wiley & Sons, Inc.: Hoboken, NJ, 1981.

[5] Sun, S.; Sariciftci, N. S.; Eds. *Organic Photovoltaics: Mechanisms, Materials, and Devices*; Taylor & Francis: Boca Raton, FL, 2005.

[6] Hagen, K.; Ed. *Organic Electronics: Materials, Manufacturing, and Applications*; Wiley-VCH Verlag GmbH & Co. KGaA: Weinheim, Germany, 2006.

[7] Shaheen, S. E.; Ginley, D. S.; Jabbour, G. E. *MRS Bull.* **2005**, *30*, 10–15.

[8] Loo, Y. L.; McCulloch, I. *MRS Bull.* **2008**, *33*, 653–658.

[9] Forrest, S. R. *MRS Bull.* **2005**, *30*, 28–32.

[10] de Boer, R. W. I.; Gershenson, M. E.; Morpurgo, A. F.; Podzorov, V. *Phys. Status Solidi A* **2004**, *201*, 1302–1331.

[11] Tang, Q.; Jiang, L.; Tong, Y.; Li, H.; Liu, Y.; Wang, Z.; Hu, W.; Liu, Y.; Zhu, D. *Adv. Mater.* **2008**, *20*, 2947–2951.

[12] Anthony, J. E.; Brooks, J. S.; Eaton, D. L.; Parkin, S. R. *J. Am. Chem.. Soc.* **2001**, *123*, 9482–9483.

[13] Kim, C. S.; Lee, S.; Gomez, E. D.; Anthony, J. E.; Loo, Y. L. *Appl. Phys. Lett.* **2008**, *93*, 103302.

[14] Lim, Y. F.; Shu, Y; Parkin, S. R.; Anthony, J. E; Malliaras, G. G. *J. Mater. Chem.* **2009**, *19*, 3049–3056.

[15] Ong, B. S.; Wu, Y.; Liu, P. *J. Am. Chem. Soc.* **2004**, *126*, 3378–3379.

[16] McCulloch, I.; Heeney, M.; Bailey, C.; Genevicius, K.; MacDonald, I.; Shkunov, M.; Sparrowe, D.; Tiemey, S.; Wagner, R.; Zhang, W.; Chabinyc, M. L.; Kline, R. J.; McGehee, M. D.; Toney, M. F. *Nat. Mater.* **2006**, *5*, 328–333.

[17] Dimitrakopoulos, C. D.; Malenfant, P. R. L. *Adv. Mater.* **2002**, *14*, 99–117.

[18] Newman, C. R.; Frisbie, C. D.; da Silva Filho, D. A.; Brédas, J. L.; Ewbank, P. C.; Mann, K. R. *Chem. Mater.* **2004**, *16*, 4436–4451.

[19] Tang, C. W. *Appl. Phys. Lett.* **1986**, *48*, 183–185.

[20] Mutolo, K. L.; Mayo, E. I.; Rand, B. P.; Forrest, S. R.; Thompson, M. E. *J. Am. Chem. Soc.* **2006**, *128*, 8108–8109.

[21] Pandey, A. K.; Nunzi, J. M. *Appl. Phys. Lett.* **2006**, *89*, 213506.

[22] Schulze, K.; Riede, M.; Brier, E.; Reinold, E.; Bäuerle, P.; Leo, K. *J. Appl. Phys.* **2008**, *104*, 074511.

[23] Schulze, K.; Uhrich, C.; Schüppel, R.; Leo, K.; Pfeiffer, M.; Brier, E.; Reinold, E.; Bäuerle, P. *Adv. Mater.* **2006**, *18*, 2872–2875.

[24] Uhrich, C.; Schüppel, R.; Petrich, A.; Pfeiffer, M.; Leo, K.; Brier, E.; Kilickiran, P.; Bäuerle, P. *Adv. Funct. Mater.* **2007**, *17*, 2991–2999.

[25] Mishra, A.; Ma, C. Q.; Bäuerle, P. *Chem. Rev.* **2009**, *109*, 1141–1276.

[26] Luhman, W. A.; Holmes, R. J. *Appl. Phys. Lett.* **2009**, *94*, 153304.

[27] Janssen, R. A. J.; Hummelen, J. C.; Sariiftci, N. S. *MRS Bull.* **2005**, *30*, 33–36.

[28] Pfuetzner, S.; Meiss, J.; Petrich, A.; Riede, M.; Leo, K. *Appl. Phys. Lett.* **2009**, *94*, 223307.

[29] Hummelen, J. C.; Knight, B. W.; LePeq, F.; Wudl, F.; Yao, J.; Wilkins, C. L. *J. Org. Chem.* **1995**, *60*, 532–538.

[30] Troshin, P. A.; Hoppe, H.; Renz, J.; Egginger, M.; Mayorova, J. Y.; Goryachev, A. E.; Peregudov, A. S.; Lyubovskaya, R. N.; Gobsch, G.; Sariciftci, N. S.; Razumov, V. F. *Adv. Funct. Mater.* **2009**, *19*, 779–788.

[31] Chesterfield, R. J.; McKeen, J. C.; Newman, C. R.; Ewbank, P. C.; da Silva Filho, D. A.; Brédas, J. L.; Miller, L. L.; Mann, K. R.; Frisbie, C. D. *J. Phys. Chem. B* **2004**, *108*, 19281–19292.

[32] Li, J.; Dierschke, F.; Wu, J.; Grimsdale, A. C.; Müllen, K. *J. Mater. Chem.* **2006**, *16*, 96–100.

[33] Jurchescu, O. D.; Subramanian, S.; Kline, R. J.; Hudson, S. D.; Anthony, J. E.; Jackson, T. N.; Gundlach, D. J. *Chem. Mater.* **2008**, *20*, 6733–6737.

[34] Kline, J. R; McGehee, M. D; Kadnikova, E. N.; Liu, J.; Fréchet, J. M. J. *Adv. Mater.* **2003**, *15*, 1519–1522.

[35] Kline, J. R.; DeLongchamp, D. M.; Fischer, D. A.; Lin, E. K.; Heeney, M.; McCulloch, I.; Toney, M. F. *Appl. Phys. Lett.* **2007**, *90*, 062117.

[36] Ballantyne, A. M.; Chen, L.; Dane, J.; Hammant, T; Braun, F. M.; Heeney, M.; Duffy, W.; McCulloch, I.; Bradley, D. D. C.; Nelson, J. *Adv. Funct. Mater.* **2008**, *18*, 2373–2380.

[37] Campbell, A. J.; Bradley, D. D. C.; Antoniadis, H. *Appl. Phys. Lett.* **2001**, *79*, 2133–2135.

[38] McNeill, C. R.; Abrusci, A.; Zaumseil, J.; Wilson, R.; McKiernan, M. J.; Burroughes, J. H.; Halls, J. J. M.; Greenham, N. C.; Friend, R. H. *Appl. Phys. Lett.* **2007**, *90*, 193506.

[39] Chen, L. C.; Godovsky, D.; Inganäs, O.; Hummelen, J C.; Janssen, R. A. J.; Svensson, M.; Andersson, M. R. *Adv. Mater.* **2000**, *12*, 1367–1370.

[40] Xue, L.; Liu, L.; Gao, Q.; Wen, S.; He, J.; Tian, W. *Sol. Energ. Mat. Sol. C.* **2009**, *93*, 501–507.

[41] Shaheen, S. E.; Brabec, C. J.; Sariciftci, N. S.; Padinger, F.; Fromherz, T.; Hummelen, J. C. *Appl. Phys. Lett.* **2001**, *78*, 841–843.

[42] Tuladhar, S. M.; Sims, M.; Choulis, S. A.; Nielsen, C. B.; George, W. N.; Steinke, J. H. G.; Bradley, D. D. C.; Nelson, J. *Org. Electron.* **2009**, *10*, 562–567.

[43] Padinger, F.; Rittberger, R. S.; Sariciftci, N. S. *Adv. Funct. Mater.* **2003**, *13*, 85–88.

[44] Roncali, J. *Chem. Rev.* **1997**, *97*, 173–205.

[45] Mühlbacher, D. Scharber, M.; Morana, M.; Zhu, Z.; Waller, D.; Gaudiana, R.; Brabec, C. J. *Adv. Mater.* **2006**, *18*, 2884–2889.

[46] Svensson, M.; Zhang, F.; Veenstra, S. C; Verhees, W. J. H.; Hummelen, J. C.; Kroon, J. M.; Inganäs, O.; Andersson, M. R. *Adv. Mater.* **2003**, *15*, 988–991.

[47] Zhang, F.; Manno, W.; Andersson, I. M.; Admassie, S.; Andersson, M. R.; Inganäs, O. *Adv. Mater.* **2006**, *18*, 2169–2173.

[48] Wienk, M. M.; Turbiez, M. G. R.; Struijk, M. P.; Fonrodoan, M.; Janssen, R. A. J. *Appl. Phys. Lett.* **2006**, *88*, 153511.

[49] Dhanabalan, A.; van Duren, J. K. J.; van Hal, P. A.; van Dongen, J. L. J.; Janssen, R. A. J. *Adv. Funct. Mater.* **2001**, *11*, 255–262.

[50] Wang, X.; Perzon, E.; Delgado, J. L.; de la Cruz, P.; Zhang, F.; Langa, F.; Andersson, M. R.; Inganäs, O. *Appl. Phys. Lett.* **2004**, *85*, 5081–5083.

[51] Wang, X.; Perzon, E.; Oswald, F.; Langa, F.; Admassie, S.; Andersson, M. R.; Inganäs, O. *Adv. Mater.* **2005**, *15*, 1665–1670.

[52] Xia, Y.; Wang, L.; Deng, X.; Li, D.; Zhu, X.; Cao, Y. *Appl. Phys. Lett.* **2006**, *89*, 081106.

[53] Kim, J. Y.; Qin, Y.; Stevens, D. M.; Ugurlu, O.; Kalihari, V.; Hillmyer, M. A.; Frisbie, C. D. *J. Phys. Chem. C* **2009**, *113*, 10790–10797.

[54] Qin, Y.; Hillmyer, M. A. *Macromolecules* **2009**, in press.

[55] Moulé, A. J.; Allard, S.; Kronenberg, N. M.; Tsami, A.; Scherf, U.; Meerholz, K. *J. Phys. Chem. C* **2008**, *112*, 12583–12589.

[56] Sun, Q.; Park, K.; Dai, L. *J. Phys. Chem. C* **2009**, *113*, 7892–7897.

[57] Granström, M.; Petritsch, K.; Arias, A. C.; Lux, A.; Andersson, M. R.; Friend, R. H. *Nature* **1998**, *395*, 257–260.

[58] Yu, G.; Heeger, A. J. *J. Appl. Phys.* **1995**, *78*, 4510–4515.

[59] Koetse, M. M.; Sweelssen, J.; Hoekerd, K. T.; Schoo, H. F. M.; Veenstra, S. C.; Kroon, J. M.; Yang, X.; Loos, J. *Appl. Phys. Lett.* **2006**, *88*, 083504.

[60] Lindner, S. M.; Thelakkat, M. *Macromolecules* **2004**, *37*, 8832–8835.

[61] Sommer, M.; Hüttner, S.; Wunder, S.; Thelakkat, M. *Adv. Mater.* **2008**, *13*, 2523–2527.

[62] Zhan, X.; Tan, Z.; Domercq, B.; An, Z.; Zhang, X.; Barlow, S.; Li, Y.; Zhu, D.; Kippelen, B.; Marder, S. R. *J. Am. Chem. Soc.* **2007**, *129*, 7246–7247.

[63] Yan, H.; Chen, Z.; Zheng, Y.; Newman, C.; Quinn, J. R.; Dötz, F.; Kastler, M.; Facchetti, A. *Nature* **2009**, *457*, 679–686.

[64] de Boer, B.; Stalmach, U.; van Hutten, P. F.; Melzer, C.; Krasnikov, V. V.; Hadziioannou, G. *Polymer* **2001**, *42*, 9097–9109.

[65] van der Veen, M. H.; de Boer, B.; Stalmach, U.; van de Wetering, K. I.; Hadziioannou, G. *Macromolecules* **2004**, *37*, 3673–3684.

[66] Hadziioannou, G. *MRS Bull.* **2002**, *27*, 456–460.

[67] Roncali, J. *Chem. Soc. Rev.* **2005**, *34*, 483–495.

[68] Cravino, A. *Polym. Int.* **2007**, *56*, 943–956.

[69] van Hall, P. A.; Knol, J.; Langeveld-Voss, B. M. W.; Meskers, S. C. J.; Hummelen, J. C.; Janssen, R. A. J. *J. Phys. Chem. A* **2000**, *104*, 5974–5988.

[70] Narutaki, M.; Takimiya, K.; Otsubo, T.; Harima, Y.; Zhang, H.; Araki, Y.; Ito, O. *J. Org. Chem.* **2006**, *71*, 1761–1768.

[71] Fernández, G.; Sánchez, L.; Veldman, D.; Wienk, M. M.; Atienza, C.; Guldi, D. M.; Janssen, R. A. J.; Martín, N. *J. Org. Chem.* **2008**, *73*, 3189–3196.

[72] Baffreau, J.; Ordronneau, L.; Leroy-Lhez, S.; Hudhomme, P. *J. Org. Chem.* **2008**, *73*, 6142–6147.

[73] Li, W. S.; Yamamoto, Y.; Fukushima, T.; Saeki, A.; Seki, S.; Tagawa, S.; Masunaga, H.; Sasaki, S.; Takata, M.; Aida, T. *J. Am. Chem. Soc.* **2008**, *130*, 8886–8887.

[74] Ouhib, F.; Khoukh, A.; Ledeuil, J-B.; Martinez, H.; Desbrières, J.; Dagron-Lartigau, C. *Macromolecules* **2008**, *41*, 9736–9743.

[75] Stalmach, U.; de Boer, B.; Videlot, C.; van Hutten, P. F.; Hadziioannou, G. *J. Am. Chem. Soc.* **2000**, *122*, 5464–5472.

[76] Richard, F.; Brochon, C.; Leclerc, N.; Eckhardt, D.; Heiser, T.; Hadziioannou, G. *Macromol. Rapid Commun*. **2008**, *29*, 885–891.

[77] Marcos-Ramos, A.; Rispens, M. T.; van Duren, J. K. J.; Hummelen, J. C.; Janssen, R. A. J. *J. Am. Chem. Soc.* **2001**, *123*, 6714–6715.

[78] Sivula, K.; Ball, Z. T.; Watanabe, N.; Fréchet, J. M. J. *Adv. Mater.* **2006**, *18*, 206–210.

[79] Sommer, M.; Lang, A. S.; Thelakkat, M. *Angew. Chem., Int. Ed.* **2008**, *47*, 7901–7904.

[80] Zhang, Q.; Cirpan, A.; Russell, T. P.; Emrick, T. *Macromolecules* **2009**, *42*, 1079–1082.

[81] Boudouris, B. W.; Molins, F.; Blank, D. A.; Frisbie, C. D.; Hillmyer, M. A. *Macromolecules* **2009**, *42*, 4118–4126.

[82] Kazmerski, L. L. *J. Electron Spectrosc. Relat. Phenom.* **2006**, *150*, 105–135.

[83] Shevaleevskiy, O. *Pure Appl. Chem.* **2008**, *80*, 2079–2089.

[84] Konarka Power Plastic. http://konarka.com/index.php (June 2009), Konarka Technologies website.

[85] Li, G.; Shrotriya, V.; Huang, J.; Yao, Y.; Moriarty, T.; Emery, K.; Yang, Y. *Nat. Mater.* **2005**, *4*, 864–868.

[86] Ma, W.; Yang, C.; Gong, X.; Lee, K.; Heeger, A. J. *Adv. Funct. Mater.* **2005**, *15*, 1617–1622.

[87] Park, S. H.; Roy, A.; Beaupré, S.; Cho, S.; Coates, N.; Moon, J. S.; Moses, D.; Leclerc, M.; Lee, K.; Heeger, A. J. *Nat. Photonics* **2009**, *3*, 297–303.

[88] Brabec, C. J.; Hauch, J. A.; Schilinsky, P.; Waldauf, C. *MRS Bull.* **2005**, *30*, 50–52.

[89] Thekaekara, M. P. *Suppl. Proc. 20th Annu. Meet. Inst. Environ. Sci.* **1974**, 21.

[90] Solar Spectral Irradiance: Air Mass 1.5. http://rredc.nrel.gov/solar/spectra/am1.5/ (June 2009), National Renewable Energy Laboratory (NREL) website.

[91] Shrotriya, V.; Li, G.; Yao, Y.; Moriarty, T.; Emery, K.; Yang, Y. *Adv. Funct. Mater.* **2006**, *16*, 2016–2023.

[92] Shockley, W. *Bell Syst. Tech. J.* **1949**, *28*, 435.

[93] Lambert, J. B.; Shurvell, H. F.; Lightner, D. A.; Cooks, R. G. *Organic Structural Spectroscopy*; Prentice Hall: Upper Saddle River, NJ, 1998.

[94] *Principal Conclusions of the American Physical Society Study Group on Solar Photovoltaic Energy Conversion*, American Physical Society, New York, 1979.

[95] Mott, N. F. *Contemp. Phys.* **1969**, *10*, 125–138.

[96] Le Comber, P. G.; Spear, W. E. *Phys. Rev. Lett.* **1970**, *25*, 509–511.

[97] Vissenberg, M. C. J. M.; Matters, M. *Phys. Rev. B* **1998**, *57*, 12964–12967.

[98] Horowitz, G.; Hajlaoui, M. E.; Hajlaoui, R. *J. Appl. Phys.* **2000**, *87*, 4456–4463.

[99] Gregg, B. A.; Hanna, M. C. *J. Appl. Phys.* **2003**, *93*, 3605–3614.

[100] Gregg, B. A. *MRS Bull.* **2005**, *30*, 20–22.

[101] Simon, J. *Molecular Semiconductors*; Springer-Verlag: Berlin, Germany, 1985.

[102] Gregg, B. A.; Fox, M. A.; Bard, A. J. *J. Phys. Chem.* **1990**, *94*, 1586–1598.

[103] Pope, M.; Swenberg, C. E. *Electronic Processes in Organic Crystals and Polymers*; Oxford University Press: New York, NY, 1999.

[104] Kenkre, V. M.; Parris, P. E.; Schmidt, D. *Phys. Rev. B* **1985**, *32*, 4946–4955.

[105] Zakhidov, A. A.; Yoshino, K. *Synth. Met.* **1994**, *64*, 155–165.

[106] Gregg, B. A.; Sprague, J.; Peterson, M. *J. Phys. Chem. B* **1997**, *101*, 5362–5369.

[107] Tong, X.; Bailey-Salzman, R. F.; Wei, G.; Forrest, S. R. *Appl. Phys. Lett.* **2008**, *93*, 173304.

[108] Ameri, T.; Dennler, G.; Waldauf, C.; Denk, P.; Forberich, K.; Scharber, M. C.; Brabec, C. J.; Hingerl, K. *J. Appl. Phys.* **2008**, *103*, 084506.

[109] Meiss, J.; Riede, M. K.; Leo, K. *J. Appl. Phys.* **2009**, *105*, 063108.

[110] Scharber, M. C.; Mühlbacher, D.; Koppe, M.; Denk, P.; Walduf, C.; Heeger, A. J.; Brabec, C. J. *Adv. Mater.* **2006**, *18*, 789–794.

[111] Peumans, P.; Bulovic, V.; Forrest, S. R. *Appl. Phys. Lett.* **2000**, *76*, 2650–2652.

[112] Peumans, P.; Forrest, S. R. *Appl. Phys. Lett.* **2001**, *79*, 126–128.

[113] Xue, J.; Rand, B. P.; Uchida, S.; Forrest, S. R. *Adv. Mater.* **2005**, *17*, 66–71.

[114] Xue, J.; Rand, B. P.; Uchida, S; Forrest, S. R. *J. Appl. Phys.* **2005**, *98*, 124903.

[115] Moon, J. S.; Lee, J. K.; Cho, S.; Byun, J.; Heeger, A. J. *Nano Lett.* **2009**, *9*, 230–234.

[116] Morteani, A. C.; Sreearunothai, P.; Herz, L. M.; Friend, R. H.; Silva, C. *Phys. Rev. Lett.* **2004**, *92*, 247402.

[117] Huang, Y.; Westenhoff, S.; Avilov, I.; Sreearunothai, P.; Hodgkiss, J. M.; Deleener, C.; Friend, R. H.; Belijonne, D. *Nat. Mater.* **2008**, *7*, 483–489.

[118] Peet, J.; Senatore, M. L.; Heeger, A. J.; Bazan, G. C. *Adv. Mater.* **2009**, *21*, 1521–1527.

[119] Kim, Y.; Choulis, S. A.; Nelson, J.; Bradley, D. D. C.; Cook, S.; Durrant, J. R. *J. Mater. Sci.* **2005**, *40*, 1371–1376.

[120] Clarke, T. M.; Ballantyne, A. M.; Nelson, J.; Bradley, D. D. C.; Durrant, J. R. *Adv. Funct. Mater.* **2008**, *18*, 4029–4035.

[121] Miller, S.; Fanchini, G.; Lin, Y. Y.; Li, C.; Chen, C. W.; Su, W. F.; Chhowalla, M. *J. Mater. Chem.* **2008**, *18*, 306–312.

[122] Gregg, B. A.; Kim, Y. I. *J. Phys. Chem.* **1994**, *98*, 2412–2417.

[123] Brabec, C. J.; Cravino, A.; Meissner, D.; Sariciftci, N. S.; Fromherz, T.; Rispens, M. T; Sanchez, L.; Hummelen, J. C. *Adv. Funct. Mater.* **2001**, *11*, 374–380.

[124] Gadisa, A.; Svensson, M.; Andersson, M. R.; Inganäs, O. *Appl. Phys. Lett.* **2004**, *84*, 1609–1611.

[125] Liu, J.; Shi, Y.; Yang, Y. *Adv. Funct. Mater.* **2001**, *11*, 420–424.

[126] Stevens, D. M.; Qin, Y.; Hillmyer, M. A.; Frisbie, C. D. *J. Phys. Chem. C* **2009**, *113*, 11408–11415.

[127] Li, N.; Lassiter, B. E.; Lunt, R. R.; Wei, G.; Forrest, S. R. *Appl. Phys. Lett.* **2009**, *94*, 023307.

[128] Frohne, H.; Shaheen, S. E.; Brabec, C. J.; Müller, D. C.; Sariciftci, N. S.; Meerholz, K. *Chem. Phys. Chem.* **2002**, *3*, 795–799.

[129] Cattin, L.; Dahou, F.; Lare, Y.; Morsli, M.; Tricot, R.; Houari, S.; Mokrani, A.; Jondo, K.; Khelil, A.; Napo, K.; Bernede, J. C. *J. Appl. Phys.* **2009**, *105*, 034507.

[130] Ouyang, J.; Chu, C. W.; Chen, F. C.; Xu, Q.; Yang, Y. *Appl. Phys. Lett.* **2006**, *88*, 073508.

[131] Snaith, H. J.; Kenrick, H.; Chiesa, M.; Friend, R. H. *Polymer* **2005**, *46*, 2573–2578.

[132] Brabec, C. J.; Shaheen, S. E.; Winder, C.; Sariciftci, N. S. *Appl. Phys. Lett.* **2002**, *80*, 1288–1290.

[133] Reese, M. O.; White, M. S.; Rumbles, G.; Ginley, D. S.; Shaheen, S. E. *Appl. Phys. Lett.* **2008**, *92*, 053307.

[134] Kim, J. Y.; Kim, S. H.; Lee, H. H.; Lee, K.; Ma, W.; Gong, X.; Heeger, A. J. *Adv. Mater.* **2006**, *18*, 572–576.

[135] Rand, B. P.; Peumans, P.; Forrest, S. R. *J. Appl. Phys.* **2004**, *85*, 5757–5759.

[136] Ameri, T.; Dennler, G.; Lungenschmied, C.; Brabec, C. J. *Energ. Environ. Sci.* **2009**, *2*, 347–363.

[137] Peumans, P.; Yakimov, A.; Forrest, S. R. *J. Appl. Phys.* **2003**, *93*, 3693–3723.

[138] Lipomi, D. J.; Chiechi, R. C.; Reus, W. F.; Whitesides, G. M. *Adv. Funct. Mater.* **2008**, *18*, 3469–3477.

[139] Miyanishi, S.; Tajima, K.; Hashimoto, K. *Macromolecules* **2009**, *42*, 1610–1618.

[140] Greenham, N. C.; Moratti, S. C.; Bradley, D. D. C.; Friend, R. H.; Holmes, A. B. *Nature* **1993**, *365*, 628–630.

[141] Erb, T.; Zhokhavets, U.; Gobsch, G.; Raleva, S.; Stühn, B.; Schilinsky, P.; Waldauf, C.; Brabec, C. J. *Adv. Funct. Mater.* **2005**, *15*, 1193–1196.

[142] Zhong, H.; Yang, X.; deWith, B.; Loos, J. *Macromolecules* **2006**, *39*, 218–223.

[143] Müller, C.; Ferenczi, T. A. M.; Campoy-Quiles, M.; Frost, J. M.; Bradley, D. D. C.; Smith, P.; Stingelin-Stutzmann, N.; Nelson, J. *Adv. Mater.* **2008**, *20*, 3510–3515.

[144] Kim, J. Y.; Frisbie, C. D. *J. Phys. Chem. C* **2008**, *112*, 17726–17736.

[145] Ball, Z. T.; Sivula, K.; Fréchet, J. M. J. *Macromolecules* **2006**, *39*, 70–72.

[146] Lee, J. K.; Ma, W. L.; Brabec, C. J.; Yuen, J.; Moon, J. S.; Kim, J. Y.; Lee, K.; Bazan, G. C.; Heeger, A. J. *J. Am. Chem. Soc.* **2008**, *130*, 3619–3623.

[147] Coates, N. E.; Hwang, I. W.; Peet, J.; Bazan, G. C; Moses, D.; Heeger, A. J. *Appl. Phys. Lett.* **2008**, *93*, 072105.

[148] Watkins, P. K.; Walker, A. B.; Verschoor, G. L. B. *Nano Lett.* **2005**, *5*, 1814–1818.

[149] Yang, F.; Forrest, S. R. *ACS Nano* **2008**, *2*, 1022–1032.

[150] Coakley, K. M.; Liu, Y.; McGehee, M. D.; Frindell, K. L.; Stuckey, G. D. *Adv. Funct. Mater.* **2003**, *13*, 301–306.

[151] Coakley, K. M.; McGehee, M. D. *Appl. Phys. Lett.* **2003**, *83*, 3380–3382.

[152] Kuo, C. Y.; Tang, W. C.; Gau, C.; Guo, T. F.; Jeng, D. Z. *Appl. Phys. Lett.* **2008**, *93*, 033307.

[153] Hampton, M. J.; Williams, S. S.; Zhou, Z.; Nunes, J.; Ko, D. H.; Templeton, J. L.; Samulski, E. T.; DeSimone, J. M. *Adv. Mater.* **2008**, *20*, 2667–2673.

[154] Williams, S. S.; Hampton, M. J.; Gowrishankar, V.; Ding, I. K.; Templeton, J. L.; Samulski, E. T.; DeSimone, J. M.; McGehee, M. D. *Chem. Mater.* **2008**, *20*, 5229–5234.

[155] Olson, D. C.; Piris, J.; Collins, R. T.; Shaheen, S. E.; Ginley, D. S. *Thin Solid Films* **2005**, *496*, 26–29.

[156] Olson, D. C.; Shaheen, S. E.; Collins, R. T.; Ginley, D. S. *J. Phys. Chem. C* **2007**, *111*, 16670–16678.

[157] Olson, D. C.; Lee, Y. J.; White, M. S.; Kopidakis, N.; Shaheen, S. E.; Ginley, D. S.; Voigt, J. A.; Hsu, J. W. P. *J. Phys. Chem. C* **2008**, *112*, 9544–9547.

[158] Monson, T. C.; Lloyd, M. T.; Olson, D. C.; Lee, Y. J.; Hsu, J. W. P. *Adv. Mater.* **2008**, *20*, 4755–4759.

[159] Lloyd, M. T.; Prasankumar, R. P.; Sinclair, M. B.; Mayer, A. C.; Olson, D. C.; Hsu, J. W. P. *J. Mater. Chem.* **2009**, *19*, 4609–4614.

[160] Xi, H.; Wei, Z.; Duan, Z.; Xu, W.; Zhu, D. *J. Phys. Chem. C* **2008**, *112*, 19934–19938.

[161] Boudouris, B. W.; Frisbie, C. D.; Hillmyer, M. A. *Macromolecules* **2008**, *41*, 67–75.

4 Nanoporous Poly(3-alkylthiophene) Thin Films Generated from Block Copolymer Templates[†]

4.1 Overview

We report the synthesis and characterization of a new series of rod-coil block copolymers, regioregular poly(3-alkylthiophene)-*b*-polylactide (P3AT-PLA), where the alkyl chain in the polythiophene moiety is either six or twelve carbons in length. After utilizing a controlled polymerization technique to synthesize end-functionalized P3AT, these polymers were used as macroinitiators for the controlled ring-opening polymerization (ROP) of D,L-lactide. The block copolymers were characterized by ^{1}H NMR spectroscopy, size exclusion chromatography (SEC), differential scanning calorimetry (DSC), thermogravimetric analysis (TGA), wide-angle x-ray scattering (WAXS), ultraviolet-visible (UV-Vis) light spectroscopy, and atomic force microscopy (AFM). In thin films of these materials (ca. 35 nm thickness), microphase separated domains are formed while the crystallinity of the P3AT majority phase is maintained. Upon chemical etching of the PLA block, we observed a nanopitted film where the crystallinity of the P3AT phase remains; characteristic pits are on the order of 35 nm in diameter with depths of up to 10 nm. The increase in the exposed surface area of the semiconducting polymer (~150% that of the planar film) could be useful in a variety of organic electronic applications.

4.2 Introduction

Poly(3-alkylthiophenes) (P3ATs) have garnered much attention in the organic electronics community due to their high charge transport performance, their chemically tunable electronic properties, and their processability from a variety of solvents.[1-3] Poly(3-alkylthiophenes) are among the leading polymer semiconductors for application in organic field-effect transistors (OFETs),[4-6] volatile organic chemical (VOC)

[†] Reproduced with permission from B. W. Boudouris, C. D. Frisbie, and M. A. Hillmyer, *Macromolecules* **2008**, *41*, 67–75. Copyright 2008 American Chemical Society.

sensors,[7,8] and plastic solar cells.[9-14] Optimizing performance for these applications necessitates precise control of thin film structure,[15-17] and the use of molecular design to control polythiophene thin film morphology continues to be an active area of research. In this report we describe a novel class of polythiophene-containing block copolymers that can produce a nanoporous P3AT film structure.

Theoretical studies[18-20] have predicted and experimental efforts[21-25] have demonstrated that thin films of diblock copolymers can self-assemble into many types of well-ordered nanostructures on a variety of substrates after being cast from a number of solvents. In most of these cases, both segments of the diblock copolymer contain single-bond carbon-carbon backbone repeat units and thus are considered flexible (or coil-like) in the melt.[26] By selecting the appropriate components of the diblock system, selective etching of the minority phase can lead to nanoporous materials that are useful for applications ranging from separations to templates for nanolithography.[27] In contrast to coil-coil diblock copolymer systems, some polymers contain more rigid backbone bonds that are deemed rod-like in nature, and these are found in many semiconducting polymers, including P3ATs. In a manner similar to their coil-like counterparts, the thermodynamic behavior of rod-coil systems has been investigated both theoretically[28-30] and experimentally.[31-34] While experimental efforts have focused on the phase behavior of rod-coil block copolymer systems and their potential uses in organic electronics applications,[35-44] specific efforts with P3AT block copolymer systems are more uncommon.[7,45-47] This is, in part, because only recently have the synthetic tools become available to generate well-defined P3AT-containing block copolymers.[48]

P3ATs have been traditionally synthesized by electrochemical[49] and oxidative[50,51] polymerizations. However, these resultant polymers tend to be ill-defined with large polydispersities and nonspecific end groups. Recently, the McCullough group showed that highly regioregular, low polydispersity P3ATs could be fabricated via the Grignard metathesis (GRIM) method[52] and that end groups could be controlled via a simple in situ end-capping procedure.[48,53] With the realization of end group control, block copolymers containing P3AT and a more coil-like segment (*e.g.*,

polystyrene and polymethylacrylate) have been prepared and tested in organic electronic devices.[45,46,54,55] The addition of the second block not only seems to have an effect on the crystallinity of the materials but also leads to new morphological behavior. Preliminary findings, however, have explored only a handful of insulating moieties and have shown little difference in the thin film microstructure upon changing the second block except in the case of poly(2-vinylpyridine).[46,47,55,56] By expanding the inventory of insulating blocks covalently bonded to the P3AT segment, a better understanding can be gained regarding how the chemical nature of the second block affects P3AT self-assembly. Furthermore, incorporating chemical functionality into the second block allows for the tailoring of thin films that could be useful for enhanced optoelectronic applications.

Polylactide (PLA) has been shown to be a biodegradable and versatile moiety in forming well-ordered block copolymer monoliths and thin films with a variety of morphologies.[57-59] Since the ester linkage in the flexible backbone of the PLA can be selectively etched via a gentle alkaline bath, nanoporous templates with pore sizes on the order of 20 nm can be generated readily in a variety of polymeric matrices without damaging the matrix material.[27,60,61] In P3AT-containing block copolymers, distinguishing the spatial regimes of the amorphous component of the P3AT block from the coil-like second block via direct imaging techniques can be difficult. By using a block that can be selectively etched, topological changes in the film before and after etching (*e.g.*, using atomic force microscopy) can be monitored and can help reveal the thin film structure.

In this paper we report the stepwise synthesis of poly(3-alkylthiophene)-*b*-polylactide block copolymers (P3AT-PLA) by the controlled polymerization of D,L-lactide[62-64] from hydroxyl-terminated poly(3-alkylthiophenes) (P3AT-OH) which form microphase separated thin films with domains on the order of 30 nm. The PLA can be selectively etched from the films leading to P3AT films with high porosities. Nanoporous P3AT films could lead to enhanced performance of organic electronic devices such as sensors and solar cells. For example, the porous-P3AT film could lead

to better sensitivity in detection of VOC vapors in field-effect transistor devices. Also, pitted P3AT block copolymer films could be backfilled with an electron-accepting material, such as buckminsterfullerene (C_{60}), and the enhanced P3AT/C_{60} contact may facilitate better exciton dissociation and charge collection in ordered bulk heterojunction solar cells.[65,66] These possibilities have motivated our efforts to develop strategies that lead to nanoporous P3AT films.

4.3 Experimental

General Methods. The ^{1}H NMR spectra were measured on a Varian VI-500 spectrometer using deuterated chloroform (Cambridge) solutions containing ~1 wt % polymer. Size exclusion chromatography (SEC) data were collected on a Hewlett-Packard 1100 series equipped with a Hewlett-Packard 1047A refractive index (RI) detector and three Jordi poly(divinylbenzene) columns of 10^4, 10^3, and 500 Å pore sizes. Tetrahydrofuran (THF) at 40 °C was used as the mobile phase at a flow rate of 1 mL/min and the SEC was calibrated with polystyrene standards (Polymer Laboratories). Differential scanning calorimetry (DSC) measurements were acquired using a TA Q1000 calorimeter. The samples were first annealed at 250 °C and then cooled to –50 °C at a rate of 10 °C/min. The results shown are for the final sample heating at a rate of 10 °C/min. An indium standard was used to calibrate the instrument and nitrogen was used as the purge gas. Thermogravimetric analysis (TGA) was performed with a Perkin Elmer TGA 7 in a nitrogen atmosphere with a heating rate of 10 °C/min. Wide-angle x-ray scattering (WAXS) data were collected in the diffraction angular range of 3–30° (2θ) by a Bruker-AXS D5005 microdiffractometer. The crystalline peaks were referenced from known reflection values[67] and deconvoluted using the curve-fitting software, JADE 7 (CMI). Film thicknesses were estimated by scratching the polymer film and measuring the step change with a KLA-Tencor P16 profilometer. Ultraviolet-visible (UV-Vis) light absorption spectra of polymer thin films were taken on a Spectronic Genesys 5 spectrometer over a wavelength range of 300–900 nm using a bare ITO-coated glass substrate as a blank. Atomic force microscopy (AFM) images

were taken with a Veeco Metrology Nanoscope IIIa microscope operating in tapping mode.

Materials. All reagents and solvents were used as received from Sigma-Aldrich unless otherwise noted. Degassed THF and toluene were purified by passage through an activated alumina column and were collected in flame-dried, air-free flasks. D,L-lactide was purified by recrystallization from ethyl acetate followed by drying under reduced pressure and was stored in an inert atmosphere glove box.

Synthesis of Hydroxyl-terminated Poly(3-alkylthiophene) (P3AT-OH). A modified method similar to that of the McCullough group was used for the synthesis of hydroxyl-terminated poly(3-alkylthiophene)s.[54] A typical polymerization is described for the hydroxyl-terminated poly(3-dodecylthiophene (P3DDT-OH) (Table 4.1). The polymerization was performed in a flame-dried 250 mL reaction flask containing a Teflon-coated magnetic stir bar. To the flask, ~150 mL of anhydrous THF was added via cannula. 2,5-dibromo-3-dodecylthiophene (6.6 g, 16 mmol) and a solution of 1 M *tert*-butylmagnesium chloride in THF (16 mL, 16 mmol) were added to the THF solvent under N_2. The reaction was placed in an oil bath and heated to reflux for 1.5 h. After cooling the solution to room temperature, 1,3-bis(diphenylphosphino)propane nickel (II) chloride [Ni(dppp)Cl_2] (0.098 g, 0.18 mmol) was added as a solid under N_2 and the reaction was allowed to stir for 1 h. A solution of 1 M vinylmagnesium bromide in THF (3 mL, 3 mmol) was added under N_2 and the reaction was allowed to stir for 1 h prior to precipitation in methanol. The polymer was collected and purified via Soxhlet extraction with methanol, hexane, and chloroform, sequentially. The concentrated chloroform fraction was precipitated in methanol and the vinyl-terminated poly(3-dodecylthiophene) (P3DDT-vinyl) was washed with methanol, collected, and dried overnight under reduced pressure.

The reaction to convert the P3DDT-vinyl end groups to hydroxyl end groups was carried out in a flame-dried 250 mL reaction flask containing a Teflon-coated magnetic stir bar. After flame-drying, 80 mL of anhydrous THF was added via cannula. P3DDT-vinyl (0.8 g, 0.06 mmol) and a 0.5 M solution of 9-borobicyclononane (9-BBN)

in THF (13 mL, 6.5 mmol) were added to the reaction flask under N_2. The flask was placed in an oil bath and heated to 45 °C for 24 h. At this point, 6 M NaOH in deionized water (8 mL, 48 mmol) was added to the reaction flask under N_2. The reaction was cooled to room temperature and a 30 wt % hydrogen peroxide aqueous solution (Mallinckrodt Chemicals, 8 mL) was added to the reaction flask. Heat was reapplied and the solution was allowed to stir at 45 °C for 24 h. The reaction was then cooled to room temperature and precipitated in methanol. The polymer was filtered, washed with methanol and deionized water, and dried under vacuum overnight.

Characterization of a representative **P3HT-OH**. ^{1}H NMR (500 MHz, $CDCl_3$): δ_H 0.9 (t, 3H), 1.3 (m, 6H), 1.7 (t, 2H), 2.8 (t, 2H), 3.0 (t, 2H), 3.9 (m, 2H), 6.9 (s, 48H); SEC: M_n: 12100, PDI: 1.3.

Characterization of a representative **P3DDT-OH**. ^{1}H NMR (500 MHz, $CDCl_3$): δ_H 0.9 (t, 3H), 1.3 (m, 18H), 1.7 (t, 2H), 2.8 (t, 2H), 3.0 (t, 2H), 3.9 (m, 2H), 6.9 (s, 50H); SEC: M_n: 18900, PDI: 1.3.

Synthesis of Poly(3-alkylthiophene)-*b*-Polylactide (P3AT-PLA). Macroinitiated ring-opening polymerizations of lactide are well-known, and we have used a method similar to one previously reported for the polymerization of lactide using hydroxyl-terminated polystyrene as the macroinitiator.[68] The details for the example polymerization of P3DDT(13)-PLA(2) are as follows. P3DDT-OH (0.161 g, 0.013 mmol) was dried under reduced pressure in a reaction flask at 110 °C for 24 hours. The flask was then sealed and transferred inside of a glove box where toluene (1.4 mL) was used to dissolve the P3DDT-OH. A solution of 1 M triethyl aluminum ($AlEt_3$) in toluene (13 μL, 0.013 mmol) was also added in order to have equal molar amounts of $AlEt_3$ and P3DDT-OH present to form the macroinitiator. The reaction was then sealed and brought outside the glove box to be placed in an oil bath at 90 °C for 16 h. At this point, the reaction mixture was cooled and transferred back inside the glove box and D,L-lactide (0.21 g, 1.4 mmol) was added. The reaction was capped and returned to the oil bath where it was heated at 90 °C for an additional 5 h. The reaction was cooled to room temperature, quenched with ~2 M HCl (1 mL, 2 mmol), and precipitated in

methanol. After filtering and washing with methanol, the polymer was dried overnight under vacuum.

Characterization of **P3HT(8)-PLA(1)**. ^{1}H NMR (500 MHz, $CDCl_3$): main chain P3HT peaks are the same as for **P3HT-OH** with δ_H 1.6 (m, 3H), 3.1 (t, 2H), 4.3 (m, 3H), 5.2 (m, 14H); SEC: M_n: 12500, PDI: 1.3.

Characterization of **P3HT(8)-PLA(3)**. ^{1}H NMR (500 MHz, $CDCl_3$): main chain P3HT peaks are the same as for **P3HT-OH** with δ_H 1.6 (m, 3H), 3.1 (t, 2H), 4.4 (m, 3H), 5.2 (m, 45H); SEC: M_n: 12900, PDI: 1.3.

Characterization of **P3HT(8)-PLA(31)**. ^{1}H NMR (500 MHz, $CDCl_3$): main chain P3HT peaks are the same as for **P3HT-OH** with δ_H 1.6 (m, 3H), 3.1 (t, 2H), 4.4 (m, 3H), 5.2 (m, 430H); SEC: M_n: 15000, PDI: 1.5.

Characterization of **P3DDT(13)-PLA(2)**. ^{1}H NMR (500 MHz, $CDCl_3$): main chain P3DDT peaks are the same as for **P3DDT-OH** with δ_H 1.6 (m, 3H), 3.1 (t, 2H), 4.4 (m, 3H), 5.2 (m, 27H); SEC: M_n: 21200, PDI: 1.4.

Characterization of **P3DDT(13)-PLA(3)**. ^{1}H NMR (500 MHz, $CDCl_3$): main chain P3DDT peaks are the same as for **P3DDT-OH** with δ_H 1.6 (m, 3H), 3.1 (t, 2H), 4.4 (m, 3H), 5.2 (m, 35H); SEC: M_n: 21900, PDI: 1.3.

P3AT Series Thin Film Preparation. Solutions of P3AT-OH and P3AT-PLA were made by dissolving 20 mg of polymer in 1 mL of 1,2-dichlorobenzne (DCB) and allowing the solutions to stir at 60 °C under inert atmosphere overnight. ITO-coated glass substrates (Delta Technologies) were sonicated for 10 min sequentially in acetone, chloroform, and isopropanol and dried with compressed N_2. Solutions were passed through a 0.45 μm syringe filter and spun-cast onto the substrates using the slow-drying technique developed by Li et al.[11] The solutions were deposited on the substrates and the rotation rate was increased from 0 to 700 rpm over the course of ~2 seconds and held at 700 rpm for 60 sec. The wet films were then transferred to a Petri dish and covered to allow for slow evaporation of the DCB, which led to drying times on the order of 1 h. After the films were dry, they were transferred into inert atmosphere and

annealed for 1 h at 165 °C. The thicknesses of all of the films, as measured by profilometry, were 37 ± 4 nm.

Etching of the P3AT Series Thin Films. As described previously, a 0.5 M solution of NaOH in water/methanol (60/40 v/v) was used to etch the PLA moiety from the block copolymer thin films.[57] The samples were etched for up to 72 h at room temperature and were then washed with deionized water and dried with compressed N_2. The removal of PLA was monitored by ^{1}H NMR spectroscopy.

4.4 Results and Discussion

Synthesis of P3AT-PLA. The new method for synthesizing P3AT block copolymers that contain PLA is shown in Figure 4.1. The first step in forming these block copolymers was to generate vinyl-terminated poly(3-alkylthiophene) homopolymers. These polymers were synthesized using the Grignard metathesis (GRIM) method and subsequent end-capping with vinyl magnesium bromide.[48] Soxhlet extractions can be used to fractionate P3ATs.[69,70] To remove small molecular weight polymers and any residual reagents from the polymerization reaction, the polymers were Soxhlet extracted with methanol, hexane, and chloroform in a sequential manner. In the chloroform fraction of the P3AT-vinyl polymers there was not complete addition of the vinyl group to the end of the polymer chains for the P3HT-vinyl (~92% functionality) and P3DDT-vinyl (~95% functionality) precursors. This causes a small amount of residual P3AT homopolymer to be present in all of the samples discussed below. The chloroform fraction of the vinyl-terminated polymers (P3AT-vinyl) was then converted to hydroxyl-terminated poly(3-alkylthiophenes) (P3AT-OH) via hydroboration and oxidation of the end group in a process similar to that described by the McCullough group.[54] The P3AT-OH homopolymers exhibited narrow molecular weight distributions ($M_w / M_n = 1.3$) by SEC (Table 4.1) which is typical for polymers synthesized via the GRIM method.[71] These P3AT-OH homopolymers were used as controls in the block copolymer thin film studies described below and were also the starting materials for the synthesis of P3AT-PLA.

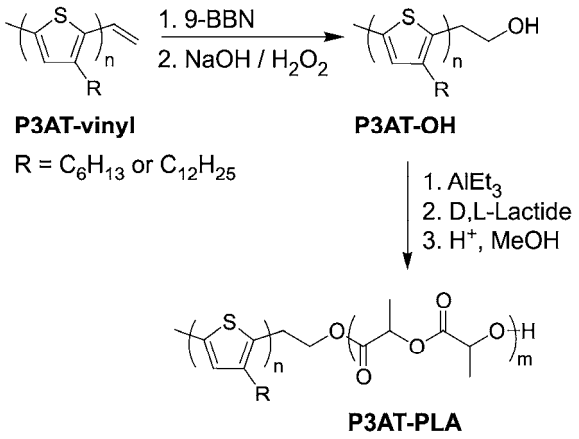

Figure 4.1. Synthetic scheme for the formation of P3AT-PLA diblock copolymers. The R group was either C_6H_{13} [poly(3-hexylthiophene)] or $C_{12}H_{25}$ [poly(3-dodecylthiophene)]

The use of aluminum alkoxide initiators to create polylactide with a narrow molecular weight distribution via ring-opening polymerizations (ROPs) has been studied previously.[62-64] In the current system, triethylaluminum was used to convert the P3AT-OH to the corresponding aluminum alkoxide macroinitiator. It was this macroinitiator that was used in the ring-opening polymerization of D,L-lactide to yield the atactic form of PLA.[72] By varying the conversion of lactide, the molecular weight of the PLA block was controlled (Table 4.1).

Table 4.1. Characterization of P3AT-PLA samples.

Sample[a]	M_n [b] (kg/mol) P3AT	M_n [b] (kg/mol) PLA	M_n (kg/mol) Total	M_w/M_n [c]	w_{PLA} [d]	T_g(°C) [e] P3AT	T_g(°C) [f] PLA	T_m(°C) P3AT	Crystallinity [g] (%)
P3HT-OH	8.0		8.0	1.3		–17		218	18
P3HT(8) - PLA(1)	8.0	0.9	8.9	1.3	0.10	–20	43	223	14
P3HT(8) - PLA(3)	8.0	3.2	11.2	1.3	0.29	–18	42	219	13
P3HT(8) - PLA(31)	8.0	31.0	39.0	1.5	0.79	–21	45	221	12
P3DDT-OH	12.5		12.5	1.3				158	52
P3DDT(13) - PLA(2)	12.5	1.7	14.2	1.4	0.12			149	28
P3DDT(13) - PLA(3)	12.5	2.5	15.0	1.3	0.17			152	26

[a] P3HT-OH is the homopolymer of the poly(3-hexylthiophene)-b-polylactide series symbolized by P3HT(X)-PLA(Y) where the P3HT has a molecular weight of X kg/mol and the PLA has a molecular weight of Y kg/mol. P3DDT-OH is the homopolymer of the poly(3-dodecylthiophene)-b-polylactide series symbolized by P3DDT(X)-PLA(Y) where the P3DDT has a molecular weight of X kg/mol and the PLA has a molecular weight of Y kg/mol. [b] As determined by ^{1}H NMR spectroscopy. [c] As determined by SEC versus polystyrene standards. [d] $w_{PLA} = M_n(\text{PLA}) / [M_n(\text{PLA}) + M_n(\text{P3AT})]$. [e] The glass transition temperature of P3DDT was not prominent enough to be observed in either the homopolymer or diblock copolymers of the series. [f] A broad peak associated with the side-chain melting of the P3DDT samples hindered the appropriate identification of the PLA glass transition temperature in the P3DDT series. [g] As determined by the ratio of the enthalpy of melting for the P3AT fraction of the sample relative to the infinite enthalpy of melting reported in the literature for the P3AT (see discussion in the text).

Molecular Characterization of P3AT-PLA. To observe the conversion of P3AT-vinyl to P3AT-OH and P3AT-OH to P3AT-PLA, ^{1}H NMR spectroscopy was used to monitor the resonances of the end groups associated with each of these three types of polymers. The molecular weights of the P3AT-OH homopolymers were determined by ^{1}H NMR spectroscopy using end group analysis, and these molecular weights were used in all further computations. Calculations were based on NMR determined molecular weights due to the fact that SEC calculated molecular weights of rod-like polymers (specifically polythiophenes) versus polystyrene standards can overestimate the true molecular weight of the polymer by over a factor of 2.[73] By observing the chemical shifts and splitting patterns in the spectra we are able to see full conversions of the P3AT-OH to P3AT-PLA (Figure 4.2). In both the P3HT and P3DDT cases, there is a clear shift of both of the methylene resonances (a and b in Figure 4.2) upon the addition of polylactide along with the appearance of resonances associated

with the terminal repeat unit of the PLA moiety. The presence of peaks at 3.0 ppm and 3.9 ppm for the P3AT-OH end groups were in good agreement with previous reports.[54] The appearance of the peak at 4.4 ppm upon the addition of PLA was consistent with the terminal lactide repeat unit and appears at the same chemical shift as the methylene protons between the P3AT and PLA chains (b in Figure 4.2).[74] Additionally, integration of the area under the end group peaks before and after lactide polymerizations were in good agreement with the predicted structures.

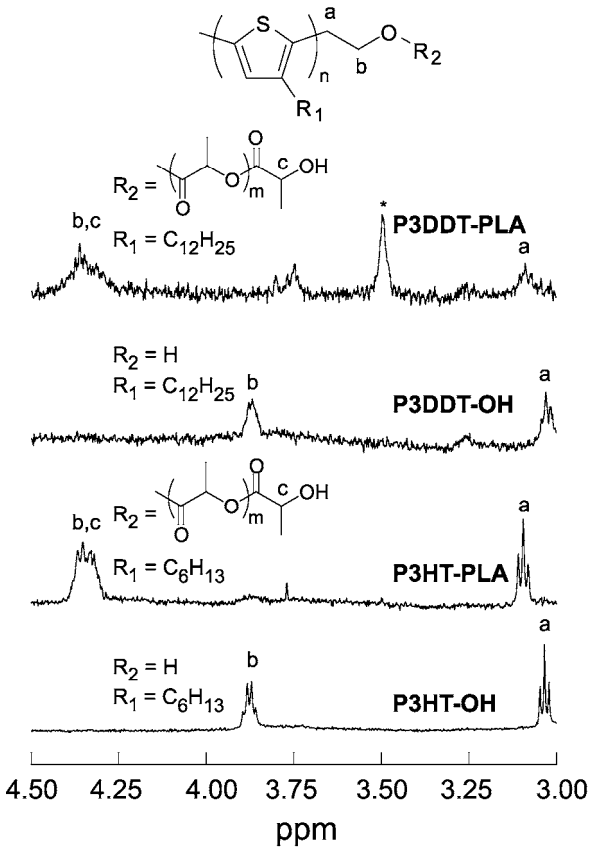

Figure 4.2. ^{1}H NMR spectra of P3HT-OH and a representative block copolymer for the P3HT-PLA series along with the ^{1}H NMR spectra of P3DDT-OH and a representative block copolymer for the P3DDT-PLA series. All polymers were dissolved in $CDCl_3$. The * at ~3.5 ppm in the P3DDT-PLA spectrum is a signal due to residual methanol present in the sample.

Figure 4.3 shows the entire ^{1}H NMR spectra of a representative P3AT-PLA block copolymer with the resonances of backbone atoms in PLA (b and c). The areas

under these peaks were integrated and the relative intensities were compared with the already determined main-chain resonances associated with the P3AT segment (a) to gauge the molecular weight of the PLA segment. Due to the relatively high molecular weight of P3AT present in this sample, the end group peaks shown in Figure 4.2 are not clearly visible in the full ^{1}H NMR spectrum.

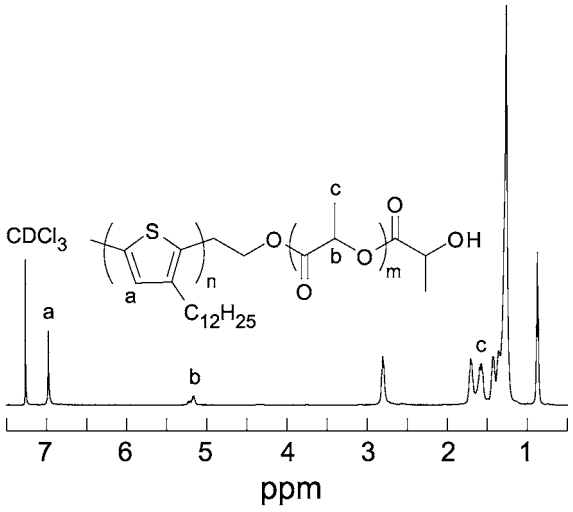

Figure 4.3. ^{1}H NMR spectrum of a representative block copolymer, P3DDT(13)-PLA(2), in $CDCl_3$. The unlabeled peaks upfield of 3.5 ppm are associated with the dodecyl side chain of this polymer.

The molecular weight distributions of the homopolymer and diblock copolymer materials were evaluated by SEC, and the results show a general trend of constant or slightly increasing polydispersity with the length of the PLA chain. This is consistent with the concepts of the equilibrium polymerization and growing polydispersities with growing reactions times for the PLA moiety.[75] In addition to monitoring the polydispersities of the block copolymers SEC traces show clear, monomodal distributions after the addition of the PLA block, reaffirming the results offered by end group integration, which suggest all PLA present in the samples is covalently bound to the P3AT chains (see Figure 4.4). We believe the small shift in elution volume reflects the rod-coil nature of P3AT-PLA type polymers. Since the addition of a short, flexible PLA block only slightly impacts the overall hydrodynamic volume of the rather rigid and bulky P3AT segment, shifts in retention volume are smaller than would be expected

for a coil-coil system but are still clear and consistently shifted to lower elution volumes as the molecular weight of the PLA moiety is increased.

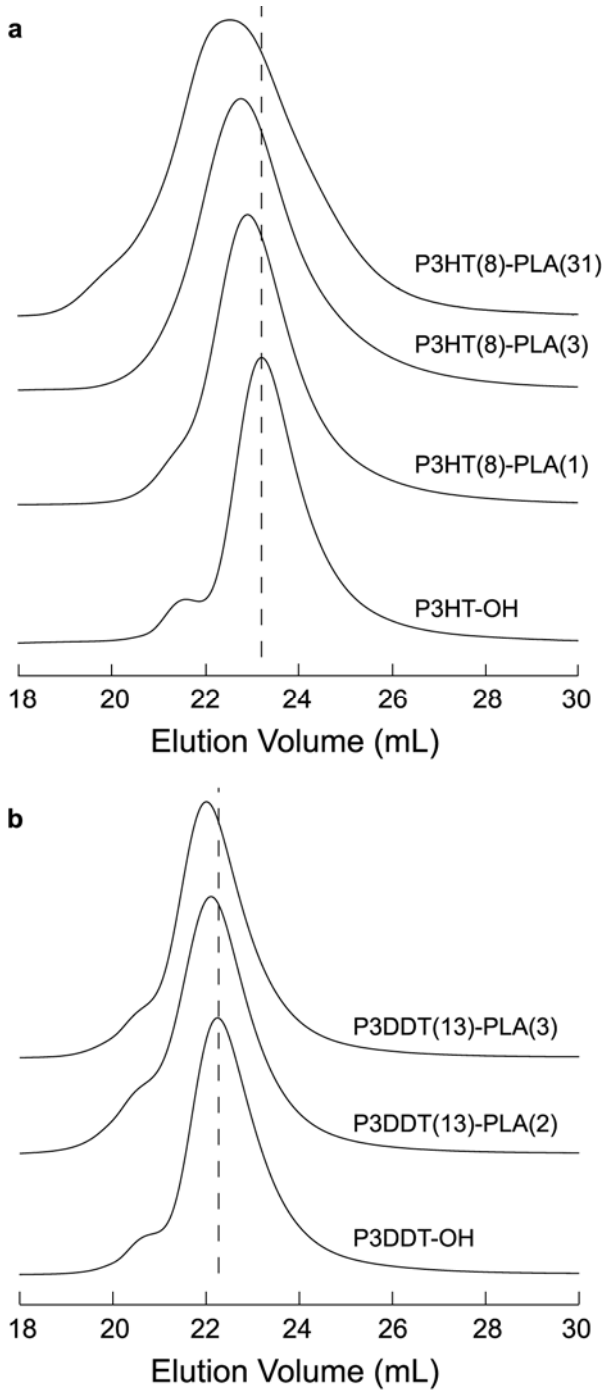

Figure 4.4. SEC traces of the (a) P3HT-PLA series and (b) P3DDT-PLA series with THF as the mobile phase. Dashed lines are guides for the eye through the apex of the SEC trace of the P3AT homopolymer chromatogram.

Thermal characterization of P3HT-PLA. The polymers were subjected to DSC analysis in order to observe the melting points and glass transitions of the materials, gauge the crystallinity of the P3AT segments, and verify the presence of microphase separated domains. The appearance of distinct glass transition temperatures for P3HT (T_g ~ –20 °C) and PLA (T_g ~43 °C) (Figure 4.5), which are consistent with literature values, support P3AT-PLA microphase separation.[76-78] The amount of polymer that was crystalline in the sample was determined by integrating the area under the melting peak in each of the three samples, normalizing the values by the amount of P3HT present in the sample, and comparing this with the literature value for the enthalpy of fusion for an ideal P3HT crystal, ΔH_m^{∞} = 99 J/g.[79] Since the atactic PLA is prevented from being included in the crystalline matrix, the existence of PLA in the block copolymer slightly lowers the amount of crystallinity in the diblock copolymers versus the homopolymer (see Table 4.1). One concern observed during the course of these measurements was the relatively high melting temperature (T_m ~220 °C) of the P3HT segment.[79-81] Previous reports have indicated that thermal degradation of PLA occurs at or below 220 °C.[57]

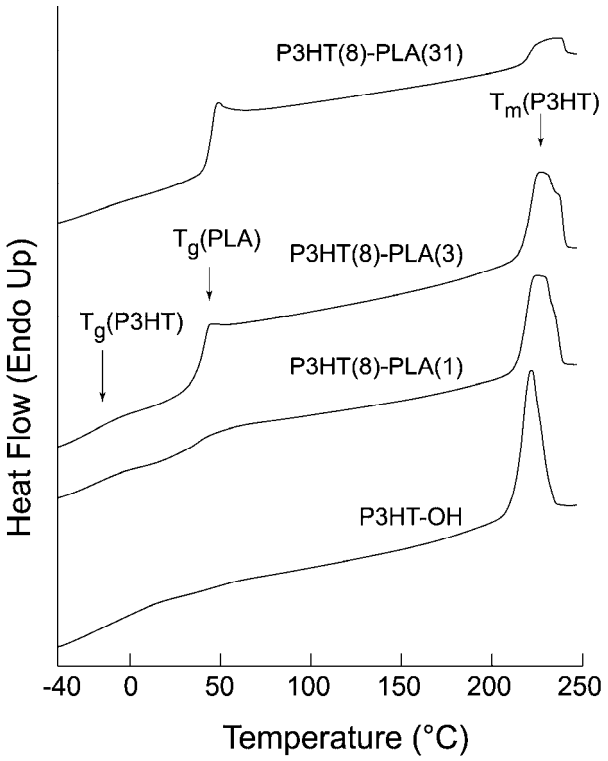

Figure 4.5. DSC traces of P3HT-PLA series at 10 °C/min showing the separate glass transitions for P3HT, PLA, and the melting temperature of P3HT. The scans shown were collected after annealing at 250 °C and then cooling to –50 °C.

Thermal characterization of P3DDT-PLA. To avoid the possible thermal degradation problem associated with the P3HT-based diblock copolymers, the P3DDT series was synthesized since it is well-known that the melting temperature of P3ATs decreases as the length of the alkyl chain is increased.[82,83] As previously seen in the literature, P3DDT has two melting transitions. The first is a broad peak spanning 25–80 °C and is associated with the melting of ordered alkyl groups in the material due to the high regioregularity of the polymer and the rather long side chains.[84] Due to the broadness of the signal related to the side chain melting of the P3DDT, discerning the glass transition of the PLA was difficult. The main chain melting peak (T_m ~150 °C) occurs at a much lower temperature than that of P3HT and the value of ΔH_m^{∞} is much smaller at 55 J/g.[79] The multiple signals present in the main chain melting peak of the P3DDT, are consistent with previous literature accounts and have been attributed to a

combination of melting processes.[79,82] The amount of crystallinity present in the P3DDT homopolymer was much greater than that of the P3HT homopolymer, but the addition of the PLA segment had the same qualitative effect on the crystallinity of the diblock copolymers in the series. With the melting temperature of the P3DDT block being lower than the degradation temperature of PLA, thermal processing of these diblock copolymers is more tractable.

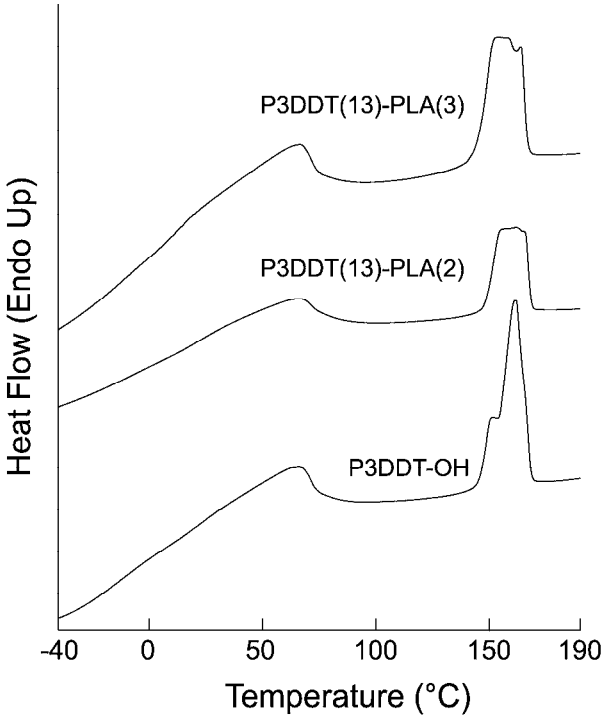

Figure 4.6. DSC traces of P3DDT-PLA series at 10 °C/min showing the broad side-chain relaxation process for P3DDT and the melting temperature of P3DDT. The scans shown were collected after annealing at 250 °C and then cooling to –50 °C. The glass transition of PLA is obscured for all samples due to the side-chain relaxation of P3DDT.

In order to verify the ability of the P3DDT-PLA to be processed above the melting temperature of the semiconducting segment, thermogravimetric (TGA) measurements were performed to observe the onset of PLA degradation in these polymers. As shown in Figure 4.7a, the onset of PLA degradation begins at ~200 °C with nearly all of the PLA degraded by 280 °C. The midpoint of the weight loss plateau

regions of P3DDT(13)-PLA(2) and P3DDT(13)-PLA(3) are at 87% and 82%, respectively, which corresponds well with the weight fraction of PLA in the block copolymers (see Table 4.1). Figure 4.7b shows the effect of holding the P3DDT-PLA polymers at ~10 °C above the melting temperature of the P3DDT for 1 h. While there is some noise due to the relatively small window of weight fraction plotted, processing the polymers above the melting temperature of P3DDT will not cause significant degradation of PLA over the course of the experiment. Despite the fact that P3HT outperforms P3DDT in charge transport measurements, we performed all structural and thin film experiments on the P3DDT-PLA series for this reason.[85,86]

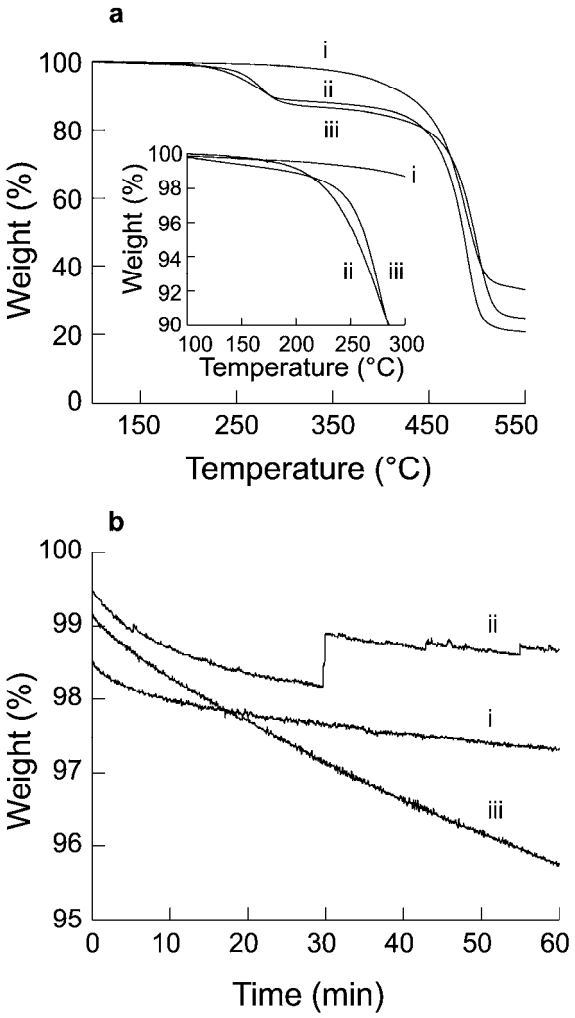

Figure 4.7. (a) Weight loss with respect to temperature of (i) P3DDT-OH, (ii) P3DDT(13)-PLA(2), and (iii) P3DDT(13)-PLA(3) in nitrogen at a heating scan rate of 10 °C/min. The inset highlights the large amount of weight loss in the block copolymers around the melting temperature of P3HT. (b) Weight loss with respect to time of (i) P3DDT-OH, (ii) P3DDT(13)-PLA(2), and (iii) P3DDT(13)-PLA(3) at a constant temperature of 165 °C in nitrogen. The P3DDT(13)-PLA(2) trace shows some noise at ~30 min due to a jostling of the instrument.

Wide Angle X-ray Scattering (WAXS). WAXS was employed to observe the effect of the PLA block on the crystallinity of P3DDT. The signal at lower scattering angles is indexed as the (100) reflection and is associated with the layered structure of the P3DDT main chain folding into the crystalline matrix. Since the lamellae of the

P3DDT structure is known to be significant and that the packing is highly interdigitated, the (200) and (300) reflections are also prominent in the homopolymer chains.[82,87,88] This high degree of ordering leads to a large fraction of crystalline domains in the polymer (also reflected by the DSC measurements). Since the P3DDT alkyl side chains are rather long, they can interpenetrate the overlaying lamellae structure of the main chain and this is the cause for the side chain crystallization (melting) observed in the DSC thermograms. As PLA was incorporated into the block copolymers the crystalline peaks remained but were broadened due to the incorporation of the amorphous PLA domains.

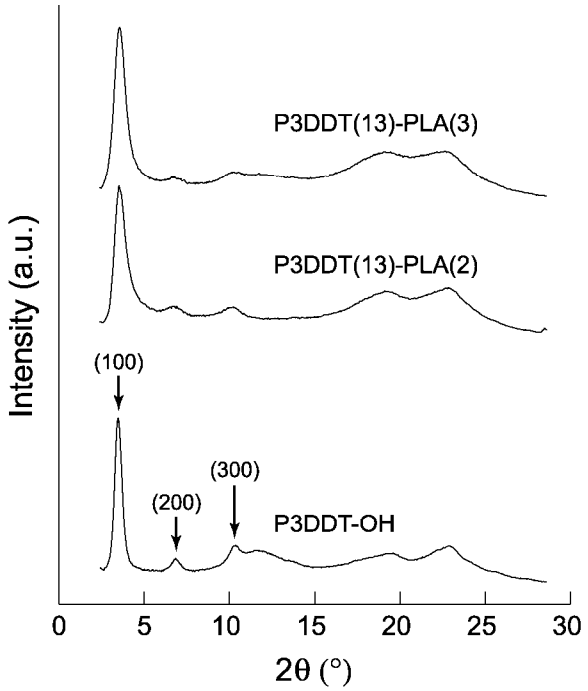

Figure 4.8. WAXS patterns of the P3DDT-PLA series with arrows showing the first three lamellae reflections of the homopolymer.

Ultraviolet-Visible (UV-Vis) Light Absorbance. P3AT thin films are often used as the primary light absorbers and electron donors in organic photovoltaic devices.[10,11] For the block copolymers to be useful in this application they must absorb light as the P3AT homopolymers do. We show the results of increasing the amount of

PLA relative to P3DDT in the block copolymer samples and the corresponding decrease of light absorption in the wavelength range of 400-600 nm. In order to help induce organization of the P3DDT chains during the spin-coating process, the slow-drying technique developed by Li et al. was used.[11] This slow casting procedure leads to reasonably well-ordered films even prior to annealing since the slow drying of the 1,2-dichlorobenzene (over the course of ~1 h) gives the polymer chains sufficient time to organize prior to locking into a semicrystalline structure (Figure 4.9a). As expected, decreasing the amount of P3DDT in the sample decreases the relative amount of light absorbed. Despite the fact that the absorbencies of the block copolymer films were lower than that of the homopolymer, spectra of all films showed three maxima over the range of P3DDT absorption. The shoulder at ~625 nm is related to vibronic absorption and is an indicator that there a high degree of ordering in both the homopolymer and block copolymers despite the presence of the amorphous PLA.[89] Annealing of the films in inert atmosphere leads to a slight increase in absorption for the block copolymer thin films relative to the homopolymer as the polymer chains are given more of an opportunity to reorganize into an ordered structure (Figure 4.9b). In addition, a blue shift in the main absorbance peak of the homopolymer and block copolymer films is seen upon annealing. The shift between the as-spun and annealed films is likely due to the relatively rapid cooling of the annealed film as compared to the slower solvent evaporation in the spin-coating process. The longer solvent annealing process presumably leads to a more organized structure and concomitant shift of the principal absorption to a longer wavelength. After chemical etching of the films (see Experimental Section), the absorbance spectrum of the homopolymer and block copolymers remains unchanged, consistent with the idea that the sacrificial PLA block is selectively etched while leaving the semicrystalline matrix intact (Figure 4.9c). ^{1}H NMR experiments on both the P3DDT(13)-PLA(2) and P3DDT(13)-PLA(3) etched block copolymer films show that ~45% of the PLA is removed after 72 h of etching in the 0.5 M NaOH in water/methanol (60/40 v/v) bath. This amount of residual PLA was as low as we could achieve given the current etching technique. We believe that

removal of PLA could be increased by increasing mass transport either by convective or diffusive means. While there is a residual amount of PLA left in the pitted block copolymer film (see next section), we have previously shown that having even a much larger amount of insulating material (greater than 40 wt %) has only a small affect on charge generation and conduction when incorporated into the active layer of blended bulk heterojunction organic photovoltaic (OPV) cells with a soluble fullerene.[90] The alkaline etching times used in these experiments suggest that P3DDT preferentially wets the ITO substrate since the films are remarkably stable in the etching bath for multiple days. The formation of a selective monolayer has been observed in other PLA block copolymer systems and varies based upon the substrate and surface treatment conditions.[57] We have observed similar block copolymer films dewet from other substrates over the course of much shorter etching periods.

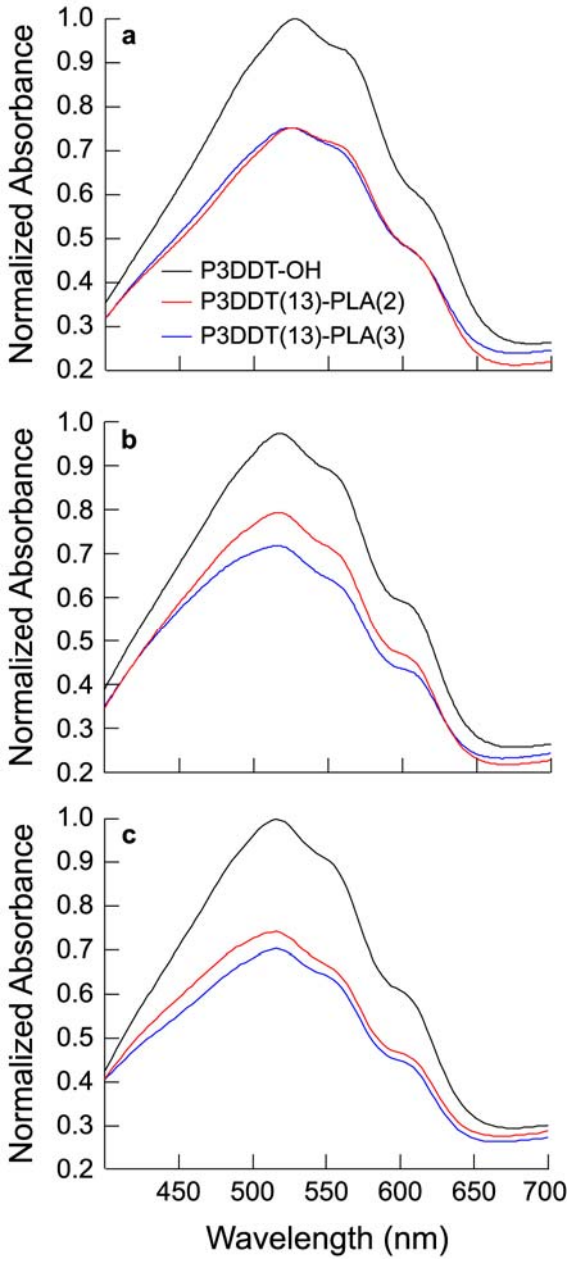

Figure 4.9. UV-Vis light absorbance spectra of P3DDT-PLA series thin films (a) as-spun from 1,2-dichlorobenzene, (b) after annealing in inert atmosphere, and (c) after etching the films in a solution of 0.5 M NaOH in water/methanol (60/40 v/v) for 72 h to selectively remove the PLA segment from the diblock copolymers.

Thin Film Imaging. In order to observe the morphology of the block copolymer films atomic force microscopy (AFM) was employed in tapping mode in order to

minimize damage to the soft materials. Prior to etching, the homopolymer and block copolymer thin films show little change in surface height across the scan area of the microscope image (Figures 4.10a, b, c). After placing the films in the etching bath for 72 h, the P3DDT-OH remains a smooth film intact with no apparent surface pitting (Figure 4.10d). On the other hand, the block copolymer films show discrete pits in the P3DDT matrices (Figure 4.10e and f). In both the P3DDT(13)-PLA(2) and P3DDT(13)-PLA(3) polymers the pits in the films are irregularly shaped with characteristic "diameters" on the order of 35 ± 15 nm and depths of 8 ± 2 nm. We note that the pits may have larger depths than we report and that accurate measurements might be limited by the resolution of the tip of the microscope. Assuming the pits to be cylindrical in nature and 8 nm in depth, the increase in surface area of the pitted structures over the original planar structures is 47%. Phase separation may be dominated by P3DDT crystallization as opposed to the amorphous coil-*b*-coil systems where microphase separation is dominated by enthalpic interactions between the constituent monomers. Accordingly, the PLA must fill space not occupied by the crystalline domains of the P3DDT. This leads to pits with various diameters and geometries upon etching of the PLA. This type of phase separation has been seen in other P3AT block copolymer systems where polythiophene is the majority phase.[47]

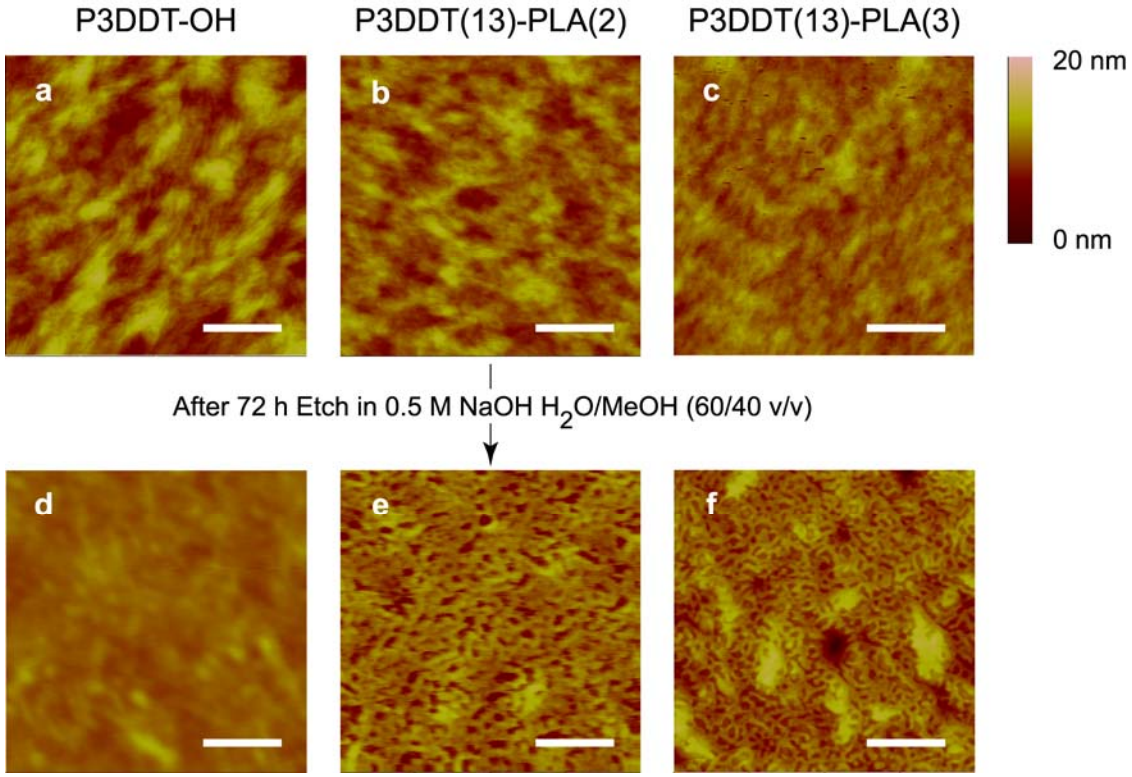

Figure 4.10. Tapping mode AFM height images of thin films of (a) P3DDT-OH, (b) P3DDT(13)-PLA(2), and (c) P3DDT(13)-PLA(3) prior to etching and (d) P3DDT-OH, (e) P3DDT(13)-PLA(2), and (f) P3DDT(13)-PLA(3) after exposure to an alkaline solution. Scale bars represent 250 nm.

4.5 Summary

We have shown the synthesis and molecular characterization of a new series of semiconducting-*b*-insulating block copolymers, P3AT-PLA, via two controlled polymerization steps. After exploring the thermal properties of these materials, we find that there is an advantage, in terms of processability, in using poly(3-dodecylthiophene) as the semiconducting moiety. By using the polymer with the longer alkyl side chain, we find a reduced melting point and, thus, as evidenced by DSC and TGA, annealing can be performed at temperatures lower than the degradation temperature of PLA. WAXS and DSC data shows that the lamellae structure of bulk P3DDT is maintained with the addition of PLA segments but the overall crystallinity of the polymers is

slightly reduced as the amount of PLA present is increased. The materials are easily dissolved in a variety of organic solvents and were spun-cast from a high boiling point solvent in order to generate thin films with a high degree of P3DDT ordering. After etching the P3DDT-PLA thin films with a gentle alkaline bath, we find pitted domains on the nanoscale where the PLA has been selectively removed without affecting the P3DDT crystalline structure as evidenced by AFM, ^{1}H NMR spectroscopy, and UV-Vis absorption experiments. The facile synthesis and easy processability of these block copolymers leads to pitted films, which could be incorporated into a variety of organic electronic devices in order to improve performance. Two examples include greater sensitivity in VOC detection devices due to higher surface area for VOC-P3DDT interaction and improved contact between electron-donating and accepting materials in OPVs.

4.6 Acknowledgements

This work was funded by the Initiative for Renewable Energy and the Environment (IREE) at the University of Minnesota and the Xcel Energy Renewable Development Fund. We thank Ryan Wold for help with WAXS data collection and Dr. Rajeswari M. Kasi and Derek M. Stevens for helpful discussions.

4.7 References

[1] Skotheim, T.; Reynolds, J.; Elsembauer, R.; Eds. *Handbook of Conducting Polymers*; Marcel Dekker: New York, 1998.

[2] Nalwa, H. S.; Ed. *Handbook of Organic Conductive Molecules and Polymers*; J. Wiley & Sons: New York, 1996.

[3] McCullough, R. D. *Adv. Mater.* **1998**, *10*, 93–116.

[4] Wang, G.; Swensen, J.; Moses, D.; Heeger, A. J. *J. Appl. Phys.* **2003**, *93*, 6137–6141.

[5] Sirringhaus, H. *Adv. Mater.* **2005**, *17*, 2411–2425.

[6] Panzer, M. J.; Frisbie, C. D. *Adv. Funct. Mater.* **2006**, *16*, 1051–1056.

[7] Li, B.; Sauvé, G.; Iovu, M. C.; Jeffries-EL, M.; Zhang, R.; Cooper, J.; Santhanam, S.; Schultz, L.; Revelli, J. C.; Kusne, A. G.; Kowlewski, T.; Snyder, J. L.; Weiss, L. E.; Fedder, G. K.; McCullough, R. D.; Lambeth, D. N. *Nano Lett.* **2006**, *6*, 1598–1602.

[8] McQuade, D. T.; Pullen, A. E.; Swager, T. M. *Chem. Rev.* **2000**, *100*, 2537–2574.

[9] Padinger, F.; Rittberger, R. S.; Sariciftci, N. S. *Adv. Funct. Mater.* **2003**, *13*, 85–88.

[10] Reyes-Reyes, M.; Kim, K.; Carroll, D. L. *Appl. Phys. Lett.* **2005**, *87*, 083506.

[11] Li, G.; Shrotriya, V.; Huang, J.; Yao, Y.; Moriarty, T.; Emery, K.; Yang, Y. *Nat. Mater.* **2005**, *4*, 864–868.

[12] Kim, J. Y.; Lee, K.; Coates, N. E.; Moses, D.; Nguyen, T.; Dante, M.; Heeger, A. J. *Science* **2007**, *317*, 222–225.

[13] Sun, S.; Sariciftci, N. S., Eds. *Organic Photovoltaics: Mechanisms, Materials, and Devices*; Taylor & Francis: Boca Raton, FL, 2005.

[14] Janssen, R. A. J.; Hummelen, J. C.; Sariciftci, N. S. *MRS Bull.* **2005**, *30*, 33–36.

[15] Brabec, C. J.; Hauch, J. A.; Schilinsky, P.; Waldauf, C. *MRS Bull.* **2005**, *30*, 50–52.

[16] Chirvase, D.; Parisi, J.; Hummelen, J. C.; Dyakonov, V. *Nanotechnology* **2004**, *15*, 1317–1323.

[17] Zhang, R.; Li, B.; Iovu, M. C.; Jeffries-EL, M.; Sauvé, G.; Cooper, J.; Jia, S.; Tristram-Nagle, S.; Smilgies, D. M.; Lambeth, D. N.; McCullough, R. D.; Kowalewski, T. *J. Am. Chem. Soc.* **2006**, *128*, 3480–3481.

[18] Bates, F. S.; Fredrickson, G. H. *Annu. Rev. Phys. Chem.* **1990**, *41*, 525–557.

[19] Shull, K. R. *Macromolecules* **1992**, *25*, 2122–2133.

[20] Alexander-Katz, A.; Fredrickson, G. H. *Macromolecules* **2007**, *40*, 4075–4087.

[21] Russell, T. P.; Coulon, G.; Deline, V. R.; Miller, D. C. *Macromolecules* **1989**, *22*, 4600–4606.

[22] Menelle, A.; Russell, T. P.; Anastasiadis, S. H.; Satija, S. K.; Majkrzak, C. F. *Phys. Rev. Lett.* **1992**, *68*, 67–70.

[23] Sikka, M.; Singh, N.; Karim, A.; Bates, F. S.; Satija, S. K.; Majkrzak, C. F. *Phys. Rev. Lett.* **1993**, *70*, 307–310.

[24] Morkved, T. L.; Lu, M.; Urbas, A. M.; Ehrichs, E. E.; Jaeger, H. M.; Mansky, P.; Russell, T. P. *Science* **1996**, *273*, 931–933.

[25] Huang, E.; Rockford, L.; Russell, T. P.; Hawker, C. J. *Nature* **1998**, *31*, 757–758.

[26] Hiemenz, P. C.; Lodge, T. P. *Polymer Chemistry*; CRC Press: Boca Raton, FL, 2007.

[27] Hillmyer, M. A. *Adv. Polym. Sci.* **2005**, *190*, 137–181.

[28] Halperin, A. *Macromolecules* **1990**, *23*, 2724–2731.

[29] Williams, D. R. M.; Fredrickson, G. H. *Macromolecules* **1992**, *25*, 3561–3568.

[30] Matsen, M. W.; Barrett, C. *J. Chem. Phys.* **1998**, *109*, 4108–4118.

[31] Radzilowski, L. H.; Wu, J. L.; Stupp, S. I. *Macromolecules* **1993**, *26*, 879–882.

[32] Chen, J. T.; Thomas, E. L.; Ober, C. K.; Hwang, S. S. *Macromolecules* **1995**, *28*, 1688–1697.

[33] Chen, J. T.; Thomas, E. L.; Ober, C. K.; Mao, G. P. *Science* **1996**, *273*, 343–346.

[34] Park, J.; Thomas, E. L. *Macromolecules* **2004**, *37*, 3532–3535.

[35] Jenekhe, S. A.; Chen, X. L. *Science* **1999**, *283*, 372–375.

[36] Jenekhe, S. A.; Chen, X. L. *J. Phys. Chem. B* **2000**, *104*, 6332–6335.

[37] Chen, X. L.; Jenekhe, S. A. *Macromolecules* **2000**, *33*, 4610–4612.

[38] de boer, B.; Stalmach, U.; van Hutten, P. F.; Melzer, C.; Krasnikov, V. V.; Hadziioannou, G. *Polymer* **2001**, *42*, 9097–9109.

[39] de Boer, B.; Stalmach, U.; Nijland, H.; Hadziioannou, G. *Adv. Mater.* **2000**, *12*, 1581–1583.

[40] Hadziioannou, G. *MRS Bull.* **2002**, *27*, 456–460.

[41] van der Veen, M. H.; de Boer, B.; Stalmach, U.; van de Wetering, K. I.; Hadziioannou, G. *Macromolecules* **2004**, *37*, 3673–3684.

[42] Olsen, B. D.; Segalman, R. A. *Macromolecules* **2005**, *38*, 10127–10137.

[43] Olsen, B. D.; Segalman, R. A. *Macromolecules* **2006**, *39*, 7078–7083.

[44] Olsen, B. D.; Li, X.; Wang, J.; Segalman, R. A. *Macromolecules* **2007**, *40*, 3287–3295.

[45] Sauvé, G.; McCullough, R. D. *Adv. Mater.* **2007**, *19*, 1822–1825.

[46] Iovu, M. C.; Craley, R.; Jeffries-EL, M.; Krankowski, A. B.; Zhang, R.; Kowalewski, T.; McCullough, R. D. *Macromolecules* **2007**, *40*, 4733–4735.

[47] Dai, C.; Yen, W.; Lee, Y.; Ho, C.; Su, W. *J. Am. Chem. Soc.* **2007**, *129*, 11036–11038.

[48] Jeffries-EL, M.; Sauvé, G.; McCullough, R. D. *Macromolecules* **2005**, *38*, 10346–10352.

[49] Hotta, S.; Rughooputh, S. D. D. V.; Heeger, A. J.; Wudl, F. *Macromolecules* **1987**, *20*, 212–215.

[50] Sugimoto, R.; Takeda, S.; Gu, H. B.; Yoshino, K. *Chem. Express* **1986**, *1*, 635–638.

[51] Hotta, S.; Soga, M.; Sonoda, N. *Synth. Met.* **1988**, *26*, 267–279.

[52] Loewe, R. S.; Khersonsky, S. M.; McCullough, R. D. *Adv. Mater.* **1999**, *11*, 250–253.

[53] Jeffries-EL, M.; Sauvé, G.; McCullough, R. D. *Adv. Mater.* **2004**, *16*, 1017–1019.

[54] Iovu, M. C.; Jeffries-EL, M.; Sheina, E. E.; Cooper, J. R.; McCullough, R. D. *Polymer* **2005**, *46*, 8582–8586.

[55] Iovu, M. C.; Jeffries-EL, M.; Zhang, R.; Kowalewski, T.; McCullough, R. D. *J. Polym. Sci. A* **2006**, *43*, 1991–2000.

[56] Liu, J.; Sheina, E.; Kowalewski, T.; McCullough, R. D. *Agnew. Chem., Int. Ed.* **2002**, *41*, 329–332.

[57] Olayo-Valles, R.; Guo, S.; Lund, M. S.; Leighton, C.; Hillmyer, M. A. *Macromolecules* **2005**, *38*, 10101–10108.

[58] Mao, H.; Hillmyer, M. A. *Soft Matter* **2006**, *2*, 57–59.

[59] Ha, J.; Hillmyer, M. A.; Ward, M. D. *J. Phys. Chem. B* **2005**, *109*, 1392–1399.

[60] Olayo-Valles, R.; Lund, M. S.; Leighton, C.; Hillmyer, M. A. *J. Mater. Chem.* **2004**, *14*, 2729–2731.

[61] Kubo, T.; Parker, J. S.; Hillmyer, M. A.; Leighton, C. *Appl. Phys. Lett.* **2007**, *90*, 233113.

[62] Schmidt, S. C.; Hillmyer, M. A. *Macromolecules* **1999**, *32*, 4794–4801.

[63] Kricheldorf, H.; Berl, M.; Scharnagle, N. *Macromolecules* **1988**, *21*, 286–293.

[64] Wang, Y.; Hillmyer, M. A. *Macromolecules* **2000**, *33*, 7395–7403.

[65] Coakley, K. M.; Liu, Y.; Goh, C.; McGehee, M. D. *MRS Bull.* **2005**, *30*, 37–40.

[66] Olson, D. C.; Piris, J.; Collins, R. T.; Shaheen, S. E.; Ginley, D. S. *Thin Solid Films* **2006**, *496*, 26–29.

[67] Tashiro, K.; Kobayashi, M.; Kawai, T.; Yoshino, K. *Polymer* **1997**, *38*, 2867–2879.

[68] Zalusky, A. S.; Olayo-Valles, R.; Wolf, J. H.; Hillmyer, M. A. *J. Am. Chem. Soc.* **2002**, *124*, 12761–12773.

[69] Trznadel, M.; Pron, A.; Zagorska, M.; Chrzaszcz, R.; Pielichowski, J. *Macromolecules* **1998**, *31*, 5051–5058.

[70] Merlo, J. A.; Frisbie, C. D. *J. Phys. Chem. B* **2004**, *108*, 19169–19179.

[71] Iovu, M. C.; Sheina, E. E.; Gil, R. R.; McCullough, R. D. *Macromolecules* **2005**, *38*, 8649–8656.

[72] Li, S. *J. Biomed. Mater. Res.* **1999**, 48, 342–353.

[73] Liu, J.; Loewe, R. S.; McCullough, R. D. *Macromolecules* **1999**, *32*, 5777–5785.

[74] Fan, Y.; Chen, G.; Tanaka, J.; Tateishi, T. *Biomacromolecules* **2005**, *6*, 3051–3056.

[75] Dubois, Ph.; Jacobs, C.; Jérôme, R.; Teyssié, Ph. *Macromolecules* **1991**, *24*, 2266–2270.

[76] Kuila, B. K.; Nandi, A. K. *Macromolecules* **2004**, *37*, 8577–8584.

[77] Miyauchi, S.; Kondo, T.; Oshima, K.; Yamauchi, T.; Shimomura, M.; Mitomo, H. *J. Appl. Poly. Sci.* **2000**, *77*, 3069–3076.

[78] Anderson, K. S.; Hillmyer, M. A. *Polymer* **2006**, *47*, 2030–2035.

[79] Malik, S.; Nandi, A. K. *J. Poly. Sci. B* **2002**, *40*, 2073–2085.

[80] Yang, C.; Orfino, F. P.; Holdcroft, S. *Macromolecules* **1996**, *29*, 6510–6517.

[81] Gurau, M. C.; Delongchamp, D. M.; Vogel, B. M.; Lin, E. K.; Fischer, D. A.; Sambasivan, S.; Richter, L. J. *Langmuir* **2007**, *23*, 834–842.

[82] Causin, V.; Marega, C.; Marigo, A.; Valentini, L.; Kenny, J. M. *Macromolecules* **2005**, *38*, 409–415.

[83] Zhao, Y.; Keroack, D.; Yuan, G.; Massicotte, A. *Macromol. Chem. Phys.* **1997**, *198*, 1035–1049.

[84] Liu, S. L.; Chung, T. S. *Polymer* **2000**, *41*, 2781–2793.

[85] Park, Y. D.; Kim, D. H.; Jang, Y.; Cho, J. H.; Hwang, M.; Lee, H. S.; Lim, J. A.; Cho, K. *Organic Electronics* **2006**, *7*, 514–520.

[86] Babel, A.; Jenekhe, S. A. *Synth. Met.* **2005**, *148*, 169–173.

[87] Chen, S.; Lee, S. *Polymer* **1995**, *36*, 1719–1723.

[88] Prosa, T. J.; Moulton, J.; Heeger, A. J.; Winokur, M. J. *Macromolecules* **1999**, *32*, 4000–4009.

[89] Sunderberg, M.; Inganäs, O.; Stafström, S.; Gustafsson, G.; Sjögren, B. *Solid State Commun.* **1989**, *71*, 435–439.

[90] Boudouris, B. W.; Kasi, R. M.; Frisbie, C. D.; Hillmyer, M. A. *PMSE Preprints* **2006**, *95*, 103.

5 Polythiophene Regioregularity and Block Copolymer Microstructure

5.1 Overview

The microstructures of polylactide-*b*-poly(3-alkylthiophene)-*b*-polylactide (PLA-P3AT-PLA) triblock copolymers are reported for two series of P3AT-based samples where the number of thiophene repeat units was kept approximately constant for the two different sets. In one series the polythiophene moiety was synthesized in a manner to yield a regioregular polymer with an alkyl side chain length of twelve carbons. Poly(3-hexylthiophene) (P3HT) with an irregular arrangement of side chains (regiorandom) was used in the second set of polythiophene-containing block copolymers. In both instances the end groups of the polythiophenes were manipulated, and the polymers subsequently were used as difunctional macroinitiators for the ring-opening polymerization (ROP) of D,L-lactide. The molecular and thermal properties of the triblock copolymers were characterized by ^{1}H NMR spectroscopy, size exclusion chromatography (SEC), and differential scanning calorimetry (DSC). Powder wide-angle and small-angle x-ray scattering (WAXS and SAXS) revealed that the bulk microstructures of the block copolymers were greatly influenced by the regioregularity of the polythiophene segment. The microphase separations of regioregular polythiophenes were dominated by the crystallization of the semiconducting polymer. The regiorandom polythiophene-based block copolymers were completely amorphous with the microstructures set by the enthalpic and entropic characteristics of the constituent macromolecules. By manipulating the regiospecificity of the semiconducting moiety, we have overcome a large and commonly encountered obstacle, crystallization-induced phase separation, in the self-assembly of polythiophene-based block copolymers. Using these new macromolecules, a better understanding of how to tune the microphase separation of polythiophene-containing block copolymers could be obtained, and this may prove extremely useful in numerous organic electronic applications.

5.2 Introduction

Soluble polythiophene derivatives such as poly(3-alkylthiophenes) (P3ATs) have been intensely studied in the organic electronics community recently. These polymers are promising because they transport holes efficiently (μ_h ~0.1-1 $cm^2\ V^{-1}s^{-1}$), can be processed from a wide selection of organic solvents, have relatively low band gaps (E_g ~1.9 eV), and, by modification of their chemical structure, have tunable optoelectronic properties.[1-4] Specifically, thiophene-containing polymers have risen to the forefront of high performance, bulk heterojunction organic photovoltaics (OPVs) with power conversion efficiencies of ~5-6%.[5-7] Because separation of the bound electron-hole pairs (excitons) created upon photon absorption is crucial to photocurrent generation in OPVs, the exciton diffusion length (L_d ~10–40 nm) is critical to device performance.[8-11] Therefore, controlling the microstructure of the active layers in these devices is important if high efficiency devices are to be fabricated.[12,13] With this in mind, we have synthesized polythiophene-based triblock copolymers that self-assemble into distinct domains with characteristic spacings on the order of the exciton diffusion length.

Polythiophene derivatives have been the preeminent hole-conducting semiconductors, and soluble fullerene derivatives have been used predominantly as the electron-conducting materials in organic photovoltaics.[9,14-16] Currently, the microstructure of the active layers of these devices is manipulated by controlling the coating[5] and post-processing conditions[5,17-20] of the organic layer. While some groups have attempted to understand the phase behavior of polythiophene-fullerene solid solutions,[21,22] the most efficient solar cells are still fabricated with a kinetically trapped active layer morphology. This leads to decreased device performance with time as the morphology is altered with exposure to ambient conditions and solar illumination.[23,24] Consequently, researchers have begun to look at ordered bulk heterojunction active layers,[25-27] which have been predicted to perform better than blended bulk heterojunction active layers.[28,29] In these systems, the active layer morphologies are

well-ordered and the domain spacings and geometries ideally would be tuned to find maxima in device efficiencies.

Block copolymer thin films were predicted,[30-32] and subsequently proven, to self-assemble into ordered microstructures on the nanometer length scale.[33-37] In the most common cases, the constituents of the block copolymers were macromolecules with flexible carbon-carbon backbones. These polymers adopt Gaussian, random walk chain configurations (coil) in the melt.[38-40] On the other hand, polythiophenes, and many other semiconducting polymers, have rigid polymer backbone bonds, and adopt much stiffer configurations (rod) in the melt making the microstructure of rod-containing block copolymers harder to predict than coil-coil block copolymers. In rod-coil block copolymers, the enthalpy and entropy terms used in modeling the phase behavior of coil-coil block copolymers must be supplemented by one parameter that accounts for the ratio of the rod and coil block lengths and another that accounts for the self-alignment of the rigid rod segments.[41-45] Recently, the phase behavior of P3AT-containing block copolymers has become of increasing interest.[46-58] However, obtaining long-range, well-ordered microstructures in diblock and triblock copolymers composed of a P3AT and a coil-like polymer has been difficult to achieve in practice. In fact, only poly(3-hexylthiophene)-*b*-poly(2-vinylpyridine) (P3HT-P2VP) has been shown to form ordered microstructures, and this only occurred after very specific solvent annealing conditions were used.[50] Generally, this lack of long-range ordered is attributed to the crystallization of the highly regioregular polythiophene moiety dominating the observed phase separation. Therefore, in these block copolymer systems, kinetically trapped polythiophene lamellae microstructures are commonly observed.

The McCullough group greatly advanced the synthetic protocols for P3ATs with the introduction of the Grignard metathesis (GRIM) method.[59] Not only does this reaction pathway yield highly regioregular polythiophenes with high molecular weights and low polydispersities, but it also allows for the in situ end-capping of the polymer chains with a functional group.[60] However, end-capping of the polymer chains is not always complete. If this is the case, using these P3ATs as macroinitiators can result in

residual P3AT homopolymer present in the ensuing P3AT-coil block copolymer. Traditionally, the regioregular, semicrystalline polythiophenes generated by the GRIM method have been desired due to their enhanced optoelectronic properties relative to their regiorandom, non-crystalline counterparts. However, amorphous polythiophenes may prove more useful in generating ordered block copolymer microstructures as has been the case with PPV-based rod-coil block copolymers.[61-64]

In this paper we report the stepwise synthesis of polylactide-*b*-poly(3-alkylthiophene)-*b*-polylactide block copolymers (PLA-P3AT-PLA) by the controlled polymerization of D,L-lactide[65-67] from hydroxyl-terminated poly(3-alkylthiophenes) (HO-P3AT-OH). Note that we have previously shown the utility of using polylactide as the coil block as it can be easily and selectively etched from a P3AT matrix.[54] By altering the P3AT moiety, we have synthesized two distinct series of PLA-P3AT-PLA block copolymers: 1) regioregular poly(3-dodecylthiophene) (*Re*P3DDT) and 2) regiorandom poly(3-hexylthiophene) (*Ra*P3HT). In both series, the average number of thiophene units is approximately the same and the terminal melting (or glass) transition temperature of the P3AT is below the degradation temperature of PLA (T_d ~200 °C).[68] Powder x-ray scattering data indicate that phase separation is dominated by crystallization in the regioregular P3AT case. However, the completely amorphous block copolymers form domains that are not established due to crystallization of the polythiophene block (ca 30 nm), which are on the order of the exciton diffusion length. The possibility of systematically tuning the size and *non-kinetically controlled* morphologies of semiconducting block copolymers, which can be used to generate nanoporous templates, has motivated our efforts to develop block copolymers with a regiorandom P3AT midblock.

5.3 Experimental

General Methods. The ^{1}H NMR spectra were measured on a Varian VI-500 spectrometer using deuterated chloroform (Cambridge) solutions containing ~1 wt % polymer. Size exclusion chromatography (SEC) data were collected on an Agilent 1100 series equipped with a Hewlett-Packard 1047A refractive index (RI) detector and an

Agilent Ultraviolet visible (UV-Vis) light detector (path length = 10 mm) and three PLgel 5μm MIXED-C columns. Chloroform at 35 °C was used as the mobile phase at a flow rate of 1 mL/min and the SEC was calibrated with polystyrene (PS) standards (Polymer Laboratories). Differential scanning calorimetry (DSC) measurements were acquired using a TA Q1000 calorimeter. The samples were first annealed at 260 °C and then cooled to –60 °C at a rate of 10 °C/min. The results shown are for the final sample heating at a rate of 10 °C/min. An indium standard was used to calibrate the instrument and nitrogen was used as the purge gas. Wide-angle x-ray scattering (WAXS) data of polymer powders were collected at room temperature in the diffraction angular range of 3–30° (2θ) by a Bruker-AXS D5005 microdiffractometer. No annealing treatments were preformed prior to data collection. The crystalline peaks were referenced from known reflection values[69] and deconvoluted using the curve-fitting software, JADE 7 (CMI). Small-angle x-ray scattering (SAXS) experiments were performed at the Advanced Photon Source (APS) at Argonne National Laboratories at Sector 5-ID-D beamline. The beamline is maintained by the Dow-Northwestern-Dupont Collaborative Access Team (DND-CAT). Scattering intensity was monitored by a Mar 165 mm diameter CCD detector with a resolution of 2048 x 2048. The two-dimensional scattering patterns were azimuthally integrated to afford one-dimensional profiles presented as spatial frequency (q) versus scattered intensity. The powder SAXS samples were annealed at 180 °C and then cooled to 50 °C. The spectra shown below were acquired at 50 °C.

Materials. All reagents and solvents were used as received from Sigma-Aldrich unless otherwise noted. Degassed tetrahydrofuran (THF) and toluene were purified by passage through an activated alumina column and were collected in flame-dried, air-free flasks. D,L-lactide was purified by recrystallization from toluene followed by drying under reduced pressure and was stored in an inert atmosphere glove box.

Synthesis of Hydroxyl-terminated Regioregular Poly(3-dodecylthiophene) (HO-P3DDT-OH). A modified method similar to that of the McCullough group was used for the synthesis of dihydroxyl-terminated poly(3-alkylthiophene)s.[70,71] A typical polymerization is described for the hydroxyl-terminated poly(3-dodecylthiophene)

(HO-P3DDT-OH) (Table 5.1). The polymerization was performed in a flame-dried 250 mL reaction flask containing a Teflon-coated magnetic stir bar. To the flask, ~80 mL of anhydrous THF was added via cannula. 2,5-dibromo-3-dodecylthiophene (8.5 g, 20.6 mmol) and a solution of 2 M *tert*-butylmagnesium chloride in diethyl ether (10.3 mL, 20.6 mmol) were added to the THF solvent under Ar. The reaction was heated to reflux for 1.5 h. After cooling the solution to room temperature, 1,3-bis(diphenylphosphino)propane nickel (II) chloride [Ni(dppp)Cl_2] (0.035 g, 0.065 mmol) was added as a solid under Ar. The reaction was then allowed to stir for 70 min at room temperature under Ar. The reaction was quenched with 5 mL of 2 M hydrochloric acid (HCl) and precipitated in methanol. The polymer was collected and purified via Soxhlet extraction with methanol, hexane, and chloroform, sequentially. The concentrated chloroform fraction was precipitated in methanol and the hydrogen/bromine-terminated poly(3-dodecylthiophene) (H-P3DDT-Br) was washed with methanol, collected, and dried overnight under reduced pressure.

The end groups of P3DDT were converted to protons by a magnesium-halogen exchange.[70] In this reaction, 100 mL of anhydrous THF was added to a flame-dried reaction flask using a cannula under Ar. H-P3DDT-Br (1.71 g, 0.081 mmol) was added to the reaction flask as a solid under Ar. Then 2 M *tert*-butylmagnesium chloride in diethyl ether (10.0 mL, 20.0 mmol) was added to the reaction flask, and the reaction was heated to reflux. After allowing the reaction to reflux for 2 h, it was cooled to room temperature. 10.0 mL of 2 M hydrogen chloride were slowly added to quench the reaction. The hydrogen/hydrogen-terminated polymer (P3DDT) was precipitated in methanol and then purified by Soxhlet extraction with methanol and chloroform.

The Vilsmeier reaction was used to synthesize *bis*-aldehyde poly(3-dodecylthiophene) (HCO-P3DDT-COH).[72] Here, 100 mL of anhydrous toluene were added to a flame-dried reaction flask. P3DDT (1.48 g, 0.07 mmol), *N*-methylformanilide (8.5 mL), and phosphorous oxychloride ($POCl_3$) (5.5 mL) were added to the reaction flask under Ar. The reaction was heated to 75 °C and stirred at this temperature for 24 h. The reaction was then cooled to room temperature, and 80 mL of

a concentrated aqueous sodium acetate solution (35 g solid in 100 mL water) was added to the reaction mixture under Ar. The components were allowed to stir overnight at room temperature. Afterwards, the organic and aqueous phases were separated and the toluene fraction was washed with HPLC-grade water. The toluene fraction was then concentrated and precipitated in methanol. HCO-P3DDT-COH was then Soxhlet extracted with methanol and chloroform.

Reduction of the aldehyde end groups led to the dihydroxyl-functionalized poly(3-dodecylthiophene) (HO-*Re*P3DDT-OH). HCO-P3DDT-COH (0.32 g, 0.015 mmol) was dissolved in 50 mL of anhydrous THF under Ar. A 1 M solution of lithium aluminumhydride ($LiAlH_4$) in THF was added to the reaction flask under Ar using a gas-tight, deoxygenated syringe (0.5 mL, 0.5 mmol). The reaction was stirred at room temperature for 40 min and then quenched with 0.5 mL of 1 M HCl. The polymer was precipitated in methanol and Soxhlet extracted with methanol and chloroform.

Characterization of **HO-*Re*P3DDT-OH**. ^{1}H NMR (500 MHz, $CDCl_3$): δ_H 0.87 (t, 3H), 1.29 (m, 18H), 1.70 (t, 2H), *2.60 (t, 4H)*, 2.80 (t, 2H), *4.77 (d, 4H)*, 6.9 (s, 83H); SEC: M_n: 34800, PDI: 1.9. Italicized entries correspond to end group proton resonances.

Synthesis of Hydroxyl-terminated Regiorandom Poly(3-hexylthiophene) (HO-*Ra*P3HT-OH). Regiorandom poly(3-hexylthiophene) with hydrogen/bromine end groups (H-P3HT-Br) was purchased from Rieke Metals. End group modifications were made in manners analogous to those described above for HO-*Re*P3DDT-OH.

Characterization of **HO-*Ra*P3HT-OH**. ^{1}H NMR (500 MHz, $CDCl_3$): δ_H 0.89 (m, 3H), 1.34 (m, 6H), 1.65 (d, 2H), 2.68 (d, 2H), *4.78 (m, 4H)*, 7.00 (m, 75H); SEC: M_n: 39100, PDI: 4.6. Italicized entries correspond to end group proton resonances.

Synthesis of Polylactide-*b*-Poly(3-alkylthiophene)-*b*-Polylactide (PLA-P3AT-PLA). We have used a common catalyst, tin octanoate [$Sn(oct)_2$], for the ring-opening polymerization (ROP) of D,L-lactide with HO-P3AT-OH polymers acting as macroinitiators. The details for the example polymerization of PLA-*Re*P3DDT(0.38)-PLA(34) (Table 5.1) are as follows. HO-*Re*P3DDT-OH (0.057 g, 5.4 μmol OH groups) was freeze-dried under reduced vacuum with liquid nitrogen (LN_2) overnight. The flask

was then sealed and transferred inside of a glove box where toluene (4.0 mL) was used to dissolve the HO-*Re*P3DDT-OH. D,L-lactide was then added to the reaction flask (0.077 g, 5.4 mmol). A solution of 0.494 μM tin octanoate in toluene (0.47 mL, 0.232 μmol) was also added in order to have one mole of tin for every 20 moles of hydroxyl groups. The reaction was then sealed and brought outside the glove box to be placed in an oil bath at 110 °C for 5 h. The reaction was cooled to room temperature and quenched with ~2 M HCl (1 mL, 2 mmol). The polymerization was stopped at a ~20% conversion of lactide, and then precipitated in methanol. After filtering and washing with methanol, the polymer was dried overnight under vacuum.

Characterization of **PLA-*Re*P3DDT(0.72)-PLA(8)**. ^{1}H NMR (500 MHz, $CDCl_3$): main chain P3DDT peaks are the same as for **HO-*Re*P3DDT-OH** with δ_H 1.57 (m, 3H), 4.35 (t, 2H), 5.20 (m, 112H); SEC: M_n: 67900, PDI: 2.2.

Characterization of **PLA-*Re*P3DDT(0.39)-PLA(33)**. ^{1}H NMR (500 MHz, $CDCl_3$): main chain P3DDT peaks are the same as for **HO-*Re*P3DDT-OH** with δ_H 1.57 (m, 3H), 4.35 (t, 2H), 5.20 (m, 460H); SEC: M_n: 97200, PDI: 2.0.

Characterization of **PLA-*Re*P3DDT(0.37)-PLA(35)**. ^{1}H NMR (500 MHz, $CDCl_3$): main chain P3HT peaks are the same as for **HO-*Re*P3DDT-OH** with δ_H 1.57 (m, 3H), 4.35 (t, 2H), 5.20 (m, 481H); SEC: M_n: 102100, PDI: 1.9.

Characterization of **PLA-*Ra*P3HT(0.56)-PLA(11)**. ^{1}H NMR (500 MHz, $CDCl_3$): main chain P3DDT peaks are the same as for **HO-*Ra*P3HT-OH** with δ_H 1.57 (m, 3H), 4.35 (t, 2H), 5.20 (m, 156H); SEC: M_n: 70000, PDI: 3.6.

Characterization of **PLA-*Ra*P3HT(0.46)-PLA(14)**. ^{1}H NMR (500 MHz, $CDCl_3$): main chain P3HT peaks are the same as for **HO-*Ra*P3HT-OH** with δ_H 1.57 (m, 3H), 4.35 (t, 2H), 5.20 (m, 198H); SEC: M_n: 65400, PDI: 4.4.

Characterization of **PLA-*Ra*P3HT(0.35)-PLA(24)**. ^{1}H NMR (500 MHz, $CDCl_3$): main chain P3HT peaks are the same as for **HO-*Ra*P3HT-OH** with δ_H 1.57 (m, 3H), 4.35 (t, 2H), 5.20 (m, 326H); SEC: M_n: 72800, PDI: 4.9.

5.4 Results and Discussion

Synthesis of PLA-P3AT-PLA. Regioregular poly(3-dodecylthiophene) (*Re*P3DDT) was synthesized using the Grignard metathesis (GRIM) method.[59] Regiorandom poly(3-hexylthiophene) (*Ra*P3HT) was commercially available and purchased from a Rieke Metals. In both instances, the polymer was purified by Soxhlet extraction using methanol, hexane, and chloroform in a sequential manner. The methanol and hexane fractions helped to remove residual reaction materials and low molecular weight polymers while the chloroform fraction was used in further reactions.[73,74] Because the mechanism for the polymerization of *Ra*P3HT is uncontrolled, the polydispersity index (PDI) is inherently high (PDI > 2.0) for high molecular weight polymers (Chapter 2) and the molecular weight of the resulting product is difficult to predict. However, the GRIM polymerization is well-controlled,[75,76] and this allowed the molecular weight of P3DDT to be tuned such that the average number of thiophene repeat units was approximately the same for P3DDT (N_{P3DDT} ~84) and P3HT (N_{P3HT} ~75). Note that regioregular poly(3-dodecylthiophene) was favored over regioregular poly(3-hexlythiophene) because the melting temperature of P3DDT (T_m ~160 °C)[77] is below the thermal degradation temperature of polylactide, while P3HT's melting temperature is not (T_m ~220 °C).[78] HO-*Ra*P3HT-OH is amorphous and has a low glass transition temperature (T_g ~15 °C) so it can also be thermally processed without worry of damaging the PLA moiety in block copolymers (see below).

Previously (Chapter 4), we synthesized P3AT-PLA diblock copolymers.[54] In that work, the end groups of the polymers were selectively capped on one end by using vinylmagnesium bromide to quench the GRIM polymerization, and then subsequently oxidized to yield P3ATs with a mono-substituted alcohol end group. This route is not available for the current systems because regiorandom P3ATs cannot be end-functionalized in situ like the regioregular P3ATs synthesized using the GRIM polymerization route. Therefore, we have adapted a post-polymerization end group functionalization procedure previously used by the McCullough group that is amenable

to both regioregular and regiorandom P3ATs.[70] This route promotes the formation of triblock copolymers from difunctional alcohol macroinitiators (HO-P3AT-OH). An abbreviated synthetic scheme for P3AT end group functionalization and PLA-P3AT-PLA triblock copolymers is shown in Figure 5.1. Note that we have omitted the magnesium-halogen exchange reaction that converts any bromine end groups to protons, but this reaction has been described in detail elsewhere.[70,71] Because large excesses of reagents are used in each end group modification step, complete conversions at both the 2 and 5 positions of the thiophene ring are easily achieved[71] in each of the reactions all the way to the formation of HO-P3AT-OH.

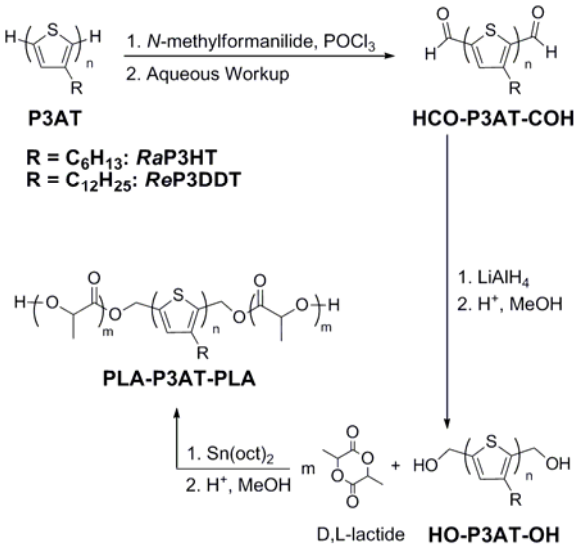

Figure 5.1. Synthetic scheme for the generation of PLA-P3AT-PLA triblock copolymers. Poly(3-dodecylthiophene) block copolymers contain a regioregular polythiophene block (*Re*P3DDT) while poly(3-hexylthiophene) block copolymers have a regiorandom semiconducting block (*Ra*P3HT).

Tin octanoate [$Sn(oct)_2$] is one of the most commonly used catalysts for the ring-opening polymerization of D,L-lactide.[79,80] It is generally accepted that the polymerization proceeds via a coordination-insertion mechanism,[79] and the use of tin octanoate allows for control over the molecular weight of the polymer.[81] In the current system, HO-P3AT-OH and $Sn(oct)_2$ combined to form a difunctional macroinitiator. It

was this macroinitiator that was used in the ring-opening polymerization of D,L-lactide to yield the atactic form of PLA.[82] By varying the initial amount of lactide present (while keeping the initial concentration and conversion of lactide constant), the molecular weight of the PLA block was changed. Multiple PLA-P3AT-PLA block copolymers were synthesized from the two parent macromolecules, HO-*Re*P3DDT-OH and HO-*Ra*P3HT-OH (Table 5.1).

Table 5.1. Characterization of PLA-P3AT-PLA samples.

Sample[a]	M_n[b] (kg/mol) P3AT	M_n[b] (kg/mol) PLA	M_w/M_n[c]	w_{P3AT}[d]	T_g (°C) P3AT	T_g (°C) PLA	T_m (°C) P3AT	Crystallinity[e] (%)
HO-*Re*P3DDT-OH	21.0		1.9		–10		156	16
PLA-*Re*P3DDT(0.72)-PLA(8)	21.0	8.1	2.2	0.72	–8	54	157	4
PLA-*Re*P3DDT(0.39)-PLA(33)	21.0	33.1	2.0	0.39	–9	56	160	5
PLA-*Re*P3DDT(0.37)-PLA(35)	21.0	34.6	1.9	0.37	–8	58	159	3
HO-*Ra*P3HT-OH	12.5		4.6		14			
PLA-*Ra*P3HT(0.56)-PLA(11)	12.5	11.0	3.6	0.53	16	48		
PLA-*Ra*P3HT(0.46)-PLA(14)	12.5	14.4	4.4	0.46	17	53		
PLA-*Ra*P3HT(0.35)-PLA(24)	12.5	23.5	4.9	0.35	15	50		

[a] HO-*Re*P3DDT-OH is the homopolymer of the polylactide-*b*-regioregular poly(3-dodecylthiophene)-*b*-polylactide series symbolized by PLA-*Re*P3DDT(X)-PLA(Y) where X is the weight fraction of polythiophene present in the polymer and the PLA has a molecular weight of Y kg/mol. HO-*Ra*P3HT-OH is the homopolymer of the polylactide-*b*-regiorandom poly(3-hexylthiophene)-*b*-polylactide series symbolized by PLA-*Ra*P3HT(X)-PLA(Y) where X is the weight fraction of polythiophene present in the polymer and the PLA has a molecular weight of Y kg/mol. [b] As determined by ^{1}H NMR spectroscopy. [c] As determined by SEC versus polystyrene standards. [d] $w_{P3AT} = M_n(P3AT) / [M_n(PLA) + M_n(P3AT)]$. [e] As determined by the ratio of the enthalpy of melting for the P3DDT fraction of the sample relative to the infinite enthalpy of melting reported in the literature for the P3DDT (see discussion in the text).

Molecular Characterization of PLA-P3AT-PLA. ^{1}H NMR spectroscopy was used to monitor the chemical shifts of the resonances associated with the protons of functionalized P3ATs. The molecular weights of the HO-P3AT-OH homopolymers were determined by ^{1}H NMR spectroscopy using end group analysis, and these molecular weights were used in all further computations. NMR-determined molecular weights were used because polythiophene molecular weights determined by SEC with polystyrene standards overestimate the true molecular weight of the polymer.[83] Figure 5.2 shows the relevant region of the ^{1}H NMR spectra and chemical structures for the HO-*Re*P3DDT-OH and HO-*Ra*P3HT-OH precursors and representative block copolymers after the addition of the PLA moieties. In both cases, the resonances

associated with the protons of the methylene alcohol shift after the addition of PLA. In fact, these signals should be shifted downfield in the PLA-P3AT-PLA cases but are not observed, presumably because they are at the same location as a main chain PLA peak (Figure 5.3). The presence of peaks at $\delta \approx 4.8$ ppm (a in Figure 5.2) for the HO-P3AT-OH end group was in good agreement with previous reports.[70] Note that for HO-*Re*P3DDT-OH the peak appears as a doublet while the signal for HO-*Ra*P3HT-OH is a doublet of doublets. This result occurs because of the relative positions of the alkyl group of the terminal repeat units on either end of the polymer chains. In the case of regioregular P3ATs the addition of the end group is almost exclusively at the 2-position of the thiophene ring, but in the case of regiorandom P3ATs there is an equal probability of having the functional group at either the 2- or 5-position of the terminal thiophene units. The appearance of the peak at $\delta \approx 4.35$ ppm (b in Figure 5.2) upon the addition of PLA was consistent with the terminal lactide repeat unit.[84] Integration of the areas under the end group and main chain peaks before and after lactide polymerizations were in good agreement with the structures shown.

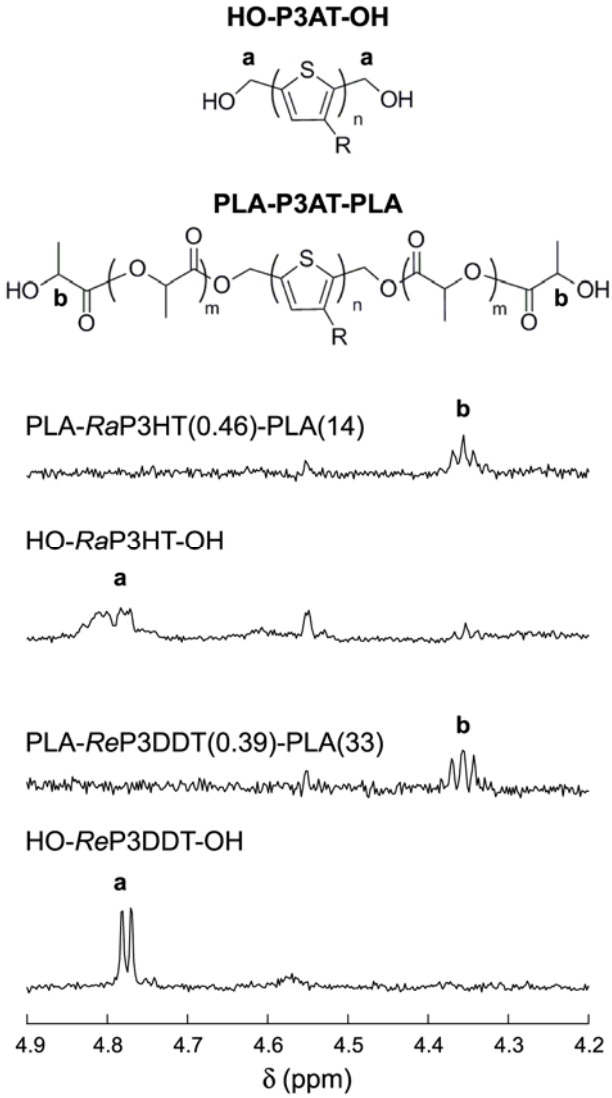

Figure 5.2. Representative ^{1}H NMR spectra of the end group regions before and after addition of the polylactide moieties to the HO-P3AT-OH macroinitiators for the regioregular (lower) and regiorandom (upper) series. Note that the protons labeled a in HO-*Ra*P3HT-OH case are doublets and have two maxima (δ ~4.78 ppm and ~4.82 ppm). This is due to the end groups having an equal probability of being attached at the 2- or 5-positions of the terminal thiophene repeat units. For HO-*Re*P3DDT-OH there is only one doublet at δ ~4.78 ppm because the end groups are exclusively attached at the 2-position of the terminal repeat units. The polymers were dissolved in deuterated chloroform and spectra were recorded at room temperature.

The full ^{1}H NMR spectra of representative PLA-*Re*P3DDT-PLA and PLA-*Ra*P3HT-PLA block copolymers are shown in Figure 5.3. Unlabeled resonances upfield

of δ = 2 ppm are related to the protons of the alkyl side groups. The resonances of backbone atoms in PLA are labeled (b and d) and are consistent with our previous reports of P3AT-PLA block copolymers.[54] Also highlighted are the proton on the thiophene ring (a) and the protons on the alpha carbon of the alkyl chains (c). The resonances associated with these protons appear quite differently depending on whether the P3AT is regioregular or regiorandom. The inset shows that in the PLA-*Re*P3DDT(0.39)-PLA(34) case proton (a) is a singlet, but it is a multiplet for PLA-*Ra*P3HT(0.46)-PLA(14).[85] In the regioregular case, almost all repeat units are linked head-to-tail (Chapter 2), while the repeat units of the regiorandom polythiophene have an equal probability of being linked head-to-tail, tail-to-tail, head-to-head, and tail-to-head. This is also the reason for the resonance at δ ≈ 2.7 ppm to appear as a singlet for the regioregular P3AT and as a doublet for the regiorandom P3AT. Finally note that because the polymers shown have relatively high molecular weights, the end group resonances are not clearly visible in the full ^{1}H NMR spectrum.

The molecular weight distributions of the homopolymers and triblock copolymer materials were evaluated by SEC, and chromatographs collected by refractive index (RI) and ultraviolet-visible (UV-Vis) light detectors are shown in Chapter 9.2. Importantly, the spectra recorded by the RI and UV-Vis detectors matched one another. These chromatographs reinforce the ^{1}H NMR end group analyses that there are no P3AT or PLA homopolymers present in the samples. The results show a general trend of constant polydispersity indices with increasing PLA molecular weight. Because the reactions were terminated at a low conversion of lactide, we would expect a narrow molecular weight distribution for the polylactide moiety that was not dependent upon the regioregularity of the polymer; however, the observed PDI values for the triblock copolymers were both above and below the polydispersity indices for the homopolymers. Small, yet clear, shifts to higher elution volumes upon the addition of higher molecular weight PLA were seen in both series, as well. We have previously observed similar behavior in P3AT-PLA diblock copolymer systems, and believe the

small shift in elution volume reflects the coil-rod-coil character of PLA-P3AT-PLA type polymers.[54]

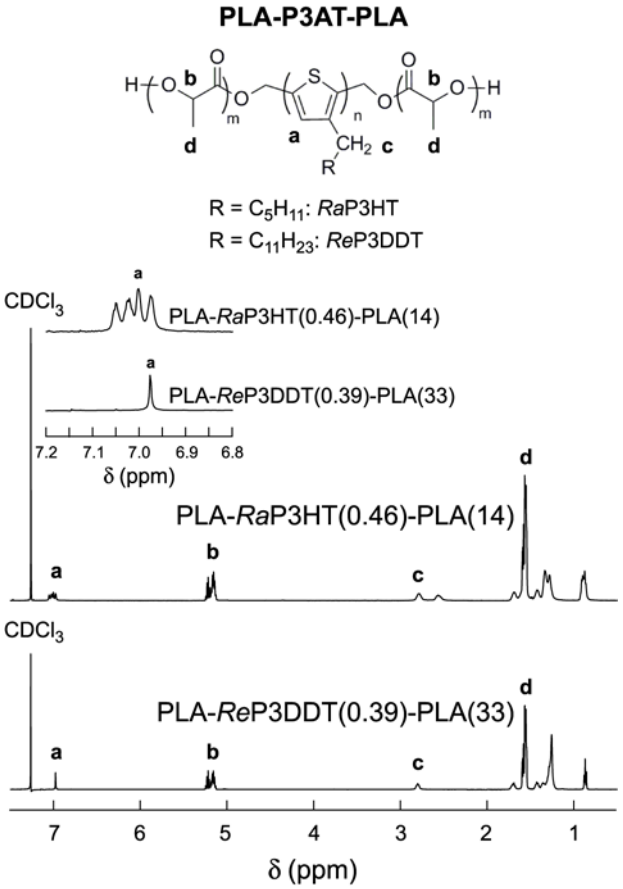

Figure 5.3. Representative ^{1}H NMR spectra of PLA-*Re*P3DDT(0.39)-PLA(33) (lower) and PLA-*Ra*P3HT(0.46)-PLA(14) (upper). The inset highlights the difference in splitting patterns between the regiorandom and regioregular polythiophenes of the main chain proton labeled (a). The unlabeled peaks upfield of δ = 2 ppm are due to the protons of the side chain. The polymers were dissolved in deuterated chloroform and spectra were recorded at room temperature.

Thermal Characterization of PLA-P3AT-PLA. The thermal transitions of the polymers were analyzed by DSC, and these transitional temperatures are summarized in Table 5.1. While the synthesis and molecular characterization of regioregular and regiorandom P3AT-containing polymers were similar, Figure 5.4 begins to illustrate the vast differences in microstructures that changes to stereospecificity can create. As is

common, three thermal transitions for HO-*Re*P3DDT-OH are observed and correspond to the glass transition temperature (T_g ~ –10 °C), side-chain melting temperature (T_{mSC} ~25–80 °C), and the main chain melting temperature (T_m ~156 °C) of the polymer.[86] The glass transition has a weak signal while the melting transition of the ordered, interdigitated dodecyl side groups is broad. As more PLA is incorporated into PLA-*Re*P3DDT-PLA these two transitions become harder to observe with both being obscured in Figure 5.4a for the PLA-*Re*P3DDT(0.39)-PLA(33) and PLA-*Re*P3DDT(0.37)-PLA(35) samples. However, the glass transition temperature can be observed at a magnified scale for all samples (not shown) and remains constant at T_g ~ –9 °C. Also present in the PLA-*Re*P3DDT-PLA samples is the glass transition temperature of polylactide (T_g ~56 °C) that increases slightly with increasing PLA molecular weight, as expected.[87] The clear separation of the P3AT and PLA glass transition temperatures in all of the block copolymer samples suggests the presence of distinct, microphase separated domains. Cleary visible in each of the *Re*P3DDT-based samples is the main chain melting transition, which remains at an approximately constant temperature of 158 °C. This relatively low melting temperature is useful for this particular polymer system as the polythiophene block can melt prior to the thermal degradation of PLA. This would not be the case if regioregular poly(3-hexylthiophene) was used as the middle block as the main chain melting temperature of P3HT is ~220 °C.[78] The reported infinite heat of melting for an ideal P3DDT crystal is ΔH_m^∞ = 55 J/g.[88] Integrating the area under the main chain melting peak of the HO-*Re*P3DDT-OH thermogram and dividing by ΔH_m^∞ yields a polymer percent crystallinity of 16%. This is much higher than any of the PLA-*Re*P3DDT-PLA triblock copolymers, which all have percent crystallinity values of ~4%. Note that the percent crystallinity values listed in Table 5.1 were normalized by the weight fraction of P3DDT present in each sample. We have observed a decrease in crystallinity of regioregular P3DDT samples upon the addition of PLA before in *Re*P3DDT-PLA block copolymers.[54] However, the four-fold decrease in crystallinity currently seen is much larger than in the diblock copolymer. We speculate that the large decrease in the amount of crystalline material in PLA-

*Re*P3DDT-PLA samples relative to *Re*P3DDT-PLA arises due to packing frustration of the polythiophene moiety. In the diblock copolymer case, one end of the P3DDT block is free to enter and leave the crystal lattice without concerning itself with a polylactide block. The triblock copolymer is not afforded this luxury, and, in order to crystallize, the ends of the P3DDT chain must carry an entire PLA block through the polythiophene crystal matrix. In fact, the actuality that the triblock copolymers crystallize at all is a testament to the severe degree of undercooling that is present in the block copolymers at room temperature.

Regiorandom P3HT-based samples are completely amorphous and the thermogram of HO-*Ra*P3HT-OH shows only a weak, broad glass transition at T_g ~14 °C (Figure 5.4b) and no apparent melting transition (measured until T = 250 °C). The glass transition of the polythiophene block in the PLA-*Ra*P3HT-PLA block copolymers is almost entirely masked by the much stronger PLA glass transition signal, but the careful observer will notice a slight signal for the PLA-*R*aP3HT(0.56)-PLA(11) and PLA-*R*aP3HT(0.46)-PLA(14) in Figure 5.4b. In an analogous manner to the case of the regioregular P3DDT-based triblock copolymer series, the glass transition temperature of both blocks are distinct and have values that are near the homopolymer glass transition temperature values, which is an indication of microphase separation. Note that as the molecular weight of the PLA blocks are increased, the signal from the glass transition increases as does the actual glass transition temperature, which are to be expected.

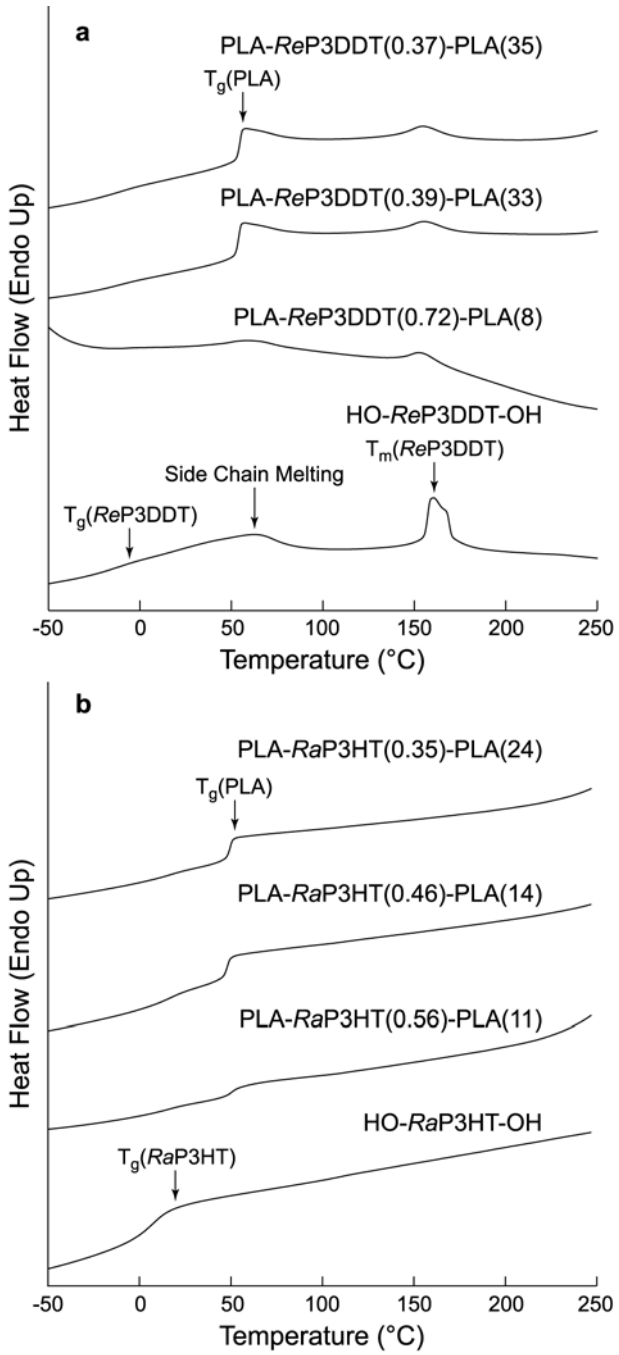

Figure 5.4. DSC thermograms of the (a) regioregular P3DDT and (b) regiorandom P3HT series. The scans shown were collected at a heating rate of 10 °C/min after annealing at 260 °C and then cooling to –60 °C. The percent crystallinity of the regioregular polythiophene components (see text for details) of HO-*Re*P3DDT-OH, PLA-*Re*P3DDT(0.70)-PLA(9), PLA-*Re*P3DDT(0.39)-PLA(33), and PLA-*Re*P3DDT(0.37)-PLA(35) were 16%, 4%, 5%, and 3%, respectively.

Wide-Angle X-ray Scattering (WAXS). The crystal structure of the homopolymers and triblock copolymers was monitored using WAXS. In agreement with DSC results, HO-*Ra*P3HT-OH showed only two broad humps ($q \approx 4$ nm^{-1}, $q \approx 15$ nm^{-1}) consistent with amorphous regimes and no crystalline reflections. As expected, no crystalline reflections were observed in the WAXS patterns of the PLA-*Ra*P3HT-PLA triblock copolymers (not shown). The regioregular polythiophene homopolymer, HO-*Re*P3DDT-OH, clearly showed the commonly observed lamellae structure with the (100), (200), and (300).[89,90] These peaks are also present (although weaker) in the PLA-*Re*P3DDT-PLA block copolymers. In agreement with the DSC results, these reflections are wider and less intense than what we have observed previously for *Re*P3DDT-PLA diblock copolymers, which suggests a lower amount of polythiophene crystallinity. Once again, we speculate that crystallinity is lowered in the triblock copolymer case due to the lack of a free polythiophene chain end, which is present in the diblock copolymer case. These spectra are also consistent with the DSC thermograms that suggested a small amount of polythiophene crystallinity even in block copolymers composed of greater than 60 wt% PLA. We note that as larger molecular weights of PLA are added to *Re*P3DDT, larger amorphous peaks grow in at higher q values (8 nm^{-1} < q < 18 nm^{-1}). This phenomenon has been observed in other PLA-containing block copolymer systems and has been ascribed to diffuse scattering due to amorphous polymer regimes.[91] The results presented here set the stage for the nanoscale phase separation observed in the SAXS data presented below. By using *Ra*P3HT-based block copolymers, we are assured that any phase separation observed in the triblock copolymers is not due to crystallization effects. This is in contrast to the kinetically driven, P3AT crystallization-induced phase separation seen in nearly every other P3AT-containing block copolymer system. Crystallization-induced phase separation is commonly observed because, as the current DSC and WAXS results have shown, only a small amount of regioregular polythiophene moiety is required to cause semicrystalline domains to form.

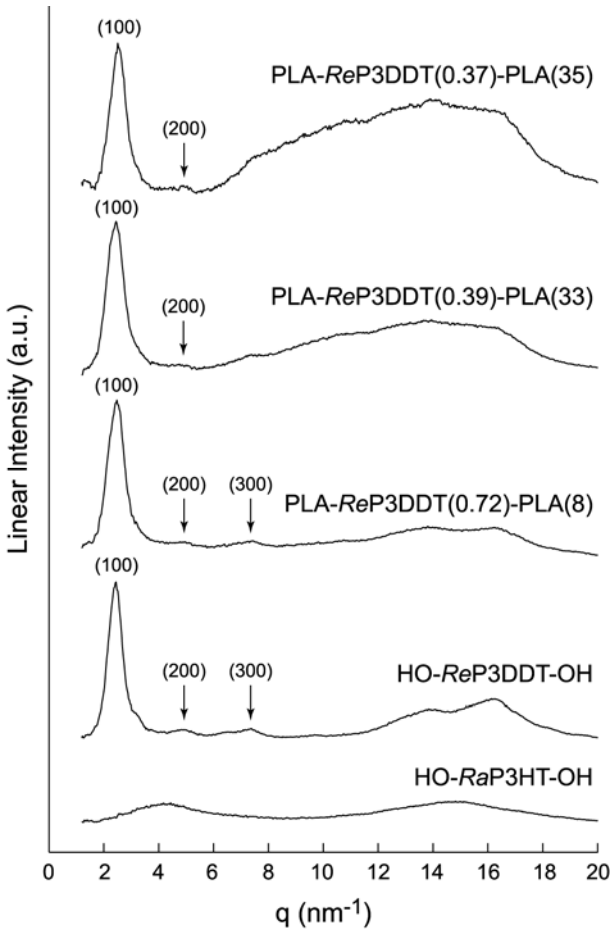

Figure 5.5. WAXS spectra of regiorandom HO-*Ra*P3HT-OH and the regioregular HO-*Re*P3DDT-OH series powders. The prominent lamellae reflections are marked for the semicrystalline samples. Note that all of the regioregular P3DDT samples exhibit the (100) and (200) reflections while the regiorandom sample does not; this confirms the melting transition (or lack thereof) results shown in Figure 5.4. No annealing treatments were performed prior to acquiring these data.

Small-Angle X-Ray Scattering (SAXS). SAXS was employed in order to observe the bulk microphase separation of the triblock copolymers. Figure 5.6a shows the spectra for the *Re*P3DDT-based block copolymer series. As expected, the HO-*Re*P3DDT-OH homopolymer showed no electron density contrast peak. The PLA-*Re*P3DDT-PLA block copolymers all showed one broad peak at relatively low q (high domain spacing) values. This peak has previously been attributed to the spacing between lamellae of crystalline P3AT (sometimes called nanofibrils) formed as the

amorphous blocks are excluded from the crystalline P3AT matrix.[46,50] Logically, as the molecular weight of the PLA blocks is increased, so is the spacing between the P3AT nanofibrils ($d \sim 40 - 70$ nm). While this domain spacing is roughly on the order of the exciton diffusion length, many groups have shown that long-range order is not achieved in this crystallization-induced type of phase separation. And, in practice, long-range order is required for block copolymers to be of use in most organic electronic applications.

In the case of the regiorandom series, HO-*Ra*P3HT-OH also does not exhibit any reflections over the q-range scanned, as expected. In contrast to the regioregular polythiophene-based block copolymers, the PLA-*Ra*P3HT-PLA block copolymers not only exhibit much more prominent first order reflections (q^*), but also show weak second order reflections that are a multiple of two from the primary reflection ($2q^*$). The domain spacing calculated from q^* suggests domain spacings of ~35 nm, very close to the length scale for exciton diffusion in organic photovoltaics. Also note that because HO-*Ra*P3HT-OH is amorphous the microphase separation cannot be the result of the polythiophene block crystallizing. The spacing between the first and second order reflections is consistent with the formation of lamellae of P3HT and PLA, but higher order reflections are required to confirm this hypothesis. The lack of higher order reflections is most likely due to the high polydispersities of the block copolymers (Table 5.1). While extremely high polydispersity (PDI) values block copolymers do not necessarily preclude the formation of long-range order, few experimental examples exist.[92,93] Despite the lack of third (or higher) order reflections, PLA-*Ra*P3HT(0.56)-PLA(11) is the first reported instance of a polythiophene-rich block copolymer that microphase separates into a structure that is not nanofibril-like. Cleary, there is an inherent difference in the mechanism of phase separation between regioregular and regiorandom polythiophene-based block copolymers and the apparent utility of the less studied *Ra*P3HT, in terms of morphological control, needs to be further investigated.

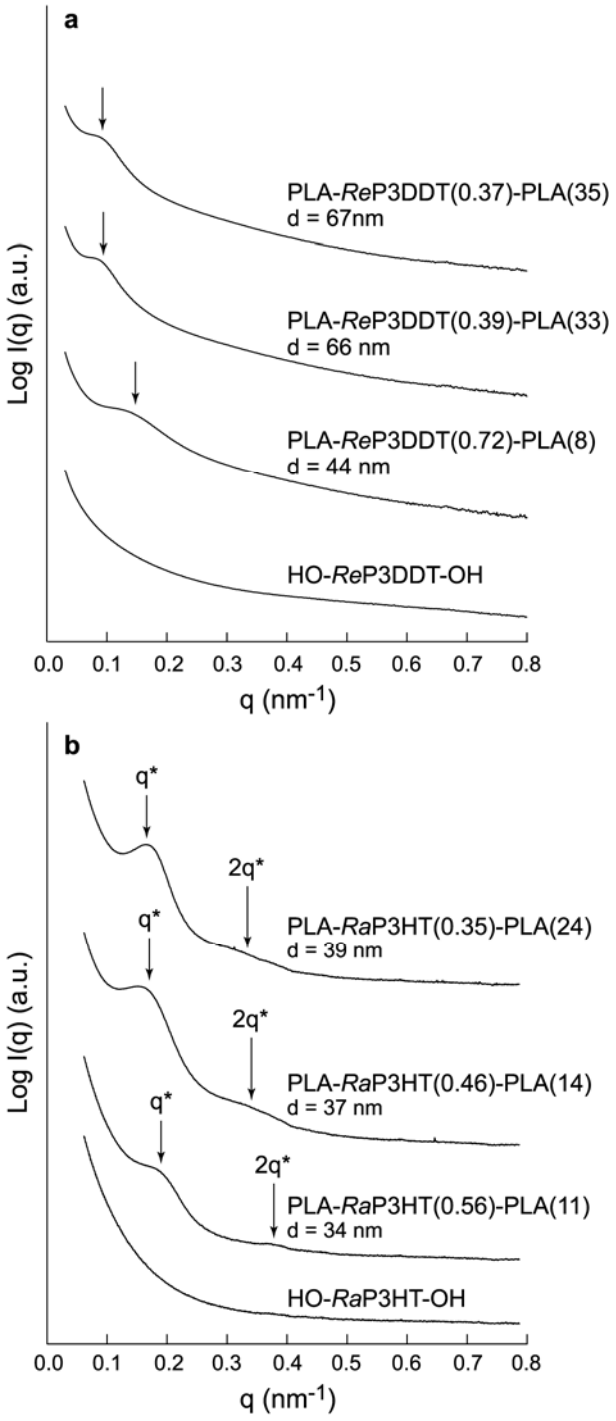

Figure 5.6. SAXS spectra of the (a) regioregular P3DDT series and (b) regiorandom P3HT series polymers taken at 50 °C. The polymers were first annealed at 180 °C and then slowly cooled back to 50 °C. The principle reflection for each sample is marked with an arrow and the domain spacing (*d*) is listed next to the sample label.

5.5 Summary

The synthesis and molecular characterization of a new class of polythiophene-containing ABA-type triblock copolymers has been shown where the middle (B) block is a polythiophene derivative and it is used as a difunctional initiator for the ring-opening polymerization of D,L-lactide. Two distinct series of block copolymers were developed that contained approximately the same number of thiophene repeat units. The first series was based on a regioregular poly(3-dodecylthiophene) precursor (HO-*Re*P3DDT-OH) that yielded PLA-*Re*P3DDT-PLA triblock copolymers, and the second series was synthesized from a regiorandom poly(3-hexylthiophene) (HO-*Ra*P3HT-OH) starting material to generate PLA-*Ra*P3HT-PLA block copolymers. Differential scanning calorimetry results showed that both of these starting, middle blocks had their terminal solid to liquid transitions below the degradation temperature of PLA. In the case of HO-*Re*P3DDT-OH, the final transition was a melting of the semicrystalline polythiophene domains at a temperature of T_m ~160 °C. HO-*Ra*P3HT-OH was completely amorphous and its terminal transition was a glass transition at T_g ~16 °C. Wide-angle x-ray scattering confirmed that the block copolymers containing regiorandom P3HT were amorphous. The *Re*P3DDT-based block copolymers continued to show reflections consistent with crystalline lamellae commonly observed in P3ATs even in block copolymers that contained high weight fractions of PLA. The ability or inability of the polythiophene block to crystallize greatly influenced the microphase separation observed in small-angle x-ray scattering experiments. We observed the regioregular polythiophene-containing block copolymer samples showed a single, broad reflection. *Ra*P3HT-based block copolymers, on the other hand, showed sharper primary reflections and even second order reflections because phase separation was controlled by crytallization. This is in contrast to the crystallization-induced phase separation commonly seen in regioregular P3AT-containing block copolymers and the *Re*P3DDT-based triblock copolymers in this work. The domain spacings for the *Ra*P3HT-based block copolymers were also much closer to the common exciton diffusion lengths in semiconducting polymers (*ca.* 37 nm). The *q*-spacing between the

primary and secondary reflections suggest that the three PLA-*Ra*P3HT-PLA block copolymers studied all assembled into lamellar morphologies, but further work is needed to confirm this initial conclusion. The difference in the mechanisms of ordering between regioregular and regiorandom P3AT-containing block copolymers is striking.

To this point, only a handful of PLA-*Ra*P3HT-PLA compositions have been explored, and many other microstructures may be available for this block copolymer system. Additionally, the domain spacing of these materials may be tuned by changing the molecular weights of the constituent polymers. These two new handles (that are not readily available in regioregular P3AT materials) can be used to develop a polythiophene-containing thin film with long-range order and tunable dimensions. Once the desired PLA-*Ra*P3HT-PLA thin film morphology is found, the PLA domains can be selectively etched to leave a nanoporous P3HT matrix, which could then be backfilled with an electron-accepting material to generate a true, all-organic ordered bulk heterojunction OPV device. It is this never before seen phase separation in P3AT-based block copolymers that makes the new class of regiorandom poly(3-hexylthiophene)-containing block copolymers so promising.

5.6 References

[1] Skotheim, T.; Reynolds, J.; Elsembauer, R.; Eds. *Handbook of Conducting Polymers*; Marcel Dekker: New York, 1998.

[2] Nalwa, H. S.; Ed. *Handbook of Organic Conductive Molecules and Polymers*; J. Wiley & Sons: New York, 1996.

[3] McCullough, R. D. *Adv. Mater.* **1998**, *10*, 93–116.

[4] Osaka, I.; McCullough, R. D. *Acc. Chem. Res.* **2008**, *41*, 1202–1214.

[5] Li, G.; Shrotriya, V.; Huang, J.; Yao, Y.; Moriarty, T.; Emery, K.; Yang, Y. *Nat. Mater.* **2005**, *4*, 864–868.

[6] Ma, W.; Yang, C.; Gong, X.; Lee, K.; Heeger, A. J. *Adv. Funct. Mater.* **2005**, *15*, 1617–1622.

[7] Park, S. H.; Roy, A.; Beaupré, S.; Cho, S.; Coates, N.; Moon, J. S.; Moses, D.; Leclerc, M.; Lee, K.; Heeger, A. J. *Nat. Photonics* **2009**, *3*, 297–303.

[8] Forrest, S. R. *MRS Bull.* **2005**, *30*, 28–32.

[9] Janssen, R. A. J.; Hummelen, J. C.; Sariciftci, N. S. *MRS Bull.* **2005**, *30*, 33–36.

[10] Gregg, B. A.; Hanna, M. C. *J. Appl. Phys.* **2003**, *93*, 3605–3614.

[11] Gregg, B. A. *MRS Bull.* **2005**, *30*, 20–22.

[12] Moon, J. S.; Lee, J. K.; Cho, S.; Byun, J.; Heeger, A. J. *Nano Lett.* **2009**, *9*, 230–234.

[13] Sun, S.; Sariciftci, N. S.; Eds. *Organic Photovoltaics: Mechanisms, Materials, and Devices*; Taylor & Francis: Boca Raton, FL, 2005.

[14] Dennler, G.; Scharber, M. C.; Brabec, C. J. *Adv. Mater.* **2009**, *21*, 1323–1338.

[15] Thompson, B. C.; Fréchet, J. M. J. *Angew. Chem., Int. Ed.* **2008**, *47*, 58–77.

[16] Peet, J.; Heeger, A. J.; Bazan, G. C. *Acc. Chem. Res.* **2009**, *ACS ASAP*.

[17] Schilinsky, P.; Waldauf, C.; Brabec, C. J. *Appl. Phys. Lett.* **2002**, *81*, 3885–3887.

[18] Padinger, F.; Rittberger, R. S.; Sariciftci, N. S. *Adv. Funct. Mater.* **2003**, *13*, 85–88.

[19] Erb, T.; Zhokhavets, U.; Gobsch, G.; Raleva, S.; Stühn, B.; Schilinsky, P.; Waldauf, C.; Brabec, C. J. *Adv. Funct. Mater.* **2005**, *15*, 1193–1196.

[20] Clarke, T. M.; Ballantyne, A. M.; Nelson, J.; Bradley, D. D. C.; Durrant, J. R. *Adv. Funct. Mater.* **2008**, *18*, 4029–4035.

[21] Müller, C.; Ferenczi, T. A. M.; Campoy-Quiles, M.; Frost, J. M.; Bradley, D. D. C.; Smith, P.; Stingelin-Stutzmann, N.; Nelson, J. *Adv. Mater.* **2008**, *20*, 3510–3515.

[22] Kim, J. Y.; Frisbie, C. D. *J. Phys. Chem. C* **2008**, *112*, 17726–17736.

[23] Günes, S.; Neugebauer, H.; Sariciftci, N. S. *Chem. Rev.* **2007**, *107*, 1324–1338.

[24] Kim, B. J.; Miyamoto, Y.; Ma, B.; Fréchet, J. M. J. *Adv. Mater.* **2009**, *19*, 1–9.

[25] Coakley, K. M.; McGehee, M. D. *Appl. Phys. Lett.* **2003**, *83*, 3380–3382.

[26] Lipomi, D. J.; Chiechi, R. C.; Reus, W. F.; Whitesides, G. M. *Adv. Funct. Mater.* **2008**, *18*, 3469–3477.

[27] Xi, H.; Wei, Z.; Duan, Z.; Xu, W.; Zhu, D. *J. Phys. Chem. C* **2008**, *112*, 19934–19938.

[28] Watkins, P. K.; Walker, A. B.; Verschoor, G. L. B. *Nano Lett.* **2005**, *5*, 1814–1818.

[29] Yang, F.; Forrest, S. R. *ACS Nano* **2008**, *2*, 1022–1032.

[30] Bates, F. S.; Fredrickson, G. H. *Annu. Rev. Phys. Chem.* **1990**, *41*, 525–557.

[31] Shull, K. R. *Macromolecules* **1992**, *25*, 2122–2133.

[32] Alexander-Katz, A.; Fredrickson, G. H. *Macromolecules* **2007**, *40*, 4075–4087.

[33] Russell, T. P.; Coulon, G.; Deline, V. R.; Miller, D. C. *Macromolecules* **1989**, *22*, 4600–4606.

[34] Menelle, A.; Russell, T. P.; Anastasiadis, S. H.; Satija, S. K.; Majkrzak, C. F. *Phys. Rev. Lett.* **1992**, *68*, 67–70.

[35] Sikka, M.; Singh, N.; Karim, A.; Bates, F. S.; Satija, S. K.; Majkrzak, C. F. *Phys. Rev. Lett.* **1993**, *70*, 307–310.

[36] Morkved, T. L.; Lu, M.; Urbas, A. M.; Ehrichs, E. E.; Jaeger, H. M.; Mansky, P.; Russell, T. P. *Science* **1996**, *273*, 931–933.

[37] Huang, E.; Rockford, L.; Russell, T. P.; Hawker, C. J. *Nature* **1998**, *31*, 757–758.

[38] Szwarc, M.; Levy, M.; Milkovich, R. *J. Am. Chem. Soc.* **1956**, *78*, 2656–2657.

[39] Schlick, S.; Levy, M. *J. Phys. Chem.* **1960**, *64*, 883–886.

[40] Hadjichristidis, N.; Pispas, S.; Floudas, G. A. *Block Copolymers: Synthetic Strategies, Physical Properties, and Applications*; John Wiley & Sons, Inc.: Hoboken, NJ, 2003.

[41] Halperin, A. *Macromolecules* **1990**, *23*, 2724–2731.

[42] Williams, D. R. M.; Fredrickson, G. H. *Macromolecules* **1992**, *25*, 3561–3568.

[43] Matsen, M. W.; Barrett, C. *J. Chem. Phys.* **1998**, *109*, 4108–4118.

[44] Pryamitsyn, V.; Ganesan, V. *J. Chem. Phys.* **2004**, *120*, 5824–5838.

[45] Olsen, B. D.; Shah, M.; Ganesan, V.; Segalman, R. A. *Macromolecules* **2008**, *41*, 6809–6817.

[46] Liu, J.; Sheina, E.; Kowalewski, T.; McCullough, R. D. *Angew. Chem., Int. Ed.* **2002**, *41*, 329–332.

[47] Tu, G.; Li, H.; Forster, M.; Heiderhoff, R.; Balk, L. J.; Scherf, U. *Macromolecules* **2006**, *39*, 4327–4331.

[48] Iovu, M. C.; Jeffries-EL, M.; Zhang, R.; Kowalewski, T.; McCullough, R. D. *J. Polym. Sci. Part A*, **2006**, *43*, 1991–2000.

[49] Sauvé, G.; McCullough, R. D. *Adv. Mater.* **2007**, *19*, 1822–1825.

[50] Dai, C.; Yen, W.; Lee, Y.; Ho, C.; Su, W. *J. Am. Chem. Soc.* **2007**, *129*, 11036–11038.

[51] Iovu, M. C.; Craley, R.; Jeffries-EL, M.; Krankowski, A. B.; Zhang, R.; Kowalewski, T.; McCullough, R. D. *Macromolecules* **2007**, *40*, 4733–4735.

[52] Sommer, M.; Lang, A. S.; Thelakkat, M. *Angew. Chem., Int. Ed.* **2008**, *47*, 7901–7904.

[53] Richard, F.; Brochon, C.; Leclerc, N.; Eckhardt, D.; Heiser, T.; Hadziioannou, G. *Macromol. Rapid Commun.* **2008**, *29*, 885–891.

[54] Boudouris, B. W.; Frisbie, C. D.; Hillmyer, M. A. *Macromolecules* **2008**, *41*, 67–75.

[55] Higashihara, T.; Ohshimizu, K.; Hirao, A.; Ueda, M. *Macromolecules* **2008**, *41*, 9505–9507.

[56] Urien, M.; Erothu, H.; Cloutet, E.; Hiorns, R. C.; Vignau, L.; Cramail, H. *Macromolecules* **2008**, *41*, 7033–7040.

[57] Higashihara, T.; Ueda, M. *React. Funct. Polym.* **2009**, *69*, 457–462.

[58] Zhang, Q.; Cirpan, A.; Russell, T. P.; Emrick, T. *Macromolecules* **2009**, *42*, 1079–1082.

[59] Loewe, R. S.; Khersonsky, S. M.; McCullough, R. D. *Adv. Mater.* **1999**, *11*, 250–253.

[60] Jeffries-EL, M.; Sauvé, G.; McCullough, R. D. *Adv. Mater.* **2004**, *16*, 1017–1019.

[61] Olsen, B. D.; Segalman, R. A. *Macromolecules* **2005**, *38*, 10127–10137.

[62] Olsen, B. D.; Segalman, R. A. *Macromolecules* **2006**, *39*, 7078–7083.

[63] Olsen, B. D.; Li, X.; Wang, J.; Segalman, R. A. *Macromolecules* **2007**, *40*, 3287–3295.

[64] Olsen, B. D.; Segalman, R. A. *Mater. Sci. Eng., R* **2008**, *62*, 37–66.

[65] Schmidt, S. C.; Hillmyer, M. A. *Macromolecules* **1999**, *32*, 4794–4801.

[66] Kricheldorf, H.; Berl, M.; Scharnagle, N. *Macromolecules* **1988**, *21*, 286–293.

[67] Wang, Y.; Hillmyer, M. A. *Macromolecules* **2000**, *33*, 7395–7403.

[68] Olayo-Valles, R.; Guo, S.; Lund, M. S.; Leighton, C.; Hillmyer, M. A. *Macromolecules* **2005**, *38*, 10101–10108.

[69] Tashiro, K.; Kobayashi, M.; Kawai, T.; Yoshino, K. *Polymer* **1997**, *38*, 2867–2879.

[70] Liu, J.; McCullough, R. D. *Macromolecules* **2002**, *35*, 9882–9889.

[71] Boudouris, B. W.; Molins, F.; Blank, D. A.; Frisbie, C. D.; Hillmyer, M. A. *Macromolecules* **2009**, *42*, 4118–4126.

[72] Witiak, D. T.; Williams, D. R.; Kakodkar, S. V. *J. Org. Chem.* **1974**, *39*, 1242–1247.

[73] Trznadel, M.; Pron, A.; Zagorska, M.; Chrzaszcz, R.; Pielichowski, J. *Macromolecules* **1998**, *31*, 5051–5058.

[74] Merlo, J. A.; Frisbie, C. D. *J. Phys. Chem. B* **2004**, *108*, 19169–19179.

[75] Loewe, R. S.; Ewbank, P. C.; Liu, J.; Zhai, L.; McCullough, R. D. *Macromolecules* **2001**, *34*, 4324–4333.

[76] Iovu, M. C.; Sheina, E. E.; Gil, R. R.; McCullough, R. D. *Macromolecules* **2005**, *38*, 8649–8656.

[77] Causin, V.; Marega, C.; Marigo, A.; Valentini, L.; Kenny, J. M. *Macromolecules* **2005**, *38*, 409–415.

[78] Kuila, B. K.; Nandi, A. K. *Macromolecules* **2004**, *37*, 8577–8584.

[79] Kricheldorf, H. R.; Kreiser-Saunders, I.; Stricker, A. *Macromolecules* **2000**, *33*, 702–709.

[80] Ryner, M.; Stridsberg, K.; Albertsson, A. C.; von Schenck, H.; Svensson, M. *Macromolecules* **2001**, *34*, 3877–3881.

[81] Dove, A. P. *Chem. Commun.* **2008**, *48*, 6446–6470.

[82] Li, S. *J. Biomed. Mater. Res.* **1999**, *48*, 342–353.

[83] Liu, J.; Loewe, R. S.; McCullough, R. D. *Macromolecules* **1999**, *32*, 5777–5785.

[84] Fan, Y.; Chen, G.; Tanaka, J.; Tateishi, T. *Biomacromolecules* **2005**, *6*, 3051–3056.

[85] Chen, T. A.; Wu, X.; Rieke, R. D. *J. Am. Chem. Soc.* **1995**, *117*, 233–244.

[86] Liu, S. L.; Chung, T. S. *Polymer* **2000**, *41*, 2781–2793.

[87] Anderson, K. S.; Hillmyer, M. A. *Polymer* **2006**, *47*, 2030–2035.

[88] Malik, S.; Nandi, A. K. *J. Poly. Sci. B* **2002**, *40*, 2073–2085.

[89] Chen, S.; Lee, S. *Polymer* **1995**, *36*, 1719–1723.

[90] Prosa, T. J.; Moulton, J.; Heeger, A. J.; Winokur, M. J. *Macromolecules* **1999**, *32*, 4000–4009.

[91] Hamilton, B. D.; Weissbuch, I.; Lahav, M.; Hillmyer, M. A.; Ward, M. D. *J. Am. Chem. Soc.* **2009**, *131*, 2588–2596.

[92] Bendejacq, D.; Ponsinet, V.; Joanicot, M.; Loo, Y. L.; Register, R. A. *Macromolecules* **2002**, *35*, 6645–6649.

[93] Lynd, N. A.; Meuler, A. J.; Hillmyer, M. A. *Prog. Polym. Sci.* **2008**, *33*, 875–893.

6 Amorphous Polythiophene-based Block Copolymers with Relatively Narrow Polydispersities

6.1 Overview

We report on a series of polythiophene-based triblock copolymers, polylactide-*b*-poly(3-dodecylthiophene-*co*-thiophene)-*b*-polylactide (PLA-coPT-PLA), synthesized using a combination of the controlled Grignard metathesis (GRIM) polymerization and ring-opening polymerization (ROP) techniques. Typically, the GRIM polymerization method yields high molecular weight, low polydispersity poly(3-alkythiophene)s (P3ATs) that are semicrystalline. By manipulating the side chain substituent groups we have synthesized a polythiophene block that is completely amorphous which also retains the advantages associated with a controlled polymerization. The molecular properties of the triblock copolymers were characterized by ^{1}H NMR spectroscopy and size exclusion chromatography (SEC). Differential scanning calorimetry (DSC) and powder wide-angle x-ray scattering (WAXS) indicated that the poly(3-dodecylthiophene-*co*-thiophene) homopolymer and the PLA-coPT-PLA block copolymers were amorphous. Despite the lack of crystalline domains, ultraviolet-visible (UV-Vis) absorption spectroscopy of polymer thin films showed that the materials have a low band gap (E_g ~1.9 eV) and a high absorption coefficient ($\alpha \approx 7.4 \times 10^4$ cm^{-1} at λ_{max} = 490 nm). The advantage of using an amorphous polythiophene block, in terms of controlling the microstructural long-range order on the nanoscale, was detailed in Chapter 5. Therefore, using these low polydispersity macromolecules to direct the microphase separation of semiconducting block copolymer thin films could prove useful for organic photovoltaic applications.

6.2 Introduction

The synthesis of new, soluble polythiophene derivatives, such as poly(3-alkylthiophenes) (P3ATs), has become increasingly important as these macromolecules are commonly used in a variety of organic electronic devices. Polythiophenes are frequently employed because they are good hole-transporting materials (μ_h ~0.1-1 cm^2

$V^{-1}s^{-1}$), have some of the narrowest band gaps of organic semiconductors (E_g ~1.9 eV), and can be processed from a wide selection of organic solvents.[1,2] Importantly, the optoelectronic properties of these polymer semiconductors can be tuned by modifying the chemical structure of the macromolecules.[3,4] In fact, thiophene-containing polymers have been the preeminent electron-donating materials in high performance, bulk heterojunction organic photovoltaics (OPVs) where the power conversion efficiencies of devices have reached ~5-6%.[5-7] In OPV devices absorption of a photon creates a bound electron-hole pair (exciton) that randomly diffuses through space (with a diffusion length, L_d ~10–40 nm) before recombining. If the exciton reaches an electron donor-acceptor interface prior to recombination the exciton can separate into a free electron and hole, which can be collected at the electrodes to add to the net photocurrent.[8-11] Thus, the microstructure of the active layers in these devices must be controlled if high efficiency devices are to be fabricated.[12,13] Currently, the morphology of the active layers of these devices is tuned by controlling the coating[5] and post-processing conditions[5,14-17] of the organic layer. The phase behavior of polythiophene-fullerene solid solutions has been studied,[18,19] but the most efficient solar cells are still fabricated with non-equilibrium active layer morphologies. Because this can result in degradation of device performance with time, researchers have begun to turn their attention towards ordered bulk heterojunction active layers.[20-22] In these systems, active layers are well-ordered and the domain spacings could be manipulated to maximize device performance, in theory.

Unlike the majority of block copolymer systems,[23-25] polythiophenes, and many other semiconducting polymers, have rigid polymer backbone bonds, and adopt stiff polymer backbone configurations (rod) in the melt. This makes the microstructure of rod-containing block copolymers harder to predict than those composed entirely of polymers that have backbone configurations which follow a Gaussian coil spatial distribution (coil) in the melt. Because of their potential application in organic electronics, the phase behavior of P3AT-containing block copolymers has been increasingly studied.[26-38] Except for the instance of poly(3-hexylthiophene)-*b*-poly(2-

vinylpyridine) (P3HT-P2VP), long-range and well-ordered structures have not been shown either in the bulk or in thin films. In fact, the P3HT-P2VP system only formed ordered microstructures after very specific solvent annealing conditions were used.[30] It is generally thought that this lack of long-range order occurs because the crystallization of the polythiophene moiety dominates any phase separation that exists in the system.

A paradigm shift in the methods for P3AT synthesis occurred when the McCullough group introduced the Grignard metathesis (GRIM) method, and this synthetic route has become the predominant method for the creation of polythiophene derivatives.[39] This reaction pathway yields highly regioregular polythiophenes with low polydispersities, and the molecular weight of the polythiophene can be tuned easily by controlling the amount of catalyst added to the reaction mixture. Traditionally, the regioregular, semicrystalline polythiophenes generated by the GRIM method have been desired due to their enhanced optoelectronic properties relative to their regiorandom, non-crystalline counterparts. However, copolymerization of thiophene monomers using the GRIM method has proven to yield non-crystalline polymers,[40,41] and these amorphous polythiophenes may prove more useful in generating ordered block copolymer microstructures.

In this paper we report the stepwise synthesis of polylactide-*b*-poly(3-dodecylthiophene-*co*-polythiophene)-*b*-polylactide block copolymers (PLA-coPT-PLA) by first generating a hydroxyl-terminated polythiophene (HO-coPT-OH) which is used as a macroinitiator for the controlled ring-opening polymerization of D,L-lactide.[42-44] The utility of the polylactide moiety in polythiophene-containing block copolymers has been shown previously.[34] The employment of the GRIM polymerization method for the synthesis of a random copolymer of polythiophene and poly(3-dodecylthiophene) generates a semiconducting midblock with a narrow molecular weight distribution. Importantly, differential scanning calorimetry (DSC) and powder x-ray scattering data indicate both the HO-coPT-OH precursor and the PLA-coPT-PLA block copolymers are completely amorphous. Also, the glass transition temperature of the PT block is below the degradation temperature of PLA (T_d ~200 °C).[45] Additionally, ultraviolet-

visible light (UV-Vis) absorption spectroscopy measurements of block copolymer thin films show that the PT block has a band gap comparable to regioregular poly(3-hexylthiophene). In Chapter 5 we showed that designing an amorphous polythiophene block allows for thermodynamically-controlled microphase separation in polylactide-*b*-poly(3-hexylthiophene)-*b*-polylactide (PLA-P3HT-PLA) block copolymer, but long-range order was not observed in this system due to the large PDI of the P3HT block.[46,47] The possibility of generating semiconducting block copolymer templates with long-range order, where the equilibrium morphologies can be systematically tuned, motivated our efforts to develop triblock copolymers with a midblock composed of two thiophene monomers.

6.3 Results and Discussion

Synthesis of PLA-coP3AT-PLA. 2,5-dibromo-3-dodecylthiophene and 2-5-dibromothiophene were copolymerized in a controlled manner using the Grignard metathesis (GRIM) method.[39] After polymerization, the product (H-coPT-Br) was purified by Soxhlet extraction using methanol, hexane, methylene chloride, and chloroform in a sequential manner. The methanol, hexane, and methylene chloride fractions helped to remove residual reaction materials and low molecular weight polymers while the chloroform fraction was used in further reactions.[48,49] The reaction scheme for the synthesis of H-coPT-Br and PLA-coPT-PLA is shown in Figure 6.1, and full experimental details may be found in Chapter 9.2. Because the GRIM polymerization is well-controlled, the HO-coPT-OH macroinitiator was kept at a reasonably low polydispersity index (PDI = 1.7).[50,51] The use of the GRIM method also allows for easy control of the polythiophene molecular weight by tuning the reaction conditions. In this work a low molecular weight polythiophene block was used intentionally to aid in molecular characterization. The copolymerization of 3-dodecylthiophene and thiophene repeat units has previously occurred using similar reaction conditions.[40,41] In these instances an equimolar feed of activated 3-dodecylthiophene (3DDT) and thiophene (T) monomers led to copolymers with a 1:1 ratio of 3DDT to T repeat units. However, we found that an equimolar mixture of

activated monomer generated a copolymer that had a 2:1 molar ratio of 3DDT:T repeat units. Despite the fact that polythiophenes polymerized using the GRIM route can be end-functionalized in situ with functional groups (*i.e.* vinyl groups) using an appropriate Grignard reaction,[52] we chose to quench the reaction with acid in order to generate difunctional macroinitiators. End-functionalization of the polythiophene to generate HO-coPT-OH occurred in a manner similar to that presented in Chapter 5.[53,54] As such, large excesses of reagents were used in all post-polymerization functionalization steps. This protocol drove all reactions to full conversion, and generated a well-defined, difunctional macroinitiator for the ring-opening polymerization of D,L-lactide to yield the atactic form of PLA.[55] Once again, the catalyst selected for the PLA polymerization was the commonly used tin octanoate [$Sn(oct)_2$].[56,57] By using $Sn(oct)_2$ we were able to easily control the molecular weight of the resultant PLA blocks.[58] The molecular weight of the PLA blocks was changed by varying the initial amount of lactide present while keeping the initial concentration and conversion of lactide constant. A series consisting of four PLA-coPT-PLA block copolymers was synthesized from the parent HO-coPT-OH molecule.

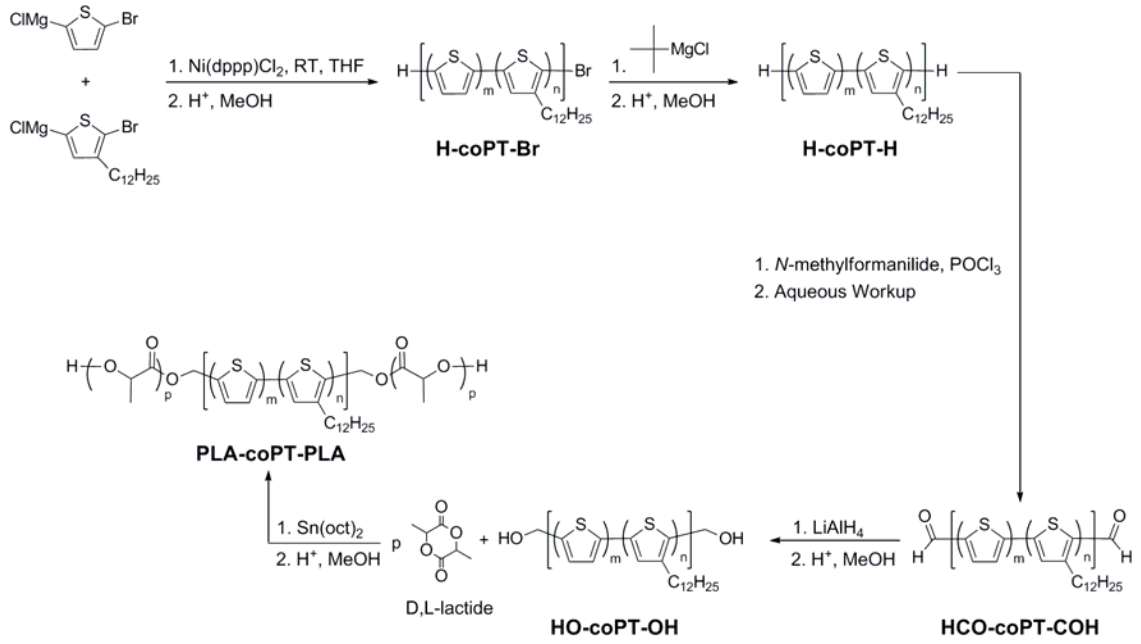

Figure 6.1. Synthetic scheme for the formation of PLA-coPT-PLA triblock copolymers. The feed ratio of activated monomers in the polymerization was equimolar. However, the resultant polymers used in this work had thiophene repeat units with m = 10 and n = 20. Note that Ni(dppp)Cl_2 is 1,3-bis(diphenylphosphino)propane nickel (II) chloride.

Molecular Characterization of PLA-coPT-PLA. ^{1}H NMR spectroscopy was used to monitor the chemical shifts of the resonances associated with the protons of functionalized coPTs. The molecular weight of the HO-coPT-OH homopolymer was determined by ^{1}H NMR spectroscopy using end group analysis, and these molecular weights were used in all further computations. The molecular weight of the coPT block for all polymers was found to be $M_n \approx 5.8$ kg/mol. As a note, the nomenclature used for the triblock copolymers in this chapter is the same as that used in Chapter 5. Therefore, a block copolymer that is composed of X% polythiophene by weight and has an overall PLA molecular weight of Y kg/mol is given the label PLA-coPT(0.X)-PLA(Y). Figure 6.2 shows the ^{1}H NMR spectra and chemical structures for the HO-coPT-OH homopolymer and a representative triblock copolymer, PLA-coPT(0.59)-PLA(4.0). The homopolymer spectra compared well with a previous report.[40] The ratio of the average number of repeat units of thiophene and 3-dodecylthiophene incorporated into the

homopolymer were determined by comparing the area under the peaks located at $\delta \approx 0.87$ ppm and $\delta \approx 7.05$ ppm. The upfield resonance is associated exclusively with the protons of the terminal CH_3 group of the dodecyl side chain. We found that there were 20 thiophene rings, on average, in the polymer chain that contained this substitution. The peak near 7 ppm, on the other hand, is associated with the protons bonded to the thiophene ring both in the unsubstituted thiophene (a, Figure 6.2) and the substituted 3-dodecylthiophene (b, Figure 6.2). Knowing that the integration value required the inclusion of 20 substituted thiophene rings, we were able to calculate an average of 10 thiophene repeat units per polymer chain. This 2:1 ratio of 3-dodecylthiophene:thiophene repeat units (n =20, m = 10) indicates the copolymer is richer in substituted thiophene than the feed stream, which had a ratio of 1:1 activated 3-dodecylthiophene:thiophene monomers. Note that previous reports of this copolymerization (using slightly different activated thiophene monomers) showed that the copolymer composition was the same as the initial feedstock.[40,41] Upon the addition of PLA to HO-coPT-OH, two large resonances are observed at $\delta \approx 1.6$ ppm (e, Figure 6.2) and $\delta \approx 5.2$ (f, Figure 6.2). These peaks are consistent with the backbone protons in the PLA blocks, which we have previously observed in polythiophene-polylactide block copolymers.[34] The inset highlights the shift in end group resonances upon the addition of polylactide. The presence of the doublet at $\delta \approx 4.75$ ppm (c, Figure 6.2) for the HO-coPT-OH agrees with a previous report[53] and the results presented in Chapter 5 for the HO-P3AT-OH polymers. This peak completely vanishes and the peak at $\delta \approx 4.35$ ppm (d, Figure 6.2) appears upon the addition of PLA. The resonance labeled d is consistent with the terminal lactide repeat unit.[59] Integration of the areas under the end group and main chain peaks before and after lactide polymerizations were in good agreement with the structures shown.

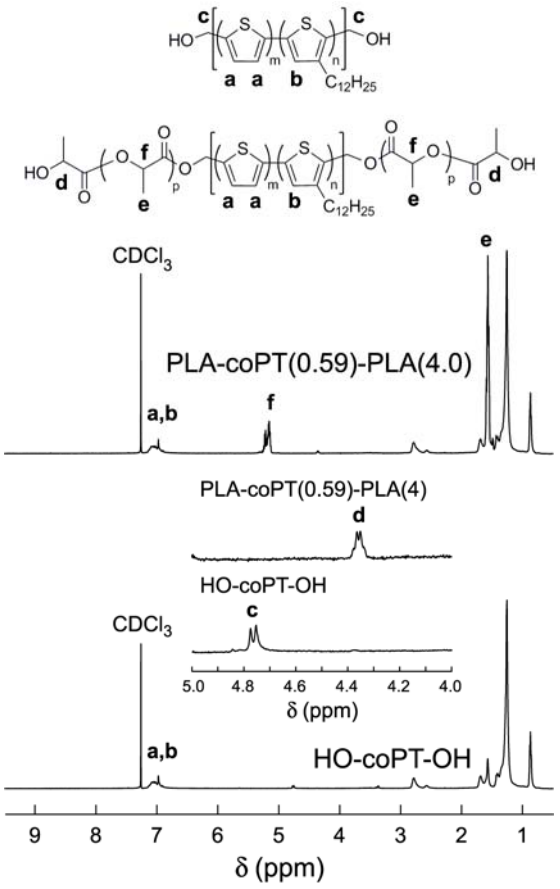

Figure 6.2. ^{1}H NMR spectra of the homopolymer (HO-coPT-OH) and a representative block copolymer [PLA-coPT(0.59)-PLA(4.0)]. The inset shows a magnified view of the region of interest for the end group resonances. The unlabeled peaks upfield of δ = 3 ppm are due to the protons of the dodecyl side chain. The polymers were dissolved in deuterated chloroform and spectra were recorded at room temperature.

The molecular weight distributions of the homopolymers and triblock copolymer materials were evaluated by SEC, and chromatographs recorded using an ultraviolet-visible (UV-Vis) light detector are shown in Figure 6.3. The results show a general trend of decreasing polydispersity indices (PDI values listed in Figure 6.3) with increasing PLA molecular weight. Narrowing of the molecular weight distribution with increasing PLA chain length was expected because the PLA polymerizations were terminated at low conversions of lactide (see Chapter 9.2). Obvious shifts to lower elution volumes upon the addition of higher molecular weight PLA was observed for all

four PLA-coPT-PLA block copolymers. The small shift in elution volume between the homopolymer and the triblock copolymers is attributed to the coil-rod-coil character of PLA-P3AT-PLA type polymers.[34] We note that for the polymer with the highest molecular weight of polylactide, PLA-coPT(0.14)-PLA(35.7), there is a low intensity signal that overlaps with the elution volume of the HO-coPT-OH precursor ($V_{elute} \approx 23.5$ mL). This shoulder corresponds to less than 10% of the signal from the main peak at $V_{elute} \approx 19.5$ mL. Therefore, any homopolymer contamination may be considered small, and, in fact, was within the experimental error in the ^{1}H NMR measurements previously discussed.

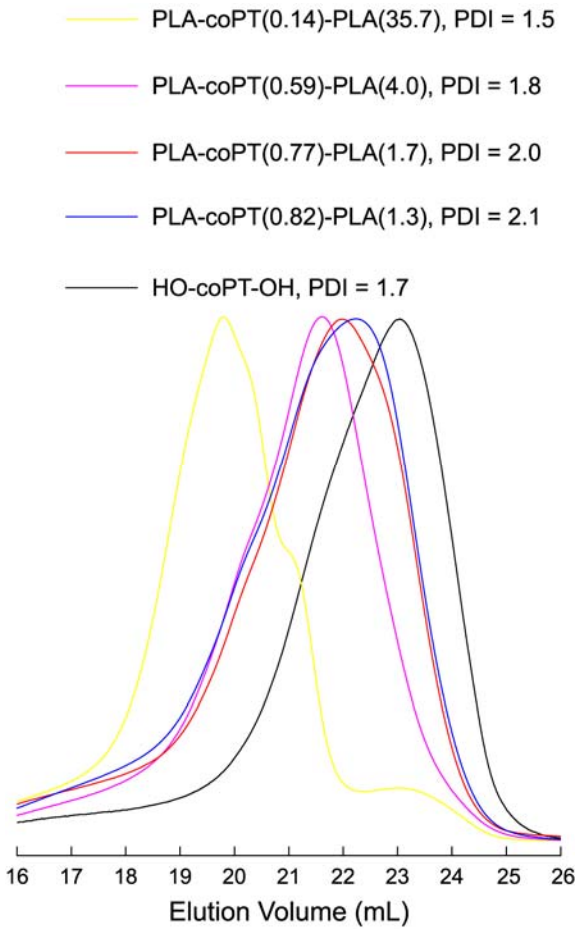

Figure 6.3. SEC chromatograms of the HO-coPT-OH precursor and PLA-coPT-PLA block copolymers with chloroform as the eluting solvent at 35 °C. The traces were obtained using a UV-Vis detector monitoring the signal at λ = 400 nm.

Thermal Characterization of PLA-coPT-PLA. Differential scanning calorimetry (DSC) was employed to analyze the thermal transitions of the polymers. The resultant thermograms indicate that there is no clear melting transition for the HO-coPT-OH homopolymer or any of the triblock copolymers over the temperature range scanned (Figure 6.4). A weak endothermic transition is seen in the HO-coPT-OH thermogram at T ≈ 35°. This signal is tentatively assigned as the glass transition temperature of HO-coPT-OH because there is no discernable glass transition at lower temperatures as is the case with homopolymer poly(3-alklythiophenes).[60] However, side-chain melting of the dodecyl substituents cannot be ruled out because it has been shown that the long alkyl side groups form crystalline regimes that melt in this temperature range.[61] Clearly, the main chain melting transition commonly observed in poly(3-dodecylthiophene) homopolymers (T_m ~156 °C) is not present, indicating a lack of main chain crystallinity.[34,62,63] Importantly, all thermal transitions of the HO-coPT-OH polymer are below the degradation temperature of PLA (T_d ~200 °C).[64] Addition of PLA to the ends of the coPT chains leads to the appearance of a signal due to the glass transition of polylactide blocks (T_g ~50 °C). This endothermic process masks the glass transition signal of the polythiophene block even in the polymer sample with the lowest weight fraction of polylactide, PLA-coPT(0.82)-PLA(1.3). This phenomenon was also seen in Chapter 5 for PLA-P3AT-PLA block copolymers when the P3AT block was amorphous (regiorandom). As expected, both the temperature and the strength of the PLA glass transition signal increase with increasing PLA molecular weight.[65] In fact, the glass transition of polylactide for the PLA-coPT(0.14)-PLA(35.7) is so large there is an overshoot in instrument response.[66] Because the signal from the glass transition of the coPT block is even weaker than in the case of PLA-*Ra*P3HT-PLA (Chapter 5), we were unable to determine if two distinct glass transitions were present; this would have been an indication of microphase separation. As such, further experimentation is required to determine if distinct, nanoscopic polymer domains form in these block copolymer systems.

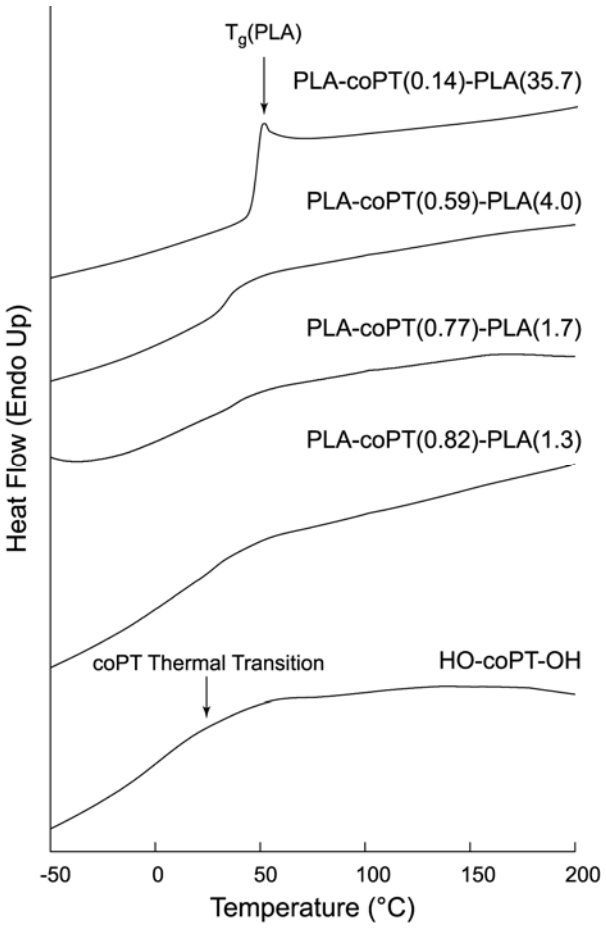

Figure 6.4. DSC thermograms of HO-coPT-OH and the PLA-coPT-PLA block copolymers. The scans shown were collected at a heating rate of 10 °C/min after annealing at 260 °C and then cooling to –60 °C. There is an overshoot instrument response at the PLA glass transition temperature for the PLA-coPT(0.14)-PLA(35.7) sample due to the high content of PLA in the sample.

Wide-Angle X-ray Scattering (WAXS). WAXS was employed to confirm the DSC results, and verify that the HO-coPT-OH homopolymer and the triblock copolymers were amorphous. As expected, only broad signals are present in the HO-coPT-OH spectrum, consistent with an amorphous material. These two broad peaks are centered at $q \approx 9$ nm^{-1}, $q \approx 15$ nm^{-1}, which is strikingly similar to the spectrum of HO-*Ra*P3HT-OH originally shown in Chapter 5 and reproduced above the dashed line in Figure 6.5. For the sake of comparison, the WAXS patterns for HO-*Re*P3DDT-OH and PLA-*Re*P3DDT(0.37)-PLA(35) also have been reproduced above the dashed line. These

spectra are reminders that in semicrystalline polythiophene-containing block copolymers (even with as little as 37 wt% P3DDT) sharp peaks are observed. These reflections are assigned the (100), (200), and (300) of the poly(3-alkylthiophene) crystal motif.[67,68] Upon addition of PLA blocks to the HO-coPT-OH macroinitiator, there is a growth in amorphous peaks at higher q values ($8\ nm^{-1} < q < 18\ nm^{-1}$). As described in Chapter 5, this additional signal is caused by diffuse scattering from the PLA domains.[69] The signal due to the PLA block in the representative PLA-coPT-PLA block copolymer, PLA-coPT(0.14)-PLA(35.7), makes observation of the coPT peak at $q \approx 15\ nm^{-1}$ impossible. Interestingly, the signal at $q \approx 9\ nm^{-1}$ is shifted to $q \approx 3\ nm^{-1}$. This shows that the addition of PLA creates larger polythiophene domain spacings, but more experiments are required to understand the driving force for this rearrangement. However, the preliminary results suggest that coPT-based block copolymers may be extremely useful in generating well-ordered block copolymer thin films over the long-range because any observed phase separation cannot be due to the crystallization of the polythiophene block.

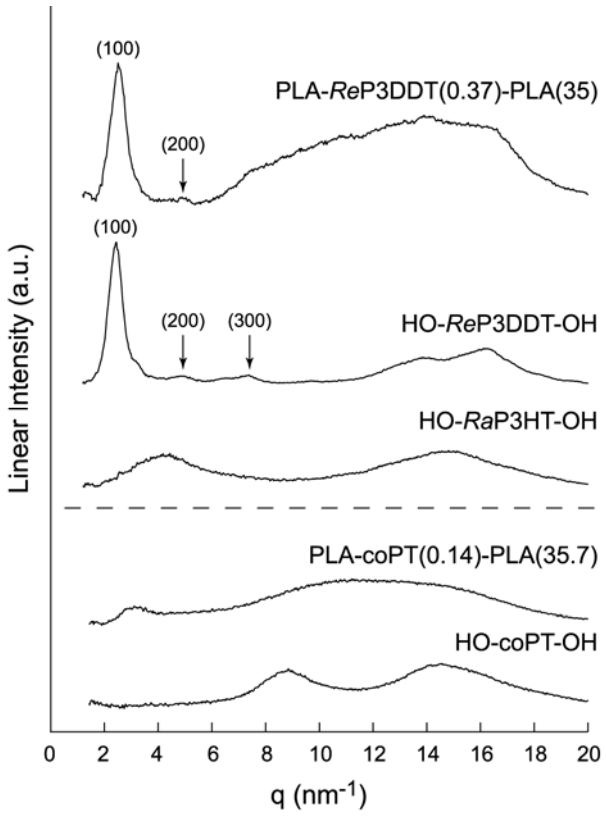

Figure 6.5. WAXS spectra of HO-coPT-OH and PLA-coPT(0.14)-PLA(35.7). Selected WAXS data reproduced from Chapter 5 also are shown above the dashed line for convenience and include: HO-*Ra*P3HT-OH, HO-*Re*P3DDT-OH, and PLA-*Re*P3DDT(0.37)-PLA(35). See Chapter 5 for full polymer characterization. The prominent lamellae reflections are marked for the semicrystalline samples. Note that all of the regioregular P3DDT samples exhibit the (100) and (200) reflections while the amorphous samples do not; this confirms the lack of melting endotherms from the data presented in Figure 6.4. No annealing treatments were performed prior to acquiring these data.

Thin Film Ultraviolet-Visible (UV-Vis) Light Absorbance Spectroscopy. The optical properties of the polymers are important when considering photovoltaic applications. As such, the UV-Vis spectra of thin films of the homopolymer and block copolymers were recorded. Thin films were fabricated by spin-coating 10 mg per 1 mL of 1,2-dichlorobenzene solutions onto glass substrates at a rotation rate of 1000 rpm for 1 min. The band gap of the polymers was determined by the onset of absorption (λ ~650 nm), and was found to be E_g ~1.9 eV regardless of the PLA content. The absorption

coefficient at the maximum absorption wavelength (λ_{max} = 490 nm) for the HO-coPT-OH homopolymer was found to be α = 7.4 x 10^4 cm^{-1}, which is comparable to a previous report[40] for thiophene copolymers and poly(3-alkythiophene) homopolymers.[70] Unlike poly(3-alkylthiophene) thin films, there are no shoulders associated with increased vibronic structure (commonly associated with crystallinity) present in the as-spun films (Chapter 4).[71] The incorporation of PLA to the ends of the coPT polymer chains does little to affect the absorption spectra of the thin films (Figure 6.6a). The absorption coefficient of the thin film (α) at the maximum absorption wavelength (λ_{max}) increases linearly as the amount of PLA decreases confirming that all light absorption in the visible window is due to the polythiophene block (Figure 6.6c). The films were also annealed in an inert atmosphere glove box at 110 °C for 48 h. This temperature was selected because it is above the glass transition temperatures of both coPT and PLA (Figure 6.4) and below the degradation temperature of PLA. The absorbance spectra of the annealed thin films are shown in Figure 6.6b. Little changes after annealing; however, there is the appearance of a small shoulder over the range of 600 nm < λ < 650 nm. This indicates an increase in ordering of the polythiophene moiety, but should not greatly affect the microphase separation of the block copolymers. As with the as-spun films, the absorption coefficient of the thin film increases as the weight fraction of the polythiophene block is increased (Figures 6.6 d). Overall, these thiophene-containing homopolymers and block copolymers have optical properties similar to commonly employed solar cell hole-conducting polymers. Importantly for potential thin film microstructural studies, the PLA-coPT-PLA block copolymers have these useful optical properties in the absence of semicrystalline regimes.

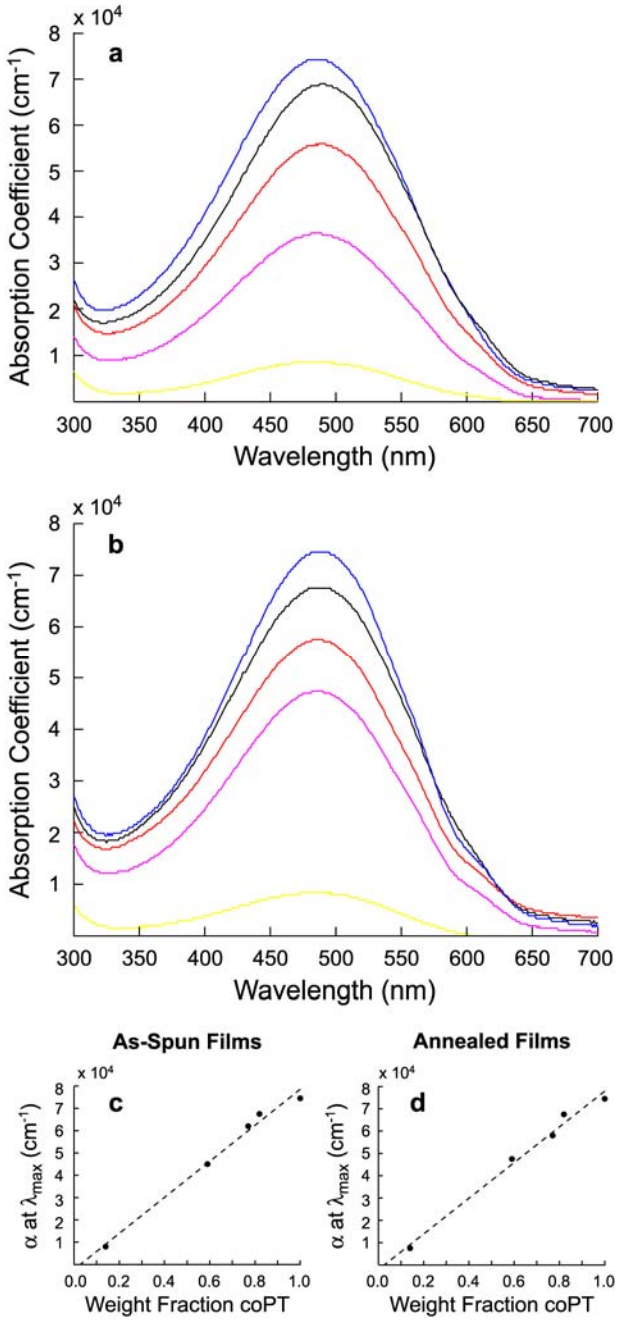

Figure 6.6. UV-Vis absorption spectra of (a) as-spun and (b) annealed HO-coPT-OH and triblock copolymer thin films on glass. The absorption coefficient (α) at the maximum absorption wavelength (λ_{max}) as a function of polythiophene content in the polymer of the (c) as-spun and (d) annealed polymer thin films. The dashed lines in (c) and (d) are linear fits for the data points plotted. All films were 20 ± 4 nm as measured by AFM. Films were annealed at 150 °C for 48 h in an inert atmosphere glove box.

6.4 Summary

We have reported on a new series of semiconducting-etchable ABA-type triblock copolymers, polylactide-*b*-poly(3-dodecylthiophene-*co*-thiophene)-*b*-polylactide (PLA-coPT-PLA). In an analogous manner to the block copolymers synthesized in Chapter 5, a difunctional alcohol (HO-coPT-OH) was used as a macroinitiator for the controlled polymerization of lactide. The molecular properties of these macromolecules were characterized by ^{1}H NMR spectroscopy and size exclusion chromatography (SEC). Because the copolymerization of thiophene used the controlled GRIM polymerization technique, the HO-coPT-OH homopolymer and PLA-coPT-PLA block copolymers were found to have relatively narrow molecular weight distributions. Importantly, copolymerization of the thiophene-based repeat units impacted the polymer structure significantly enough that the homopolymer and the block copolymers were all found to be completely amorphous based on DSC and WAXS results. Both the homopolymer and block copolymers have an optical band gap comparable to the often-used hole-conducting polymer, P3HT (E_g ~1.9 eV). Finally, the absorption coefficients of the block copolymers were found to be linearly dependent on the weight fraction of coPT present in the macromolecule. These novel block copolymers are useful because they are materials that contain a semiconducting moiety that is not crystalline and has a relatively narrow molecular weight distribution. These two properties aid in the fabrication of block copolymer thin films with tunable dimensions and long-range order. As such, PLA-coPT-PLA type block copolymers could be employed in the production all-organic ordered bulk heterojunction photovoltaic devices.

6.5 References

[1] Skotheim, T.; Reynolds, J.; Elsembauer, R.; Eds. *Handbook of Conducting Polymers*; Marcel Dekker: New York, 1998.

[2] Nalwa, H. S.; Ed. *Handbook of Organic Conductive Molecules and Polymers*; J. Wiley & Sons: New York, 1996.

[3] McCullough, R. D. *Adv. Mater.* **1998**, *10*, 93–116.

[4] Osaka, I.; McCullough, R. D. *Acc. Chem. Res.* **2008**, *41*, 1202–1214.

[5] Li, G.; Shrotriya, V.; Huang, J.; Yao, Y.; Moriarty, T.; Emery, K.; Yang, Y. *Nat. Mater.* **2005**, *4*, 864–868.

[6] Ma, W.; Yang, C.; Gong, X.; Lee, K.; Heeger, A. J. *Adv. Funct. Mater.* **2005**, *15*, 1617–1622.

[7] Park, S. H.; Roy, A.; Beaupré, S.; Cho, S.; Coates, N.; Moon, J. S.; Moses, D.; Leclerc, M.; Lee, K.; Heeger, A. J. *Nat. Photonics* **2009**, *3*, 297–303.

[8] Forrest, S. R. *MRS Bull.* **2005**, *30*, 28–32.

[9] Janssen, R. A. J.; Hummelen, J. C.; Saricifici, N. S. *MRS Bull.* **2005**, *30*, 33–36.

[10] Gregg, B. A.; Hanna, M. C. *J. Appl. Phys.* **2003**, *93*, 3605–3614.

[11] Gregg, B. A. *MRS Bull.* **2005**, *30*, 20–22.

[12] Moon, J. S.; Lee, J. K.; Cho, S.; Byun, J.; Heeger, A. J. *Nano Lett.* **2009**, *9*, 230–234.

[13] Sun, S.; Saricifici, N. S.; Eds. *Organic Photovoltaics: Mechanisms, Materials, and Devices*; Taylor & Francis: Boca Raton, FL, 2005.

[14] Schilinsky, P.; Waldauf, C.; Brabec, C. J. *Appl. Phys. Lett.* **2002**, *81*, 3885–3887.

[15] Padinger, F.; Rittberger, R. S.; Saricifici, N. S. *Adv. Funct. Mater.* **2003**, *13*, 85–88.

[16] Erb, T.; Zhokhavets, U.; Gobsch, G.; Raleva, S.; Stühn, B.; Schilinsky, P.; Waldauf, C.; Brabec, C. J. *Adv. Funct. Mater.* **2005**, *15*, 1193–1196.

[17] Clarke, T. M.; Ballantyne, A. M.; Nelson, J.; Bradley, D. D. C.; Durrant, J. R. *Adv. Funct. Mater.* **2008**, *18*, 4029–4035.

[18] Müller, C.; Ferenczi, T. A. M.; Campoy-Quiles, M.; Frost, J. M.; Bradley, D. D. C.; Smith, P.; Stingelin-Stutzmann, N.; Nelson, J. *Adv. Mater.* **2008**, *20*, 3510–3515.

[19] Kim, J. Y.; Frisbie, C. D. *J. Phys. Chem. C* **2008**, *112*, 17726–17736.

[20] Coakley, K. M.; McGehee, M. D. *Appl. Phys. Lett.* **2003**, *83*, 3380–3382.

[21] Lipomi, D. J.; Chiechi, R. C.; Reus, W. F.; Whitesides, G. M. *Adv. Funct. Mater.* **2008**, *18*, 3469–3477.

[22] Xi, H.; Wei, Z.; Duan, Z.; Xu, W.; Zhu, D. *J. Phys. Chem. C* **2008**, *112*, 19934–19938.

[23] Szwarc, M.; Levy, M.; Milkovich, R. *J. Am. Chem. Soc.* **1956**, *78*, 2656–2657.

[24] Schlick, S.; Levy, M. *J. Phys. Chem.* **1960**, *64*, 883–886.

[25] Hadjichristidis, N.; Pispas, S.; Floudas, G. A. *Block Copolymers: Synthetic Strategies, Physical Properties, and Applications*; John Wiley & Sons, Inc.: Hoboken, NJ, 2003.

[26] Liu, J.; Sheina, E.; Kowalewski, T.; McCullough, R. D. *Angew. Chem., Int. Ed.* **2002**, *41*, 329–332.

[27] Tu, G.; Li, H.; Forster, M.; Heiderhoff, R.; Balk, L. J.; Scherf, U. *Macromolecules* **2006**, *39*, 4327–4331.

[28] Iovu, M. C.; Jeffries-EL, M.; Zhang, R.; Kowalewski, T.; McCullough, R. D. *J. Polym. Sci. Part A*, **2006**, *43*, 1991–2000.

[29] Sauvé, G.; McCullough, R. D. *Adv. Mater.* **2007**, *19*, 1822–1825.

[30] Dai, C.; Yen, W.; Lee, Y.; Ho, C.; Su, W. *J. Am. Chem. Soc.* **2007**, *129*, 11036–11038.

[31] Iovu, M. C.; Craley, R.; Jeffries-EL, M.; Krankowski, A. B.; Zhang, R.; Kowalewski, T.; McCullough, R. D. *Macromolecules* **2007**, *40*, 4733–4735.

[32] Sommer, M.; Lang, A. S.; Thelakkat, M. *Angew. Chem., Int. Ed.* **2008**, *47*, 7901–7904.

[33] Richard, F.; Brochon, C.; Leclerc, N.; Eckhardt, D.; Heiser, T.; Hadziioannou, G. *Macromol. Rapid Commun.* **2008**, *29*, 885–891.

[34] Boudouris, B. W.; Frisbie, C. D.; Hillmyer, M. A. *Macromolecules* **2008**, *41*, 67–75.

[35] Higashihara, T.; Ohshimizu, K.; Hirao, A.; Ueda, M. *Macromolecules* **2008**, *41*, 9505–9507.

[36] Urien, M.; Erothu, H.; Cloutet, E.; Hiorns, R. C.; Vignau, L.; Cramail, H. *Macromolecules* **2008**, *41*, 7033–7040.

[37] Higashihara, T.; Ueda, M. *React. Funct. Polym.* **2009**, *69*, 457–462.

[38] Zhang, Q.; Cirpan, A.; Russell, T. P.; Emrick, T. *Macromolecules* **2009**, *42*, 1079–1082.

[39] Loewe, R. S.; Khersonsky, S. M.; McCullough, R. D. *Adv. Mater.* **1999**, *11*, 250–253.

[40] Thompson, B. C.; Kim, B. J.; Kavulak, D. F.; Sivula, K.; Mauldin, C.; Fréchet, J. M. J. *Macromolecules* **2007**, *40*, 7425–7428.

[41] McCullough, R. D.; Jayaraman, M. *J. Chem. Soc., Chem. Commun.* **1995**, 135–136.

[42] Schmidt, S. C.; Hillmyer, M. A. *Macromolecules* **1999**, *32*, 4794–4801.

[43] Kricheldorf, H.; Berl, M.; Scharnagle, N. *Macromolecules* **1988**, *21*, 286–293.

[44] Wang, Y.; Hillmyer, M. A. *Macromolecules* **2000**, *33*, 7395–7403.

[45] Olayo-Valles, R.; Guo, S.; Lund, M. S.; Leighton, C.; Hillmyer, M. A. *Macromolecules* **2005**, *38*, 10101–10108.

[46] Bendejacq, D.; Ponsinet, V.; Joanicot, M.; Loo, Y. L.; Register, R. A. *Macromolecules* **2002**, *35*, 6645–6649.

[47] Lynd, N. A.; Meuler, A. J.; Hillmyer, M. A. *Prog. Polym. Sci.* **2008**, *33*, 875–893.

[48] Trznadel, M.; Pron, A.; Zagorska, M.; Chrzaszcz, R.; Pielichowski, J. *Macromolecules* **1998**, *31*, 5051–5058.

[49] Merlo, J. A.; Frisbie, C. D. *J. Phys. Chem. B* **2004**, *108*, 19169–19179.

[50] Loewe, R. S.; Ewbank, P. C.; Liu, J.; Zhai, L.; McCullough, R. D. *Macromolecules* **2001**, *34*, 4324–4333.

[51] Iovu, M. C.; Sheina, E. E.; Gil, R. R.; McCullough, R. D. *Macromolecules* **2005**, *38*, 8649–8656.

[52] Jeffries-EL, M.; Sauvé, G.; McCullough, R. D. *Adv. Mater.* **2004**, *16*, 1017–1019.

[53] Liu, J.; McCullough, R. D. *Macromolecules* **2002**, *35*, 9882–9889.

[54] Boudouris, B. W.; Molins, F.; Blank, D. A.; Frisbie, C. D.; Hillmyer, M. A. *Macromolecules* **2009**, *42*, 4118–4126.

[55] Li, S. *J. Biomed. Mater. Res.* **1999**, *48*, 342–353.

[56] Kricheldorf, H. R.; Kreiser-Saunders, I.; Stricker, A. *Macromolecules* **2000**, *33*, 702–709.

[57] Ryner, M.; Stridsberg, K.; Albertsson, A. C.; von Schenck, H.; Svensson, M. *Macromolecules* **2001**, *34*, 3877–3881.

[58] Dove, A. P. *Chem. Commun.* **2008**, *48*, 6446–6470.

[59] Fan, Y.; Chen, G.; Tanaka, J.; Tateishi, T. *Biomacromolecules* **2005**, *6*, 3051–3056.

[60] Malik, S.; Nandi, A. K. *J. Poly. Sci. B* **2002**, *40*, 2073–2085.

[61] Liu, S. L.; Chung, T. S. *Polymer* **2000**, *41*, 2781–2793.

[62] Malik, S.; Nandi, A. K. *J. Poly. Sci. B* **2002**, *40*, 2073–2085.

[63] Liu, S. L.; Chung, T. S. *Polymer* **2000**, *41*, 2781–2793.

[64] Olayo-Valles, R.; Guo, S.; Lund, M. S.; Leighton, C.; Hillmyer, M. A. *Macromolecules* **2005**, *38*, 10101–10108.

[65] Anderson, K. S.; Hillmyer, M. A. *Polymer* **2006**, *47*, 2030–2035.

[66] Hiemenz, P. C.; Lodge, T. P. *Polymer Chemistry*; CRC Press: Boca Raton, FL, 2007.

[67] Chen, S.; Lee, S. *Polymer* **1995**, *36*, 1719–1723.

[68] Prosa, T. J.; Moulton, J.; Heeger, A. J.; Winokur, M. J. *Macromolecules* **1999**, *32*, 4000–4009.

[69] Hamilton, B. D.; Weissbuch, I.; Lahav, M.; Hillmyer, M. A.; Ward, M. D. *J. Am. Chem. Soc.* **2009**, *131*, 2588–2596.

[70] Thompson, B. C.; Fréchet, J. M. J. *Angew. Chem., Int. Ed.* **2008**, *47*, 58–77.

[71] Sunderberg, M.; Inganäs, O.; Stafström, S.; Gustafsson, G.; Sjögren, B. *Solid State Commun.* **1989**, *71*, 435–439.

7 Synthesis, Optical Properties, and Microstructure of a Fullerene-terminated Poly(3-hexylthiophene)[†]

7.1 Overview

End-functionalized, regioregular poly(3-hexylthiophene) (P3HT) was synthesized by a combination of a controlled polymerization technique and post-polymerization functionalization. Both ends of the polymer chains were terminated with fullerene units to create an internal electron accepting-donating-accepting molecule, methylfulleropyrrolidine-poly(3-hexylthiophene)-methylfulleropyrrolidine (C_{60}-P3HT-C_{60}). The molecular properties of the polymer were characterized using ^{1}H NMR spectroscopy, size exclusion chromatography (SEC), ultraviolet-visible (UV-Vis) absorption spectroscopy and fluorescence spectroscopy. These results show that the fullerene units are covalently bound to the polymer chain ends. Differential scanning calorimetry (DSC), wide-angle x-ray scattering (WAXS), and small-angle x-ray scattering (SAXS) were used to determine the bulk microstructure of the polymers. In addition, atomic force microscopy (AFM) was used to examine spun-cast thin films. These experiments revealed that microphase separation occurs between the main polymer chain and the fullerene end groups and suggests the creation of two distinct semicrystalline regimes in C_{60}-P3HT-C_{60} that are similar to those seen in a compositionally similar blend of P3HT and C_{60}. This comparable domain formation, coupled with the possibility of enhanced charge transfer associated with an internal donor-acceptor material, makes C_{60}-P3HT-C_{60} a promising candidate as a material in bulk heterojunction organic photovoltaics.

[†] Reproduced with permission from B. W. Boudouris, F. Molins, D. A. Blank, C. D. Frisbie, and M. A. Hillmyer, *Macromolecules* **2009**, *42*, 4118–4126. Copyright 2009 American Chemical Society.

7.2 Introduction

The search for an economical and flexible supplement to current inorganic solar cells has led to an increased interest in the development of organic photovoltaics (OPVs).[1-3] However, implementation of plastic solar cells has been thwarted by the relatively low efficiency of the devices, currently ~5% in the best cases.[4,5] To facilitate electron-hole separation, the most efficient organic devices contain two types of semiconductors: an electron donor and an electron acceptor. Regioregular poly(3-hexylthiophene)[6,7] (P3HT) has become the predominant electron-donating material used in polymer-based OPVs because of its high hole mobility (~0.1-1 $cm^2\ V^{-1}s^{-1}$), relatively low band gap (~1.9 eV), and solution processibility.[8-11] In bulk heterojunction systems, P3HT and an electron-accepting soluble fullerene derivative, [6,6]-phenyl-C_{61}-butyric acid methyl ester (PCBM), are solution blended to form an active layer in the most efficient polymer-based OPVs.[12-15] Two key criteria enhance the performance of these devices relative to other polymer-based solar cells due to the seemingly serendipitous relationship between P3HT and PCBM. First, large interfacial area and intimate contact between the fullerene and polymer phases occurs and allows for ultrafast charge separation at the donor-acceptor interface. Secondly, the materials phase separate in such a way that percolating networks form and allow for charge collection at the appropriate electrodes.[5,16-20] This critical phase separation is currently controlled through a combination of well-tuned spin-coating conditions and thermal annealing treatments in the binary system.[4,5,12,13,16]

Phase separation in single component systems of block copolymer thin films, on the other hand, have been shown to spontaneously form ~10 nm domains.[21-23] In addition to providing a pathway for intramolecular charge separation, an electron acceptor-donor-acceptor triblock copolymer affords the possibility of nanodomains formed by the microphase separation of the electron donor and the electron acceptor without the need for additional processing steps. The phase separation observed in these block copolymers could be controlled by varying the length of the constituent chains

allowing for a systematic study of charge transport behavior as a function of domain spacing.

In fact, donor-acceptor molecules previously have been synthesized using fullerene-containing hybrid moieties for application in OPV devices both as charge transport materials and as compatibilizers to enhance active layer morphology.[24-37] Particularly, some oligothiophene and oligo(*p*-phenylene vinylene) systems with fullerene end groups have been synthesized for the purpose of examining their photophysics. While some of these materials have also been used in photovoltaics,[28,29,32] the device efficiencies have so far been low, perhaps due to poor morphologies. Polymeric donor molecules with fullerene end groups, which may potentially form better films, have so far not been extensively researched.

Here we report the synthesis of a difunctional, fullerene-terminated regioregular poly(3-hexylthiophene), methylfulleropyrrolidine-poly(3-hexylthiophene)-methylfulleropyrrolidine (C_{60}-P3HT-C_{60}), through the use of a controlled polymerization and subsequent post-polymerization functionalization. The molecular properties of the polymer were characterized using ^{1}H NMR spectroscopy, size exclusion chromatography (SEC), ultraviolet-visible (UV-Vis) absorption spectroscopy, and fluorescence spectroscopy. Differential scanning calorimetry (DSC), wide-angle x-ray scattering (WAXS), small-angle x-ray scattering (SAXS), and atomic force microscopy (AFM) experiments show that this material microphase separates on the nanometer length scale. The size of the P3HT crystallite lamellae, thought to be chiefly responsible for hole transport, are scarcely affected by the inclusion of the relatively bulky end groups on the polymer. In addition, the fullerene units on the polymer chain aggregate into domains with a crystal packing that is similar to that observed for powders of a related small molecule, *N*-methylfulleropyrrolidine (NMC_{60}). The C_{60}-P3HT-C_{60} polymer also has a similar x-ray scattering pattern to that of a binary blend of P3HT and C_{60} (mixed in approximately the same weight ratio as that contained in C_{60}-P3HT-C_{60}) but with the added advantage of having the electron donor and acceptor covalently bound.

We believe that this system offers an advantage over previously studied oligothiophene-fullerene systems due to the synthetic simplicity of this molecule. The P3HT polymerization technique utilized in this work is much less labor-intensive than the step-wise routes used to grow oligothiophenes and also allows for the easy manipulation of the average number of repeat units in the chains by varying reaction conditions. The crystallization-induced phase separation of C_{60}-P3HT-C_{60} is likely to result in interesting and potentially useful morphologies. This opens up possibilities for systematic studies of OPV cells based on C_{60}-P3HT-C_{60} where the molecular weight of the P3HT block is tuned. In addition, we plan a thorough examination of the photophysics and exciton dissociation of C_{60}-P3HT-C_{60} in a solvent which will yield insight on exciton diffusion lengths in the long-chain cases, for example. These points are the motivation for studying this new, macromolecular fullerene-polythiophene-fullerene system.

7.3 Experimental

General Methods. The ^{1}H NMR spectra were measured on a Varian VI-500 spectrometer using deuterated chloroform (Cambridge) solutions containing ~1 wt % polymer. Elemental analysis was performed by Micro-Analysis, Inc., Wilmington, DE (see Chapter 9.2). As expected, the percentage of carbon and nitrogen was higher in C_{60}-P3HT-C_{60} than in P3HT; however, quantitative agreement between the calculated and measured composition was not observed. Quantitative analysis of fullerene-containing species is hampered by the incomplete combustion and retention of residual solvent.[38-40] Analytical size exclusion chromatography (SEC) data were collected on an Agilent 1100 series equipped with an Agilent Ultraviolet visible (UV-Vis) light detector (path length = 10 mm) and three PLgel 5μm MIXED-C columns. For the molecular weight and polydispersity characterizations, chloroform at 35 °C was used as the mobile phase at a flow rate of 1 mL/min and the SEC data were calibrated with polystyrene standards and known Mark-Houwink parameters for poly(3-hexylthiophene) and polystyrene (Polymer Laboratories).[41,42] Measurements using the UV-Vis signal of the SEC spectra used chloroform at room temperature as the mobile phase at a flow rate of

1 mL/min. Preparatory size exclusion chromatography (prep SEC) was performed on an Agilent 1100 series equipped with an Agilent UV-Vis light detector (path length = 10 mm) and two PLgel 10μm MIXED-D columns. Chloroform at 35 °C was used as the mobile phase at a flow rate of 6 mL/min as to keep the internal pressure of the columns approximately equal to the pressure used during analytical SEC experiments. Matrix-assisted laser desorption/ionization-mass spectroscopy (MALDI-MS) measurements were performed on a Bruker Reflex III operating in linear mode. A typical sample was prepared by mixing 5 μL of a polymer solution in THF (5 mg/mL) and 15 μL of a dithranol solution in THF (20 mg/mL). The mixture (~1 μL) was then spotted onto the plate. Cytochrome C (Bruker) was used externally for calibration.

Spectroscopic Characterization. Molar absorption coefficients were calculated using static ultraviolet-visible (UV-Vis) absorption spectra of polymer (dissolved in chloroform) solutions and were taken on a Spectronic Genesys 5 spectrometer over a wavelength range of 200–900 nm using a chloroform-containing quartz cuvette (Starna Cells, Inc.) with a 10 mm path length as a blank. Thin films for absorbance measurements were made by spin-coating polymer solution in 1,2-dichlorobenzene (10 mg/1 mL) onto glass substrates at 600 rpm for 1 min. The films were then allowed to dry slowly in a covered Petri dish in an inert atmosphere glove box.[4] Film thicknesses were estimated by scratching the polymer film and measuring the step change with a KLA-Tencor P16 profilometer. The thickness of the P3HT film was 69 ± 3 nm and the thickness of the C_{60}-P3HT-C_{60} film was 52 ± 3 nm. Fluorescence data were acquired on a FluroLog 2 fluorimeter (SPEX) with solutions of the polymers in either chloroform or toluene. A binary mixture of P3HT and [6,6]-phenyl-C_{61}-butyric acid methyl ester (PCBM) was made by dissolving the two materials with the ratio of 2.1 molar equivalents of free PCBM for every polymer chain in solutions (P3HT+PCBM). The samples were prepared to obtain an optical density 0.1 – 0.3 for C_{60}-P3HT-C_{60} and 0.1 – 0.2 for the P3HT and the P3HT+PCBM samples. Solutions of Coumarin 153 (Exciton) in MeOH were used as the quantum yield (QY) standards, and had a known value of 0.42.[43] The fluorescence intensity of the polymer samples and the standard were

independent of purging with inert gas so no precautions with regard to air were taken in these measurements. Fluorescence spectra of the polymers and standard, with an excitation wavelength of 440 nm, were collected back to back and corrected for frequency dependent detector sensitivity.

Thermal and Structural Characterization. Differential scanning calorimetry (DSC) measurements were acquired using a TA Q1000 calorimeter. The samples were first annealed at 260 °C and then cooled to –60 °C at a rate of 10 °C/min. The results shown are for the final sample heating at a rate of 10 °C/min. An indium standard was used to calibrate the instrument and nitrogen was used as the purge gas. Wide-angle x-ray scattering (WAXS) data were collected in the diffraction angular range of $3^\circ \le 2\theta \le 31^\circ$ by a Bruker-AXS D5005 microdiffractometer. The crystalline peaks were deconvoluted using the curve-fitting software, JADE 8 (CMI). Small-angle x-ray scattering (SAXS) measurements were made on a home-built beamline at the University of Minnesota and used Copper Kα radiation (λ = 1.54 Å) as the x-ray source. All data were corrected for detector response characteristics. Atomic force microscopy (AFM) images were taken with a Veeco Metrology (previously Digital Instruments) Nanoscope IIIa Multimode microscope operating in tapping mode in the repulsive regime under inert atmosphere. The probe tips were fabricated by Mikromasch USA (NSC15/AlBS tips, resonant frequency 265–400 kHz, and spring constant 40 N/m).

Blending of P3HT/C_{60} Mixture. In order to make a binary blend of P3HT and C_{60} in approximately the same weight ratio as that of the C_{60}-P3HT-C_{60} polymer, 30 mg of P3HT and 8 mg of C_{60} were dissolved in 10 mL of chloroform. This led to a blend with a 0.21 weight fraction of C_{60} ($w_{C_{60}} = 0.21$). The solution was allowed to stir at room temperature until the mixture was completely dissolved. At this point the solution was drop cast into a tin pan and allowed to dry. The mixture (P3HT/C_{60} mixture) was recovered from the pan and dried overnight under vacuum.

P3HT and C_{60}-P3HT-C_{60} Thin Film Preparation. Solutions of P3HT and C_{60}-P3HT-C_{60} were made by dissolving 3 mg of polymer in 1 mL of 1,2-dichlorobenzne (DCB) and allowing the solutions to stir at 60 °C under inert atmosphere overnight.

Silicon wafers with a 3000 Å thermally grown silicon oxide layer were used as the substrates for the films. Solutions were passed through a 0.45 μm syringe filter and the solutions were deposited on the substrates. The rotation rate was then increased from 0 to 2000 rpm over the course of ~5 seconds and held at 2000 rpm for 60 sec inside an inert atmosphere glove box. The films were then annealed in inert atmosphere for 10 min at 150 °C.

7.4 Results and Discussion

Synthesis of C_{60}-P3HT-C_{60}. Regioregular poly(3-hexylthiophene) was synthesized using the controlled Grignard Metathesis (GRIM) polymerization method and yielded P3HT with a narrow molecular weight distribution (M_w/M_n = 1.3).[44] To remove any small molecular weight impurities residual in the reaction mixture,[45] the polymer was purified using a Soxhlet extraction apparatus with methanol, acetone, and chloroform in a sequential manner. The chloroform fraction was then used in the subsequent reactions. The P3HT was initially designed to have a lower molecular weight to aid in molecular characterization. Our experience with higher molecular weight P3HT derivatives suggests that the influence of chain length on the end group reactivity is not a significant concern. The utility of end-functionalized P3HTs has previously been shown in the synthesis of polythiophene-containing block copolymers,[46-48] and the post-polymerization functionalization route for the synthesis of C_{60}-P3HT-C_{60} is shown in Figure 7.1.

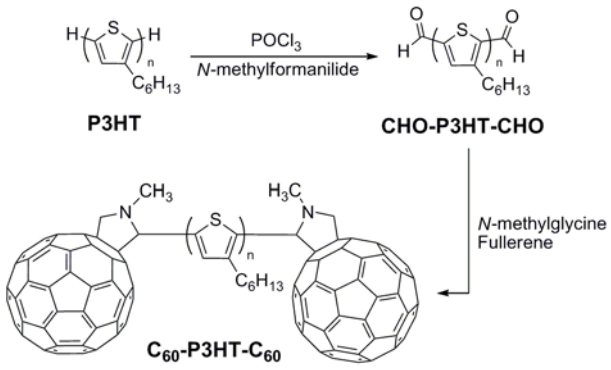

Figure 7.1. Synthetic route for the target molecule, methylfulleropyrrolidine-poly(3-hexylthiophene)-methylfulleropyrrolidine (C_{60}-P3HT-C_{60}).

After converting the bromine-hydrogen end-capped polymer (H-P3HT-Br) to the proton-terminated polymer (P3HT) by use of a magnesium-halogen reaction,[49] the P3HT was converted to the *bis*-aldehyde terminated molecule (CHO-P3HT-CHO) in a Vilsmeier-Haack reaction with phosphorus oxychloride and *N*-methylformanilide used in excess.[50] Finally, the polymer was converted to the desired product, methylfulleropyrrolidine-poly(3-hexylthiophene)-methylfulleropyrrolidine (C_{60}-P3HT-C_{60}), by using an excess of *N*-methylglycine and fullerene to drive the 1,3-dipolar cylcoaddition (Prato) reaction to completion as in analogous reactions previously shown in the literature for small molecules.[24-30,51] Preparatory size exclusion chromatography (prep SEC) was utilized to separate the polymer from the excess fullerene. Figure 9.2 shows a representative prep SEC chromatogram of the separation procedure illustrating the large retention time difference between the elution of the C_{60}-P3HT-C_{60} and unreacted fullerene making for the facile collection of only the polymer. The polymer was collected from the elution times (t_{elute}) of 22 min < t_{elute} < 33 min.[52]

Molecular Structure of C_{60}-P3HT-C_{60}. To determine the molecular weight distribution of the polymers, analytical size exclusion chromatography (SEC) was performed on the macromolecules with a UV-Vis detector that was also capable of collecting the UV-Vis spectrum of the polymer as the material eluted through the column over the absorption range of both P3HT and C_{60}. The molecular weight distribution of the P3HT did not change during the Vilsmeier reaction step in generating

CHO-P3HT-CHO. However, there is a significant amount of coupling that occurs during the addition of fullerene to the end of the polymer chains and is reflected by the second peak on the SEC trace shown in Figure 7.2a. The coupling caused the molecular weight to increase from M_n ~5,400 g mol^{-1} to M_n ~7,600 g mol^{-1} (41% increase) and for the molecular weight distribution to increase from M_w/M_n ~1.3 to M_w/M_n ~1.8 as measured by SEC against polystyrene standards and with the data corrected using published Mark-Houwink parameters.[41,42] The increase in molecular weight is also reflected in the ^{1}H NMR measurements with integration of the polymer end groups showing an increase from M_n ~4,500 g mol^{-1} for CHO-P3HT-CHO to M_n ~6,700 g mol^{-1} for C_{60}-P3HT-C_{60} (48% increase). Control reactions run at similar conditions to the Prato reaction without the fullerene present showed that chain coupling was still a major problem in the reaction process. However, simply refluxing chlorobenzene with P3HT dissolved in solution does not lead to chain coupling. This suggests that the macromolecular azomethine ylide intermediate generated in situ from the reaction of CHO-P3HT-CHO and *N*-methylglycine is required for the coupling of the polymer chains. While previous reports of the dimerization of thiocarbonyl[53] and thiophenedicarboxaldehyde-containing[54] ylide intermediates imply a possible mechanism for this coupling, further experiments are required to confirm this observation. Despite the chain coupling that occurs during the C_{60} addition step, the UV-Vis absorption spectra obtained at the two peaks (t_{elute} = 21.2 min and t_{elute} = 22.3 min) in the C_{60}-P3HT-C_{60} SEC chromatogram shown in Figure 7.2b agree with ^{1}H NMR spectroscopy (see below) and suggest that every polymer chain has both ends terminated with fullerene. The uncoupled C_{60}-P3HT-C_{60} polymer chain shows a more pronounced fullerene absorption signal at λ = 330 nm than the coupled C_{60}-P3HT-C_{60} polymer chains since the fullerene is now a larger percent of the composition of the uncoupled chains. In addition, it is apparent that the unreacted fullerene is no longer present in the C_{60}-P3HT-C_{60} sample as depicted in the full SEC traces shown in Figure 9.3.

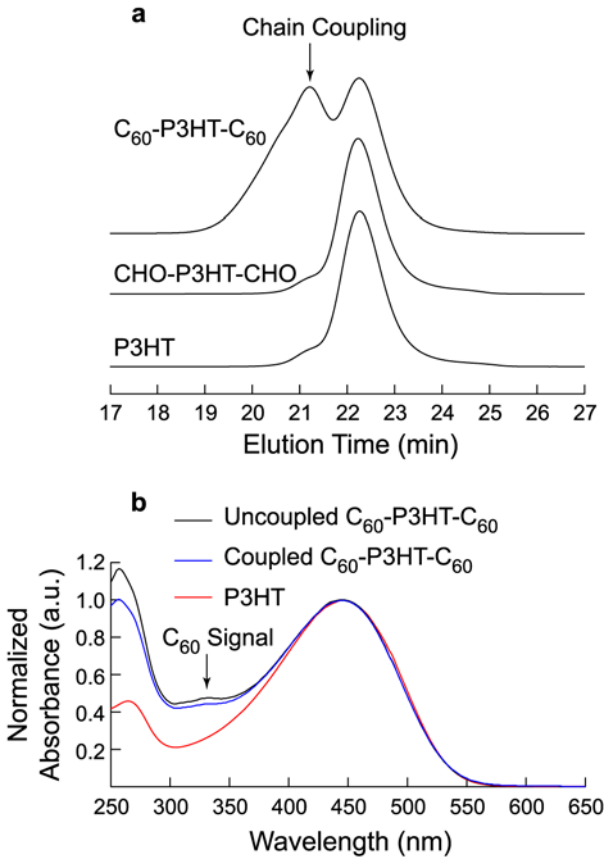

Figure 7.2. (a) SEC chromatograms of C_{60}-P3HT-C_{60} and the polymer precursors with chloroform as the eluting solvent at 35 °C. The traces were obtained using a UV-Vis detector monitoring the signal at λ = 400 nm. The traces are offset vertically for clarity. (b) The online UV-Vis spectra at room temperature for the P3HT precursor and C_{60}-P3HT-C_{60} in chloroform at the two maxima in the SEC plots for the coupled polymer (t_{elute} = 21.2 min) and uncoupled polymer (t_{elute} = 22.3 min).

The conversion of end groups during the post-polymerization functionalization was monitored using ^{1}H NMR spectroscopy, matrix-assisted laser desorption/ionization-mass spectroscopy (MALDI-MS), and ultraviolet-visible (UV-Vis) light spectroscopy. The molecular weights of the P3HT polymers were determined by ^{1}H NMR spectroscopy using end group analysis, and these molecular weights were used in all further computations. While calculations were based on NMR determined molecular weights Mark-Houwink-corrected SEC molecular weights were similar to those (< 6 repeat units difference) determined by end group integrations. The molecular

structures of CHO-P3HT-CHO and C_{60}-P3HT-C_{60} along with the ^{1}H NMR spectrum of C_{60}-P3HT-C_{60} are shown in Figure 7.3. Figures 7.3b and 7.3c show the relevant ^{1}H NMR spectra regimes for the end groups of CHO-P3HT-CHO and C_{60}-P3HT-C_{60}, respectively. End group integration showed complete conversion of the aldehyde-terminated polymer to the fullerene-terminated polymer. The peaks around δ ~10 ppm in the CHO-P3HT-CHO spectrum are due to the substitution of the aldehyde group at either the 2-position of the terminal thiophene ring (higher intensity) or the 5-position of the thiophene ring (lower intensity).[49] This is also reflected in the C_{60}-P3HT-C_{60} spectrum as the e' protons show two resonances with a small difference in chemical shift. The chemical shifts and splitting patterns of the end groups were also in agreement with previous reports[24,28] with the protons labeled e' and g having integrations of 2:2:2. Note that the protons labeled g are diastereotopic due to the adjacent stereocenter. The coupling constant of the resonance at δ ~5.0 ppm is J = 9.5 Hz and the coupling constant of the resonance at δ ~4.2 ppm is J = 10 Hz, which is consistent with reported literature values for small molecule systems.[24]

Matrix-assisted laser desorption/ionization-mass spectrometry (MALDI-MS) measurements were also performed to verify the end group functionality of C_{60}-P3HT-C_{60}. Two major sets of peaks were observed with the first type associated with C_{60}-P3HT-C_{60}. As observed in other fullerene-capped systems,[55-57] the second major set corresponds to P3HT moieties where both fullerene units have fragmented from the polymer chain during the desorption/ionization process to yield species with m/z = [C_{60}-P3HT-C_{60}] – 1440 (Figure 9.4).

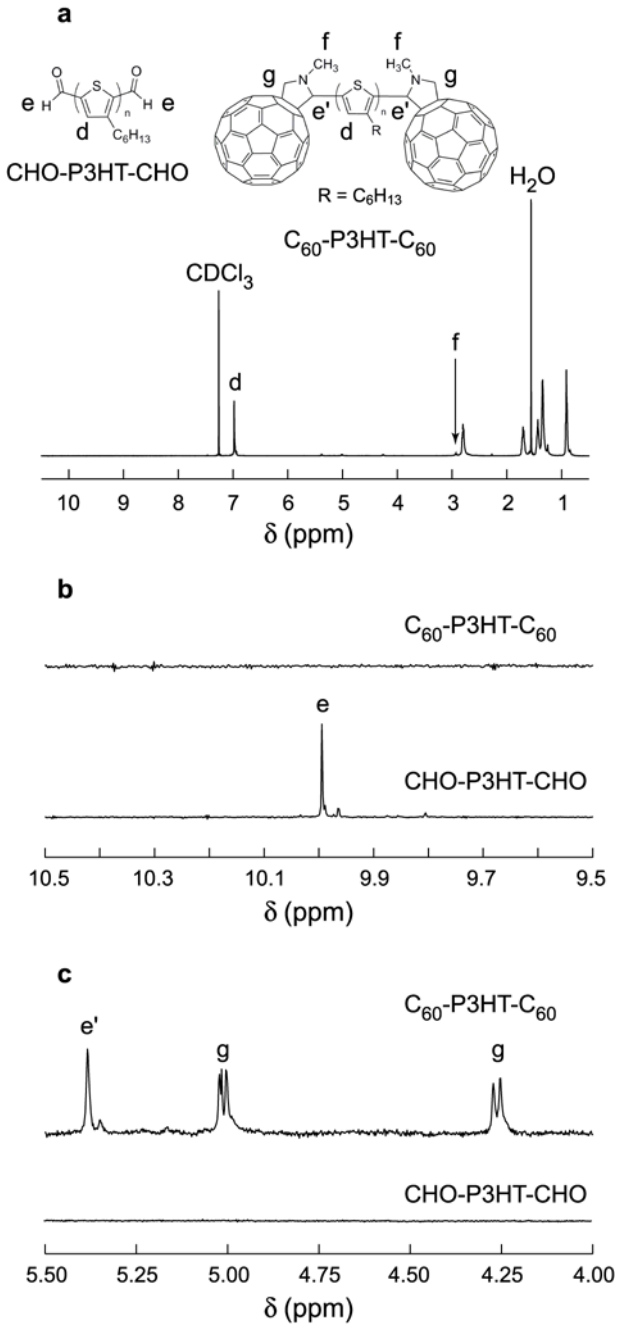

Figure 7.3. ^{1}H NMR spectra of (a) C_{60}-P3HT-C_{60}, (b) the region near δ = 10 ppm showing the disappearance of the aldehyde proton signal upon addition of fullerene, and (c) the region near δ = 5 ppm showing the appearance of the signals related to the fullerene end groups. The unlabeled peaks upfield of δ = 5 ppm in Figure 7.3a are from the alkyl group protons. The coupling constant of the resonance at δ ~4.3 ppm is J = 9.5 Hz and the coupling constant of the resonance at δ ~5.0 ppm is J = 10 Hz.

To verify the amount of fullerene end groups per polymer chain determined by ^{1}H NMR spectroscopy, absorbance at selected wavelengths versus concentration of species plots were constructed to determine the molar absorption coefficient of P3HT and C_{60}. These molar absorption coefficients were found using the slope of the linear fits shown in Figures 7.4b and 7.4c for wavelengths of λ = 330 nm in the fullerene system and λ = 330 nm and 448 nm in the P3HT system. The molar absorption coefficients were found to be $\varepsilon_{330} = 5.3 \times 10^4\ M^{-1}cm^{-1}$ for fullerene and $\varepsilon_{330} = 5.5 \times 10^4\ M^{-1}cm^{-1}$ and $\varepsilon_{448} = 20 \times 10^4\ M^{-1}cm^{-1}$ for P3HT. From this point a system of linear equations involving two variables and two unknowns was solved using the Beer-Lambert Law. Because the connection between the donor and acceptor contained one non-conjugated bond the molar absorption coefficients are likely not significantly affected by covalent attachment.[58]

$$A_{330}^{Total} = A_{330}^{P3HT} + A_{330}^{C_{60}} = \varepsilon_{330}^{P3HT} b\left[P3HT\right]_{330} + \varepsilon_{330}^{C_{60}} b\left[C_{60}\right]_{330} \quad (7.1)$$

$$A_{448}^{Total} = A_{448}^{P3HT} + A_{448}^{C_{60}} = \varepsilon_{448}^{P3HT} b\left[P3HT\right]_{448} + \varepsilon_{448}^{C_{60}} b\left[C_{60}\right]_{448} \approx \varepsilon_{448}^{P3HT} b\left[P3HT\right]_{448} \quad (7.2)$$

In these equations A_i is the total absorbance of the polymer at wavelength i at room temperature from the solution spectra shown in Figure 7.4a, b is the path length of the detection cell (10 mm), and [X] is the concentration of species X. Equation 7.2 becomes simplified because the absorbance of fullerene at λ = 448 nm is approximately zero. Using the NMR-determined molecular weight (M_n ~6,700 g mol^{-1}) for the main chain of the polymer (this includes the coupled and uncoupled chains), and 1552 g mol^{-1} for the molecular weight of methylfulleropyrrolidine end groups we find the theoretical weight fraction of the fullerene end groups is $w_{C_{60}} = 0.19$ for C_{60}-P3HT-C_{60}. Solving for the actual composition using Equations 7.1 and 7.2 yields a value of $w_{C_{60}} = 0.14$ for fullerene-capped polymer, in reasonable agreement with the predicted value. Utilizing the two equations above and the raw data obtained prior to normalization of the plots shown in Figure 7.4b we find that the UV-Vis data indicate the fullerene end-functionalization is slightly lower than the ^{1}H NMR spectroscopy data suggests but the

results are in relatively good agreement and indicate that the majority of the polymer chains are capped on both ends with fullerene units.

Thin film UV-Vis absorbance spectra were also acquired for P3HT and C_{60}-P3HT-C_{60}. As shown in Figure 7.4d, both spectra exhibit four local maxima over the range of the P3HT absorption; included in these maxima is a shoulder at $\lambda \approx 625$ nm which is associated with vibronic structure and is an indication of crystalline order consistent with the wide-angle x-ray scattering data (see Figure 7.7). The C_{60}-P3HT-C_{60} spectrum contains a small shoulder at $\lambda \approx 330$ nm, and a significant increase in the thin film absorption relative to P3HT at $\lambda \approx 275$ nm is also present. Both of these observations are consistent with absorption of fullerene species. The absorption coefficients calculated at the maximum absorption wavelength ($\lambda = 552$ nm) were $\alpha_{P3HT} = 5.0 \times 10^4\ cm^{-1}$ and $\alpha_{C_{60}-P3HT-C_{60}} = 6.2 \times 10^4\ cm^{-1}$ for the P3HT and C_{60}-P3HT-C_{60} films, respectively.

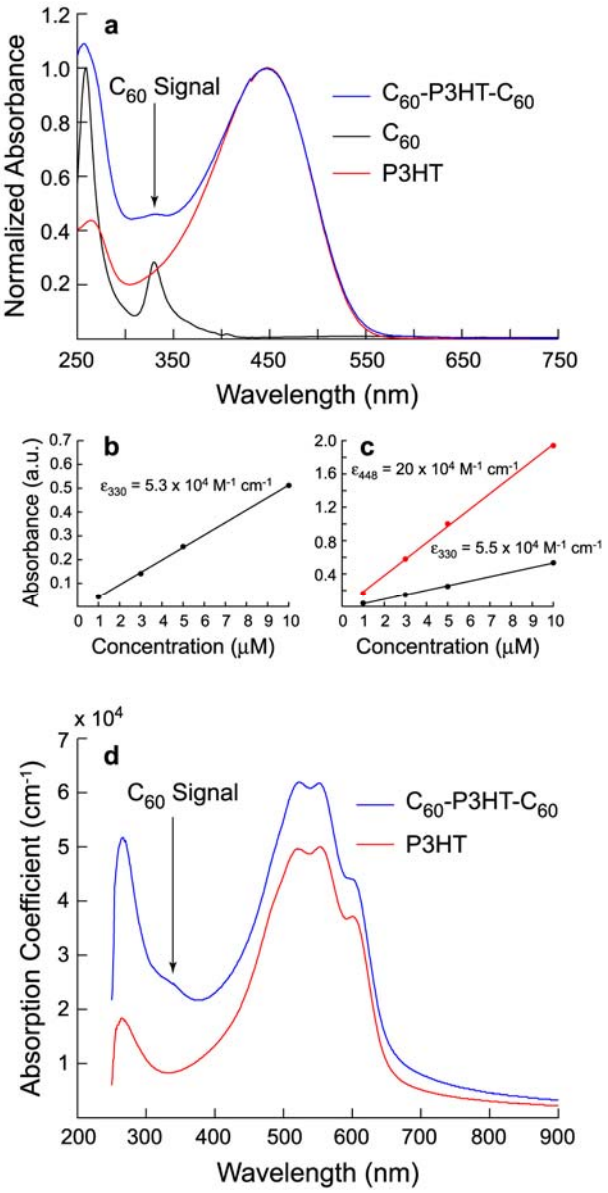

Figure 7.4. (a) UV-Vis absorption data of 5 μM solutions of P3HT, C_{60}, and C_{60}-P3HT-C_{60} in chloroform at room temperature. Absorbance as a function of concentration in chloroform solutions for (b) C_{60} and (c) P3HT at selected wavelengths (λ = 330 nm and λ = 448 nm). (d) UV-Vis absorption coefficients for thin films of P3HT (d ~70 nm) and C_{60}-P3HT-C_{60} (d ~52 nm) spun-coat from 1,2-dichlorobenzene solutions.

Importantly, fluorescence quenching experiments were performed on chloroform solutions of the polymers (Figure 7.5a). The emission spectra of all polymers show a primary peak and a shoulder at higher wavelengths, which is consistent with previous

reports.[28] The calculated quantum yield of the C_{60}-P3HT-C_{60} polymer is 0.03 which is seven times less than the quantum yields of both P3HT and a mixture of unbound P3HT and PCBM (P3HT+PCBM) where 2.1 equivalents of free PCBM were added to the solution for every polymer chain. The highly soluble fullerene derivative PCBM was used in place of C_{60} to ensure that the quencher was dissolved in solution with P3HT. Figure 7.5b shows fluorescence quenching measurements of the same three samples dissolved in toluene. Significant quenching is once again seen in the C_{60}-P3HT-C_{60} molecule relative to the other systems. Previous studies have shown that when quenching occurs in a similar manner both in chloroform and toluene that energy transfer is the likely means of relaxation;[27,28,59-61] however, ultrafast spectroscopy measurements are required to confirm that electron transfer does not account for at least a fraction of the quenching in the chloroform system.

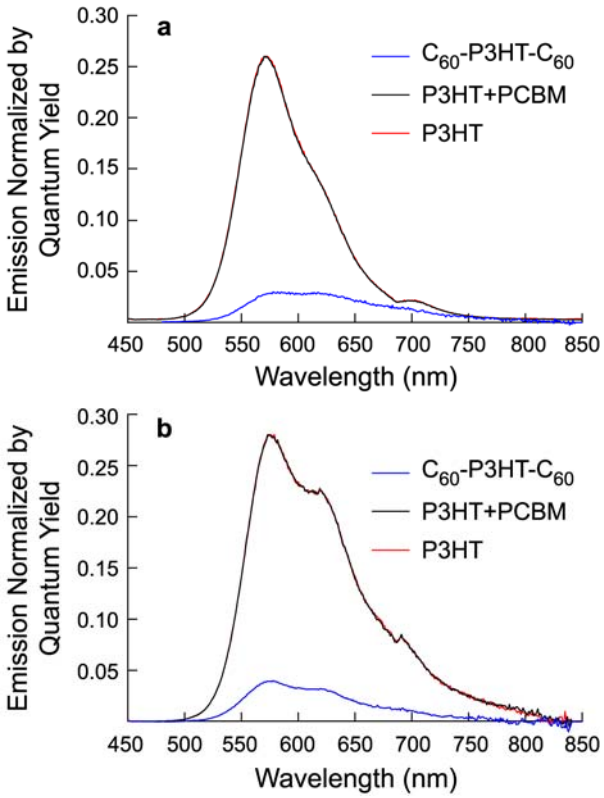

Figure 7.5. Fluorescence spectra for P3HT, P3HT+PCBM, and C_{60}-P3HT-C_{60} in (a) chloroform and (b) toluene where the emission signal has been normalized by the quantum yield of each of the samples.

We have concluded that the polymer, C_{60}-P3HT-C_{60}, is a mixture of two types of polymer chains and contains a bimodal distribution of these chains with the majority of all types of polymer chains terminated on both ends with fullerene groups. The distribution of the uncoupled polymer chains is the same as the CHO-P3HT-CHO starting material. The size distribution of these molecules is centered about 27 thiophene repeat units per polymer chain and this type of polymer chain composes 52% of the bimodal mixture by weight. The coupled P3HT chains contain an ill-defined linkage along the backbone of the polythiophene chain and have a distribution twice the length of the uncoupled chains on average. This average is centered on 54 thiophene repeat units per polymer chain, and the coupled chains compose the remainder (48% by weight) of the bimodal mixture. We are confident that the UV-Vis spectroscopic signals

(and the subsequent x-ray diffraction pattern reflections) associated with fullerene can be attributed to the *end groups of the polymer chain* and not due to unreacted, free C_{60} present in what would be a mixture of polymer and small molecule.

Thermal and Microstructural Characterization of C_{60}-P3HT-C_{60}.

We used DSC to determine the melting temperatures of the polymer and fullerene samples and to estimate the amount of P3HT crystallinity in the polymers (Figure 7.6). As previously seen in the literature, C_{60} undergoes a first order phase transition around –11 °C and this peak is associated with a crystal rearrangement from a simple cubic structure to a face-centered cubic crystal packing.[62] The melting transition of C_{60} was not observed in the temperature range scanned. Unlike the parent C_{60} molecule, *N*-methylfulleropyrrolidine (NMC_{60}) does not experience the simple cubic to face-centered cubic crystal packing transition presumably due to the substituents of NMC_{60}. This molecule also does not exhibit a melting endotherm in the temperature range scanned. As is commonly seen in P3HT, two melting transitions were observed in the H-P3HT-H molecule. The first transition is a broad transition ranging from T ~50 °C to T ~75 °C and is associated with the side-chain melting of interdigitated hexyl groups.[63] The main chain melting of P3HT was found to be at T ~206 °C. The mixture of P3HT and C_{60} shows both the crystal transition melting temperature associated with the fullerene component and the main chain melting transition of the polythiophene. Finally, C_{60}-P3HT-C_{60} also exhibits the melting transition of the polythiophene at T ~195 °C but does not exhibit the simple cubic to face-centered cubic rearrangement because the molecule present at the end of the polymer chains is more akin to NMC_{60}, which also is incapable of the crystal rearrangement transition. The melting point depressions observed both in the P3HT/C_{60} mixture and C_{60}-P3HT-C_{60} systems are expected because the fullerene acts as an impurity that depresses the freezing (melting) temperature of the semicrystalline polymer.[64] The amount of polymer that was crystalline in the P3HT and C_{60}-P3HT-C_{60} samples was determined by integrating the area under the melting peak in each of the samples, normalizing the values by the amount of P3HT present in the sample, and comparing this with the literature value for

the enthalpy of fusion for an ideal P3HT crystal, ΔH_m^{∞} = 99 J g^{-1}.[65] The amount of polythiophene that was crystalline in each sample was 11% and 10% for the P3HT and C_{60}-P3HT-C_{60} samples, respectively, which is typical for lower molecular weight P3HTs. Therefore, the bulky end groups of the polymer chain appear to only have a minor impact on the semicrystalline nature of P3HT according to the DSC data.

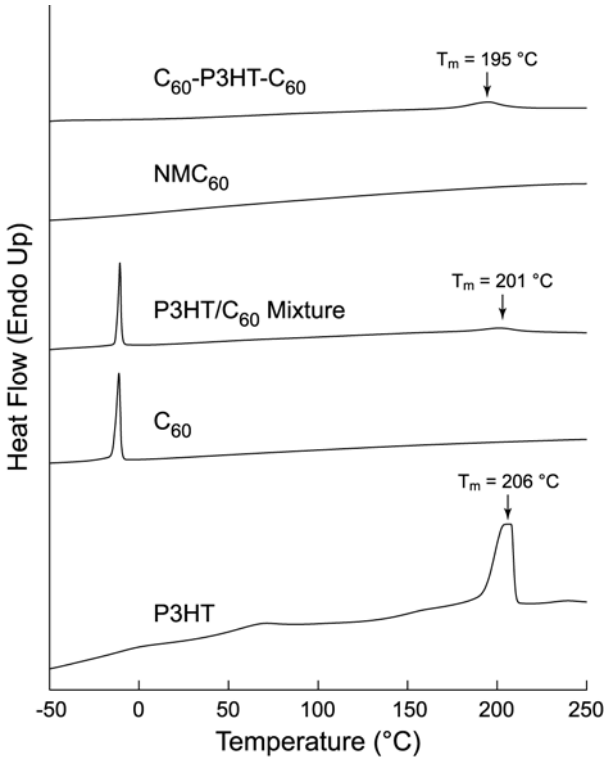

Figure 7.6. DSC thermograms of P3HT, C_{60}, the P3HT/C_{60} mixture, NMC_{60}, and C_{60}-P3HT-C_{60}. The scans shown were collected at a heating rate of 10 °C/min after annealing at 260 °C and then cooling to –60 °C. The arrows mark the P3HT main chain melting temperature of the applicable samples. The percent crystallinity of the polythiophene components (see text for details) of P3HT and C_{60}-P3HT-C_{60} were 11% and 10%, respectively.

Wide Angle X-ray Scattering (WAXS) and Small Angle X-ray Scattering (SAXS). The spectra in Figure 7.7 show the WAXS powder scattering patterns of P3HT, C_{60}, the P3HT/C_{60} mixture, NMC_{60}, and C_{60}-P3HT-C_{60}. As is common with P3HT, the first three reflections observed in Figure 7.7a are the (100), (200), and (300) peaks consistent with a lamellar morphology within the crystalline regions of the

polymer and side group interdigitation.[66] The C_{60} scattering pattern in Figure 7.7b is also consistent with previously observed results for buckminsterfullerene, which is known to have a face-centered cubic (*fcc*) crystal structure at room temperature, and shows reflections for the (111), (220), (311), and (222) indices.[62,67,68] The P3HT/C_{60} mixture spectra is a combination of the individual P3HT and C_{60} single species spectra where the (100), (200), and (300) crystalline reflections of the polythiophene phase are prominent while the (220) and (311) reflections of the fullerene phase present but are not as accentuated. However, this does suggest that the mixture contains two crystalline domains: one associated with the polythiophene and one associated with the fullerene. Figure 7.7d shows the reference spectrum of free NMC_{60} and indicates that this molecule has a very similar scattering pattern to that of free C_{60} but with reflections shifted to slightly lower q values (slightly higher domain spacings) due to the substituents present on the NMC_{60} molecule. Also present in this sample is the (200) reflection which is allowable for an *fcc* crystal lattice but not commonly observed in the case of C_{60}.[62,67,68] Much like the P3HT/C_{60} mixture, the C_{60}-P3HT-C_{60} spectra in Figure 7.7e appears to be a combination of the P3HT and NMC_{60} scattering patterns and suggests the presence of unique polythiophene and fullerene crystalline regimes because of the prescence of both the (100) P3HT peak and the (311) and (222) NMC_{60} reflections. For the three P3HT-containing samples, the average sizes of the polymer crystallites were estimated by using Scherrer's relation.[69] The sizes of the polymer crystallites were found to be 13 nm, 14 nm, and 11 nm for P3HT, the P3HT/C_{60} mixture, and C_{60}-P3HT-C_{60} samples, respectively. These values are similar with those previously seen in the literature for unannealed P3HT samples[70] and the fact that the crystallite size of the P3HT remains almost unchanged even with the bulky fullerene side groups is noteworthy. We note that peak broadening in WAXS can have other origins besides small crystallite sizes (*e.g.*, inhomogeneous strains). Nevertheless, the formation of discrete domains is consistent with the phase separation seen in other polymer-fullerene systems.[71,72]

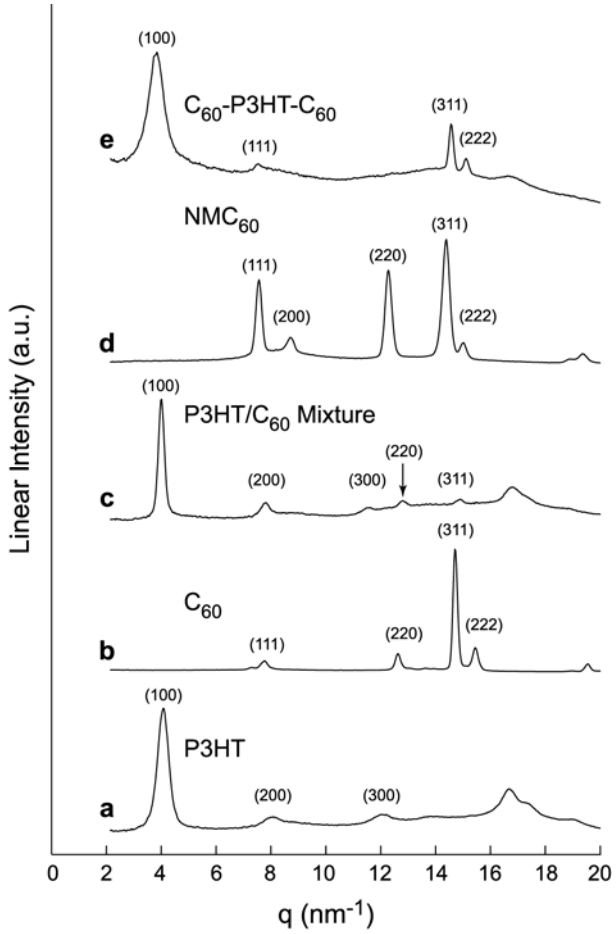

Figure 7.7. WAXS spectra of (a) P3HT, (b) C_{60}, (c) the P3HT/C_{60} mixture, (d) NMC_{60}, and (e) C_{60}-P3HT-C_{60} obtained at room temperature. The sizes of the polymer crystallites were found to be 13 nm, 14 nm, and 11 nm for P3HT, the P3HT/C_{60} mixture, and C_{60}-P3HT-C_{60}, respectively using Scherrer's relation. The spectra are offset for clarity.

In addition to WAXS spectra, SAXS was also employed to observe the domain spacing of P3HT and the C_{60}-P3HT-C_{60} triad. Figure 7.8 shows the obtained spectra at 30 °C after annealing at 220 °C for 5 min. The presence of a weak, broad peak corresponding to domain spacings of d ~13–14 nm indicate the width of the crystallite lamellae previously observed in thin films of regioregular P3HT samples cast from selected solvents.[73] In agreement with the WAXS data, the crystallite structure is more prominent in the P3HT sample over both the P3HT/C_{60} mixture and the C_{60}-P3HT-C_{60} triad.

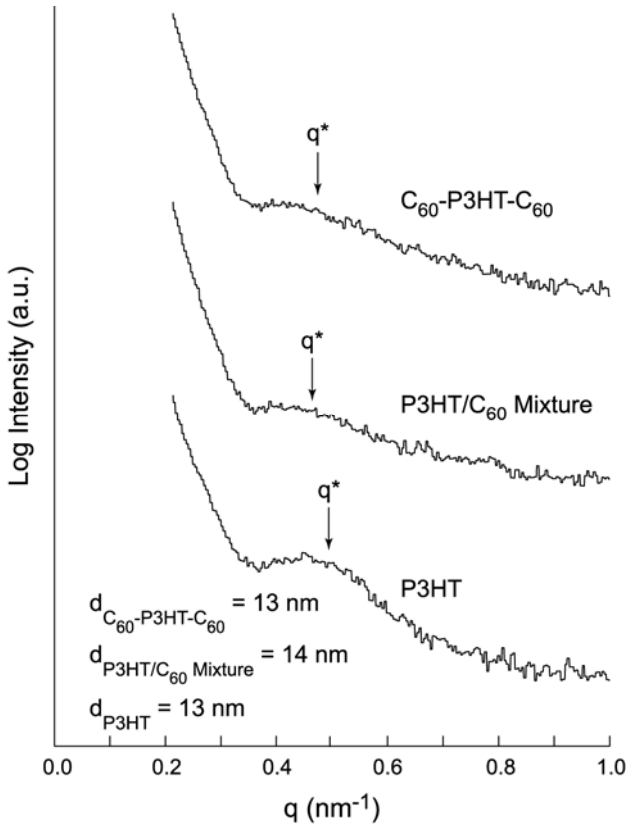

Figure 7.8. SAXS spectra at 30 °C after annealing at 220 °C for 5 min and slowly cooling to room temperature of P3HT, the P3HT/C_{60} mixture, and C_{60}-P3HT-C_{60}. The principle reflection, q*, for each sample is marked with an arrow. The corresponding domain spacings calculated from q* values for the samples are listed at the lower left-hand part of the plot.

Thin Film Imaging. As polymer thin films are important in the application of OPV devices, atomic force microscopy (AFM) operating in tapping mode was used to acquire phase images of thin films. The thin films were spun-coat onto thermally grown silicon dioxide from a 3 mg of polymer in 1 mL of 1,2-dichlorobenzene solution. The films were then annealed at 150 °C in an inert atmosphere glove box for 10 min. The phase images are shown in Figure 7.9 with the Fast Fourier Transfer (FFT) data inset in the upper left-hand corners of the images. The films are rather smooth and both have a root mean square (RMS) roughness of 0.3 nm over the 750 nm scan range shown in Figure 7.9. While the crystalline P3HT lamellae are not as distinct as shown in previous works,[46,73,74] the integration of the FFT of the films gave characteristic dimensions of 14

nm and 13 nm for the P3HT and C_{60}-P3HT-C_{60} films, respectively. These numbers compare reasonable well with the dimensions obtained for the crystallite width seen in the SAXS spectra (especially considering the inherent error due to the radius of curvature associated with the tip of the AFM cantilever) and previously in the literature, which suggests that the morphologies observed in the bulk are also present in thin films.[73,74]

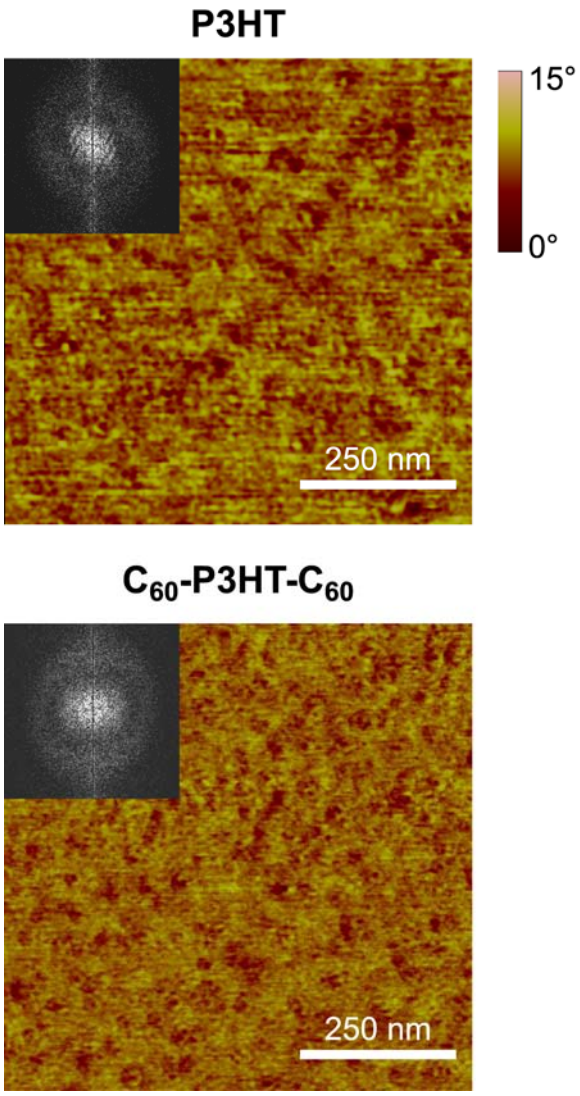

Figure 7.9. AFM phase images of thin films of P3HT and C_{60}-P3HT-C_{60} and corresponding FFT insets. Processing the FFT data showed characteristic domain dimensions of 14 nm and 13 nm for P3HT and C_{60}-P3HT-C_{60}, respectively. The films were formed by spin-coating a solution that contained 3 mg of polymer in 1 mL of 1,2-dichlorobenzene at a rotation rate of 2000 rpm for 1 min onto a silicon dioxide substrate. The films were then annealed at 150 °C for 10 min in an inert atmosphere glove box.

7.5 Summary

We have described the synthesis of fullerene end-functionalized regioregular poly(3-hexylthiophene), C_{60}-P3HT-C_{60}. We find that the final step in the reaction

sequence leads to chain coupling and speculate that this occurs through an azomethine ylide intermediate which causes a slight increase in the overall molecular weight and a larger increase in the polydispersity of the poly(3-hexylthiophene). The molecules were characterized using a variety of techniques to ensure that the majority of the polymers (including both the coupled and uncoupled polymer chains) contained covalently bound fullerene and no free C_{60}. Thermal characterization reveals that C_{60}-P3HT-C_{60} does experience a melting transition at a slightly depressed temperature from that observed in P3HT presumably due to packing frustration brought about by the relatively bulky end groups. However, the percent crystallinity of the polythiophene portion of the polymer remains approximately the same as that of the P3HT material. The powder x-ray scattering data indicate the presence of two distinct semicrystalline regimes in the C_{60}-P3HT-C_{60} polymer, which suggests that the end groups microphase separate from the main polymer chains to generate fullerene-rich and polythiophene-rich domains as was seen in a mixture of P3HT and C_{60}. The crystallite sizes of the P3HT domains were estimated to be on the order of 12 nm for both the P3HT and C_{60}-P3HT-C_{60} polymers using Scherrer's relation. Small-angle x-ray scattering on powders showed that the width of the P3HT crystallites were ~13 nm for both P3HT and C_{60}-P3HT-C_{60}. Finally, AFM phase images of thin films of the two polymers indicated that domain spacings consistent with SAXS data were also present in thin films of both of the polymer samples. The C_{60}-P3HT-C_{60} polymer behaves in a similar manner to the parent P3HT polymer in terms of light absorption, thermal properties, and microstructure. The covalent attachment of the fullerene to the polymer-chain, which may enhance charge transfer, makes this new polymer a candidate for use as an electron-donating material in organic photovoltaics.

7.6 Acknowledgements

This work was funded by the Initiative for Renewable Energy and the Environment (IREE) at the University of Minnesota and the Xcel Renewable Development Fund. Parts of this work were carried out in the University of Minnesota IT Characterization Facility, which receives partial support from the NSF through the

NNIN program. We thank Marc Rodwogin for help with prep SEC separation experiments and Benjamin D. Hamilton for help with WAXS experiments. We also thank Dr. Yang Qin and Derek M. Stevens for helpful discussions.

7.7 References

[1] Sun, S.; Sariciftci, N. S.; Eds. *Organic Photovoltaics: Mechanisms, Materials, and Devices*; Taylor & Francis: Boca Raton, FL, 2005.

[2] Shaheen, S. E.; Ginley, D. S.; Jabbour, G. E. *MRS Bull.* **2005**, *30*, 10–15.

[3] Günes, S.; Neugebauer, H.; Sariciftci, N. S. *Chem. Rev.* **2007**, *107*, 1324–1338.

[4] Li, G.; Shrotriya, V.; Huang, J.; Yao, Y.; Moriarty, T.; Emery, K.; Yang, Y. *Nat. Mater.* **2005**, *4*, 864–868.

[5] Ma, W.; Yang, C.; Gong, X.; Lee, K.; Heeger, A. J. *Adv. Funct. Mater.* **2005**, *15*, 1617–1622.

[6] Loewe, R. S.; Khersonsky, S. M.; McCullough, R. D. *Adv. Mater.* **1999**, *11*, 250–253.

[7] Chen, T. A.; Wu, X.; Rieke, R. D. *J. Am. Chem. Soc.* **1995**, *117*, 233–244.

[8] Skotheim, T.; Reynolds, J.; Elsembauer, R.; Eds. *Handbook of Conducting Polymers*; Marcel Dekker: New York, 1998.

[9] Osaka, I.; McCullough, R. D. *Acc. Chem. Res.* **2008**, *41*, 1202–1214.

[10] Nalwa, H. S.; Ed. *Handbook of Organic Conductive Molecules and Polymers*; J. Wiley & Sons: New York, 1996.

[11] McCullough, R. D. *Adv. Mater.* **1998**, *10*, 93–116.

[12] Schilinsky, P.; Waldauf, C.; Brabec, C. J. *Appl. Phys. Lett.* **2002**, *81*, 3885–3887.

[13] Padinger, F.; Rittberger, R. S.; Sariciftci, N. S. *Adv. Funct. Mater.* **2003**, *13*, 85–88.

[14] Janssen, R. A. J.; Hummelen, J. C.; Sariciftci, N. S. *MRS Bull.* **2005**, *30*, 33–36.

[15] Thompson, B. C.; Fréchet, J. M. J. *Angew. Chem., Int. Ed.* **2008**, *47*, 58–77.

[16] Chirvase, D.; Parisi, J.; Hummelen, J. C.; Dyakonov, V. *Nanotechnology* **2004**, *15*, 1317–1323.

[17] Nguyen, L. H.; Hoppe, H.; Erb, T.; Günes, S.; Gobsch, G.; Sariciftci, N. S. *Adv. Funct. Mater.* **2007**, *17*, 1071–1078.

[18] Müller, C.; Ferenczi, T. A. M.; Campoy-Quiles, M.; Frost, J. M.; Bradley, D. D. C.; Smith, P.; Stingelin-Stutzmann, N.; Nelson, J. *Adv. Mater.* **2008**, *20*, 3510–3515.

[19] Campoy-Quiles, M.; Ferenczi, T.; Agostinelli, T.; Etchegoin, P. G.; Kim, Y.; Anthopoulos, T. D.; Stavrinou, P. N.; Bradley, D. D. C.; Nelson, J. *Nat. Mater.* **2008**, *7*, 158–164.

[20] Xin, H.; Ren, G.; Kim, F. S.; Jenekhe, S. A. *Chem. Mater.* **2008**, *20*, 6199–6207.

[21] Bates, F. S.; Fredrickson, G. H. *Annu. Rev. Phys. Chem.* **1990**, *41*, 525–557.

[22] Russell, T. P.; Coulon, G.; Deline, V. R.; Miller, D. C. *Macromolecules* **1989**, *22*, 4600–4606.

[23] Morkved, T. L.; Lu, M.; Urbas, A. M.; Ehrichs, E. E.; Jaeger, H. M.; Mansky, P.; Russell, T. P. *Science* **1996**, *273*, 931–933.

[24] Hadziioannou, G. *MRS Bull.* **2002**, *27*, 456–460.

[25] Roncali, J. *Chem. Soc. Rev.* **2005**, *34*, 483–495.

[26] Cravino, A. *Polym. Int.* **2007**, *56*, 943–956.

[27] van Hall, P. A.; Knol, J.; Langeveld-Voss, B. M. W.; Meskers, S. C. J.; Hummelen, J. C.; Janssen, R. A. J. *J. Phys. Chem. A* **2000**, *104*, 5974–5988.

[28] Narutaki, M.; Takimiya, K.; Otsubo, T.; Harima, Y.; Zhang, H.; Araki, Y.; Ito, O. *J. Org. Chem.* **2006**, *71*, 1761–1768.

[29] Fernández, G.; Sánchez, L.; Veldman, D.; Wienk, M. M.; Atienza, C.; Guldi, D. M.; Janssen, R. A. J.; Martín, N. *J. Org. Chem.* **2008**, *73*, 3189–3196.

[30] Baffreau, J.; Ordronneau, L.; Leroy-Lhez, S.; Hudhomme, P. *J. Org. Chem.* **2008**, *73*, 6142–6147.

[31] Li, W. S.; Yamamoto, Y.; Fukushima, T.; Saeki, A.; Seki, S.; Tagawa, S.; Masunaga, H.; Sasaki, S.; Takata, M.; Aida, T. *J. Am. Chem. Soc.* **2008**, *130*, 8886–8887.

[32] Ouhib, F.; Khoukh, A.; Ledeuil, J-B.; Martinez, H.; Desbrières, J.; Dagron-Lartigau, C. *Macromolecules* **2008**, *41*, 9736–9743.

[33] Stalmach, U.; de Boer, B.; Videlot, C.; van Hutten, P. F.; Hadziioannou, G. *J. Am. Chem. Soc.* **2000**, *122*, 5464–5472.

[34] de Boer, B.; Stalmach, U.; van Hutten, P. F.; Melzer, C.; Krasnikov, V. V.; Hadziioannou, G. *Polymer* **2001**, *42*, 9097–9109.

[35] Richard, F.; Brochon, C.; Leclerc, N.; Eckhardt, D.; Heiser, T.; Hadziioannou, G. *Macromol. Rapid Commun*. **2008**, *29*, 885–891.

[36] Marcos-Ramos, A.; Rispens, M. T.; van Duren, J. K. J.; Hummelen, J. C.; Janssen, R. A. J. *J. Am. Chem. Soc.* **2001**, *123*, 6714–6715.

[37] Sivula, K.; Ball, Z. T.; Watanabe, N.; Fréchet, J. M. J. *Adv. Mater.* **2006**, *18*, 206–210.

[38] Sykes, A. G; Ed. *Advances in Inorganic Chemistry*; Academic Press: New York, NY, 1996; Vol. 44.

[39] Moriyama, H.; Kobayashi, H.; Kobayashi, A.; Watanabe, T. *J. Am. Chem. Soc.* **1993**, *115*, 1187–1189.

[40] Davey, S. N.; Leigh, D. A.; Moody, A. E.; Tetler, L. W.; Wade, F. A. *J. Chem. Soc., Chem. Commun.* **1994**, 397–398.

[41] Yamamoto, T.; Oguro, D.; Kubota, K. *Macromolecules* **1996**, *29*, 1833–1835.

[42] de Koning, G. J. M.; Lemstra, P. J. *Polymer* **1993**, *34*, 4089–4094.

[43] Lewis, J. E.; Maroncelli, M. *Chem. Phys. Lett.* **1998**, *282*, 197–203.

[44] Loewe, R. S.; Ewbank, P. C.; Liu, J.; Zhai, L.; McCullough, R. D. *Macromolecules* **2001**, *34*, 4324–4333.

[45] Trznadel, M.; Pron, A.; Zagorska, M.; Chrzaszcz, R.; Pielichowski, J. *Macromolecules* **1998**, *31*, 5051–5058.

[46] Sauvé, G.; McCullough, R. D. *Adv. Mater.* **2007**, *19*, 1822–1825.

[47] Dai, C.; Yen, W.; Lee, Y.; Ho, C.; Su, W. *J. Am. Chem. Soc.* **2007**, *129*, 11036–11038.

[48] Boudouris, B. W.; Frisbie, C. D.; Hillmyer, M. A. *Macromolecules* **2008**, *41*, 67–75.

[49] Liu, J.; McCullough, R. D. *Macromolecules* **2002**, *35*, 9882–9889.

[50] Witiak, D. T.; Williams, D. R.; Kakodkar, S. V. *J. Org. Chem.* **1974**, *39*, 1242–1247.

[51] Maggini, M.; Scorrano, G.; Prato, M. *J. Am. Chem. Soc.* **1993**, *115*, 9798–9799.

[52] See Chapter 9.2 for detailed synthetic procedures.

[53] El-Sayed, I.; Hazell, R. G.; Madsen, J. Ø.; Norrby, P-O.; Senning, A. *Eur. J. Org. Chem.* **2003**, *5*, 813–815.

[54] Elandaloussi, E. H.; Frère, P.; Richomme, P.; Orduna, J.; Garin, J.; Roncali, J. *J. Am. Chem. Soc.* **1997**, *119*, 10774–10784.

[55] Fazio, M. A.; Lee, P. O.; Shuster, D. I. *Org. Lett.* **2008**, *10*, 4979–4982.

[56] Ballenweg, S.; Gleiter, R.; Krätschmer, W. *Synth. Met.* **1996**, *77*, 209–212.

[57] Baffreau, J.; Ordronneau, L.; Lhez-Leroy, S.; Hudhomme, P. *J. Org. Chem.* **2008**, *73*, 6142–6147.

[58] Lambert, J. B.; Shurvell, H. F.; Lightner, D. A.; Cooks, R. G. *Organic Structural Spectroscopy*; Prentice Hall: Upper Saddle River, NJ, 1998.

[59] Yamashiro, T.; Aso, Y.; Otsubo, T.; Tang, H.; Harima, Y.; Yamashita, K. *Chem. Lett.* **1999**, 443–444.

[60] Fujitsuka, M.; Ito, O.; Yamashiro, T.; Aso, Y.; Otsubo, T. *J. Phys. Chem. A* **2000**, *104*, 4876–4881.

[61] Fujitsuka, M.; Matsumoto, K.; Ito, O.; Yamashiro, T.; Aso, Y.; Otsubo, T.; *Res. Chem. Intermed.* **2001**, *27*, 73–88.

[62] Heiny, P. A.; Fischer, J. E.; McGhie, A. R.; Romanow, W. J.; Denenstein, A. M.; McCauley, Jr., J. P.; Smith, III, A. B.; Cox, D. E. *Phys. Rev. Lett.* **1991**, *66*, 2911–2914.

[63] Liu, S. L.; Chung, T. S. *Polymer* **2000**, *41*, 2781–2793.

[64] Sperling, L. H. *Introduction to Polymer Science, 3rd Ed.*; John Wiley & Sons, Inc.: Hoboken, NJ, 2001.

[65] Malik, S.; Nandi, A. K. *J. Poly. Sci. B* **2002**, *40*, 2073–2085.

[66] Causin, V.; Marega, C.; Marigo, A.; Valentini, L.; Kenny, J. M. *Macromolecules* **2005**, *38*, 409–415.

[67] Cagiao, M. E.; Pozdnyakov, A. O.; Krumova, M.; Kudryavtsev, V. V.; Balta Callejà, F. J. *Compos. Sci. Technol.* **2007**, *67*, 2175–2182.

[68] Li, J. Q.; Zhao, Z. X.; Li, Y. L.; Zhu, D. B.; Gan, Z. Z.; Yin, D. L. *Physica C* **1992**, *196*, 135–140.

[69] Cullity, B. D. *Elements of X-Ray Diffraction, 2nd Ed.*; Addison-Wesley Publishing Company, Inc.: Reading, MA, 1978.

[70] Erb, T.; Zhokhavets, U.; Gobsch, G.; Raleva, S.; Stühn, B.; Schilinsky, P.; Waldauf, C.; Brabec, C. J. *Adv. Funct. Mater.* **2005**, *15*, 1193–1196.

[71] Moulé, A. J.; Meerholz, K. *Adv. Mater.* **2008**, *20*, 240–245.

[72] Zhong, H.; Yang, X.; deWith, B.; Loos, J. *Macromolecules* **2006**, *39*, 218–223.

[73] Zhang, R.; Li, B.; Iovu, M. C.; Jeffries-EL, M.; Sauve, G.; Cooper, J.; Jia, S.; Tristram-Nagle, S.; Smilgies, D. M.; Lambeth, D. N.; McCullough, R. D.; Kowalewski, T. *J. Am. Chem. Soc.* **2006**, *128*, 3480–3481.

[74] Liu, J.; Sheina, E.; Kowalewski, T.; McCullough, R. D. *Angew. Chem., Int. Ed.* **2002**, 41, 329–332.

8 Future Work

Projects related to the work presented in Chapters 4–7 either have been started or enthusiastically talked about during the course of the research presented in this thesis. These proposed activities are tangential to: 1) using completely amorphous polythiophene-containing block copolymers as nanoporous templates for the fabrication of all-organic ordered bulk heterojunctions, or 2) studying internal electron acceptor-donor-acceptor type macromolecules and their potential uses as compatibilizers in blended bulk heterojunction photovoltaic devices. Here, preliminary results for these experiments are presented, and future directions for these projects are suggested.

8.1 The Structure of Amorphous, Semiconducting Block Copolymers

Chapter 6 demonstrated a synthetic route that allowed for the creation of a series of polythiophene-containing block copolymers, polylactide-*b*-poly(3-dodecylthiophene-*co*-thiophene)-*b*-polylactide (PLA-coPT-PLA). The motivation for synthesizing these macromolecules was they were both completely amorphous and had relatively narrow molecular weight distributions because well-controlled polymerization mechanisms were utilized. It was suggested that these two properties would lead to thin film microphase separation with long-range order in a manner analogous to behavior observed previously in poly(phenylene vinylene)-based (PPV) block copolymer systems.[1-5] Here, the preliminary results of the thin film microstructures observed using atomic force microscopy (AFM) are presented. Recall from Chapters 5 and 6 that the nomenclature used for these block copolymers was PLA-coPT(X)-PLA(Y) for a block copolymer that had a thiophene weight fraction of X and an overall polylactide molecular weight of Y kg/mol. The ^{1}H NMR determined molecular weight of all the coPT blocks was 5.8 kg/mol with an average coPT moiety that contained 10 thiophene and 20 3-dodecylthiophene repeat units.

Figure 8.1 shows the AFM phase images acquired in tapping mode of the block copolymer thin films on glass substrates after annealing in inert atmosphere at 110 °C for 48 h. Despite the poor film quality, interesting phase separation was observed.

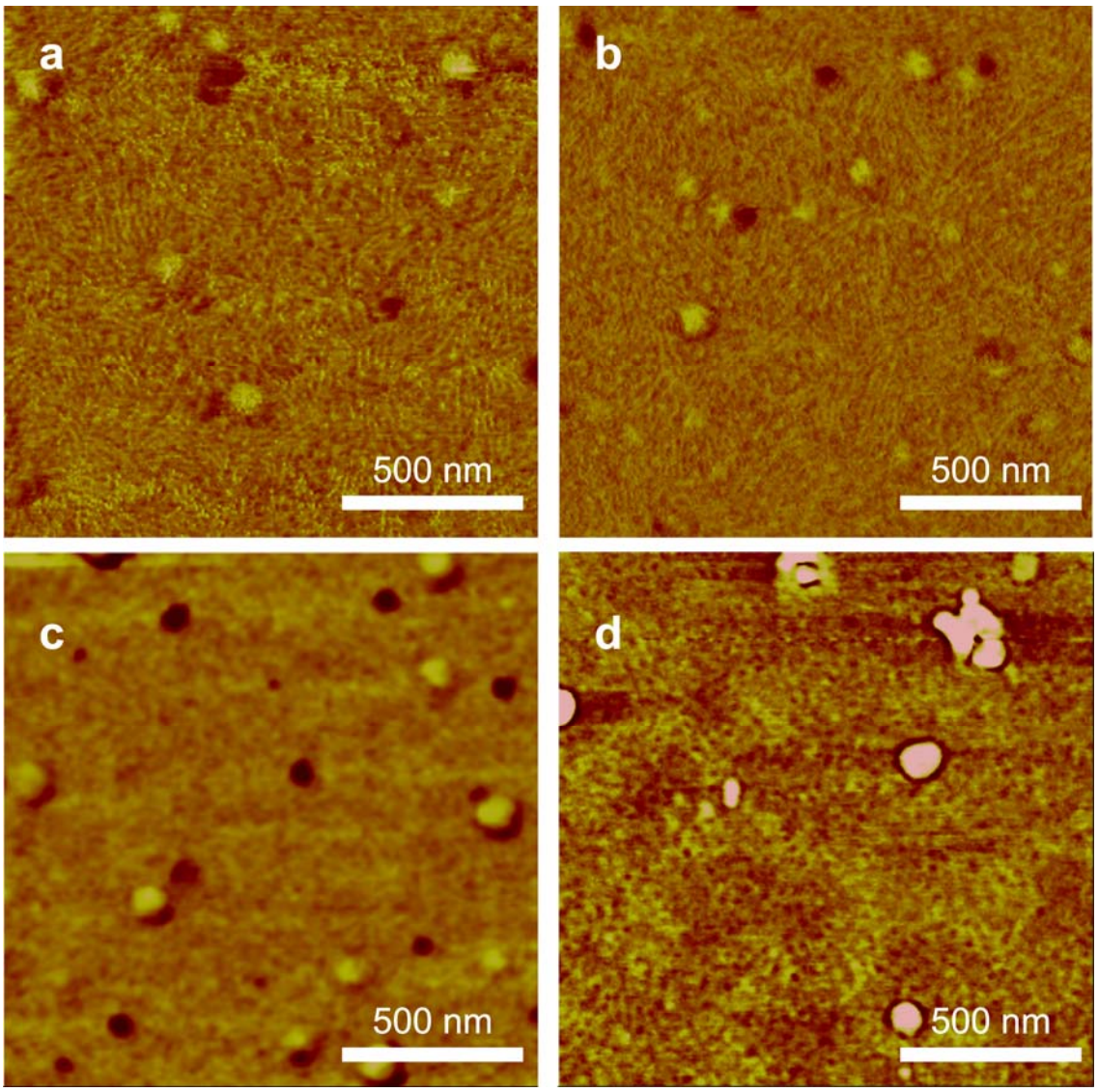

Figure 8.1. AFM thin film phase images of (a) PLA-coPT(0.82)-PLA(1.3), (b) PLA-coPT(0.77)-PLA(1.7), (c) PLA-coPT(0.59)-PLA(4.0), and (d) PLA-coPT(0.14)-PLA(35.7). The films were spun-coat from 10 mg of polymer in 1 mL of 1,2-dichlorobenzene solutions onto glass substrates at a rotation rate of 1000 rpm for 1 min. Final film thicknesses were all 20 ± 4 nm as measured by AFM. The films were annealed at 110 °C in inert atmosphere for 48 h. The phase scale for all images is 40°.

As expected, the only signal that was present in the phase image of the homopolymer film (not shown) was due to differences in the film topology across the scan. The two coPT-rich block copolymer thin films showed a lamellae structure that lacks long-range order (Figure 8.1a,b). This was reminiscent of results for semicrystalline regioregular

poly(3-alkylthiophene)-based block copolymers.[6-15] These images suggested that even in the absence of semicrystalline regimes, there was a strong driving force for alignment of the rod blocks in these coil-rod-coil triblock copolymers when the rod moiety was the majority phase. The characteristic domain spacings (determined by integration of the Fast Fourier Transforms (FFTs) of the images) were 37 nm and 40 nm for the PLA-coPT(0.82)-PLA(1.3) and PLA-coPT(0.77)-PLA(1.7) films, respectively. Because the microstructure of the block copolymer thin films did not change, an increase in domain spacing with increased polylactide molecular weight was expected. Surprisingly, no phase separation was observed for the PLA-coPT(0.59)-PLA(4.0) thin film, perhaps due to poor film quality. Another possibility was that one of the moieties greatly preferred the film-air interface for this block copolymer composition, creating a "skin" layer of one of the blocks. If this were the case, the AFM would be unable to detect any microstructure that may exist underneath this layer. In the PLA-coPT(0.14)-PLA(35.7) case, the polylactide block was the majority phase, and striking phase separation is observed. Figure 8.1d showed a film that appeared to have cylinders of coPT embedded in a PLA matrix where the cylinders were perpendicular to the substrate. Similar phase behavior for coil-rich block copolymers has been observed previously for the poly(3-hexylthiophene)-*b*-poly(2-vinylpyridine) (P3HT-P2VP) system.[7] The characteristic domain spacing of this film was also 40 nm. It should be noted that because this was a two-dimensional image, these domains could also be attributed to spheres of coPT in a PLA matrix. Further experiments would be required to clarify this point.

The AFM images shown here suggested that PLA-coPT-PLA block copolymers may provide a method to generate well-ordered, microphase separated thin films with long-range order. A relatively low molecular weight polythiophene block was used in the preliminary study to aid in molecular characterization. In future experiments, the molecular weight of this segment should be increased to help drive phase separation. Additionally, only a handful of triblock copolymer compositions have been studied. A full phase diagram for this system should be constructed to determine the triblock copolymer composition that would be most practical for photovoltaic studies. Because

the chemistry developed for the PLA-coPT-PLA block copolymers utilized the well-controlled Grignard metathesis (GRIM) polymerization method,[16] tuning the molecular weight and generating large amounts of the HO-coPT-OH macroinitiator could be achieved in a relatively facile manner. The post-polymerization functionalization of the polythiophene homopolymer also was useful because the thiophene moiety could be composed of many different types of thiophene repeat units. In fact, if it is found that coPT is not as promising as anticipated, other thiophene derivatives could be polymerized to yield amorphous polythiophenes.[17,18] One of these, or other side chain-modified polythiophenes, could be used as the midblock to generate a new class of polylactide-polythiophene-polylactide block copolymers for study.

8.2 Infiltration of Nanoporous Thin Films with an Electron Acceptor

An additional step is required for the complete fabrication of an all-organic ordered bulk heterojunction even after successful ordering of polythiophene-polylactide thin films and removal of the sacrificial PLA block (see Chapter 3). The nanoporous, polythiophene film must be subsequently backfilled with an electron accepting material. In this process, the electron accepting material ideally would completely coat the walls of the pores, and also leave a skin layer on top of the polythiophene matrix. The thin top layer would separate the electron donor from the cathode. However, this is not necessarily required as some sort of buffer material could easily be deposited atop the electron-accepting material either by thermal evaporation or from a solution composed of an orthogonal solvent. Three chief routes to achieving nanopore infiltration with an electron-accepting material have been discussed critically: 1) thermal evaporation of a n-type small molecule, 2) melt processing an n-type polymer, and 3) solution deposition of a soluble n-type small molecule derivative. A detailed description of the three techniques and possible advantages and disadvantages follows.

Thermal evaporation of a small molecule perhaps is the most instinctive of the three methods listed above because it harkens to the strategy employed when making the first organic photovoltaic (OPV) device, which was composed entirely of small molecules.[19] Additionally, the final thickness of the electron acceptor film is tuned

easily when thermal evaporation is employed. This allows for the systematic study of the effect of film thickness on device performance, and can insure the fabricator that a sufficiently thick electron acceptor layer has been deposited so that there are no areas where the electron donor and cathode are in contact. While many small molecules are available for evaporation, buckminsterfullerene (C_{60}) is one of the best candidates for use. First, the optoelectronic properties of C_{60}, including a large absorption window in the visible spectrum and a long diffusion length (L_d ~40 nm),[20] are some of the best for electron-accepting materials used in OPVs. Secondly, the highest performing bulk heterojunction solar cells use fullerene derivatives as the electron acceptors and polythiophene derivatives as the electron donors.[21-23] In order to make a more direct comparison with these systems than has been done with inorganic-organic hybrid ordered bulk heterojunctions, it would be useful to infiltrate the nanoporous polythiophene with fullerene. Finally, any packing frustration that could occur due to the confined geometry in the pores may not impact device performance as drastically for the case of buckminsterfullerene relative to other small molecule electron acceptors because C_{60} is a symmetric molecule. Despite the advantages listed, the thermal evaporation of C_{60} into a nanoporous polythiophene film could have one serious limitation. For the theoretically ideal scenario of high aspect ratio pores,[24,25] it could prove extremely difficult to achieve complete infiltration of the small molecule to the bottom of the pore. In fact, it is more likely fullerene crystals will heterogeneously nucleate at the edges, and subsequently grow across the top of the pores. This would essentially create a voided bilayer device that would almost certainly perform poorly.

In order to overcome the problem of a non-continuous active layer, an n-type polymer could be infiltrated into high aspect ratio nanopores from the melt. In this scenario, an n-type polymer with a glass transition temperature lower than that of the polythiophene matrix would be deposited on top of the nanoporous film. The polymer would then be heated in vacuum and, if necessary, force would be applied to the top of the polymer melt to aid in pore infiltration. Note that a fair amount of materials engineering would be required to determine the optimal melting times, temperatures,

and necessary forces. However, this would allow for an all-organic ordered bulk heterojunction where the nanopores are completely filled with electron-accepting material. Unfortunately, the fabrication strategy presented may be difficult to achieve in practice. First, there are only a handful of n-type polymers that have adequate electronic properties (see Chapter 3). Additionally, known amorphous polythiophenes have glass transition temperatures just slightly above room temperature. Therefore, any energy used to heat the n-type polymer into the melt most likely would lead to structural failure of the polythiophene matrix. Finally, even if a polythiophene with a glass transition temperature significantly higher than the glass transition temperature of the n-type polymer was found, all-polymer organic photovoltaics generally have much poorer performance than polymer-fullerene devices.[26,27]

In a manner analogous to the blended bulk heterojunction case, perhaps the most promising method for nanopores infiltration relies on the use of soluble fullerene derivatives. Once again, fine tuning the coating conditions would be required to reach an optimum device performance, but many different coating techniques would be available to the researcher. Here, the key hurdle to overcome is finding an orthogonal solvent for the fullerene derivatives. The most commonly used fullerene derivative, [6,6]-phenyl-C_{61}-butyric acid methyl ester (PCBM), is soluble only in good solvents for polythiophenes. On the other hand, water-soluble fullerene derivatives have been developed for biological and medical applications.[28,29] These molecules could be useful for the currently discussed procedure as we have demonstrated previously that nanoporous polythiophene films are stable for at least 72 h in aqueous alkaline solutions.[11] After infiltration of the aqueous fullerene solution, the water could be allowed to slowly evaporate leaving well-coated pore walls. Unfortunately, the optical and electronic properties of water soluble fullerene derivatives have not been explored. Obviously, a better understanding of these materials properties, which are crucial to device performance, must be obtained before water soluble fullerenes are used in devices. If these materials have even a semblance of the charge transport ability of C_{60}

or PCBM, however, this fabrication strategy could prove useful in generating all-organic ordered bulk heterojunction photovoltaic devices.

8.3 Continuing C_{60}-P3HT-C_{60} Synthetic and Microstructural Research

Building from the work presented in Chapter 7, a series of methylfulleropyrrolidine-poly(3-hexylthiophene)-methylfulleropyrrolidine (C_{60}-P3HT-C_{60}) polymers were synthesized with varying P3HT molecular weights. The same reaction pathway presented earlier was used here, which resulted in ^{1}H NMR spectra that were nearly identical to those presented in Figure 7.3.[30] Figure 8.2a shows the size exclusion chromatography (SEC) traces of the polymers with chloroform at 35 °C as the mobile phase. As expected, the elution time is shifted to lower values as the ^{1}H NMR determined average number of repeat units ($\overline{N}$) is increased from $\overline{N} = 10$ to $\overline{N} = 141$.

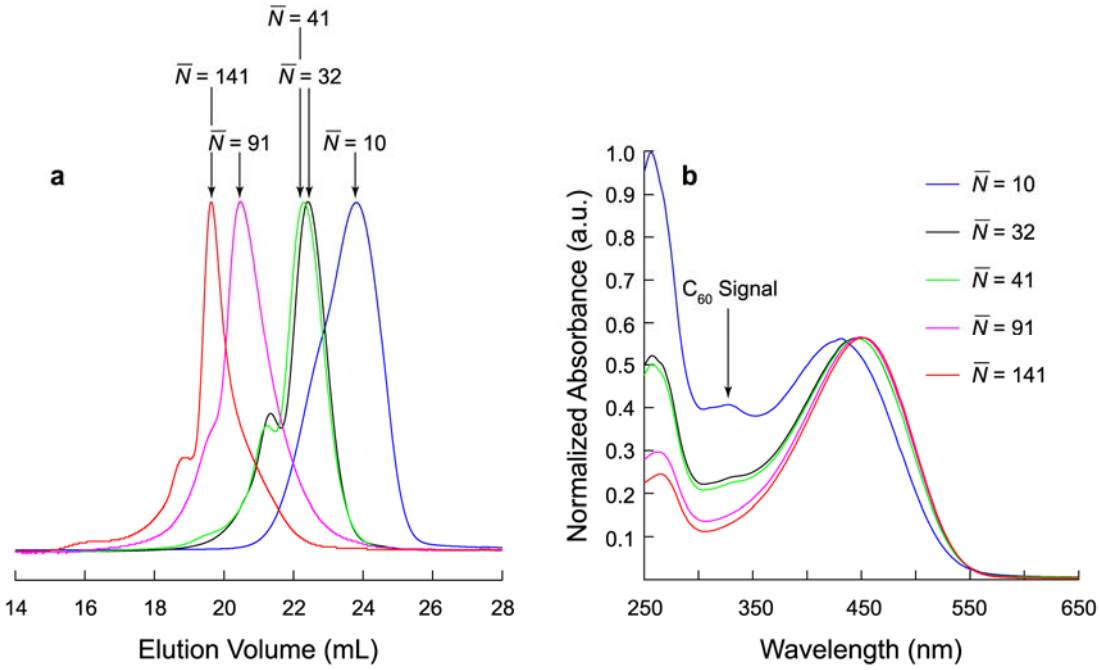

Figure 8.2. (a) SEC chromatograms of the series of newly synthesized C_{60}-P3HT-C_{60} polymers with varying average numbers of P3HT repeat units ($\overline{N}$) with chloroform as the eluting solvent at 35 °C. Traces were obtained using a UV-Vis detector monitoring the signal at λ = 400 nm. (b) Online UV-Vis spectra for the C_{60}-P3HT-C_{60} polymers in chloroform taken at the elution volume at the maximum signal of each of the SEC traces. A local maximum in C_{60} absorbance (see Chapter 7) is marked at $\lambda \approx 330$ nm.

Note that the reaction conditions of the fullerene addition reaction were modified slightly from those used in Chapter 7. The polymer concentration for the reaction was diluted by ~10-fold. This procedural change eliminated the large amount of coupling observed in the C_{60}-P3HT-C_{60} polymer of Chapter 7. The high molecular weight shoulders of the polymers shown in Figure 8.2a were also present in the chromatograms of the homopolymer precursors. In fact, high molecular weight shoulders have been commonly observed in the synthesis of P3HT and have been attributed to coupling of the growing polythiophene chains during quenching of the polymerization.[31]

The ultraviolet-visible (UV-Vis) light absorbance spectra shown in Figure 8.2b were recorded during the elution of the C_{60}-P3HT-C_{60} through the SEC columns. The recorded spectra shown were for the elution volume with the maximum detector signal of each chromatogram. Qualitatively, the spectra of all of the polymers appeared similar except for the C_{60}-P3HT-C_{60} polymer with ten average repeat units. The longer wavelength maximum was blue shifted with λ_{max} = 432 nm while the other polymers have λ_{max} = 451 nm. This was consistent with previous reports of the absorption spectra of small and large molecular weight polythiophenes.[32] Also note that the fullerene signal at $\lambda \approx 330$ nm becomes less prevalent as the molecular weight of the P3HT was increased. Because C_{60} was only present on the end groups of the P3HT chains, the relative amount of fullerene present in the C_{60}-P3HT-C_{60} polymers decreased as the average polymer chain length is increased.[30] This series of internal electron acceptor-donor-acceptor polymers should be useful in applications ranging from the basic science of charge transfer (*e.g.* ultrafast spectroscopy of isolated polymer chains in solution)[33,34] to applied device physics (*e.g.* C_{60}-P3HT-C_{60} thin films for ambipolar organic transistors and photovoltaics).[35-37]

Preliminary experiments that study the morphologies of neat and blended (with PCBM) C_{60}-P3HT-C_{60} polymer thin films have already begun for the polymer series with 10 average repeat units. Note that a C_{60}-P3HT-C_{60} polymer with 10 repeat units on average was composed of 48 wt% fullerene and 52 wt% P3HT. Figure 8.3 shows the tapping mode AFM phase images of two different thin films that were spun-coat from a

2 mg of solid per 1 mL of toluene solution onto silicon dioxide substrates at a rotation rate of 1000 rpm for 1 min. Figure 8.3a shows the neat thin film of proton-terminated poly(3-hexylthiophene) (H-P3HT-H) while Figure 8.3b shows a film that is 50 wt% H-P3HT-H and 50 wt% PCBM.

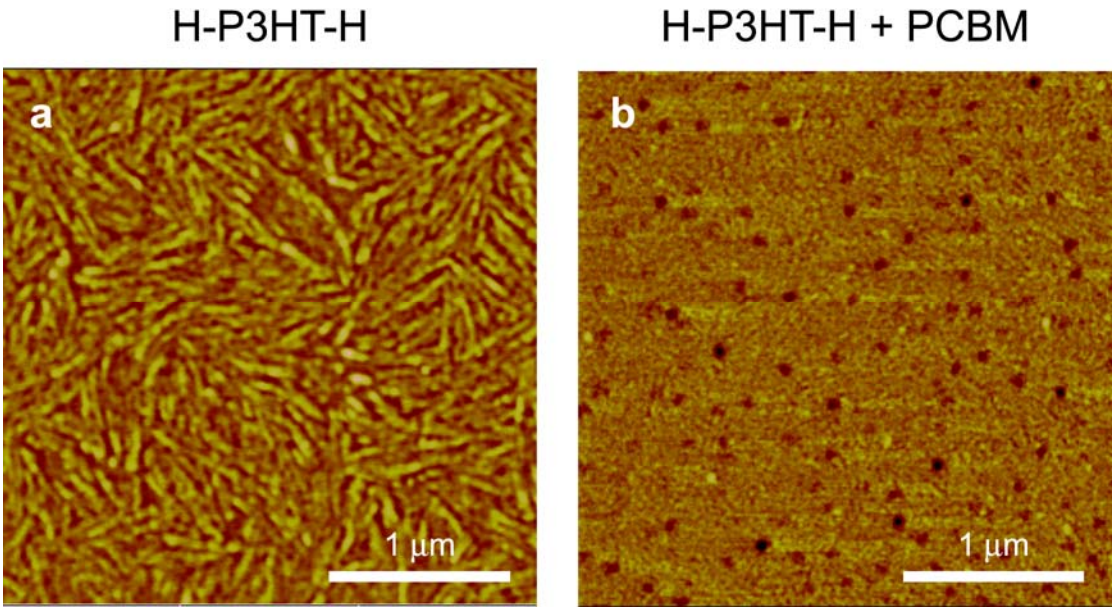

Figure 8.3. Tapping mode AFM thin film phase images of (a) neat H-P3HT-H and (b) H-P3HT-H + PCBM. The films were spun coat from 2 mg of solid in 1 mL of toluene solutions onto silicon dioxide substrates at a rotation rate of 1000 rpm for 1 min. The H-P3HT-H + PCBM film is 50 wt% H-P3HT-H and 50 wt% PCBM.

The neat H-P3HT-H film showed the commonly observed semicrystalline nanofibril structure with the long direction of most lamellae spanning greater than 100 nm.[38-40] Upon addition of 50 wt% PCBM, the thin film morphology drastically changes with the lamellar structure completely broken. Spherical domains of a second phase are formed. In compositionally similar mixtures, formation of these domains previously has been attributed to nucleation of the PCBM phase that precipitated from the fullerene-polythiophene solid solution.[41,42]

Figure 8.4 shows the analogous thin film images for the C_{60}-P3HT-C_{60} polymer with 10 average repeat units. Also spun-coat from a 2 mg of solid per 1 mL of toluene

solution onto silicon dioxide substrates at a rotation rate of 1000 rpm for 1 min, these films demonstrated strikingly different behavior than the films of Figure 8.3.

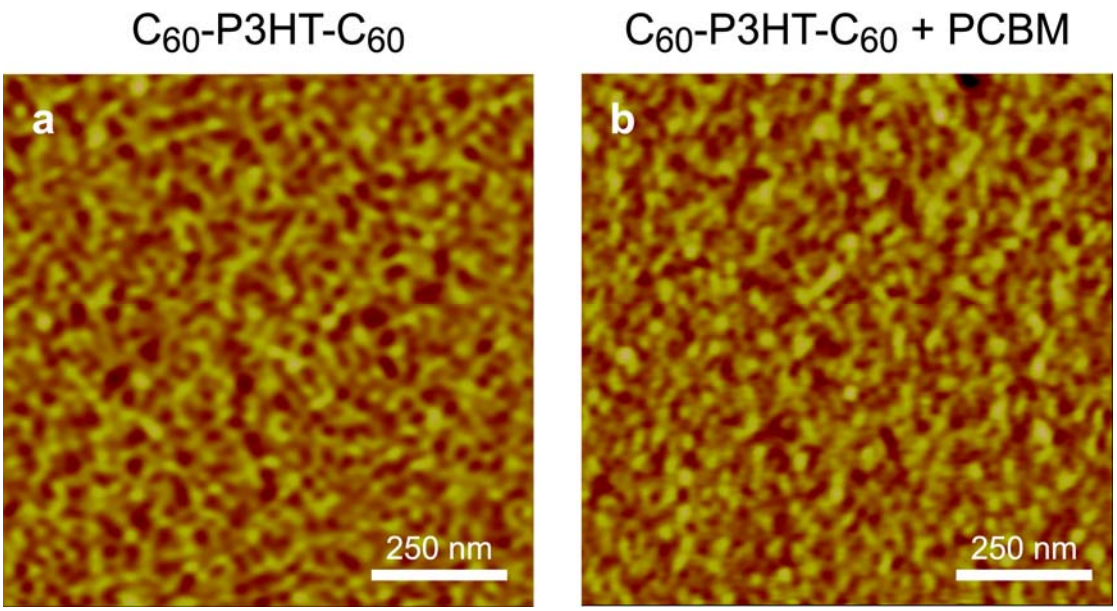

Figure 8.4. Tapping mode AFM thin film phase images of (a) neat C_{60}-P3HT-C_{60} and (b) C_{60}-P3HT-C_{60} + PCBM. The films were spun coat from 2 mg of solid in 1 mL of toluene solutions onto silicon dioxide substrates at a rotation rate of 1000 rpm for 1 min. The C_{60}-P3HT-C_{60} + PCBM film is 50 wt% C_{60}-P3HT-C_{60} and 50 wt% PCBM. Note that the magnifications of the images in this figure were 3X greater than the magnifications of the images shown in Figure 8.3.

The most obvious discrepancy between the H-P3HT-H films and the C_{60}-P3HT-C_{60} films was that the micron-scale phase separation of the former was not observed in latter. In order to discern any phase separation, a significantly higher magnification was used for the C_{60}-P3HT-C_{60} and C_{60}-P3HT-C_{60} + PCBM films (note the difference in scale bars between Figures 8.3 and 8.4). The lamellar structure observed in the semicrystalline H-P3HT-H film was not observed in the C_{60}-P3HT-C_{60} film. Unlike the higher molecular weight C_{60}-P3HT-C_{60} discussed in Chapter 7, the relatively low molecular weight polymer may have been prevented from crystallizing due to the fullerene end groups. More detailed x-ray scattering data would be required to confirm this hypothesis. Nevertheless, it was promising that the phase separation observed in the

neat C_{60}-P3HT-C_{60} film was of the same scale as the C_{60}-P3HT-C_{60} + PCBM film. Also noteworthy was the fact that both films microphase separated into domains with sizes comparable to that of the exciton diffusion length. This suggested that this low molecular weight C_{60}-P3HT-C_{60} polymer may be useful as a component (either neat or in a mixture with PCBM) in organic photovoltaic devices.

8.4 C_{60}-P3HT-C_{60} Compatibilizers in Bulk Heterojunction OPVs[†]

The efficiencies of the highest performing bulk heterojunction solar cells decrease with exposure to heat and light.[43,44] This phenomenon has been attributed to the fact that these cells are fabricated with a kinetically trapped morphology which changes as thermal and radiative energy is introduced to the thin film. As such, researchers have begun to use additives to stabilize the polymer-fullerene microstructures of newly minted OPV devices, and have been met with some improvement in device lifetimes.[43-45] Block copolymers have been commonly employed as compatibilizers to prevent the macrophase separation of polymer blends, and to promote the formation of nano and microstructured materials.[46,47] With this in mind, the C_{60}-P3HT-C_{60} polymer that was synthesized in Chapter 7 was used as a compatibilizer in polythiophene-fullerene bulk heterojunction organic photovoltaic devices.

The device fabrication procedure was similar to that used by Li et al. (Figure 8.5).[48] Indium-doped tin oxide (ITO) coated glass substrates (sheet resistance 8–12 ohm/sq) were sonicated sequentially in acetone, chloroform, and isopropanol for 10 min, and then dried with compressed nitrogen. The substrates were then exposed to a UV-ozone treatment for 5 min. Immediately following this procedure, an aqueous poly(ethylene dioxythiophene) doped with poly(styrene sulfonate) (PEDOT:PSS) solution was spun-coat onto the ITO substrates (thickness ca. 25 nm). The devices were transferred to an inert atmosphere glove box and baked for 10 min at 110 °C to remove any residual water. Solutions containing 30 mg of solid per 1 mL of 1,2-dichlorobenzene had been stirring overnight at 65 °C and contained three components in

[†] We thank Derek M. Stevens for testing the organic photovoltaic devices discussed in this section.

various weight ratios. The three components were: 1) high molecular weight ($M_n \approx 55$ kg/mol as quoted from the manufacturer) P3HT purchased from Rieke Metals, 2) PCBM, and 3) C_{60}-P3HT-C_{60} ($M_n \approx 8.2$ kg/mol, $\overline{N} = 40$, see Chapter 7). The amount of compatibilizer (C_{60}-P3HT-C_{60}) added was varied to gauge whether addition of this component improved device stability. However, the total weight fractions of P3HT (with mass from the Rieke P3HT and C_{60}-P3HT-C_{60}) and fullerene (with mass from the PCBM and C_{60}-P3HT-C_{60}) were kept at a 1:1 ratio. These solutions were passed through a 0.45 μm syringe filter and spun-coat onto the PEDOT:PSS coated substrates at a rotation rate of 600 rpm for 1 min. The wet films were removed from the spin-coater and allowed to finish drying in covered Petri dishes (~1 hr). Upon drying, the films were transferred to an evaporator and the aluminum cathodes (~80–100 nm thick) were evaporated onto the film at a deposition rate of ~0.35 nm/s.

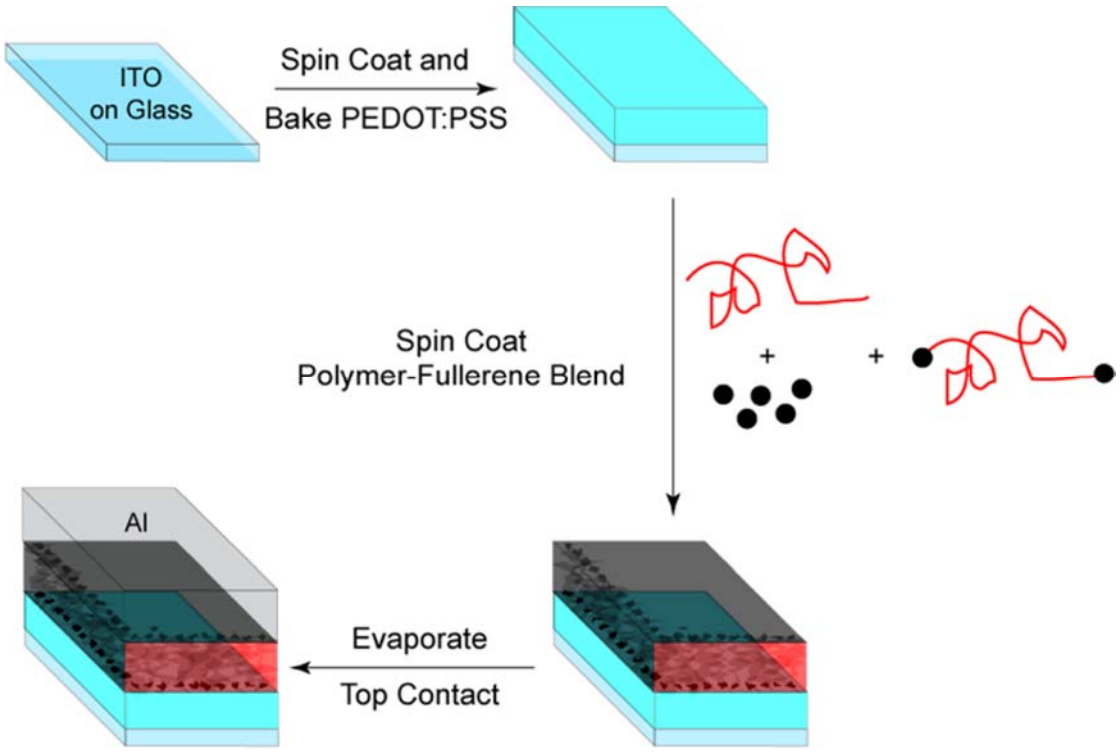

Figure 8.5. Illustration of blended bulk heterojunction device fabrication strategy. The red line symbolizes the high molecular weight P3HT purchased from Rieke Metals, and the black dots represent PCBM. The red line with black dot end points symbolizes the C_{60}-P3HT-C_{60} polymer that is added in varying quantities to the bulk heterojunction mixture.

Note the x-axis of future figures refers to the weight percentage of C_{60}-P3HT-C_{60} present in the devices. These values reflect the amount of the p-type material that is composed of the compatibilizer. For example, a 25 wt% C_{60}-P3HT-C_{60} solution would contain 3.75 mg of C_{60}-P3HT-C_{60}, 11.25 mg of Rieke P3HT, and 14.30 mg of PCBM with the reminder of the fullerene (0.70 mg present in the C_{60}-P3HT-C_{60}). Device testing used a similar experimental design as previously reported.[49] Patterning of the ITO anodes and aluminum cathodes allowed for the fabrication of 6 devices with active areas of 9 mm^2 per ~1 in^2 substrate. The illumination source for testing was a 150 W Xe arc lamp with an AM 1.5G filter. A series of neutral density filters modulated the incident light intensity which was measured using a multifunctional optical meter and

broadband thermopile detector. Reported data are average values over typically six devices, measured in air.

The performance parameters for the unannealed (as-spun) devices as a function of the amount of compatibilizer in the film are shown in Figure 8.6. There is a dramatic decrease in short-circuit current (J_{sc}) upon the addition of compatibilizer. In fact, the addition of less than 10 wt% C_{60}-P3HT-C_{60} nearly halved J_{sc}, and this value continued to decrease as more C_{60}-P3HT-C_{60} was added to the thin film composition (Figure 8.6a). On the other hand, the open-circuit voltage (V_{oc}) of the devices remains approximately constant ($V_{oc} \approx 0.4$ V) for C_{60}-P3HT-C_{60} loadings up to 55 wt%. The fill factor (*FF*) of the devices also initially decreased with increased C_{60}-P3HT-C_{60} loading before leveling at $FF \approx 20\%$ for devices composed of 12–55 wt% C_{60}-P3HT-C_{60}. Multiplication of these three parameters and division by the input illumination power (see Chapter 3) allowed the final device power conversion efficiencies (η) to be calculated. Because V_{oc} and *FF* were approximately constant, the efficiency values followed the trend of the short-circuit current density and decreased with increasing amounts C_{60}-P3HT-C_{60}. We note that even the performance of the device devoid of C_{60}-P3HT-C_{60} was substantially lower than previously reported,[21,22] but we were unable to completely justify this result. However, the more general outcome of decreasing short-circuit current with increasing C_{60}-P3HT-C_{60} loading suggested that the compatibilizer adversely affected charge transport in the devices. This may have been due to the small molecular weight of the C_{60}-P3HT-C_{60} polymer used in these blends as it has been shown previously that polythiophene-fullerene bulk heterojunctions composed of higher molecular weight P3HT have better device performance.[50] However, the charge transport properties of neat compatibilizer must be explored to truly understand any effects related to the internal electron donor-acceptor nature of the C_{60}-P3HT-C_{60}.

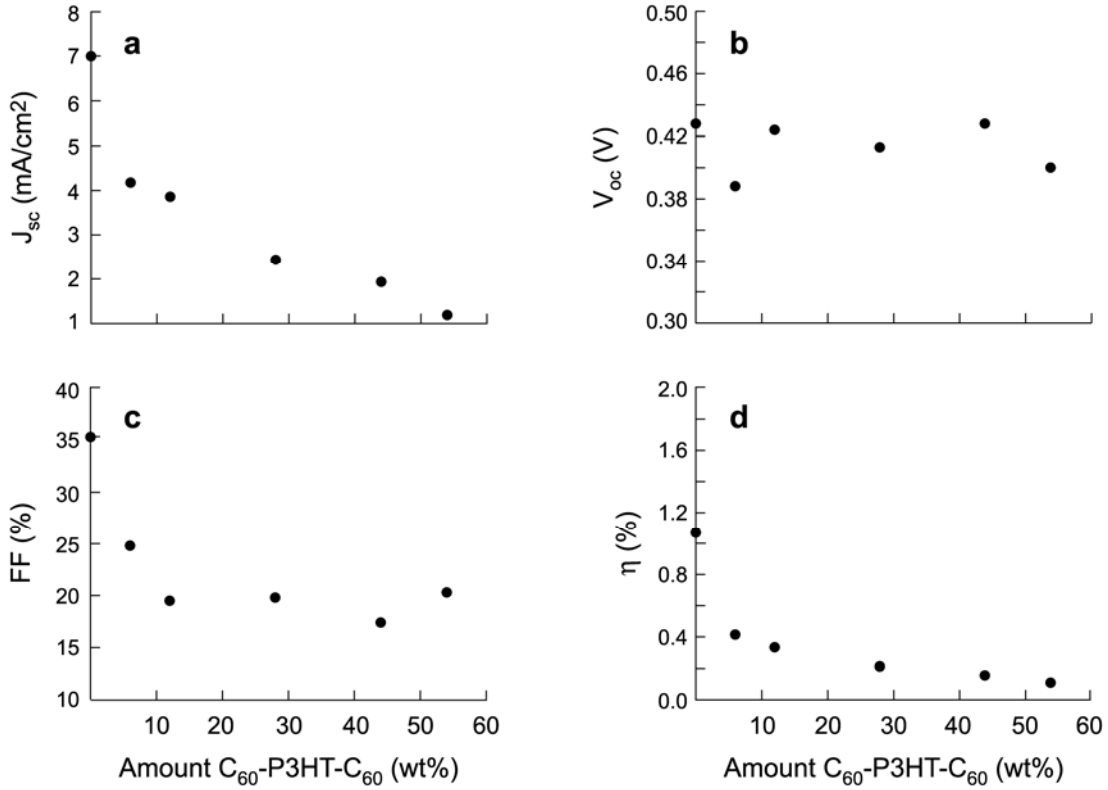

Figure 8.6. Performance parameters: (a) short-circuit current density (J_{sc}), (b) open-circuit voltage (V_{oc}), (c) fill factor (*FF*), and (d) power conversion efficiency (η) for the unannealed (as-spun) devices as a function of the weight fraction of C_{60}-P3HT-C_{60} added. All data were acquired in ambient conditions under a white light power source with a power density of P_{in} = 100 mW/cm^2. Each data point represents the average value for six devices.

After testing, the devices were transferred to an inert atmosphere glove box where they were annealed for 20 min at 150 °C. The devices were then retested, and the performance parameters are shown in Figure 8.7. While the average power conversion efficiency of the 0 wt% C_{60}-P3HT-C_{60} device dropped from 1.1% to 0.8% it still outperformed all of the devices that contained the compatibilizer (Figure 8.7d). The open-circuit voltage of all of the devices increased from $V_{oc} \approx 0.4$ V to $V_{oc} \approx 0.6$ V, but the short-circuit current density and fill factor decreased for active layers containing less than 10 wt% C_{60}-P3HT-C_{60}. This decrease in J_{sc} and *FF* suggested a change in the active layer morphology that resulted in a less than optimal thin film microstructure. On

the other hand, the J_{sc} and *FF* were hardly affected by annealing for active layers that contained greater than 10 wt% C_{60}-P3HT-C_{60}. This may, in fact, indicate that C_{60}-P3HT-C_{60} indeed stabilizes the active layer microstructure during the annealing process. Because the devices were tested in ambient conditions, however, air exposure effects may have also played a role in the device performance change that we could not decouple from the annealing effect.

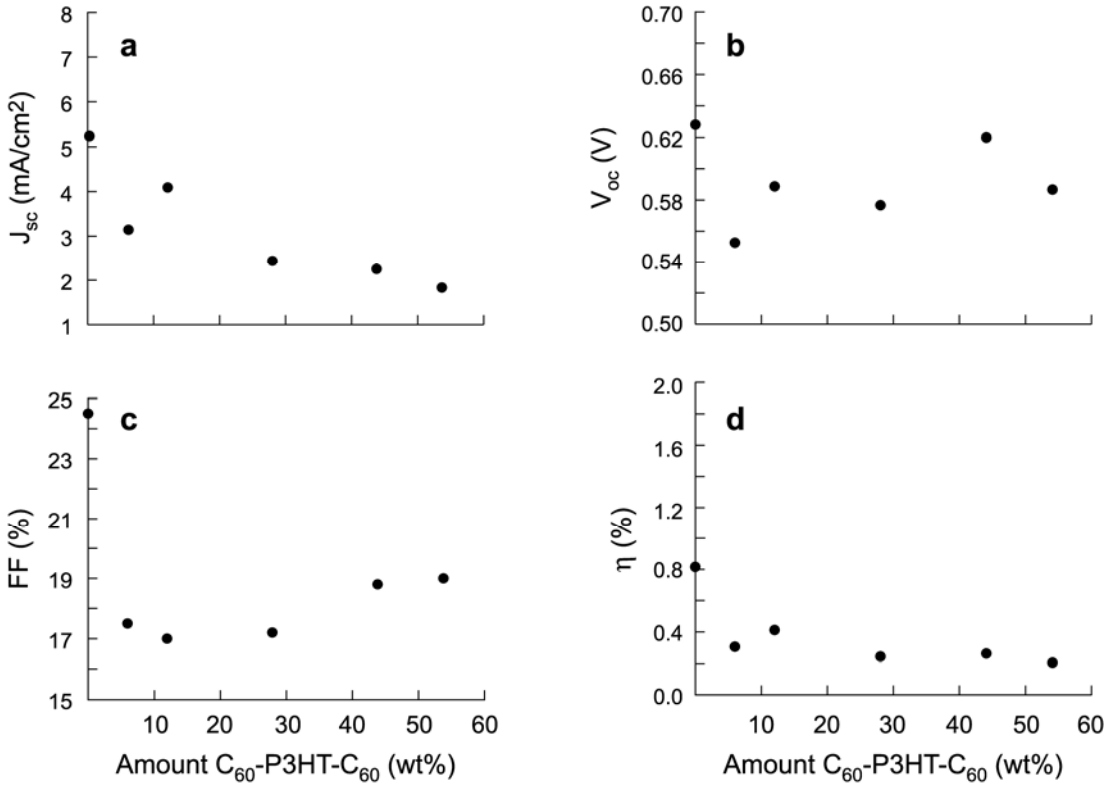

Figure 8.7. Performance parameters: (a) short-circuit current density (J_{sc}), (b) open-circuit voltage (V_{oc}), (c) fill factor (*FF*), and (d) power conversion efficiency (η) as a function of the weight fraction of C_{60}-P3HT-C_{60} added for the devices after annealing in an inert atmosphere glove box for 20 min at 150 °C. All data were acquired in ambient conditions under a white light power source with a power density of P_{in} = 100 mW/cm^2. Each data point represents the average value for six devices.

The devices were returned to the inert atmosphere glove box, and annealed for another 7.67 h (8 h total) at 150 °C. Figure 8.8 shows the normalized power conversion efficiencies (PCEs) of the devices as a function of annealing time. All device

efficiencies were normalized by the power conversion efficiency for the as-spun film (*i.e.*, the data points in Figure 8.6d). Here, it was observed that for devices with active layers that contained less than 10 wt% C_{60}-P3HT-C_{60} the device performance decreased with short and long annealing times. On the other hand, devices that contained 12 and 28 wt% C_{60}-P3HT-C_{60} achieved higher power conversion efficiencies with a short annealing time, and then returned to approximately the same performance, relative to the unannealed devices, for the longer annealing time. Devices that contained 44 wt% and 54 wt% loadings of C_{60}-P3HT-C_{60} greatly improved their relative performance levels for short annealing times. While device performance fell after 8 h of annealing, the normalized PCE was still greater than 1.0. As with other compatibilizers,[45] these data indicated that the addition of C_{60}-P3HT-C_{60} did improve the long-term stability of the polymer-fullerene solar cells. However, more experiments are required in order to develop C_{60}-P3HT-C_{60} with better electronic properties. The obvious first step would be to use a higher molecular weight C_{60}-P3HT-C_{60} synthesized in the previous section to enhance hole transport in the compatibilizers.

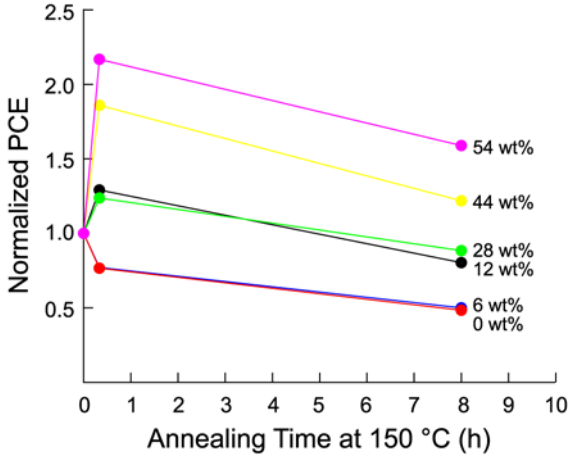

Figure 8.8. Normalized power conversion efficiencies (PCEs) of blended bulk heterojunction devices as a function of annealing time at 150 °C for various ternary blend compositions. The percentages to the right of the terminal data points indicate the weight percentage of C_{60}-P3HT-C_{60} compatibilizer present in the active layer. Note that PCE values were normalized to the initial power conversion efficiency for the as-spun active layer device (*i.e.* annealing time = 0 h). The lines serve as guides to the eye.

Hopefully, the preliminary results shown above will motivate the future experiments suggested in this chapter. By expanding on this work, a better understanding of how molecular design affects the active layer morphology and device performance may be realized. The major theme of this thesis has been that iterative, rational design of semiconducting polymers can be achieved, and that this methodology could provide a means to systematically study how the nanoscopic molecular properties of polymers influence macroscopic organic photovoltaic device parameters. Hopefully, the results presented here and in earlier chapters offer new students a trail on which to start related future endeavors.

8.5 References

[1] Olsen, B. D.; Segalman, R. A. *Macromolecules* **2005**, *38*, 10127–10137.

[2] Olsen, B. D.; Segalman, R. A. *Macromolecules* **2006**, *39*, 7078–7083.

[3] Olsen, B. D.; Segalman, R. A. *Macromolecules* **2007**, *40*, 6922–6929.

[4] Olsen, B. D.; Shah, M.; Ganesan, V.; Segalman, R. A. *Macromolecules* **2008**, *41*, 6809–6817.

[5] Olsen, B. D.; Segalman, R. A. *Mater. Sci. Eng., R* **2008**, *62*, 37–66.

[6] Liu, J.; Sheina, E.; Kowalewski, T.; McCullough, R. D. *Angew. Chem., Int. Ed.* **2002**, *41*, 329–332.

[7] Dai, C.; Yen, W.; Lee, Y.; Ho, C.; Su, W. *J. Am. Chem. Soc.* **2007**, *129*, 11036–11038.

[8] Iovu, M. C.; Craley, R.; Jeffries-EL, M.; Krankowski, A. B.; Zhang, R.; Kowalewski, T.; McCullough, R. D. *Macromolecules* **2007**, *40*, 4733–4735.

[9] Sommer, M.; Lang, A. S.; Thelakkat, M. *Angew. Chem., Int. Ed.* **2008**, *47*, 7901–7904.

[10] Richard, F.; Brochon, C.; Leclerc, N.; Eckhardt, D.; Heiser, T.; Hadziioannou, G. *Macromol. Rapid Commun.* **2008**, *29*, 885–891.

[11] Boudouris, B. W.; Frisbie, C. D.; Hillmyer, M. A. *Macromolecules* **2008**, *41*, 67–75.

[12] Higashihara, T.; Ohshimizu, K.; Hirao, A.; Ueda, M. *Macromolecules* **2008**, *41*, 9505–9507.

[13] Urien, M.; Erothu, H.; Cloutet, E.; Hiorns, R. C.; Vignau, L.; Cramail, H. *Macromolecules* **2008**, *41*, 7033–7040.

[14] Higashihara, T.; Ueda, M. *React. Funct. Polym.* **2009**, *69*, 457–462.

[15] Zhang, Q.; Cirpan, A.; Russell, T. P.; Emrick, T. *Macromolecules* **2009**, *42*, 1079–1082.

[16] Loewe, R. S.; Khersonsky, S. M.; McCullough, R. D. *Adv. Mater.* **1999**, *11*, 250–253.

[17] Ohshimizu, K.; Ueda, M. *Macromolecules* **2008**, *41*, 5289–5294.

[18] Sivula, K.; Luscombe, C. K.; Thompson, B. C. Fréchet, J. M. J. *J. Am. Chem. Soc.* **2006**, *128*, 13988–13989.

[19] Tang, C. W. *Appl. Phys. Lett.* **1986**, *48*, 183–185.

[20] Peumans, P.; Yakimov, A.; Forrest, S. R. *J. Appl. Phys.* **2003**, *93*, 3693–3723.

[21] Li, G.; Shrotriya, V.; Huang, J.; Yao, Y.; Moriarty, T.; Emery, K.; Yang, Y. *Nat. Mater.* **2005**, *4*, 864–868.

[22] Ma, W.; Yang, C.; Gong, X.; Lee, K.; Heeger, A. J. *Adv. Funct. Mater.* **2005**, *15*, 1617–1622.

[23] Park, S. H.; Roy, A.; Beaupré, S.; Cho, S.; Coates, N.; Moon, J. S.; Moses, D.; Leclerc, M.; Lee, K.; Heeger, A. J. *Nat. Photonics* **2009**, *3*, 297–303.

[24] Watkins, P. K.; Walker, A. B.; Verschoor, G. L. B. *Nano Lett.* **2005**, *5*, 1814–1818.

[25] Yang, F.; Forrest, S. R. *ACS Nano* **2008**, *2*, 1022–1032.

[26] Halls, J. J. M.; Walsh, C. A.; Greenham, N. C.; Marseglia, E. A.; Friend, R. H.; Moratti, S. C.; Holmes, A. B. *Nature* **1995**, *376*, 498–500.

[27] McNeill, C. R.; Abrusci, A.; Zaumseil, J.; Wilson, R.; McKiernan, M. J.; Burroughes, J. H.; Halls, J. J. M.; Greenham, N. C.; Friend, R. H. *Appl. Phys. Lett.* **2007**, *90*, 193506.

[28] Tokuyama, H.; Yamago, S.; Nakamura, E.; Shiraki, T.; Sugluar, Y. *J. Am. Chem. Soc.* **1993**, *115*, 7918–7919.

[29] Nakamura, E.; Isobe, H. *Acc. Chem. Res.* **2003**, *36*, 807–815.

[30] Boudouris, B. W.; Molins, F.; Blank, D. A.; Frisbie, C. D.; Hillmyer, M. A. *Macromolecules* **2009**, *42*, 4118–4126.

[31] Miyakoshi, R.; Yokoyama, A.; Yokozawa, T. *Macromol. Rapid Commun.* **2004**, *25*, 1663–1666.

[32] Trznadel, M.; Pron, A.; Zagorska, M.; Chrzaszcz, R.; Pielichowski, J. *Macromolecules* **1998**, *31*, 5051–5058.

[33] Wells, N. P.; Boudouris, B. W.; Hillmyer, M. A.; Blank, D. A. *J. Phys. Chem. C* **2007**, *111*, 15404–15414.

[34] Wells, N. P.; Blank, D. A. *Phys. Rev. Lett.* **2008**, *100*, 086403.

[35] Narutaki, M.; Takimiya, K.; Otsubo, T.; Harima, Y.; Zhang, H.; Araki, Y.; Ito, O. *J. Org. Chem.* **2006**, *71*, 1761–1768.

[36] Fernández, G.; Sánchez, L.; Veldman, D.; Wienk, M. M.; Atienza, C.; Guldi, D. M.; Janssen, R. A. J.; Martín, N. *J. Org. Chem.* **2008**, *73*, 3189–3196.

[37] Ouhib, F.; Khoukh, A.; Ledeuil, J-B.; Martinez, H.; Desbrières, J.; Dagron-Lartigau, C. *Macromolecules* **2008**, *41*, 9736–9743.

[38] Liu, J.; Sheina, E.; Kowalewski, T.; McCullough, R. D. *Angew. Chem., Int. Ed.* **2002**, *41*, 329–332.

[39] Zhang, R.; Li, B.; Iovu, M. C.; Jeffries-EL, M.; Sauvé, G.; Cooper, J.; Jia, S.; Tristram-Nagle, S.; Smilgies, D. M.; Lambeth, D. N.; McCullough, R. D.; Kowalewski, T. *J. Am. Chem. Soc.* **2006**, *128*, 3480–3481.

[40] Dai, C.; Yen, W.; Lee, Y.; Ho, C.; Su, W. *J. Am. Chem. Soc.* **2007**, *129*, 11036–11038.

[41] Müller, C.; Ferenczi, T. A. M.; Campoy-Quiles, M.; Frost, J. M.; Bradley, D. D. C.; Smith, P.; Stingelin-Stutzmann, N.; Nelson, J. *Adv. Mater.* **2008**, *20*, 3510–3515.

[42] Kim, J. Y.; Frisbie, C. D. *J. Phys. Chem. C* **2008**, *112*, 17726–17736.

[43] Gunes, S.; Neugebauer, H.; Sariciftci, N. S. *Chem. Rev.* **2007**, *107*, 1324–1338.

[44] Kim, B. J.; Miyamoto, Y.; Ma, B.; Fréchet, J. M. J. *Adv. Mater.* **2009**, *19*, 1–9.

[45] Ball, Z. T.; Sivula, K.; Fréchet, J. M. J. *Macromolecules* **2006**, *39*, 70–72.

[46] Hiemenz, P. C.; Lodge, T. P. *Polymer Chemistry*; CRC Press: Boca Raton, FL, 2007.
[47] Sperling, L. H. *Introduction to Polymer Science, 3rd Ed.*; John Wiley & Sons, Inc.: Hoboken, NJ, 2001.

[48] Li, G.; Shrotriya, V.; Huang, J.; Yao, Y.; Moriarty, T.; Emery, K.; Yang, Y. *Nat. Mater.* **2005**, *4*, 864–868.

[49] Stevens, D. M.; Qin, Y.; Hillmyer, M. A.; Frisbie, C. D. *J. Phys. Chem. C* **2009**, *113*, 11408–11415.

[50] Ma, W.; Kim, J. Y.; Lee, K.; Heeger, A. J. *Macromol. Rapid Commun.* **2007**, *28*, 1776–1780.

Bibliography

Abetz, V.; Simon, P. F. W. *Adv. Polym. Sci.* **2005**, *189*, 125–212.

Ace Glass, Inc. http://www.aceglass.com/ (July 2009), Ace Glass, Inc Homepage.

Adamus, G.; Kowalczuk, M. *Biomacromolecules* **2008**, *9*, 696–703.

Alexander-Katz, A.; Fredrickson, G. H. *Macromolecules* **2007**, *40*, 4075–4087.

Ameri, T.; Dennler, G.; Lungenschmied, C.; Brabec, C. J. *Energ. Environ. Sci.* **2009**, *2*, 347–363.

Anderson, K. S.; Hillmyer, M. A. *Polymer* **2006**, *47*, 2030–2035.

Anthony, J. E.; Brooks, J. S.; Eaton, D. L.; Parkin, S. R. *J. Am. Chem.. Soc.* **2001**, *123*, 9482–9483.

Asakawa, K.; Hiraoka, T.; Hieda, H.; Sakurai, M.; Kamata, Y.; Naito, K. *J. Photopolym. Sci. Tech.* **2002**, *15*, 465–470.

Asakura, S.; Hozumi, A.; Fuwa, A. *J. Vac. Sci. Technol., A* **2005**, *23*, 1137–1140.

Askari, S. H.; Rughooputh, S. D.; Wudl, F.; Heeger, A. J. *Polymer Preprints* **1989**, *30*, 157–160.

Babel, A.; Jenekhe, S. A. *Synth. Met.* **2005**, *148*, 169–173.

Baffreau, J.; Ordronneau, L.; Leroy-Lhez, S.; Hudhomme, P. *J. Org. Chem.* **2008**, *73*, 6142–6147.

Ball, Z. T.; Sivula, K.; Fréchet, J. M. J. *Macromolecules* **2006**, *39*, 70–72.

Ballantyne, A. M.; Chen, L.; Dane, J.; Hammant, T; Braun, F. M.; Heeney, M.; Duffy, W.; McCulloch, I.; Bradley, D. D. C.; Nelson, J. *Adv. Funct. Mater.* **2008**, *18*, 2373–2380.

Ballenweg, S.; Gleiter, R.; Krätschmer, W. *Synth. Met.* **1996**, *77*, 209–212.

Bates, F. S.; Fredrickson, G. H. *Annu. Rev. Phys. Chem.* **1990**, *41*, 525–557.

Bates, F. S.; Schulz, M. F.; Khandpur, A. K.; Förster, S.; Rosedale, J. H. *Faraday Discuss.* **1994**, *98*, 7–18.

Bendejacq, D.; Ponsinet, V.; Joanicot, M.; Loo, Y. L.; Register, R. A. *Macromolecules* **2002**, *35*, 6645–6649.

Bender, J. L.; Corbin, P. S.; Fraser, C. L.; Metcalf, D. H.; Richardson, F. S.; Thomas, E. L.; Urbas, A. M. *J. Am. Chem. Soc.* **2002**, *124*, 8526–8527.

Black, C. T.; Guarini, K. W.; Milkove, K. R.; Baker, S. M.; Russell, T. P.; Tuominen, M. T. *Appl. Phys. Lett.* **2001**, *79*, 409–411.

Boger, T; Heibel, A. K.; Sorensen, C. M. *Ind. Eng. Chem. Res.* **2004**, *43*, 4602–4611.

Bonduelle, C.; Martin-Vaca, B.; Cossio, F. P.; Bourissou, D. *Chem.–Eur. J.* **2008**, *14*, 5304–5312.

Boudouris, B. W.; Kasi, R. M.; Frisbie, C. D.; Hillmyer, M. A. *PMSE Preprints* **2006**, *95*, 103.

Boudouris, B. W.; Frisbie, C. D.; Hillmyer, M. A. *Macromolecules* **2008**, *41*, 67–75.

Boudouris, B. W.; Molins, F.; Blank, D. A.; Frisbie, C. D.; Hillmyer, M. A. *Macromolecules* **2009**, *42*, 4118–4126.

Brabec, C. J.; Cravino, A.; Meissner, D.; Sariciftci, N. S.; Fromherz, T.; Rispens, M. T; Sanchez, L.; Hummelen, J. C. *Adv. Funct. Mater.* **2001**, *11*, 374–380.

Brabec, C. J.; Shaheen, S. E.; Winder, C.; Sariciftci, N. S. *Appl. Phys. Lett.* **2002**, *80*, 1288–1290.

Brabec, C. J.; Hauch, J. A.; Schilinsky, P.; Waldauf, C. *MRS Bull.* **2005**, *30*, 50–52.

Brabec, C. J.; Durrant, J. R. *MRS Bull.* **2008**, *33*, 670–675.

Campoy-Quiles, M.; Ferenczi, T.; Agostinelli, T.; Etchegoin, P. G.; Kim, Y.; Anthopoulos, T. D.; Stavrinou, P. N.; Bradley, D. D. C.; Nelson, J. *Nat. Mater.* **2008**, *7*, 158–164.

Castelletto, V.; Hamley, I. W. *Curr. Opin. Solid State Mater Sci.* **2005**, *8*, 426–438.

Cattin, L.; Dahou, F.; Lare, Y.; Morsli, M.; Tricot, R.; Houari, S.; Mokrani, A.; Jondo, K.; Khelil, A.; Napo, K.; Bernede, J. C. *J. Appl. Phys.* **2009**, *105*, 034507.

Causin, V.; Marega, C.; Marigo, A.; Valentini, L.; Kenny, J. M. *Macromolecules* **2005**, *38*, 409–415.

Chemglass Life Sciences Website. http://www.chemglass.com (July 2009), Chemglass Scientific Apparatus.

Chen, H. Y.; Tang, H. Y.; Lin, C. C. *Macromolecules* **2006**, *39*, 3745–3752.

Chen, J. T.; Thomas, E. L.; Ober, C. K.; Hwang, S. S. *Macromolecules* **1995**, *28*, 1688–1697.

Chen, J. T.; Thomas, E. L.; Ober, C. K.; Mao, G. P. *Science* **1996**, *273* 343–346.

Chen, J. Z.; Zhang, C. X.; Sun, Z. Y.; Zheng, Y. S.; An, L. J. *J. Chem. Phys.* **2006**, *124*, 104907.

Chen, L. C.; Godovsky, D.; Inganäs, O.; Hummelen, J C.; Janssen, R. A. J.; Svensson, M.; Andersson, M. R. *Adv. Mater.* **2000**, *12*, 1367–1370.

Chen, S.; Lee, S. *Polymer* **1995**, *36*, 1719–1723.

Chen, T. A.; Wu, X.; Rieke, R. D. *J. Am. Chem. Soc.* **1992**, *114*, 10087–10088.

Chen, X. L.; Jenekhe, S. A. *Macromolecules* **2000**, *33*, 4610–4612.

Chesterfield, R. J.; McKeen, J. C.; Newman, C. R.; Ewbank, P. C.; da Silva Filho, D. A.; Brédas, J. L.; Miller, L. L.; Mann, K. R.; Frisbie, C. D. *J. Phys. Chem. B* **2004**, *108*, 19281–19292.

Chirvase, D.; Parisi, J.; Hummelen, J. C.; Dyakonov, V. *Nanotechnology* **2004**, *15*, 1317–1323.

Chmura, A. J.; Cousins, D. M.; Davidson, M. G.; Jones, M. D.; Lunn, M. D.; Mahon, M. F. *Dalton Trans.* **2008**, 1437–1443.

Clarke, T. M.; Ballantyne, A. M.; Nelson, J.; Bradley, D. D. C.; Durrant, J. R. *Adv. Funct. Mater.* **2008**, *18*, 4029–4035.

Coakley, K. M.; Liu, Y.; McGehee, M. D.; Frindell, K. L.; Stuckey, G. D. *Adv. Funct. Mater.* **2003**, *13*, 301–306.

Coakley, K. M.; McGehee, M. D. *Appl. Phys. Lett.* **2003**, *83*, 3380–3382.

Coakley, K. M.; Liu, Y.; Goh, C.; McGehee, M. D. *MRS Bull.* **2005**, *30*, 37–40.

Coates, N. E.; Hwang, I. W.; Peet, J.; Bazan, G. C; Moses, D.; Heeger, A. J. *Appl. Phys. Lett.* **2008**, *93*, 072105.

Cochran, E. W.; Garcia-Cervera, C. J.; Fredrickson, G. H. *Macromolecules* **2006**, *39*, 2449–2451.

Connor, E. F.; Nyce, G. W.; Myers, M.; Mock, A.; Hedrick, J. L. *J. Am. Chem. Soc.* **2002**, *124*, 914–915.

Cravino, A. *Polym. Int.* **2007**, *56*, 943–956.

Crossland, E. J. W.; Ludwigs, S.; Hillmyer, M. A.; Steiner, U. *Soft Matter* **2007**, *3*, 94–98.

Crossland, E. J. W.; Nedelcu, M.; Ducati, C.; Ludwigs, S.; Hillmyer, M. A.; Steiner, U.; Snaith, H. J. *Nano Lett.* **2008**, *ACS ASAP*.

Crossland, E. J. W.; Kamperman, M.; Nedelcu, M.; Ducati, C.; Wiesner, U.; Smilgies, D. M.; Toombes, G. E. S.; Hillmyer, M. A.; Ludwigs, S.; Steiner, U.; Snaith, H. J. *Nano Lett.* **2008**, *ACS ASAP*.

Cullity, B. D. *Elements of X-Ray Diffraction, 2nd Ed.*; Addison-Wesley Publishing Company, Inc.: Reading, MA, 1978.

Dai, C.; Yen, W.; Lee, Y.; Ho, C.; Su, W. *J. Am. Chem. Soc.* **2007**, *129*, 11036–11038.

Darling, T. R.; Davis, T. P.; Fryd, M.; Gridnev, A. A.; Haddleton, D. M.; Ittel, S. D.; Matheson, Jr., R. R.; Moad, G.; Rizzardo, E. *J. Polym. Sci., Polym. Poly. Chem.* **2000**, *38*, 1706–1708.

Davey, S. N.; Leigh, D. A.; Moody, A. E.; Tetler, L. W.; Wade, F. A. *J. Chem. Soc., Chem. Commun.* **1994**, 397–398.

de Boer, B.; Stalmach, U.; Nijland, H.; Hadziioannou, G. *Adv. Mater.* **2000**, *12*, 1581–1583.

de Boer, B.; Stalmach, U.; van Hutten, P. F.; Melzer, C.; Krasnikov, V. V.; Hadziioannou, G. *Polymer* **2001**, *42*, 9097–9109.

de Boer, R. W. I.; Gershenson, M. E.; Morpurgo, A. F.; Podzorov, V. *Phys. Status Solidi A* **2004**, *201*, 1302–1331.

de Cuendias, A.; Le Hellaye, M.; Lecommandoux, S.; Cloutet, E.; Cramail, H. *J. Mater. Chem.* **2005**, *15*, 3264–3267.

de Genes, P. G. *Scaling Concepts in Polymer Physics*; Cornell University Press: Ithaca, NY, 1979.

de Koning, G. J. M.; Lemstra, P. J. *Polymer* **1993**, *34*, 4089–4094.

Dennler, G.; Scharber, M. C.; Brabec, C. J. *Adv. Mater.* **2009**, *21*, 1323–1338.

Dhanabalan, A.; van Duren, J. K. J.; van Hal, P. A.; van Dongen, J. L. J.; Janssen, R. A. J. *Adv. Funct. Mater.* **2001**, *11*, 255–262.

Dimitrakopoulos, C. D.; Malenfant, P. R. L. *Adv. Mater.* **2002**, *14*, 99–117.

Doi, M.; Edwards, S. F. *The Theory of Polymer Dynamics*; Oxford University Press: New York, NY, 1986.

Dove, A. P. *Chem. Commun.* **2008**, *48*, 6446–6470.

du Boullay, O. T.; Marchal, E.; Martin-Vaca, B.; Cossio, F. P.; Bourissou, D. *J. Am. Chem. Soc.* **2006** *128*, 16442–16443.

Dubois, Ph.; Jacobs, C.; Jérôme, R.; Teyssié, Ph. *Macromolecules* **1991**, *24*, 2266–2270.

El-Sayed, I.; Hazell, R. G.; Madsen, J. Ø.; Norrby, P-O.; Senning, A. *Eur. J. Org. Chem.* **2003**, *5*, 813–815.

Erb, T.; Zhokhavets, U.; Gobsch, G.; Raleva, S.; Stühn, B.; Schilinsky, P.; Waldauf, C.; Brabec, C. J. *Adv. Funct. Mater.* **2005**, *15*, 1193–1196.

Fan, Y.; Chen, G.; Tanaka, J.; Tateishi, T. *Biomacromolecules* **2005**, *6*, 3051–3056.

Fazio, M. A.; Lee, P. O.; Shuster, D. I. *Org. Lett.* **2008**, *10*, 4979–4982.

Fernández, G.; Sánchez, L.; Veldman, D.; Wienk, M. M.; Atienza, C.; Guldi, D. M.; Janssen, R. A. J.; Martín, N. *J. Org. Chem.* **2008**, *73*, 3189–3196.

Flory, P. J. *J. Chem. Phys.* **1942**, *10*, 51–61.

Flory, P.J. *Principles of Polymer Chemistry*; Cornell University Press: Ithaca, NY, 1953.

Floudas, G.; Vazaiou, B.; Schipper, F.; Ulrich, R.; Wiesner, U.; Iatrou, H.; Hadjichristidis, N. *Macromolecules* **2001**, *34*, 2947–2957.

Forrest, S. R. *MRS Bull.* **2005**, *30*, 28–32.

François, B.; Widawski, G.; Rawiso, M.; Cesar, B. *Synth. Met.* **1995**, *69*, 463–466.

Frohne, H.; Shaheen, S. E.; Brabec, C. J.; Müller, D. C.; Sariciftci, N. S.; Meerholz, K. *Chem. Phys. Chem.* **2002**, *3*, 795–799.

Fujitsuka, M.; Ito, O.; Yamashiro, T.; Aso, Y.; Otsubo, T. *J. Phys. Chem. A* **2000**, *104*, 4876–4881.

Fujitsuka, M.; Matsumoto, K.; Ito, O.; Yamashiro, T.; Aso, Y.; Otsubo, T.; *Res. Chem. Intermed.* **2001**, *27*, 73–88.

Gadisa, A.; Svensson, M.; Andersson, M. R.; Inganäs, O. *Appl. Phys. Lett.* **2004**, *84*, 1609–1611.

Granström, M.; Petritsch, K.; Arias, A. C.; Lux, A.; Andersson, M. R.; Friend, R. H. *Nature* **1998**, *395*, 257–260.

Greenham, N. C.; Moratti, S. C.; Bradley, D. D. C.; Friend, R. H.; Holmes, A. B. *Nature* **1993**, *365*, 628–630.

Gregg, B. A.; Fox, M. A.; Bard, A. J. *J. Phys. Chem.* **1990**, *94*, 1586–1598.

Gregg, B. A.; Kim, Y. I. *J. Phys. Chem.* **1994**, *98*, 2412–2417.

Gregg, B. A.; Sprague, J.; Peterson, M. *J. Phys. Chem. B* **1997**, *101*, 5362–5369.

Gregg, B. A.; Hanna, M. C. *J. Appl. Phys.* **2003**, *93*, 3605–3614.

Gregg, B. A. *MRS Bull.* **2005**, *30*, 20–22.

Guarini, K. W.; Black, C. T.; Milkove, K. R.; Sandstrom, R. L. *J. Vac. Sci. Technol. B* **2001**, *19*, 2784–2788.

Günes, S.; Neugebauer, H.; Sariciftci, N. S. *Chem. Rev.* **2007**, *107*, 1324–1338.

Guo, S.; Rzayev, J.; Bailey, T. S.; Zalusky, A. S.; Olayo-Valles, R.; Hillmyer, M. A. *Chem. Mater.* **2006**, *18*, 1719–1721.

Gurau, M. C.; Delongchamp, D. M.; Vogel, B. M.; Lin, E. K.; Fischer, D. A.; Sambasivan, S.; Richter, L. J. *Langmuir* **2007**, *23*, 834–842.

Ha, J.; Hillmyer, M. A.; Ward, M. D. *J. Phys. Chem. B* **2005**, *109*, 1392–1399.

Hadjichristidis, N.; Pispas, S.; Floudas, G. A. *Block Copolymers: Synhtetic Strategies, Physical Properties, and Applications*; John Wiley & Sons, Inc.: Hoboken, NJ, 2003.

Hadziioannou, G. *MRS Bull.* **2002**, *27*, 456–460.

Hagen, K.; Ed. *Organic Electronics: Materials, Manufacturing, and Applications*; Wiley-VCH Verlag GmbH & Co. KGaA: Weinheim, Germany, 2006.

Hajduk, D. A.; Takenouchi, H.; Hillmyer, M. A.; Bates, F. S.; Vigild, M. E.; Almdal, K. *Macromolecules* **1997**, *30*, 3788–3795.

Halls, J. J. M.; Walsh, C. A.; Greenham, N. C.; Marseglia, E. A.; Friend, R. H.; Moratti, S. C.; Holmes, A. B. *Nature* **1995**, *376*, 498–500.

Halperin, A. *Macromolecules* **1990**, *23*, 2724–2731.

Hamilton, B. D.; Weissbuch, I.; Lahav, M.; Hillmyer, M. A.; Ward, M. D. *J. Am. Chem. Soc.* **2009**, *131*, 2588–2596.

Hampton, M. J.; Williams, S. S.; Zhou, Z.; Nunes, J.; Ko, D. H.; Templeton, J. L.; Samulski, E. T.; DeSimone, J. M. *Adv. Mater.* **2008**, *20*, 2667–2673.

Harrison, C.; Park, M.; Chaikin, P. M.; Register, R. A.; Adamson, D. H. *J. Vac. Sci. Technol. B* **1998**, *16*, 544–552.

Hasegawa, H.; Tanaka, H.; Yamasaki, K.; Hashiomto, T. *Macromolecules* **1987**, *20*, 1651–1662.

Heiny, P. A.; Fischer, J. E.; McGhie, A. R.; Romanow, W. J.; Denenstein, A. M.; McCauley, Jr., J. P.; Smith, III, A. B.; Cox, D. E. *Phys. Rev. Lett.* **1991**, *66*, 2911–2914.

Herman, D. S.; Kinning, D. J.; Thomas, E. L.; Fetters, L. J. *Macromolecules* **1987**, *20*, 2940–2942.

Hiemenz, P. C.; Lodge, T. P. *Polymer Chemistry*; CRC Press: Boca Raton, FL, 2007.

Higashihara, T.; Ohshimizu, K.; Hirao, A.; Ueda, M. *Macromolecules* **2008**, *41*, 9505–9507.

Higashihara, T.; Ueda, M. *React. Funct. Polym.* **2009**, *69*, 457–462.

Higashimura, T.; Aoshima, S.; Sawamoto, M. *Makromol. Chem. Macromol. Symp.* **1998**, *14*, 457–471.

Hillmyer, M. A. *Adv. Polym. Sci.* **2005**, *190*, 137–181.

Hillmyer, M. A. *J. Polym. Sci. Pol. Phys.* **2007**, *45*, 3249–3251.

Ho, C. C.; Lee, Y. H.; Dai, C. A.; Segalman, R. A.; Su, W. F. *Macromolecules* **2009**, *42*, 4208–4219.

Holyst, R.; Schick, M. *J. Chem. Phys.* **1992**, *96*, 730–739.

Horowitz, G.; Hajlaoui, M. E.; Hajlaoui, R. *J. Appl. Phys.* **2000**, *87*, 4456–4463.

Hotta, S.; Rughooputh, S. D. D. V.; Heeger, A. J.; Wudl, F. *Macromolecules* **1987**, *20*, 212–215.

Hotta, S.; Soga, M.; Sonoda, N. *Synth. Met.* **1988**, *26*, 267–279.

Hsieh, H. L.; Quirk, R. P. *Anionic Polymerization, Principles and Practical Applications*; Marcel Dekker, Inc.: New York, NY, 1996.

Hsueh, M. L.; Huang, B. H.; Wu, J. C.; Lin, C. C. *Macromolecules* **2005**, *38*, 9482–9487.

Huang, E.; Rockford, L.; Russell, T. P.; Hawker, C. J. *Nature* **1998**, *31*, 757–758.

Huang, Y.; Westenhoff, S.; Avilov, I.; Sreearunothai, P.; Hodgkiss, J. M.; Deleener, C.; Friend, R. H.; Belijonne, D. *Nat. Mater.* **2008**, *7*, 483–489.

Huggins, M. L. *J. Am. Chem. Soc.***1942**, *64*, 1712–1719.

Hummelen, J. C.; Knight, B. W.; LePeq, F.; Wudl, F.; Yao, J.; Wilkins, C. L. *J. Org. Chem.* **1995**, *60*, 532–538.

Iovu, M. C.; Jeffries-EL, M.; Sheina, E. E.; Cooper, J. R.; McCullough, R. D. *Polymer* **2005**, *46*, 8582–8586.

Iovu, M. C.; Sheina, E. E.; Gil, R. R.; McCullough, R. D. *Macromolecules* **2005**, *38*, 8649–8656.

Iovu, M. C.; Jeffries-EL, M.; Zhang, R.; Kowalewski, T.; McCullough, R. D. *J. Polym. Sci. Part A*, **2006**, *43*, 1991–2000.

Iovu, M. C.; Craley, R.; Jeffries-EL, M.; Krankowski, A. B.; Zhang, R.; Kowalewski, T.; McCullough, R. D. *Macromolecules* **2007**, *40*, 4733–4735.

Janssen, R. A. J.; Hummelen, J. C.; Sariciftci, N. S. *MRS Bull.* **2005**, *30*, 33–36.

Jeffries-EL, M.; Sauvé, G.; McCullough, R. D. *Adv. Mater.* **2004**, *16*, 1017–1019.

Jeffries-EL, M.; Sauvé, G.; McCullough, R. D. *Macromolecules* **2005**, *38*, 10346–10352.

Jenekhe, S. A.; Chen, X. L. *Science* **1999**, *283*, 372–375.

Jenekhe, S. A.; Chen, X. L. *J. Phys. Chem. B* **2000**, *104*, 6332–6335.

Johnson, B. J. S.; Wolf, J. H.; Zalusky, A. S.; Hillmyer, M. A. *Chem. Mater.* **2004**, *16*, 2909–2917.

Joo, W.; Yang, S. Y.; Kim, J. K.; Jinnai, H. *Langmuir* **2008**, *24*, 12612–12617.

Jurchescu, O. D.; Subramanian, S.; Kline, R. J.; Hudson, S. D.; Anthony, J. E.; Jackson, T. N.; Gundlach, D. J. *Chem. Mater.* **2008**, *20*, 6733–6737.

Kasperczyk, J. E. *Macromolecules* **1995**, *28*, 3937–3939.

Kazmerski, L. L. *J. Electron Spectrosc. Relat. Phenom.* **2006**, *150*, 105–135.

Kenkre, V. M.; Parris, P. E.; Schmidt, D. *Phys. Rev. B* **1985**, *32*, 4946–4955.

Khandpur, A. K.; Förster, S.; Bates, F. S.; Hamley, I.; Ryan, A. J.; Almdal, K.; Mortensen, K. *Macromolecules* **1995**, *28*, 8796–8806.

Kim, B. J.; Miyamoto, Y.; Ma, B.; Fréchet, J. M. J. *Adv. Mater.* **2009**, *19*, 1–9.

Kim, C. S.; Lee, S.; Gomez, E. D.; Anthony, J. E.; Loo, Y. L. *Appl. Phys. Lett.* **2008**, *93*, 103302.

Kim, J. K.; Lee, J. I.; Lee, D. H. *Macromol. Res.* **2008**, *16*, 267–292.

Kim, J. Y.; Kim, S. H.; Lee, H. H.; Lee, K.; Ma, W.; Gong, X.; Heeger, A. J. *Adv. Mater.* **2006**, *18*, 572–576.

Kim, J. Y.; Lee, K.; Coates, N. E.; Moses, D.; Nguyen, T.; Dante, M.; Heeger, A. J. *Science* **2007**, *317*, 222–225.

Kim, J. Y.; Frisbie, C. D. *J. Phys. Chem. C* **2008**, *112*, 17726–17736.

Kim, J. Y.; Qin, Y.; Stevens, D. M.; Ugurlu, O.; Kalihari, V.; Hillmyer, M. A.; Frisbie, C. D. *J. Phys. Chem. C* **2009**, *113*, 10790–10797.

Kim, Y.; Choulis, S. A.; Nelson, J.; Bradley, D. D. C.; Cook, S.; Durrant, J. R. *J. Mater. Sci.* **2005**, *40*, 1371–1376.

Kittel, C. *Introduction to Solid State Physics, 8th Ed.*; John Wiley & Sons, Inc.: Hoboken, NJ, 2005.

Kline, J. R; McGehee, M. D; Kadnikova, E. N.; Liu, J.; Fréchet, J. M. J. *Adv. Mater.* **2003**, *15*, 1519–1522.

Kline, J. R.; DeLongchamp, D. M.; Fischer, D. A.; Lin, E. K.; Heeney, M.; McCulloch, I.; Toney, M. F. *Appl. Phys. Lett.* **2007**, *90*, 062117.

Koetse, M. M.; Sweelssen, J.; Hoekerd, K. T.; Schoo, H. F. M.; Veenstra, S. C.; Kroon, J. M.; Yang, X.; Loos, J. *Appl. Phys. Lett.* **2006**, *88*, 083504.

Konarka Power Plastic. http://konarka.com/index.php (June 2009), Konarka Technologies website.

Kossmehl, G.; Samandari, M. *Makromol. Chem.* **1985**, *186*, 1565–1574.

Kowalski, A.; Duda, A.; Penczek, S. *Macromol. Rapid Commun.* **1998**, *19*, 567–572.

Kowalski, A.; Duda, A.; Penczek, S. *Macromolecules* **1998**, *31*, 2114–2122.

Kress, J.; Osborn, J. A. *J. Am. Chem. Soc.* **1983**, *105*, 6346–6347.

Kretzschmann, H.; Meier, H. *Tetrahedron Lett.* **1991**, *32*, 5059–5062.

Kricheldorf, H.; Berl, M.; Scharnagle, N. *Macromolecules* **1988**, *21*, 286–293.

Kricheldorf, H. R.; Kreiser-Saunders, I.; Stricker, A. *Macromolecules* **2000**, *33*, 702–709.

Kubo, T.; Parker, J. S.; Hillmyer, M. A.; Leighton, C. *Appl. Phys. Lett.* **2007**, *90*, 233113.

Kuila, B. K.; Nandi, A. K. *Macromolecules* **2004**, *37*, 8577–8584.

Kuo, C. Y.; Tang, W. C.; Gau, C.; Guo, T. F.; Jeng, D. Z. *Appl. Phys. Lett.* **2008**, *93*, 033307.

Kuo, S.; Huang, W.; Huang, C.; Chan, S.; Chang, F. *Macromolecules* **2004**, *37*, 4164–4173.

Lambert, J. B.; Shurvell, H. F.; Lightner, D. A.; Cooks, R. G. *Organic Structural Spectroscopy*; Prentice Hall: Upper Saddle River, NJ, 1998.

Le Comber, P. G.; Spear, W. E. *Phys. Rev. Lett.* **1970**, *25*, 509–511.

Lee, J. I.; Cho, S. H.; Park, S. M.; Kim, J. K.; Kim, J. K.; Yu, J. W.; Kim, Y. C.; Russell, T. P. *Nano Lett.* **2008**, *8*, 2315–2320.

Lee, J. K.; Ma, W. L.; Brabec, C. J.; Yuen, J.; Moon, J. S.; Kim, J. Y.; Lee, K.; Bazan, G. C.; Heeger, A. J. *J. Am. Chem. Soc.* **2008**, *130*, 3619–3623.

Lee, J.; Kim, Y.; Do, Y. *Inorg. Chem.* **2007**, *46*, 7701–7703.

Lee, Y.; Fukukawa, K.; Bang, J.; Hawker, C. J.; Kim, J. K. *J. Polym. Sci. Part A*, **2008**, *46*, 8200–8205.

Leibler, L. *Macromolecules* **1980**, *13*, 1602–1617.

Lewis, J. E.; Maroncelli, M. *Chem. Phys. Lett.* **1998**, *282*, 197–203.

Li, B.; Sauvé, G.; Iovu, M. C.; Jeffries-EL, M.; Zhang, R.; Cooper, J.; Santhanam, S.; Schultz, L.; Revelli, J. C.; Kusne, A. G.; Kowlewski, T.; Snyder, J. L.; Weiss, L. E.; Fedder, G. K.; McCullough, R. D.; Lambeth, D. N. *Nano Lett.* **2006**, *6*, 1598–1602.

Li, G.; Shrotriya, V.; Huang, J.; Yao, Y.; Moriarty, T.; Emery, K.; Yang, Y. *Nat. Mater.* **2005**, *4*, 864–868.

Li, J. Q.; Zhao, Z. X.; Li, Y. L.; Zhu, D. B.; Gan, Z. Z.; Yin, D. L. *Physica C* **1992**, *196*, 135–140.

Li, J.; Dierschke, F.; Wu, J.; Grimsdale, A. C.; Müllen, K. *J. Mater. Chem.* **2006**, *16*, 96–100.

Li, N.; Lassiter, B. E.; Lunt, R. R.; Wei, G.; Forrest, S. R. *Appl. Phys. Lett.* **2009**, *94*, 023307.

Li, S. *J. Biomed. Mater. Res.* **1999**, *48*, 342–353.

Li, W. S.; Yamamoto, Y.; Fukushima, T.; Saeki, A.; Seki, S.; Tagawa, S.; Masunaga, H.; Sasaki, S.; Takata, M.; Aida, T. *J. Am. Chem. Soc.* **2008**, *130*, 8886–8887.

Li, W.; Wang, H.; Yu, L. *Macromolecules* **1999**, *32*, 3034–3044.

Lim, Y. F.; Shu, Y; Parkin, S. R.; Anthony, J. E; Malliaras, G. G. *J. Mater. Chem.* **2009**, *19*, 3049–3056.

Lin, J. W. P.; Dudek, L. P. *J. Polym. Sci., Poly. Chem.* **1980**, *18*, 2869–2873.

Lindner, S. M.; Thelakkat, M. *Macromolecules* **2004**, *37*, 8832–8835.

Lipomi, D. J.; Chiechi, R. C.; Reus, W. F.; Whitesides, G. M. *Adv. Funct. Mater.* **2008**, *18*, 3469–3477.

Liu, J.; Loewe, R. S.; McCullough, R. D. *Macromolecules* **1999**, *32*, 5777–5785.

Liu, J.; Shi, Y.; Yang, Y. *Adv. Funct. Mater.* **2001**, *11*, 420–424.

Liu, J.; McCullough, R. D. *Macromolecules* **2002**, *35*, 9882–9889.

Liu, J.; Sheina, E.; Kowalewski, T.; McCullough, R. D. *Angew. Chem., Int. Ed.* **2002**, *41*, 329–332.

Liu, S. L.; Chung, T. S. *Polymer* **2000**, *41*, 2781–2793.

Lloyd, M. T.; Prasankumar, R. P.; Sinclair, M. B.; Mayer, A. C.; Olson, D. C.; Hsu, J. W. P. *J. Mater. Chem.* **2009**, *19*, 4609–4614.

Lo, K. H.; Tseng, W. H.; Ho, R. M. *Macromolecules* **2007**, *40*, 2621–2624.

Loewe, R. S.; Khersonsky, S. M.; McCullough, R. D. *Adv. Mater.* **1999**, *11*, 250–253.

Loewe, R. S.; Ewbank, P. C.; Liu, J.; Zhai, L.; McCullough, R. D. *Macromolecules* **2001**, *34*, 4324–4333.

Lohse, D. J.; Hadijichristidis, N. *Curr. Opin. Colloid In.* **1997**, *2*, 171–176.

Loo, Y. L.; McCulloch, I. *MRS Bull.* **2008**, *33*, 653–658.

Lou, X. D.; Detrembleur, C.; Jérôme, R. *Macromol. Rapid Commun.* **2003**, *24*, 161–172.

Luhman, W. A.; Holmes, R. J. *Appl. Phys. Lett.* **2009**, *94*, 153304.

Lynd, N. A.; Hillmyer, M. A. *Macromolecules* **2005**, *38*, 8803–8810.

Lynd, N. A.; Meuler, A. J.; Hillmyer, M. A. *Prog. Polym. Sci.* **2008**, *33*, 875–893.

Ma, W.; Yang, C.; Gong, X.; Lee, K.; Heeger, A. J. *Adv. Funct. Mater.* **2005**, *15*, 1617–1622.

Ma, W.; Kim, J. Y.; Lee, K.; Heeger, A. J. *Macromol. Rapid Commun.* **2007**, *28*, 1776–1780.

Maggini, M.; Scorrano, G.; Prato, M. *J. Am. Chem. Soc.* **1993**, *115*, 9798–9799.

Malik, S.; Nandi, A. K. *J. Poly. Sci. B* **2002**, *40*, 2073–2085.

Mao, H.; Hillmyer, M. A. *Soft Matter* **2006**, *2*, 57–59.

Marcos-Ramos, A.; Rispens, M. T.; van Duren, J. K. J.; Hummelen, J. C.; Janssen, R. A. J. *J. Am. Chem. Soc.* **2001**, *123*, 6714–6715.

Matsen, M. W.; Schick, M. *Phys. Rev. Lett.* **1994**, *72*, 2660–2663.

Matsen, M. W.; Bates, F. S. *Macromolecules* **1996**, *29*, 1091–1098.

Matsen, M. W; Bates, F. S. *J. Polym. Sci. Pol. Phys.* **1997**, *35*, 945–952.

Matsen, M. W.; Barrett, C. *J. Chem. Phys.* **1998**, *109*, 4108–4118.

Matsen, M. W.; Thompson, R. B. *J. Chem. Phys.* **1999**, *111*, 7139–7146.

Matsen, M. W. *J. Phys.–Condens. Mat.* **2002**, *14*, R21–R47.

Matyjaszewski, K. (Ed.) *Controlled/Living Polymerization: Progress in ATRP, NMP, and RAFT*; Oxford University Press: New York, NY, 2000.

Matyjaszewski, K. *Chem. Rev.* **2001**, *101*, 2921–2990.

McCulloch, I.; Heeney, M.; Bailey, C.; Genevicius, K.; MacDonald, I.; Shkunov, M.; Sparrowe, D.; Tiemey, S.; Wagner, R.; Zhang, W.; Chabinyc, M. L.; Kline, R. J.; McGehee, M. D.; Toney, M. F. *Nat. Mater.* **2006**, *5*, 328–333.

McCullough, R. D.; Lowe, R. D. *J. Chem. Soc., Chem. Commun.* **1992**, *1*, 70–72.

McCullough, R. D.; Jayaraman, M. *J. Chem. Soc., Chem. Commun.* **1995**, 135–136.

McCullough, R. D. *Adv. Mater.* **1998**, *10*, 93–116.

McNeill, C. R.; Abrusci, A.; Zaumseil, J.; Wilson, R.; McKiernan, M. J.; Burroughes, J. H.; Halls, J. J. M.; Greenham, N. C.; Friend, R. H. *Appl. Phys. Lett.* **2007**, *90*, 193506.

McQuade, D. T.; Pullen, A. E.; Swager, T. M. *Chem. Rev.* **2000**, *100*, 2537–2574.

Meiss, J.; Riede, M. K.; Leo, K. *J. Appl. Phys.* **2009**, *105*, 063108.

Menelle, A.; Russell, T. P.; Anastasiadis, S. H.; Satija, S. K.; Majkrzak, C. F. *Phys. Rev. Lett.* **1992**, *68*, 67–70.

Merlo, J. A.; Frisbie, C. D. *J. Phys. Chem. B* **2004**, *108*, 19169–19179.

Miao, Y.; Bazan, G. C. *J. Am. Chem. Soc.* **1994**, *116*, 9379–9380.

Miller, S.; Fanchini, G.; Lin, Y. Y.; Li, C.; Chen, C. W.; Su, W. F.; Chhowalla, M. *J. Mater. Chem.* **2008**, *18*, 306–312.

Mishra, A.; Ma, C. Q.; Bäuerle, P. *Chem. Rev.* **2009**, *109*, 1141–1276.

Misner, M. J.; Skaff, H.; Emrick, T.; Russell, T. P. *Adv. Mater.* **2003**, *15*, 811–814.

Miyakoshi, R.; Yokoyama, A.; Yokozawa, T. *Macromol. Rapid Commun.* **2004**, *25*, 1663–1666.

Miyamoto, M.; Sawamoto, M.; Higashimura, T. *Macromolecules* **1984**, *17*, 265–268.

Miyamoto, M.; Sawamoto, M.; Higashimura, T. *Macromolecules* **1984**, *17*, 2228–2230.

Miyanishi, S.; Tajima, K.; Hashimoto, K. *Macromolecules* **2009**, *42*, 1610–1618.

Miyauchi, S.; Kondo, T.; Oshima, K.; Yamauchi, T.; Shimomura, M.; Mitomo, H. *J. Appl. Poly. Sci.* **2000**, *77*, 3069–3076.

Moad, G.; Rizzardo, E.; Thang, S. H. *Aust. J. Chem.* **2005**, *58*, 379–410.

Monson, T. C.; Lloyd, M. T.; Olson, D. C.; Lee, Y. J.; Hsu, J. W. P. *Adv. Mater.* **2008**, *20*, 4755–4759.

Moon, J. S.; Lee, J. K.; Cho, S.; Byun, J.; Heeger, A. J. *Nano Lett.* **2009**, *9*, 230–234.

Moriyama, H.; Kobayashi, H.; Kobayashi, A.; Watanabe, T. *J. Am. Chem. Soc.* **1993**, *115*, 1187–1189.

Morkved, T. L.; Lu, M.; Urbas, A. M.; Ehrichs, E. E.; Jaeger, H. M.; Mansky, P.; Russell, T. P. *Science* **1996**, *273*, 931–933.

Morteani, A. C.; Sreearunothai, P.; Herz, L. M.; Friend, R. H.; Silva, C. *Phys. Rev. Lett.* **2004**, *92*, 247402.

Mott, N. F. *Contemp. Phys.* **1969**, *10*, 125–138.

Moulé, A. J.; Allard, S.; Kronenberg, N. M.; Tsami, A.; Scherf, U.; Meerholz, K. *J. Phys. Chem. C* **2008**, *112*, 12583–12589.

Moulé, A. J.; Meerholz, K. *Adv. Mater.* **2008**, *20*, 240–245.

Mühlbacher, D. Scharber, M.; Morana, M.; Zhu, Z.; Waller, D.; Gaudiana, R.; Brabec, C. J. *Adv. Mater.* **2006**, *18*, 2884–2889.

Müller, C.; Ferenczi, T. A. M.; Campoy-Quiles, M.; Frost, J. M.; Bradley, D. D. C.; Smith, P.; Stingelin-Stutzmann, N.; Nelson, J. *Adv. Mater.* **2008**, *20*, 3510–3515.

Muller, M.; Schick, M. *Macromolecules* **1996**, *29*, 8900–8903.

Mutolo, K. L.; Mayo, E. I.; Rand, B. P.; Forrest, S. R.; Thompson, M. E. *J. Am. Chem. Soc.* **2006**, *128*, 8108–8109.

Nakamura, E.; Isobe, H. *Acct. Chem. Res.* **2003**, *36*, 807–815.

Nalwa, H. S.; Ed. *Handbook of Organic Conductive Molecules and Polymers*; J. Wiley & Sons: New York, 1996.

Narutaki, M.; Takimiya, K.; Otsubo, T.; Harima, Y.; Zhang, H.; Araki, Y.; Ito, O. *J. Org. Chem.* **2006**, *71*, 1761–1768.

Newman, C. R.; Frisbie, C. D.; da Silva Filho, D. A.; Brédas, J. L.; Ewbank, P. C.; Mann, K. R. *Chem. Mater.* **2004**, *16*, 4436–4451.

Nguyen, L. H.; Hoppe, H.; Erb, T.; Günes, S.; Gobsch, G.; Sariciftci, N. S. *Adv. Funct. Mater.* **2007**, *17*, 1071–1078.

Nguyen, S. T.; Johnson, L. K.; Grubbs, R. H. *J. Am. Chem. Soc.* **1992**, *114*, 3974–3975.

Odian, G. *Principles of Polymerization, 4th Ed.*; John Wiley & Sons, Inc: Hoboken, NJ, 2004.

Ohshimizu, K.; Ueda, M. *Macromolecules* **2008**, *41*, 5289–5294.

Olayo-Valles, R.; Lund, M. S.; Leighton, C.; Hillmyer, M. A. *J. Mater. Chem.* **2004**, *14*, 2729–2731.

Olayo-Valles, R.; Guo, S.; Lund, M. S.; Leighton, C.; Hillmyer, M. A. *Macromolecules* **2005**, *38*, 10101–10108.

Olsen, B. D.; Segalman, R. A. *Macromolecules* **2005**, *38*, 10127–10137.

Olsen, B. D.; Segalman, R. A. *Macromolecules* **2006**, *39*, 7078–7083.

Olsen, B. D.; Segalman, R. A. *Macromolecules* **2007**, *40*, 6922–6929.

Olsen, B. D.; University of California – Berkeley: Doctoral Thesis, 2007.

Olsen, B. D.; Segalman, R. A. *Mater. Sci. Eng., R* **2008**, *62*, 37–66.

Olsen, B. D.; Shah, M.; Ganesan, V.; Segalman, R. A. *Macromolecules* **2008**, *41*, 6809–6817.

Olson, D. A.; Chen, L.; Hillmyer, M. A. *Chem. Mater.* **2008**, *20*, 869–890.

Olson, D. C.; Piris, J.; Collins, R. T.; Shaheen, S. E.; Ginley, D. S. *Thin Solid Films* **2005**, *496*, 26–29.

Olson, D. C.; Piris, J.; Collins, R. T.; Shaheen, S. E.; Ginley, D. S. *Thin Solid Films* **2006**, *496*, 26–29.

Olson, D. C.; Shaheen, S. E.; Collins, R. T.; Ginley, D. S. *J. Phys. Chem. C* **2007**, *111*, 16670–16678.

Ong, B. S.; Wu, Y.; Liu, P. *J. Am. Chem. Soc.* **2004**, *126*, 3378–3379.

Osaka, I.; McCullough, R. D. *Acc. Chem. Res.* **2008**, *41*, 1202–1214.

Ouhib, F.; Khoukh, A.; Ledeuil, J-B.; Martinez, H.; Desbrières, J.; Dagron-Lartigau, C. *Macromolecules* **2008**, *41*, 9736–9743.

Ouyang, J.; Chu, C. W.; Chen, F. C.; Xu, Q.; Yang, Y. *Appl. Phys. Lett.* **2006**, *88*, 073508.

Padinger, F.; Rittberger, R. S.; Sariciftci, N. S. *Adv. Funct. Mater.* **2003**, *13*, 85–88.

Pandey, A. K.; Nunzi, J. M. *Appl. Phys. Lett.* **2006**, *89*, 213506.

Panzer, M. J.; Frisbie, C. D. *Adv. Funct. Mater.* **2006**, *16*, 1051–1056.

Park, J.; Thomas, E. L. *Macromolecules* **2004**, *37*, 3532–3535.

Park, M.; Chaikin, P. M.; Register, R. A.; Adamson, D. H. *Appl. Phys. Lett.* **2001**, *79*, 257–259.

Park, M.; Harrison, C.; Chaikin, P. M.; Register, R. A.; Adamson, D. H. *Science* **1997**, *276*, 1401–1404.

Park, S. H.; Roy, A.; Beaupré, S.; Cho, S.; Coates, N.; Moon, J. S.; Moses, D.; Leclerc, M.; Lee, K.; Heeger, A. J. *Nat. Photonics* **2009**, *3*, 297–303.

Park, Y. D.; Kim, D. H.; Jang, Y.; Cho, J. H.; Hwang, M.; Lee, H. S.; Lim, J. A.; Cho, K. *Organic Electronics* **2006**, *7*, 514–520.

Peet, J.; Heeger, A. J.; Bazan, G. C. *Acc. Chem. Res.* **2009**, *ACS ASAP*.

Peet, J.; Senatore, M. L.; Heeger, A. J.; Bazan, G. C. *Adv. Mater.* **2009**, *21*, 1521–1527.

Peng, J.; Kim, D. H.; Knoll, W.; Xuan, Y.; Li, B.; Han, Y. *J. Chem. Phys.* **2006**, *125*, 64702.

Peumans, P.; Bulovic, V.; Forrest, S. R. *Appl. Phys. Lett.* **2000**, *76*, 2650–2652.

Peumans, P.; Forrest, S. R. *Appl. Phys. Lett.* **2001**, *79*, 126–128.

Peumans, P.; Yakimov, A.; Forrest, S. R. *J. Appl. Phys.* **2003**, *93*, 3693–3723.

Pfuetzner, S.; Meiss, J.; Petrich, A.; Riede, M.; Leo, K. *Appl. Phys. Lett.* **2009**, *94*, 223307.

Phillip, W. A.; Rzayev, J.; Hillmyer, M. A.; Cussler, E. L. *J. Membrane Sci.* **2006**, *286*, 144–152.

Phillip, W. A.; Martono, E.; Chen, L.; Hillmyer, M. A.; Cussler, E. L. *J. Membrane Sci.* **2009**, *337*, 39–46.

Pierret, R. F. *Advanced Semiconductor Fundamentals, 2nd Ed.*; Prentice Hall: Upper Saddle River, NJ, 2002.

Piotti, M. E. *Curr. Opin. Solid State Mater. Sci.* **2000**, *4*, 539–547.

Pope, M.; Swenberg, C. E. *Electronic Processes in Organic Crystals and Polymers*; Oxford University Press: New York, NY, 1999.

Principal Conclusions of the American Physical Society Study Group on Solar Photovoltaic Energy Conversion, American Physical Society, New York, 1979.

Prosa, T. J.; Moulton, J.; Heeger, A. J.; Winokur, M. J. *Macromolecules* **1999**, *32*, 4000–4009.

Pryamitsyn, V.; Ganesan, V. *J. Chem. Phys.* **2004**, *120*, 5824–5838.

Qin, Y.; Hillmyer, M. A. *Macromolecules* **2009**, in press.

Qu, G.; Jiang, F.; Zhang, S.; Usuda, S. *Mater. Lett.* **2007**, *61*, 3421–3424.

Quirk, R. P.; Lee, B. *Polym. Int.* **1992**, *27*, 359–367.

Radzilowski, L. H.; Wu, J. L.; Stupp, S. I. *Macromolecules* **1993**, *26*, 879–882.

Rand, B. P.; Peumans, P.; Forrest, S. R. *J. Appl. Phys.* **2004**, *85*, 5757–5759.

Reese, M. O.; White, M. S.; Rumbles, G.; Ginley, D. S.; Shaheen, S. E. *Appl. Phys. Lett.* **2008**, *92*, 053307.

Rehahn, M.; Schlüter, A. D. *Makromol. Chem., Rapid Commun.* **1985**, *11*, 375–379.

Reyes-Reyes, M.; Kim, K.; Carroll, D. L. *Appl. Phys. Lett.* **2005**, *87*, 083506.

Richard, F.; Brochon, C.; Leclerc, N.; Eckhardt, D.; Heiser, T.; Hadziioannou, G. *Macromol. Rapid Commun.* **2008**, *29*, 885–891.

Roncali, J. *Chem. Rev.* **1997**, *97*, 173–205.

Roncali, J. *Chem. Soc. Rev.* **2005**, *34*, 483–495.

Russell, T. P.; Coulon, G.; Deline, V. R.; Miller, D. C. *Macromolecules* **1989**, *22*, 4600–4606.

Ryner, M.; Stridsberg, K.; Albertsson, A. C.; von Schenck, H.; Svensson, M. *Macromolecules* **2001**, *34*, 3877–3881.

Rzayev, J.; Hillmyer, M. A. *Macromolecules* **2005**, *38*, 3–5.

Rzayev, J.; Hillmyer, M. A. *J. Am. Chem. Soc.* **2005**, *127*, 13373–13379.

Sauvé, G.; McCullough, R. D. *Adv. Mater.* **2007**, *19*, 1822–1825.

Scharber, M. C.; Mühlbacher, D.; Koppe, M.; Denk, P.; Wadauf, C.; Heeger, A. J.; Brabec, C. J. *Adv. Mater.* **2006**, *18*, 789–794.

Scherf, U.; Gutacker, A.; Koenen, N. *Acct. Chem. Res.* **2008**, *41*, 1086–1097.

Schilinsky, P.; Waldauf, C.; Brabec, C. J. *Appl. Phys. Lett.* **2002**, *81*, 3885–3887.

Schlick, S.; Levy, M. *J. Phys. Chem.* **1960**, *64*, 883–886.

Schmidt, S. C.; Hillmyer, M. A. *Macromolecules* **1999**, *32*, 4794–4801.

Schrock, R. R.; DePue, R. T.; Feldman, J.; Schaverien, C. J.; Dewan, J. C.; Liu, A. H. *J. Am. Chem. Soc.* **1988**, *110*, 1423–1435.

Schulz, M. F.; Khanpur, A. K; Bates, F. S.; Almdal, K.; Mortensen, K.; Hajduk, D. A.; Gruner, S. M. *Macromolecules* **1996**, *29*, 2857–2867.

Schulze, K.; Uhrich, C.; Schüppel, R.; Leo, K.; Pfeiffer, M.; Brier, E.; Reinold, E.; Bäuerle, P. *Adv. Mater.* **2006**, *18*, 2872–2875.

Schulze, K.; Riede, M.; Brier, E.; Reinold, E.; Bäuerle, P.; Leo, K. *J. Appl. Phys.* **2008**, *104*, 074511.

Semenov, A. N.; Vasilenko, S. V. *Zh. Eksp. Teor. Fiz.* **1986**, *90*, 124–140.

Semenov, A. N. *Mol. Cryst. Liq. Cryst.* **1991**, *209*, 191–199.

Shaheen, S. E.; Brabec, C. J.; Sariciftci, N. S.; Padinger, F.; Fromherz, T.; Hummelen, J. C. *Appl. Phys. Lett.* **2001**, *78*, 841–843.

Shaheen, S. E.; Ginley, D. S.; Jabbour, G. E. *MRS Bull.* **2005**, *30*, 10–15.

Sheina, E. E.; Liu, J.; Iovu, M. C.; Laird, D. W.; McCullough, R. D. *Macromolecules* **2004**, *37*, 3526–3528.

Shevaleevskiy, O. *Pure Appl. Chem.* **2008**, *80*, 2079–2089.

Shockley, W. *Bell Syst. Tech. J.* **1949**, *28*, 435.

Shrotriya, V.; Li, G.; Yao, Y.; Moriarty, T.; Emery, K.; Yang, Y. *Adv. Funct. Mater.* **2006**, *16*, 2016–2023.

Shull, K. R. *Macromolecules* **1992**, *25*, 2122–2133.

Sikka, M.; Singh, N.; Karim, A.; Bates, F. S.; Satija, S. K.; Majkrzak, C. F. *Phys. Rev. Lett.* **1993**, *70*, 307–310.

Simon, J. *Molecular Semiconductors*; Springer-Verlag: Berlin, Germany, 1985.

Singh, C.; Goulian, M.; Liu, A. J.; Frederickson, G. H. *Macromolecules* **1994**, *27*, 2974–2986.

Sirringhaus, H. *Adv. Mater.* **2005**, *17*, 2411–2425

Sivula, K.; Ball, Z. T.; Watanabe, N.; Fréchet, J. M. J. *Adv. Mater.* **2006**, *18*, 206–210.

Sivula, K.; Luscombe, C. K.; Thompson, B. C. Fréchet, J. M. J. *J. Am. Chem. Soc.* **2006**, *128*, 13988–13989.

Skotheim, T.; Reynolds, J.; Elsembauer, R.; Eds. *Handbook of Conducting Polymers*; Marcel Dekker: New York, 1998.

Smith, A. P.; Fraser, C. L. *Macromolecules* **2002**, *35*, 594–596.

Snaith, H. J.; Kenrick, H.; Chiesa, M.; Friend, R. H. *Polymer* **2005**, *46*, 2573–2578.

Solar Spectral Irradiance: Air Mass 1.5. http://rredc.nrel.gov/solar/spectra/am1.5/ (June 2009), National Renewable Energy Laboratory (NREL) website.

Sommer, M.; Hüttner, S.; Wunder, S.; Thelakkat, M. *Adv. Mater.* **2008**, *13*, 2523–2527.

Sommer, M.; Lang, A. S.; Thelakkat, M. *Angew. Chem., Int. Ed.* **2008**, *47*, 7901–7904.

Sperling, L. H. *Introduction to Polymer Science, 3rd Ed.*; John Wiley & Sons, Inc.: Hoboken, NJ, 2001.

Stalmach, U.; de Boer, B.; Videlot, C.; van Hutten, P. F.; Hadziioannou, G. *J. Am. Chem. Soc.* **2000**, *122*, 5464–5472.

Stalmach, U.; de Boer, B.; Post, A. D.; van Hutten, P. F.; Hadziioannou, G. *Angew. Chem., Int. Ed.* **2001,** *40*, 428–430.

Stevens, D. M.; Qin, Y.; Hillmyer, M. A.; Frisbie, C. D. *J. Phys. Chem. C* **2009**, *113*, 11408–11415.

Stille, J. K. *Angew. Chem., Int. Ed. Engl.* **1986**, *25*, 508 –524.

Stoykovich, M. P.; Müller, M.; Kim, S. O.; Solak, H. H.; Edwards, E. W.; de Pablo, J. J.; Nealey, P. F. *Science* **2005**, *308*, 236–239.

Sugimoto, R.; Takeda, S.; Gu, H. B.; Yoshino, K. *Chem. Express* **1986**, *1*, 635–638.

Sun, Q.; Park, K.; Dai, L. *J. Phys. Chem. C* **2009**, *113*, 7892–7897.

Sun, S.; Sariciftci, N. S., Eds. *Organic Photovoltaics: Mechanisms, Materials, and Devices*; Taylor & Francis: Boca Raton, FL, 2005.

Sunderberg, M.; Inganäs, O.; Stafström, S.; Gustafsson, G.; Sjögren, B. *Solid State Commun.* **1989**, *71*, 435–439.

Suzuki, A. *J. Organomet. Chem.* **1999**, *576*, 147–168.

Svensson, M.; Zhang, F.; Veenstra, S. C; Verhees, W. J. H.; Hummelen, J. C.; Kroon, J. M.; Inganäs, O.; Andersson, M. R. *Adv. Mater.* **2003**, *15*, 988–991.

Sykes, A. G; Ed. *Advances in Inorganic Chemistry*; Academic Press: New York, NY, 1996; Vol. 44.

Sze, S. M. *Physics of Semiconductor Devices, 2nd Ed.*; John Wiley & Sons, Inc.: Hoboken, NJ, 1981.

Szwarc, M. *Nature* **1956**, *178*, 1168–1169.

Szwarc, M.; Levy, M.; Milkovich, R. *J. Am. Chem. Soc.* **1956**, *78*, 2656–2657.

Tang, C. W. *Appl. Phys. Lett.* **1986**, *48*, 183–185.

Tang, Q.; Jiang, L.; Tong, Y.; Li, H.; Liu, Y.; Wang, Z.; Hu, W.; Liu, Y.; Zhu, D. *Adv. Mater.* **2008**, *20*, 2947–2951.

Tashiro, K.; Kobayashi, M.; Kawai, T.; Yoshino, K. *Polymer* **1997**, *38*, 2867–2879.

Tew, G. N.; Pralle, M. U.; Stupp, S. I. *J. Am. Chem. Soc.* **1999**, *121*, 9852–9866.

Thekaekara, M. P. *Suppl. Proc. 20th Annu. Meet. Inst. Environ. Sci.* **1974**, 21.

Thermo Scientific. http://www.thermo.com/ (July 2009), Thermo Scientific Website.

Thomas, E. L.; Alward, D. B.; Kinning, D. J.; Martin, D. C.; Handlin, D. L., Jr.; Fetters, L. J. *Macromolecules* **1986**, *19*, 2197–2202.

Thompson, B. C.; Kim, B. J.; Kavulak, D. F.; Sivula, K.; Mauldin, C.; Fréchet, J. M. J. *Macromolecules* **2007**, *40*, 7425–7428.

Thompson, B. C.; Fréchet, J. M. J. *Angew. Chem., Int. Ed.* **2008**, *47*, 58–77.

Thurn-Albrecht, T.; Schotter, J.; Kästle, G. A.; Emley, N.; Shibauchi, T.; Krusin-Elbaum, L.; Guarini, K.; Black, C. T.; Tuominen, M. T.; Russell, T. P. *Science* **2000**, *290*, 2126–2129.

Tokuyama, H.; Yamago, S.; Nakamura, E.; Shiraki, T.; Sugluar, Y. *J. Am. Chem. Soc.* **1993**, *115*, 7918–7919.

Tong, X.; Bailey-Salzman, R. F.; Wei, G.; Forrest, S. R. *Appl. Phys. Lett.* **2008**, *93*, 173304.

Troshin, P. A.; Hoppe, H.; Renz, J.; Egginger, M.; Mayorova, J. Y.; Goryachev, A. E.; Peregudov, A. S.; Lyubovskaya, R. N.; Gobsch, G.; Sariciftci, N. S.; Razumov, V. F. *Adv. Funct. Mater.* **2009**, *19*, 779–788.

Trznadel, M.; Pron, A.; Zagorska, M.; Chrzaszcz, R.; Pielichowski, J. *Macromolecules* **1998**, *31*, 5051–5058.

Tu, G.; Li, H.; Forster, M.; Heiderhoff, R.; Balk, L. J.; Scherf, U. *Macromolecules* **2006**, *39*, 4327–4331.

Tuladhar, S. M.; Sims, M.; Choulis, S. A.; Nielsen, C. B.; George, W. N.; Steinke, J. H. G.; Bradley, D. D. C.; Nelson, J. *Org. Electron.* **2009**, *10*, 562–567.

Uhrich, C.; Schüppel, R.; Petrich, A.; Pfeiffer, M.; Leo, K.; Brier, E.; Kilickiran, P.; Bäuerle, P. *Adv. Funct. Mater.* **2007**, *17*, 2991–2999.

Urien, M.; Erothu, H.; Cloutet, E.; Hiorns, R. C.; Vignau, L.; Cramail, H. *Macromolecules* **2008**, *41*, 7033–7040.

van der Veen, M. H.; de Boer, B.; Stalmach, U.; van de Wetering, K. I.; Hadziioannou, G. *Macromolecules* **2004**, *37*, 3673–3684.

van Hall, P. A.; Knol, J.; Langeveld-Voss, B. M. W.; Meskers, S. C. J.; Hummelen, J. C.; Janssen, R. A. J. *J. Phys. Chem. A* **2000**, *104*, 5974–5988.

Vissenberg, M. C. J. M.; Matters, M. *Phys. Rev. B* **1998**, *57*, 12964–12967.

Wanamaker, C. L.; O'Leary, L. E.; Lynd, N. A.; Hillmyer, M. A.; Tolman, W. B. *Biomacromolecules* **2007**, *8*, 3634–3640.

Wang, G.; Swensen, J.; Moses, D.; Heeger, A. J. *J. Appl. Phys.* **2003**, *93*, 6137–6141.

Wang, X.; Perzon, E.; Delgado, J. L.; de la Cruz, P.; Zhang, F.; Langa, F.; Andersson, M. R.; Inganäs, O. *Appl. Phys. Lett.* **2004**, *85*, 5081–5083.

Wang, X.; Perzon, E.; Oswald, F.; Langa, F.; Admassie, S.; Andersson, M. R.; Inganäs, O. *Adv. Mater.* **2005**, *15*, 1665–1670.

Wang, Y.; Hillmyer, M. A. *Macromolecules* **2000**, *33*, 7395 – 7403.

Watkins, P. K.; Walker, A. B.; Verschoor, G. L. B. *Nano Lett.* **2005**, *5*, 1814–1818.

Wells, N. P.; Boudouris, B. W.; Hillmyer, M. A.; Blank, D. A. *J. Phys. Chem. C* **2007**, *111*, 15404–15414.

Wells, N. P.; Blank, D. A. *Phys. Rev. Lett.* **2008**, *100*, 086403.

Wienk, M. M.; Turbiez, M. G. R.; Struijk, M. P.; Fonrodoan, M.; Janssen, R. A. J. *Appl. Phys. Lett.* **2006**, *88*, 153511.

Williams, C. K.; Breyfogle, L. E.; Choi, S. K.; Nam, W.; Young, V. G.; Hillmyer, M. A.; Tolman, W. B. *J. Am. Chem. Soc.* **2003**, *125*, 11350–11359.

Williams, D. R. M.; Fredrickson, G. H. *Macromolecules* **1992**, *25*, 3561–3568.

Williams, S. S.; Hampton, M. J.; Gowrishankar, V.; Ding, I. K.; Templeton, J. L.; Samulski, E. T.; DeSimone, J. M.; McGehee, M. D. *Chem. Mater.* **2008**, *20*, 5229–5234.

Witiak, D. T.; Williams, D. R.; Kakodkar, S. V. *J. Org. Chem.* **1974**, *39*, 1242–1247.

Xi, H.; Wei, Z.; Duan, Z.; Xu, W.; Zhu, D. *J. Phys. Chem. C* **2008**, *112*, 19934–19938.

Xia, Y.; Wang, L.; Deng, X.; Li, D.; Zhu, X.; Cao, Y. *Appl. Phys. Lett.* **2006**, *89*, 081106.

Xin, H.; Ren, G.; Kim, F. S.; Jenekhe, S. A. *Chem. Mater.* **2008**, *20*, 6199–6207.

Xue, J.; Rand, B. P.; Uchida, S.; Forrest, S. R. *Adv. Mater.* **2005**, *17*, 66–71.

Xue, J.; Rand, B. P.; Uchida, S; Forrest, S. R. *J. Appl. Phys.* **2005**, *98*, 124903.

Xue, L.; Liu, L.; Gao, Q.; Wen, S.; He, J.; Tian, W. *Sol. Energ. Mat. Sol. C.* **2009**, *93*, 501–507.

Yamamoto, T.; Sanechika, K.; Yamamoto, A. *J. Polym. Sci., Polym. Lett. Ed.* **1980**, *18*, 9–12.

Yamamoto, T.; Oguro, D.; Kubota, K. *Macromolecules* **1996**, *29*, 1833–1835.

Yamashiro, T.; Aso, Y.; Otsubo, T.; Tang, H.; Harima, Y.; Yamashita, K. *Chem. Lett.* **1999**, 443–444.

Yan, H.; Chen, Z.; Zheng, Y.; Newman, C.; Quinn, J. R.; Dötz, F.; Kastler, M.; Facchetti, A. *Nature* **2009**, *457*, 679–686.

Yang, C.; Orfino, F. P.; Holdcroft, S. *Macromolecules* **1996**, *29*, 6510–6517.

Yang, F.; Forrest, S. R. *ACS Nano* **2008**, *2*, 1022–1032.

Yokoyama, A.; Miyakoshi, R.; Yokozawa, T. *Macromolecules* **2004**, *37*, 1169–1171.

Yu, G.; Heeger, A. J. *J. Appl. Phys.* **1995**, *78*, 4510–4515.

Zakhidov, A. A.; Yoshino, K. *Synth. Met.* **1994**, *64*, 155–165.

Zalusky, A. S.; Olayo-Valles, R.; Wolf, J. H.; Hillmyer, M. A. *J. Am. Chem. Soc.* **2002**, *124*, 12761–12773.

Zhan, X.; Tan, Z.; Domercq, B.; An, Z.; Zhang, X.; Barlow, S.; Li, Y.; Zhu, D.; Kippelen, B.; Marder, S. R. *J. Am. Chem. Soc.* **2007**, *129*, 7246–7247.

Zhang, F.; Manno, W.; Andersson, I. M.; Admassie, S.; Andersson, M. R.; Inganäs, O. *Adv. Mater*. **2006**, *18*, 2169–2173.

Zhang, Q.; Cirpan, A.; Russell, T. P.; Emrick, T. *Macromolecules* **2009**, *42*, 1079–1082.

Zhang, R.; Li, B.; Iovu, M. C.; Jeffries-EL, M.; Sauve, G.; Cooper, J.; Jia, S.; Tristram-Nagle, S.; Smilgies, D. M.; Lambeth, D. N.; McCullough, R. D.; Kowalewski, T. *J. Am. Chem. Soc.* **2006**, *128*, 3480–3481.

Zhao, Y.; Keroack, D.; Yuan, G.; Massicotte, A. *Macromol. Chem. Phys.* **1997**, *198*, 1035–1049.

Zheng, W.; Wang, Z. G. *Macromolecules* **1995**, *28*, 7215–7223.

Zhong, H.; Yang, X.; deWith, B.; Loos, J. *Macromolecules* **2006**, *39*, 218–223.

9 Appendix

9.1 Copyright Permissions

The material presented in Chapters 4 and 7 was originally published in *Macromolecules* as:

"Nanoporous Poly(3-alkylthiophene) Thin Films Generated from Block Copolymer Templates," B. W. Boudouris, C. D. Frisbie, and M. A. Hillmyer, *Macromolecules* **2008**, *41*, 67–75.

"Synthesis, Optical Properties, and Microstructure of a Fullerene-terminated Poly(3-hexylthiophene)," B. W. Boudouris, F. Molins, D. A. Blank, C. D. Frisbie, and M. A. Hillmyer, *Macromolecules* **2009**, *42*, 4118–4126.

The American Chemical Society (ACS) guidelines for including published material in theses are posted on the Internet at http://pubs.acs.org/page/copyright/permissions.html by clicking on the link associated with the file "dissertation.pdf". The text of "dissertation.pdf" follows, which grants permission from the ACS to use the material in Chapters 4 and 7.

Thank you for your request for permission to include **your** paper(s) or portions of text from **your** paper(s) in your thesis. Permission is now automatically granted; please pay special attention to the implications paragraph below. The Copyright Subcommittee of the Joint Board/Council Committees on Publications approved the following:

Copyright permission for published and submitted material from theses and dissertations
ACS extends blanket permission to students to include in their theses and dissertations their own articles, or portions thereof, that have been published in ACS journals or submitted to ACS journals for publication, provided that the ACS copyright credit line is noted on the appropriate page(s).

Publishing implications of electronic publication of theses and dissertation material
Students and their mentors should be aware that posting of theses and dissertation material on the Web prior to submission of material from that thesis or dissertation to an ACS journal may affect publication in that journal. Whether Web posting is considered prior publication may be evaluated on a case-by-case basis by the journal's editor. If an ACS journal editor considers Web posting to be "prior publication", the paper will not be accepted for publication in that journal. If you intend to submit your unpublished paper to ACS for publication, check with the appropriate editor prior to posting your manuscript electronically.

9.2 Supporting Information for Results of Selected Chapters

The following data and experimental procedures appear as supporting information for selected chapters of this thesis. Please refer to the appropriate chapter for any information not provided in the figure captions.

9.2.1 Chapter 5 Supporting Information

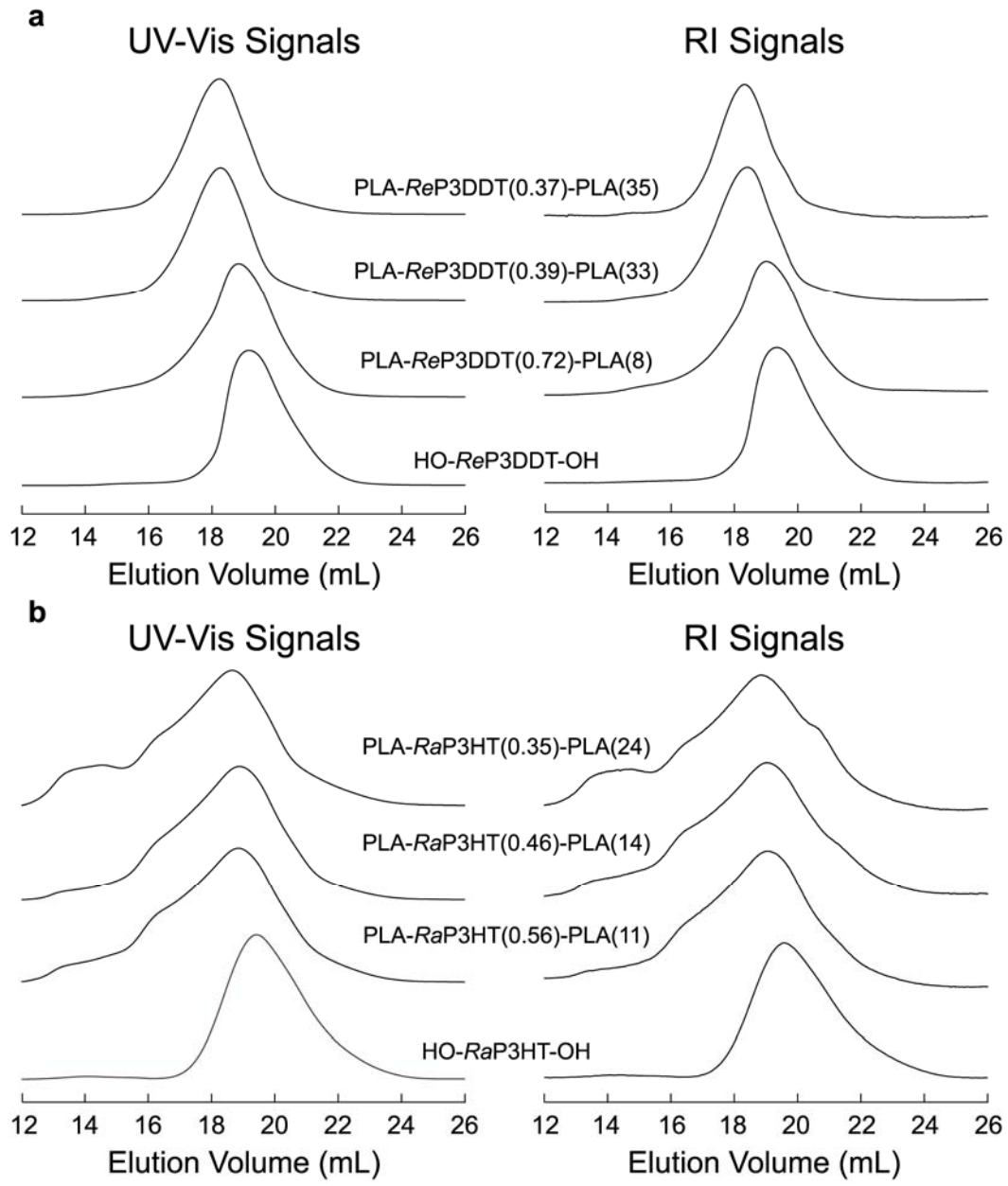

Figure 9.1. SEC chromatograms of the (a) regioregular poly(3-dodecylthiophene) and (b) regiorandom poly(3-hexylthiophene) series with chloroform as the eluting solvent at 35 °C. The traces on the left are from the UV-Vis detector and the traces on the right are from the RI detector. The traces obtained using a UV-Vis detector monitored the signal at $\lambda = 400$ nm.

9.2.2 Chapter 6 Supporting Information

General Methods. The ^{1}H NMR spectra were measured on a Varian VI-500 spectrometer using deuterated chloroform (Cambridge) solutions containing ~1 wt % polymer. Size exclusion chromatography (SEC) data were collected on an Agilent 1100 series equipped with an Agilent Ultraviolet visible (UV-Vis) light detector (path length = 10 mm) and three PLgel 5μm MIXED-C columns. Chloroform at 35 °C was used as the mobile phase at a flow rate of 1 mL/min and the SEC was calibrated with polystyrene (PS) standards (Polymer Laboratories). Differential scanning calorimetry (DSC) measurements were acquired using a TA Q1000 calorimeter. The samples were first annealed at 260 °C and then cooled to –60 °C at a rate of 10 °C/min. The results shown are for the final sample heating at a rate of 10 °C/min. An indium standard was used to calibrate the instrument and nitrogen was used as the purge gas. Wide-angle x-ray scattering (WAXS) data of polymer powders were collected at room temperature in the diffraction angular range of 3–30° (2θ) by a Bruker-AXS D5005 microdiffractometer. No annealing treatments were preformed prior to data collection. The crystalline peaks were referenced from known reflection values[1] and deconvoluted using the curve-fitting software, JADE 7 (CMI). Film thicknesses were estimated by scratching the polymer film and measuring the step change with a Veeco Metrology Nanoscope IIIa atomic force microscope (AFM) operating in tapping mode. Ultraviolet-visible (UV-Vis) light absorption spectra of polymer thin films were taken on a Spectronic Genesys 5 spectrometer over a wavelength range of 200–900 nm using a glass substrate as a blank. Solutions of HO-coPT-OH and PLA-coPT-PLA were made by dissolving 10 mg of polymer in 1 mL of 1,2-dichlorobenzne (DCB) and allowing the solutions to stir at 65 °C under inert atmosphere overnight. Glass substrates were sonicated for 10 min in isopropanol and dried with compressed nitrogen. Solutions were passed through a 0.45 μm syringe filter and spun-cast onto the substrates at a rotation rate of 1000 rpm for 60 sec. The thicknesses of all of the films, as measured using the AFM, were 20 ± 4 nm. The annealed films were placed in an inert atmosphere glove box and heated to 110 °C for 48 h on a hot plate.

Materials. All reagents and solvents were used as received from Sigma-Aldrich unless otherwise noted. Degassed tetrahydrofuran (THF) and toluene were purified by passage through an activated alumina column and were collected in flame-dried, air-free flasks. D,L-lactide was purified by recrystallization from toluene followed by drying under reduced pressure and was stored in an inert atmosphere glove box.

Synthesis of Hydroxyl-terminated Poly(3-dodecylthiophene-*co*-thiophene) (HO-coPT-OH). This procedure is a modified version of the original methodology presented by the McCullough group in 2002.[2] 80 mL of anhydrous THF was added to a flame-dried reaction flask (Flask 1) using a cannula. 2,5-dibromothiophene (2.0 g, 8.3 mmol) and a solution of ~2 M *tert*-butylmagnesium chloride in diethyl ether (4.2 mL, 8.4 mmol) were added to the THF solvent under Ar. The reaction was heated to reflux for 1.5 h and then cooled to room temperature. In a separate flame-dried reaction flask (Flask 2), 2,5-dibromo-3-dodecylthiophene (3.5 g, 8.3 mmol) and a solution of ~2 M *tert*-butylmagnesium chloride in diethyl ether (4.2 mL, 8.4 mmol) were mixed in ~150 mL of anhydrous THF under Ar. The reaction was refluxed for 1.5 h and then allowed to cool to room temperature. The reaction solution from Flask 1 was then added to Flask 2 using a cannula under inert atmosphere. After stirring the reaction for 5 min to insure proper mixing, 1,3-bis(diphenylphosphino)propane nickel (II) chloride [Ni(dppp)Cl_2] (0.228 g, 0.45 mmol) was added as a solid under Ar. This meant that there was 2.5 mole% loading of catalyst on a total activated monomer basis. The reaction was then allowed to stir for 12 h at room temperature under Ar. The reaction was quenched with 12 mL of 1 M hydrochloric acid (HCl) and precipitated in methanol. The polymer was collected and purified via Soxhlet extraction with methanol, hexane, methylene chloride, and chloroform, sequentially. The concentrated chloroform fraction, hydrogen/bromine-terminated poly(3-dodecylthiophene-*co*-thiophene) (H-coPT-Br), was dried overnight under reduced pressure and used in all future reactions. Note that this material was not as soluble in the reaction solvents as poly(3-alkylthiophene)s. Therefore, a larger amount of solvent was used in the end-functionalization reactions in order to guarantee the polymer precursor was completely dissolved.

A magnesium-halogen exchange was used to convert the end groups of H-coPT-Br to protons.[2] In this reaction, 250 mL of anhydrous THF was added to a flame-dried reaction flask using a cannula under Ar. H-coPT-Br (0.78 g, 0.21 mmol) was added to the reaction flask as a solid under Ar. Subsequently, ~2 M *tert*-butylmagnesium chloride in diethyl ether (11.8 mL, 23.6 mmol) was added to the reaction flask. The reaction was heated to reflux, and allowed to reflux for 2 h. The mixture was then cooled to 0 °C by application of an ice/water bath. 12.0 mL of ~2 M hydrogen chloride were slowly added to quench the reaction. The hydrogen/hydrogen-terminated polymer (H-coPT-H) was precipitated in methanol and then purified by Soxhlet extraction with methanol and chloroform.

In order to convert the H-coPT-H to the *bis*-aldehyde-terminated polymer, 250 mL of anhydrous toluene were added to a flame-dried reaction flask. H-coPT-H (0.42 g, 0.11 mmol), *N*-methylformanilide (3.0 mL), and phosphorous oxychloride ($POCl_3$) (2.0 mL) were added to the reaction flask under Ar.[3] The mixture was heated to 75 °C and stirred at this temperature for 24 h. After cooling to room temperature, 80 mL of a concentrated aqueous sodium acetate solution (35 g solid in 100 mL HPLC-grade water) was added to the reaction mixture under Ar. The components were allowed to stir for 2 h. Afterwards, the organic and aqueous phases were separated and the toluene fraction was washed with HPLC-grade water. The toluene fraction was then concentrated and precipitated in methanol. HCO-coPT-COH was then Soxhlet extracted with methanol and chloroform.

Dihydroxyl-functionalized polymer (HO-coPT-OH) was synthesized by reducing HCO-coPT-COH. HCO-coPT-COH (0.26 g, 0.068 mmol) was dissolved in 250 mL of anhydrous THF under Ar. A ~1 M solution of lithium aluminumhydride ($LiAlH_4$) in THF was added to the reaction flask under Ar using a gas-tight, deoxygenated syringe (3.5 mL, 3.5 mmol). The reaction was stirred at room temperature for 40 min and then quenched with 3.5 mL of 1 M HCl. The polymer was precipitated in methanol and Soxhlet extracted with methanol and chloroform.

Characterization of **HO-coPT-OH**. ^{1}H NMR (500 MHz, $CDCl_3$): δ_H 0.87 (t, 3H), 1.26 (m, 18H), 1.57 (m, 2H), 2.68 (s, 2H), *4.76 (d, 4H)*, 7.00 (m, 40H); SEC: M_n: 5500, PDI: 1.7. Italicized entries correspond to end group proton resonances.

Synthesis of Polylactide-*b*-Poly(3-dodecylthiophene-*co*-thiophene)-*b*-Polylactide (PLA-coPT-PLA). The commonly used catalyst, tin octanoate [$Sn(oct)_2$], was used for the ring-opening polymerization (ROP) of D,L-lactide.[4,5] The HO-coPT-OH homopolymer acted as the macroinitiator. The details for the example polymerization of PLA-coPT(0.59)-PLA(4.0) (see Chapter 6 for nomenclature details) follow. HO-coPT-OH (0.030 g, 10.3 μmol OH groups) was freeze-dried under reduced vacuum with liquid nitrogen (LN_2) overnight. The flask was sealed and transferred inside of a glove box where toluene (1.2 mL) dissolved the HO-coPT-OH. The monomer, D,L-lactide, was then added to the reaction flask (0.100 g, 0.69 mmol). A solution of 2.4 mM tin octanoate in toluene (0.20 mL, 0.48 μmol) was also added ([OH]:[Sn] = 20:1). The reaction was then capped, brought outside the glove box, and placed in an oil bath at 110 °C for 4 h. The reaction was cooled to room temperature, quenched with ~2 M HCl (1 mL, 2 mmol). This quenched the polymerization at ~20% conversion of lactide. The triblock copolymer was then precipitated in methanol. After filtering and washing with methanol, the polymer was dried overnight under vacuum.

Characterization of **PLA-coPT(0.82)-PLA(1.3)**. ^{1}H NMR (500 MHz, $CDCl_3$): main chain coPT peaks are the same as for **HO-coPT-OH** with δ_H 1.57 (m, 3H), 4.35 (t, 2H), 5.20 (m, 18H); SEC: M_n: 8100, PDI: 2.1.

Characterization of **PLA-coPT(0.77)-PLA(1.7)**. ^{1}H NMR (500 MHz, $CDCl_3$): main chain coPT peaks are the same as for **HO-coPT-OH** with δ_H 1.57 (m, 3H), 4.35 (t, 2H), 5.20 (m, 24H); SEC: M_n: 9500, PDI: 2.0.

Characterization of **PLA-coPT(0.59)-PLA(4.0)**. ^{1}H NMR (500 MHz, $CDCl_3$): main chain coPT peaks are the same as for **HO-coPT-OH** with δ_H 1.57 (m, 3H), 4.35 (t, 2H), 5.20 (m, 54H); SEC: M_n: 12500, PDI: 1.8.

Characterization of **PLA-coPT(0.14)-PLA(35.7)**. ^{1}H NMR (500 MHz, $CDCl_3$): main chain coPT peaks are the same as for **HO-coPT-OH** with δ_H 1.57 (m, 3H), 4.35 (t, 2H), 5.20 (m, 497H); SEC: M_n: 36700, PDI: 1.5.

9.2.3 Chapter 7 Supporting Information†

The detailed synthetic procedure for the polymers synthesized in Chapter 7 is detailed below. Preparatory size exclusion chromatography (Prep SEC), analytical size exclusion chromatography (SEC), and matrix-assisted laser desorption/ionization mass-spectrometry (MALDI-MS) data are also shown.

Materials. All reagents and solvents were used as received from Sigma-Aldrich unless otherwise noted. Degassed tetrahydrofuran (THF) and toluene were purified by passage through an activated alumina column and were collected in flame-dried, air-free flasks. Chlorobenzene was dried overnight over calcium hydride and distilled under inert atmosphere prior to use. [C_{60}]-fullerene (99.5% purity) was purchased from American Dye Source (Quebec, Canada) and used without further purification.

Synthesis of Aldehyde-terminated Poly(3-hexylthiophene) (CHO-P3HT-CHO). A method similar to that of the McCullough group was used for the synthesis of aldehyde-terminated poly(3-hexylthiophene).[2] The polymerization of 2,5-dibromo-3-hexylthiophene was performed in a flame-dried 250 mL reaction flask. To the flask, ~80 mL of anhydrous THF were added via cannula. 2,5-dibromo-3-hexylthiophene (4.0 g, 12.3 mmol) and a solution of 2 M *tert*-butylmagnesium chloride in diethyl ether (6.2 mL, 12.4 mmol) were added to the THF solvent under Ar. The reaction was placed in an oil bath and heated to reflux for 90 min. After cooling the solution to room temperature, 1,3-bis(diphenylphosphino)propane nickel (II) chloride [Ni(dppp)Cl_2] (0.168 g, 0.31 mmol) was added as a solid under Ar and the reaction was allowed to stir for 45 min. The reaction was quenched with 8 mL of ~2 M hydrochloric acid (HCl) and precipitated in methanol. The polymer was collected and purified via Soxhlet extraction

† Reproduced with permission from the Supporting Information of B. W. Boudouris, F. Molins, D. A. Blank, C. D. Frisbie, and M. A. Hillmyer, *Macromolecules* **2009**, *42*, 4118–4126. Copyright 2009 American Chemical Society. This material is available free of charge via the Internet at http://pubs.acs.org.

with methanol, acetone, and chloroform, sequentially. The concentrated chloroform fraction was precipitated in methanol and the hydrogen/bromine terminated poly(3-hexylthiophene) (H-P3HT-Br) was collected and dried overnight under reduced pressure.

The reaction to convert the P3HT to all proton-capped end groups was carried out in a 250 mL reaction flask. After flame-drying, 100 mL of anhydrous THF was added via cannula. H-P3HT-Br (0.82 g, 0.21 mmol) was added as a solid under a stream of Ar and allowed to dissolve in the solvent. Subsequently, 20.3 mL of 2 M *tert*-butylmagnesium chloride in diethyl ether was added to the reaction flask using a deoxygenated syringe under Ar. The reaction was heated to reflux and allowed to stir for 2 h before being cooled to ~0 °C by application of an ice bath to the reaction flask. The reaction was quenched with 20 mL of ~2 M HCl and precipitated in methanol followed by Soxhlet extraction of the P3HT with methanol.

In order to convert the P3HT polymer to the aldehyde-terminated material (CHO-P3HT-CHO) ~80 mL of anhydrous toluene were added to a flame-dried 250 mL reaction flask. Proton-terminated P3HT (0.51 g, 0.13 mmol) was added to the reaction flask as a solid under Ar. *N*-methylformanilide (5.0 mL, 41 mmol) and $POCl_3$ (3.8 mL, 42 mmol) were added to the reaction flask under Ar. The reaction was heated to 75 °C and allowed to stir for 24 h. After this period of time, the reaction was cooled to room temperature and 35 g of sodium acetate dissolved in 100 mL of HPLC-grade water was added to the reaction mixture. The solution was stirred for 2 h at room temperature. After separation of the aqueous and organic phases, the toluene fraction was concentrated and precipitated in methanol. The solid was collected and washed with a Soxhlet extractor using methanol.

Characterization of **P3HT**. ^{1}H NMR (500 MHz, $CDCl_3$): δ_H 0.92 (t, 83H), 1.35 (m, 169H), 1.71 (t, 58H), 2.61 (m 4H), 2.80 (t, 50H), 6.97 (s, 27H); SEC: M_n = 5400 g mol^{-1}, PDI = 1.3; Elemental Analysis: Calculated – C = 72.23%, H = 8.46%, N = 0.00%; Found – C = 69.09%, H = 8.40%, N = 0.07%.

Characterization of **CHO-P3HT-CHO**. ^{1}H NMR (500 MHz, $CDCl_3$): same as P3HT except: δ_H 2.93 (m, 4H) and 9.97 (2H); SEC: M_n = 5400 g mol^{-1}, PDI = 1.3.

Synthesis of Methylfulleropyrrolidine-Poly(3-hexylthiophene)-Methylfulleropyrrolidine (C_{60}-P3HT-C_{60}). Approximately 40 mL of chlorobenzene were added to a 100 mL flame-dried reaction flask under Ar. CHO-P3HT-CHO (0.20 g, 0.05 mmol), *N*-methylglycine (0.036 g, 0.4 mmol), and C_{60} (0.19 g, 0.26 mmol) were added to the reaction flask as solids under Ar. After purging the reaction flask for 20 min with Ar, the reaction was heated to reflux and allowed to stir for 24 h. The reaction was cooled to room temperature and the chlorobenzene was removed under vacuum. The remaining solids were redissolved in chloroform and passed through a 450 nm filter to remove any insoluble materials. The solvent was removed and the polymer was redissolved in chloroform. This solution was passed through the prep SEC columns in fractions to isolate the macromolecular material.

Characterization of **C_{60}-P3HT-C_{60}**. ^{1}H NMR (500 MHz, $CDCl_3$): δ_H 0.91 (t, 121H), 1.35 (m, 251H), 1.71 (t, 73H), 2.80 (t, 77H), 2.94 (6H), 4.26 (d, 2H), 5.0 (d, 2H), 5.38 (2H), and 6.97 (s, 40H); SEC: M_n = 7600 g mol^{-1}, PDI = 1.8; Elemental Analysis: Calculated – C = 77.03%, H = 6.97%, N = 0.34%; Found – C = 70.16%, H = 7.61%, N = 0.46%.

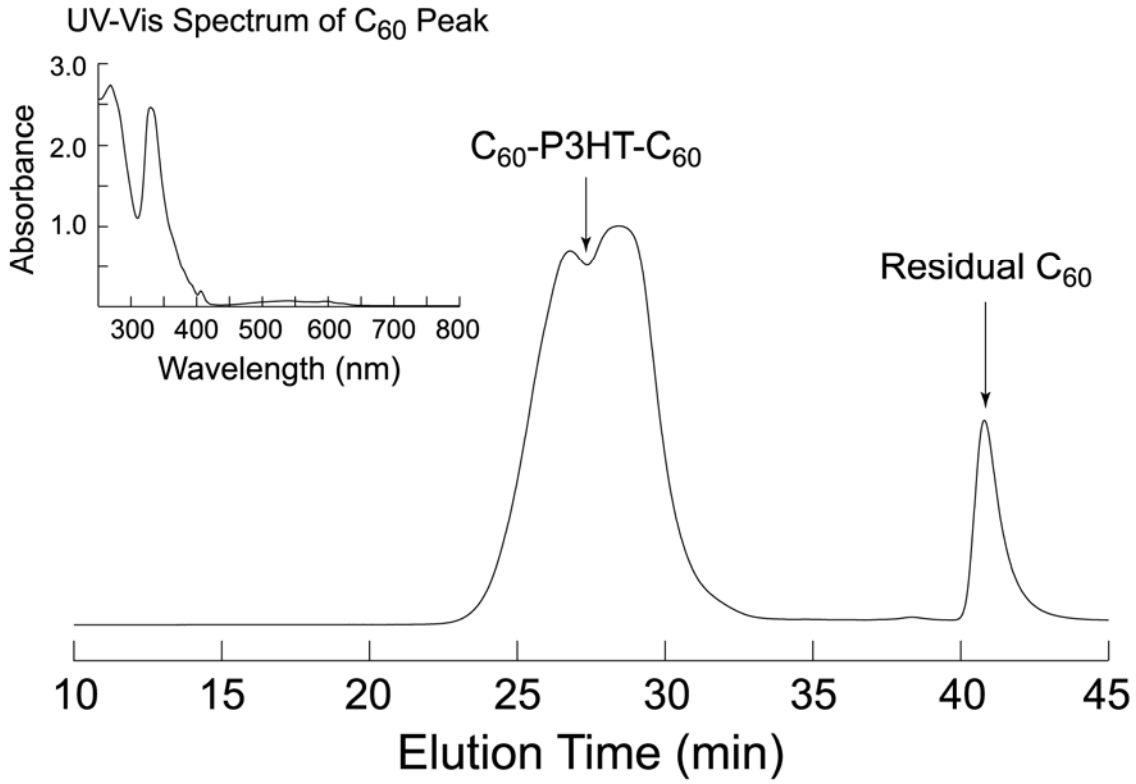

Figure 9.2. Representative prep SEC trace used in the separation of the C_{60}-P3HT-C_{60} polymer from the residual C_{60} present from the final synthesis step. The polymer was collected from 22 min < t_{elute} < 33 min. The inset shows that the peak labeled Residual C_{60} has a similar UV-Vis spectrum in chloroform to that of the known C_{60} spectrum shown in Figure 7.4a. The peaks shown both in the main part of the figure and in the inset are slightly skewed by saturation of the UV-Vis detector due to heavy loading of the polymer on the prep SEC columns.

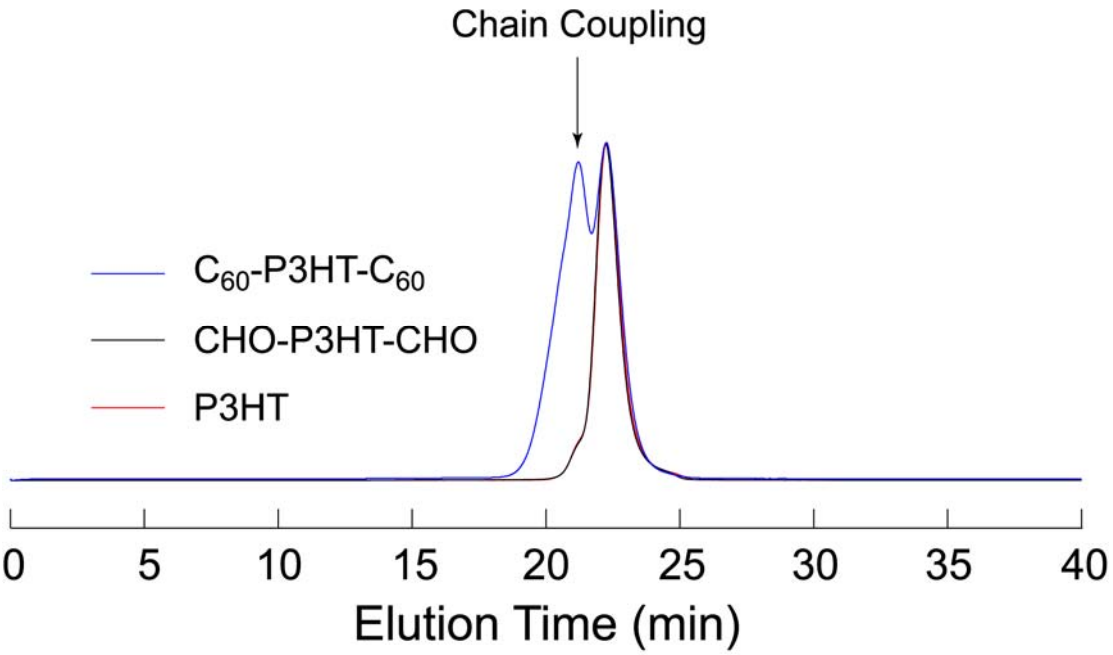

Figure 9.3. Full SEC chromatograms of C_{60}-P3HT-C_{60} and the polymer precursors with chloroform as the eluting solvent at 35 °C as shown in Figure 7.2. The traces were obtained using a UV-Vis detector monitoring the signal at λ = 400 nm. These chromatograms are over the entire elution volume of the samples and demonstrate that there is no residual fullerene present in the polymer samples.

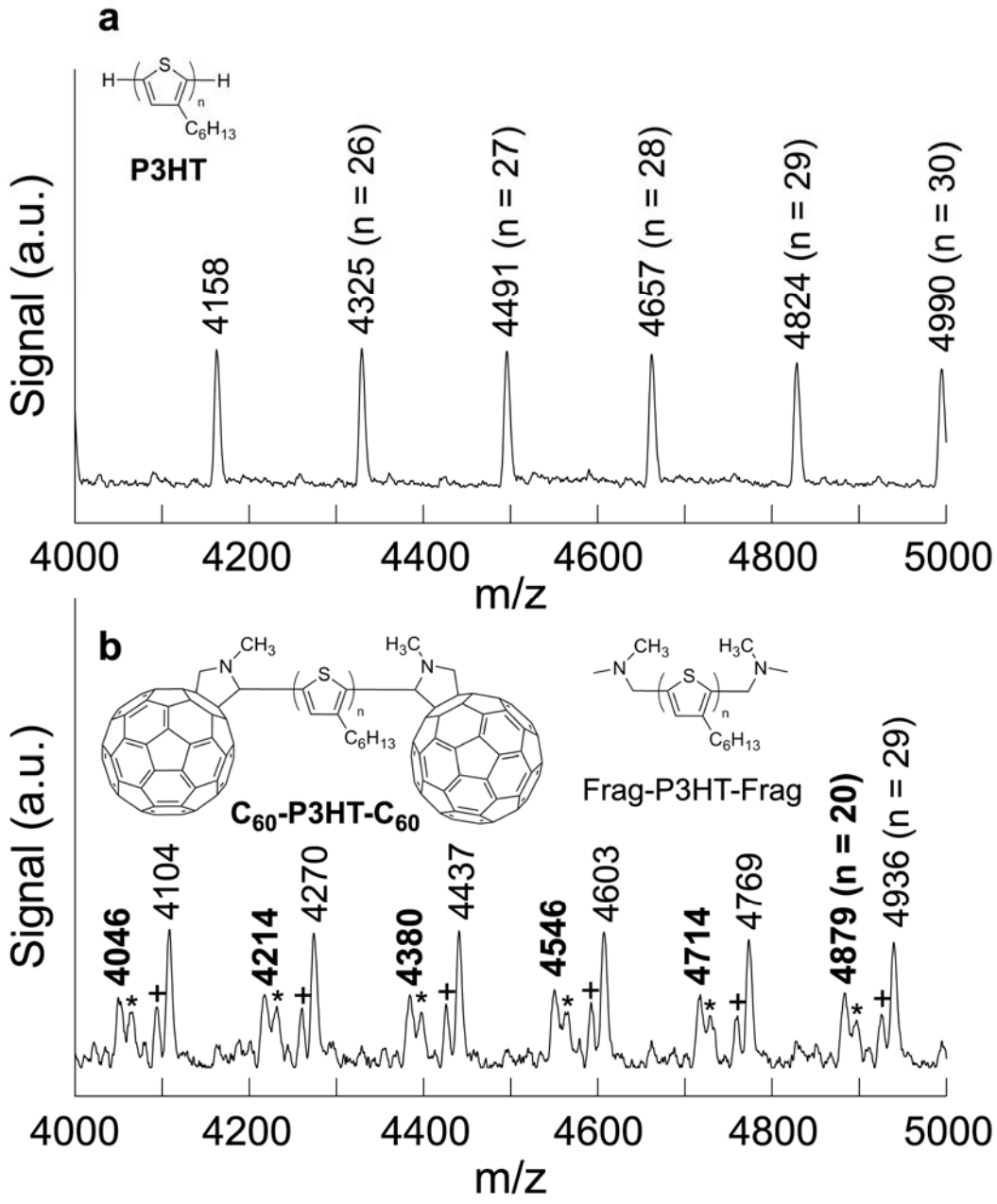

Figure 9.4. MALDI-MS spectra of (a) P3HT and (b) C_{60}-P3HT-C_{60}. The C_{60}-P3HT-C_{60} spectrum has two primary signals. We attribute the most intense signal to C_{60}-P3HT-C_{60} chains that have lost their fullerene end groups due to fragmentation (Frag-P3HT-Frag). The peaks labeled with **bold** m/z ratios are consistent with intact C_{60}-P3HT-C_{60} chains. The peaks labeled (+) and (*) are from additional fragmentation; they correspond to the loss of one CH_3 group and one CH_3-N-CH_3 group from the Frag-P3HT-Frag structure as drawn above, respectively.

9.3 Vacuum Manifold Standard Operating Procedures

A five port vacuum/inert atmosphere manifold (Schlenk line) has been assembled in the East fume hood of the Frisbie group laboratory (Room 482 Amundson Hall). Figure 9.5 depicts the layout of this fume hood with the operating and maintenance procedures of the manifold outlined below.

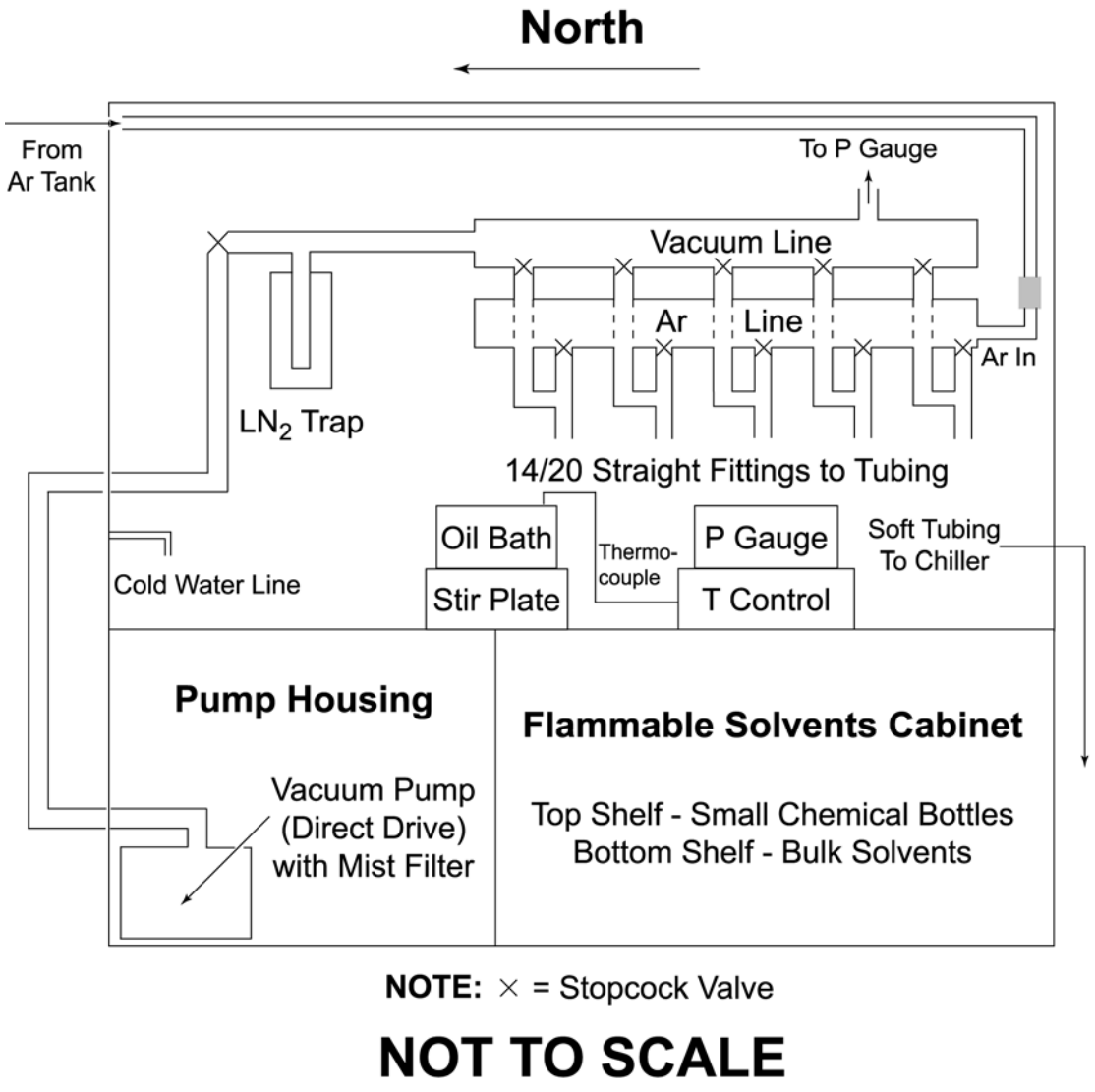

Figure 9.5. Schematic illustration of the vacuum/inert atmosphere manifold assembly in the East fume hood of 482 Amundson Hall. The shaded box in the diagram represents a gas flow meter for the argon delivery line. The schematic is not to scale.

9.3.1 Schlenk Line Design, Operation, and Maintenance

The vacuum pump for the Schlenk line is located below the bench top of the fume hood in a cabinet adjacent to the flammable solvents cabinet. This cabinet also contains spare vacuum tubing with large diameters. The vacuum pump is a direct drive pump equipped with a mist filter. There is a power switch on the pump such that the power cable can remained plugged into a power strip at all times. The vacuum pump is left running unless maintenance is being performed. A 0.5" inner diameter piece of vacuum tubing extends from the stem of the vacuum pump, and is connected to the beginning of the manifold glassware. All of the glassware used in the manifold was purchased from Chemglass (now Chemglass Life Sciences).[6] Note that any damaged part easily could be changed by purchasing a replacement part from Chemglass. A glass stem with a stopcock valve (represented by an X in Figure 9.5) connects the vacuum tubing to the glassware. This valve should be open if sub-atmospheric pressure is needed for the manifold. The valve can be closed to isolate the vacuum pump from the manifold (see below). The exit line of the glass stem is connected to a liquid nitrogen (LN_2) trap. A dewar surrounds the trap and, if necessary, can be filled with liquid nitrogen. The LN_2 trap is connected to the vacuum/inert atmosphere manifold. The current setup of the manifold has vacuum running to the top line and argon (Ar) gas running to the bottom line (Figure 9.5). This manifold has five "active" ports where vacuum or flex tubing can be attached to connect reaction, solvent, or purification flasks to vacuum or argon. Each of the active ports has two stopcock valves. One of these valves connects the port to the vacuum line and the other stopcock valve connects the line to the Ar line. Note that these valves should never be simultaneously opened. The current adapters connected to these ports are straight 14/20 connects, but other adapters may be purchased and interchanged. In addition to these active ports, there are six supplementary ports that act as inlet/outlet hookups. Three of these are not currently used and are capped with stops: 1) the port on the south side of the vacuum line, 2) the port on the north side of argon line, and 3) a port on the top side of the vacuum line. Two of the three ports in use are the inlet lines for the vacuum line (north side) and

argon line (south side). The last of the supplementary ports is on top of the vacuum manifold, and it is used as the vacuum pressure gauge hookup. An argon gas cylinder is chained to the north side of the fume hood. The regulator for the argon gas should be set at P ~2–3 psi. Polyethylene tubing runs from the regulator, through the fume hood, and into a flow meter attached to the interior of the fume hood. The tubing exits the flow meter and enters the Ar line.

When first approaching the manifold, the vacuum pump should be running, the stopcock at the glass stem should be open, and all other valves should be closed. This means that the vacuum line is under vacuum, and the pressure gauge (P gauge) reading should reflect this. The pressure gauge currently in place generally displays a pressure closer to atmospheric pressure than what the actual pressure of the vacuum line is. A general rule of thumb (based on using other pressure gauges on this vacuum line) is that a pressure reading of ~100 mTorr on the current gauge corresponds to an actual pressure of ~10 mTorr while a pressure reading of ~200 mTorr on the current gauge corresponds to an actual pressure of ~50 mTorr. A pressure reading above 200 mTorr on the current gauge should be considered poor vacuum. If a volatile solvent is to be used in the reaction/purification attached to the manifold, LN_2 should be added to the dewar, and the dewar should be raised to completely engulf the liquid nitrogen trap. Note that this needs to be done when the liquid nitrogen trap is **already under vacuum**. Otherwise, the liquid nitrogen trap may condense atmospheric oxygen! Note that the current LN_2 dewar can remain at low temperature for ~4 – 6 h before all of the liquid nitrogen evaporates. Therefore, overnight use of the liquid nitrogen trap is not currently available. If no solvents are to be used, the liquid nitrogen trap should not be filled. At this point, an air-tight flask may be attached through vacuum hose to the manifold. To evacuate the flask make sure none of the Ar line stopcocks are open, and then open the vacuum stopcock on the appropriate "active" port and watch the pressure gauge. The gauge should initially spike as gas is removed from the flask and should then decrease back to the baseline level. The amount of time required to return to baseline depends on the size of the flask used, but for moderately sized flasks, this should not take more than

1 min. To fill or purge a flask with argon, make sure all the vacuum line stopcocks are closed and open the appropriate stopcock. The flow rate of the argon gas can be controlled by a valve connected to the gas flow meter (gray box in Figure 9.5) mounted to the interior face of the fume hood. When utilization of the manifold is complete, close all of the vacuum and argon line stopcocks. If the liquid nitrogen trap was used, the following procedure will allow for safe cleaning of the system. First, close the stopcock attached to the glass stem to isolate the vacuum pump from the Schlenk line. Drop the liquid nitrogen dewar. Quickly (< 5 sec), open one of the active vacuum ports to atmosphere. Once the trap is at room temperature (~30–60 min), remove the horseshoe collar, and take down the liquid nitrogen trap. Safely dispense of the condensed liquid and clean the trap. Make sure to perform a final acetone rinse of the trap to remove any water in the trap. Allow the trap to dry and then reattach it to the manifold glassware with the horseshoe collar. Close the active port vacuum stopcock that previously was opened, and open the closed stopcock at the glass stem. The pressure of the vacuum line should return to ~150 mTorr quickly, and the line is ready for the next user.

The most important maintenance issue of the Schlenk line is changing the pump oil in the vacuum pump once every six months. Remember that this is a direct drive pump and use the appropriate pump oil. If used appropriately, the argon cylinder will last ~6 months, but a spare tank should always be on hand in case of emergency. Occasionally, substances will accidently be deposited on the walls of the vacuum/inert atmosphere manifold glassware. If this occurs, disassemble the manifold, clean the glassware with appropriate solvents, wash the glassware with water, rinse the glassware with acetone, and dry in the oven overnight to remove any residual water. If users are careful when operating the Schlenk line and the liquid nitrogen trap is used in appropriate situations, the manifold should not have to be cleaned often.

9.3.2 Operation and Maintenance of Other Fume Hood Equipment

Other pieces of useful chemistry equipment also are housed in the East fume hood. An oil bath (Ace Glassware, Inc.)[7] sits atop a stir plate, and is connected to a

temperature controller (T Control) by a thermocouple. Note that this thermocouple needs to be inserted to the bottom of the oil bath to read correctly. The thermocouple can be dislodged from the plug at the back of the temperature control box so care must be used when moving either the oil bath or temperature controller. The temperature control box is home-built so if issues arise with the system, pleas consult a departmental electronics shop on campus. While the thermocouple reads and displays the correct temperature (in °C) on the control box, the displayed temperature is usually 5–10 °C below the set point temperature. Therefore, care must be taken before walking away from the oil bath. Silicone oil is preferred as the bath medium over mineral oil as it has a higher degradation temperature. The silicone oil should be changed every 3 months or if a chemical is accidently spilled into the oil bath. On the floor just outside the south side of the fume hood sits a water chiller (Thermo Scientific).[8] This equipment allows for the circulation of water through glassware such as condensers. Flexible Tygon tubing connects the cold water source to and from the desired piece of equipment. The exit and entrance water lines are marked on the backside of the chiller. The temperature of the water can be controlled on the front panel of the water chiller. If the display panel of the chiller reads "Add", more water needs to be added to the chiller. The water level of the chiller should be kept between the minimum and maximum lines marked on the water reservoir on the front side of the water chiller. Finally, a house cold water line (equipped with an aspirator line) and sink are available on the north side of the fume hood. It is recommended that this water line be used only for pulling weak vacuum through the aspirator, and not used as a source for cooling water as the sink quickly backs up even with a modest water flow rate.

9.3.3 Safety Considerations When Working in the Fume Hood

Note that whenever working in the laboratory proper safety and personal protective equipment should be used, but those guidelines will not be listed here. This section outlines safety considerations specific to the East fume hood of 482 Amundson Hall. First, the sash of the fume hood should be raised a maximum of 18" above the bench top level, especially if open chemical containers are being used in the hood. A

stop piece is in place that reminds the user the sash should not be lifted above 18". This stop can be bypassed and the sash can be lifted to the full height; however, doing this is not recommended. When operating the vacuum/inert atmosphere manifold, make sure that the vacuum line stopcocks are never opened to atmosphere or the Ar line as this will cause overheating of the vacuum pump. Also, the liquid nitrogen dewar should only be applied to the LN_2 trap if the atmosphere of the trap has already been removed. This prevents the condensation of oxygen in the trap. If a flask is heated with the oil bath/temperature controller or the water chiller is used for cooling water, do not walk away from the setup for a long period of time (*i.e.*, overnight) until it is established that the system has reached steady state. Leaving quickly could result in fires, explosions, or floods in the laboratory! Finally, use good sense when working in the fume hood, and if questions arise, please seek assistance from the safety officer, a senior group member, or the principal investigator.

9.4 References

[1] Tashiro, K.; Kobayashi, M.; Kawai, T.; Yoshino, K. *Polymer* **1997**, *38*, 2867–2879.

[2] Liu, J.; McCullough, R. D. *Macromolecules* **2002**, *35*, 9882–9889.

[3] Witiak, D. T.; Williams, D. R.; Kakodkar, S. V. *J. Org. Chem.* **1974**, *39*, 1242–1247.

[4] Kricheldorf, H. R.; Kreiser-Saunders, I.; Stricker, A. *Macromolecules* **2000**, *33*, 702–709.

[5] Ryner, M.; Stridsberg, K.; Albertsson, A. C.; von Schenck, H.; Svensson, M. *Macromolecules* **2001**, *34*, 3877–3881.

[6] Chemglass Life Sciences Website. http://www.chemglass.com (July 2009), Chemglass Scientific Apparatus.

[7] Ace Glass, Inc. http://www.aceglass.com/ (July 2009), Ace Glass, Inc Homepage.

[8] Thermo Scientific. http://www.thermo.com/ (July 2009), Thermo Scientific Website.